Investigating the Potential of Postmortem Metabolomics in Mammalian Decomposition Studies in Outdoor Settings

A Dissertation Presented for the

Doctor of Philosophy

Degree

The University of Tennessee, Knoxville

Katharina Melanie Hoeland

December 2021

ACKNOWLEDGMENTS

I would like to thank my advisor Dr. Shawn R. Campagna for his support, patience and scientific guidance throughout my Ph.D. He gave me the freedom to set my focus early on in my graduate career toward a major focus in forensic science and let me choose projects/collaborations accordingly which ultimately shaped my future scientific direction. I am very grateful for the education I have received due to him and the University of Tennessee, Knoxville which made me grow as a person and scientist by enhancing my critical thinking and sense of integrity. I would like to also thank my committee members, Dr. Dawnie Steadman, Dr. Ampofo Darko, and Dr. Ziling (Ben) Xue for their time and dedication involved in reading and constructively criticizing my work.

Also, none of my research would have been possible without the forensic taphonomy facility in Knoxville, TN, USA and the donation of multiple bodies. Studying the processes occurring after death in a variety of different outdoor settings has an immensely valuable impact on forensic science and law enforcement agencies that cannot compete with any artificially created research environment in laboratories. Being the director of the Anthropology Research Facility (ARF) in Knoxville, it was a particular pleasure for me to work with Dr. Dawnie Steadman. Likewise, during my time in the Campagna group, I had the pleasure to work with many incredible collaborators. Their research broadened my interdisciplinary knowledge and I do not want them to feel neglected as the content of this dissertation only focuses on three selected projects. All of my colleagues guided my research in multiple discussions due to their scientific feedback which was very much appreciated. I hope that I was likewise a critical and helpful source of input. Katarina Jones, Dr. Hector Castro, and Dr. Amanda May deserve a special thank you, as they have directed and shaped my research throughout many intellectual discussions.

Lastly, and most importantly, I would like to thank my family and close friends. My family has unconditionally supported all my endeavors and they have always encouraged me and my decisions until the day I am writing this dissertation. My dear friends Haley Fielland, Simon Rotzer, and Crystal Battles – thank you for keeping up with me, listening to my endless complains and distracting me when needed most. My dear mentor Dr. Gary

Phillips, this dissertation would have probably needed many more drafts without your critical, supportive and guiding inputs. I hardly acknowledge anyone else's opinion as much as yours. I am very thankful to have met you, your incredible wife Sunny and your daughter Claire who always welcomed me and Josh like family members. That being said, thank you to my incredible boyfriend Joshua Fischer for supporting me during the hardest moments of my Ph.D.; thank you for never letting me give up and being my biggest fan. I hope you know I am yours.

ABSTRACT

By focusing on solely forensic studies, this dissertation gives an overview of three seemingly independent studies, which at a deeper level, reveal their strong interconnectivity through their forensic importance. The consistent global theme carried through all chapters circles around the application of metabolomics on biological specimens collected postmortem at an outdoor taphonomy facility in Knoxville, Tennessee, USA. The overall intention was to fill the knowledge gap around postmortem metabolomics while stressing its importance in bridging analytical chemistry and forensic science. Global postmortem metabolomics studies will contribute to the so-far conducted taphonomic groundwork by providing a better understanding of the fundamental processes of decomposition and ultimately build a more comprehensive postmortem biochemical database.

The first chapter applies postmortem metabolomics to soils and human skeletal remains obtained from a multi-individual grave. The primary goals of this study were: (1) to obtain insights into the metabolite pulse released from buried remains into grave soils at different depths of a shallow burial and (2) to assess metabolic signatures of bones using an inter- and intraindividual analysis approach.

Decomposition progresses differently below ground compared to the soil surface with impacts on rates and patterns of decomposition. In contrast to the first chapter, the second chapter faces an environmental change with a study design constructed around surface decomposition. Additionally, given that rates and patterns of decay seem to vary among species, a comprehensive omics approach including metabolomics and lipidomics was utilized to investigate species-specific metabolic signatures in soils from the cadaver decomposition island.

The final chapter completes the aforementioned studies by investigating one of the most complex of all factors – intrinsic drivers of decomposition. We evaluated the trackability of drugs through several specimens such as serum, larvae, decomposition fluid, and soils from human donors. Furthermore, comprehensive postmortem metabolomics of the same specimens provided (a) matrix-specific metabolic signatures, (b) groups of metabolites potentially useful as decomposition biomarkers, and (c) an

assessment of possible impacts of perimortem health conditions on the postmortem metabolome.

TABLE OF CONTENTS

LIST OF TABLES

LIST OF FIGURES

LIST OF ABBREVIATIONS

ADD	Accumulated degree days
ADH	Accumulated degree hours
AGC	Acquisition gain control
ANOVA	Analysis of variance
ARF	Anthropology research facility
ATP	Adenosine triphosphate
CDI	Cadaver decomposition island
COPD	Chronic obstructive pulmonary disease
CTR	Control
DF	Decomposition fluid
DS	Decomposition soil
EIC	Extracted ion chromatogram
ESI	Electrospray ionization
FC	Fold change
GC	Gas chromatography
KEGG	Kyoto encyclopedia of genes and genomes
LC-MS	Liquid chromatography - mass spectrometry
LOD	Limit of detection
LOQ	Limit of quantitation
M/Z	Mass to charge
MAVEN	Metabolomic analysis and visualization engine
MGDG	Monogalactosyldiacylglycerol
MS	Mass spectrometry
NAD	Nicotinamide adenine dinucleotide
PA	Phosphatidic acid
PE	Phosphatidylethanolamine
PG	Phosphatidylglycerol
PI	Phosphatidylinositol
PLS-DA	Partial least squares discriminant analysis

PMI	Postmortem interval
PPM	Parts per million
PS	Phosphatidylserine
RF	Random forest
RT	Retention time
sCCA	Sparce canonical correlation analysis
TBS	Total body score
TCA	Tricarboxylic acid
Tukey HSD	Tukey honest significant differences
UHPLC	Ultra-high performance liquid chromatography
VFA	Volatile fatty acid
VIP	Variable importance in projection
VOC	Volatile organic compound

INTRODUCTION

A synopsis on decomposition processes and gross postmortem changes

Death initiates a sequence of changes that degrade soft and ultimately hard tissues of a corpse. Decomposition induces noticeable macro- and microscopic alterations which occur in a fairly predictable manner, thus allowing a vague categorization of decay into a series of five (artificial) stages – fresh, bloat, active, advanced, and dry[1-4]. Although decomposition is a continuum and does not occur in discrete stages, the frequent use of stages by researchers allows for an informal, yet more uniform classification of the physical appearance of a corpse utilizing generalized terms[5]. The first stage (fresh) is associated with the mortis triad and starts immediately after death. A deceased body experiences muscle stiffness (rigor mortis), a reduction of body temperature (algor mortis), and the gravitational pooling of blood (livor mortis)[6]. As a result of a ceased blood circulation, hypoxic conditions cause cells and organelles to swell and rupture, which releases digestive enzymes responsible for cellular self-digestion (autolysis)[6, 7]. Typically, only minimal macroscopic changes are present at this stage and it lacks strong odor[8, 9]. However, flies will arrive at the body and insect invasion manifests at sites of the corpse suitable for oviposition such as natural body openings and wounds[2]. As decomposition progresses, anaerobic microbially-mediated digestion of macromolecules produces organic acids and gases which accumulate within the cadaver, ultimately causing an inflation of the abdominal area and later of other regions of the body[9, 10]. These processes are collectively summarized under the term putrefaction, marking the transitioning of the corpse into the bloating stage[10]. As the body's anaerobic intestinal bacteria (among others *Bacteroides*, *Clostridia*, and *Streptococci*) continue to break down tissue into smaller components, the internal pressure will increase up to the extent where the corpse ultimately collapses and purges putrefactive fluids[2, 7, 9, 11]. This fluid, also called decomposition fluid, forms as internal structures of the body liquefy[7]. Likewise, gasses that have formed as a by-product of decomposition get released from natural orifices causing a strong-smelling, characteristic odor[7]. The disintegration of the body enables oxygen to return to the body cavity providing ideal growth conditions for

aerobic microorganisms[7]. Additionally, fly larvae hatch and start feeding on the body. Several visible changes of the corpse are typically noticed during bloating. For example, a purple-greenish discoloration of the skin due to bacterial activity in subcutaneous capillaries (marbling), loosening of epidermis from the underlying dermis on hands and feet (skin slippage or 'degloving'), and appearance of postmortem blisters on the skin[1, 3, 6, 8, 9]. Active decay begins shortly after the release of fluids and gases into the surrounding[8]. The largest reduction of cadaveric material happens during this stage[10]. Accordingly, macromolecules along with tissue continue to break down, while entomological activity usually peaks at this period of decay[8, 9]. Purging fluids accumulate around the corpse and create a distinct 'hotspot' of fertility; referred to as cadaver decomposition island (CDI) (see below)[8]. According to *Carter et al.,* the migration of larval masses away from the food source to pupate signals the end of active decay[10]. Consequently, minimal insect activity and cadaveric material remain when decomposition proceeds into advanced decay[7]. In this stage, individual bones of the corpse are exposed to the environment, desiccated residual tissue can be found, and higher resistant material such as cartilage or hair is left to degrade[2, 8, 9]. The strong odor gradually ceases along with the purging of fluids. Lastly, the dry or skeletal stage is reached as soon as a considerably large exposure of bones dominates[2, 8, 9]. Remaining skin can adopt a leather-like appearance and closely adheres to the bones[8]. From this point onwards, the breakdown of the skeleton will continue at timeframes of years or decades until it is gradually recycled into the environment[11].

Despite the progression of the above-described stages in a predictable sequence, decomposition stages are fairly subjective and, more importantly, no two individuals are identical and decompose alike[12]. Rates and trajectories of decomposition vary strongly based on a complex and simultaneous interplay of extrinsic and intrinsic factors throughout the decomposition period[13]. Intrinsic variables refer for instance to body mass, the individuals' microbiome, and perimortem health conditions, lifestyle, or diet [2, 9, 14]. Contrasting this, extrinsic factors are either of abiotic (temperature/humidity/climate, clothing, and depositional environment such as indoor, outdoor, buried, water, soil surface) or biotic nature (i.e., microbes, arthropods, carnivores)[1, 2, 7, 13-15]. All of these

variables affect the amount of time needed for a body to decompose, and only some of them can be controlled by researchers[7, 10].

Decomposition products – The breakdown of macromolecules

Decomposition involves the enzymatic and microbially-mediated breakdown of proteins, carbohydrates, and lipids into smaller compounds and ultimately their structural monomers including amino acids, monosaccharides, and fatty acids, respectively[7, 8, 10, 16]. According to *Janaway et al*., the human body consists of approximately 20% protein, 10% fat, 1% carbohydrates, and 5% minerals – the rest is water[17]. Although there is a general understanding of the catabolism of macromolecules, the makeup of decomposition products formed during decay is highly variable based on the aforementioned influence factors. The breakdown of proteins is enzymatically catalyzed by proteases and results in the production of proteoses, peptones, polypeptides, and amino acids[7, 16]. Microorganisms further degrade amino acids via (a) deamination, (b) decarboxylation, and (c) desulfhydralation[7, 8, 16]. Deamination produces nitrogen-containing compounds such as ammonia that can either be released as gas or converted into ammonium ions nourishing for plants and microbes[4, 16]. Depending on the soil microbial community, ammonia can also undergo nitrification to yield nitrate, or alternatively, accumulate in the soil if nitrifying bacteria are missing[17]. Decarboxylation removes the carboxyl group from amino acids which produces gasses (CO_2) or, in the case of ornithine and lysine, the compounds putrescine and cadaverine, respectively[6, 7]. Indoles are also compounds produced from the breakdown of proteins[4, 16]. Sulfur-containing amino acids (e.g., cysteine, methionine) are degraded via desulfhydralation which yields hydrogen sulfide, various sulfides, or thiols[7, 8, 16]. Proteolysis occurs at a differential rate throughout the corpse, affecting organs and tissues at a varying temporal scale, hence altering the succession of gases in the decomposition odor profile. For instance, proteins in the intestines tend to degrade first followed by those in the brain, liver, and kidneys, whereas proteins in more resistant tissues such as connective tissue usually survive longer[7, 8, 16].

Carbohydrates (polysaccharides) degrade into monosaccharides (e.g., glycogen into glucose) which can then either be completely oxidized into carbon dioxide and water or result in the formation of several organic acids and alcohols[8, 11, 16]. Fungal monosaccharide degradation produces glucuronic acid, citric acid, and oxalic acid[16]. Glucose can be broken down by bacteria under aerobic conditions via the formation of pyruvic acid, lactic acid, and acetaldehyde to yield CO_2 and water[4, 16]. In contrast, restricted oxygen availability may produce lactic, butanoic, and acetic acid along with alcohols (i.e., ethanol). Methane and hydrogen sulfide are gasses resulting from bacterial carbohydrate fermentation[7, 8, 11, 16]. Collectively, these decomposition products increase the acidity in the environment surrounding a corpse[11].

Triglycerides, the main constituents of body fat (90-99%), contain three fatty acids attached to one glycerol molecule[11, 17]. Lipases are enzymes that degrade neutral lipids via a process called hydrolysis. This process yields glycerol and a mixture of saturated and unsaturated fatty acids[1, 7, 8, 11]. Further fatty acid degradation is regulated by oxygen accessibility. Broadly, an oxygen-rich environment favors oxidation of unsaturated fatty acids eventually producing aldehydes and ketones[7]. Under anaerobic conditions hydrogenation of fatty acids transforms unsaturated fatty acids (double and triple bonds) into saturated fatty acids (single bonds)[1, 7, 8, 11]. Myristic, palmitic and stearic acid are typical end products via this anaerobic route. The formation of a wax-like substance in fatty tissue (adipocere) is frequently seen in moist, oxygen-depleted environments[11]. Alternatively, lipid degradation can produce progressively shorter fatty acid chains and volatile fatty acids (VFAs), eventually resulting in the production of CO_2 and water[4, 16, 18].

Lastly, during the breakdown of macromolecules gaseous by-products, known as volatile organic compounds (VOCs), are also released. These compounds have low boiling points and high vapor pressures, thus largely contribute to the characteristic odor associated with a decomposing cadaver[7]. Among these, the most consistently reported compounds are sulfides (e.g., dimethyl sulfide), while hydrocarbons (from lipid catabolism), aldehydes, ketones, aromatic compounds, and alcohols have also been reported[19-24]. Various studies in literature investigated the ‘smell of death’ to aid postmortem interval estimations (PMI) or to scientifically elucidate components which cadaver-detection dogs or canines use to alert on[19-24].

The alteration of soil in the cadaver decomposition island (CDI)

Upon decay, decomposition products are ultimately introduced into the ecosystem for recycling. In the case of soil decomposition, the localized, nutrient-rich suite of cadaveric material creates a vertical and lateral 'hotspot' of fertility and activity – better known as cadaver decomposition island (CDI)[10, 25]. During active decay, the influx of cadaveric fluids into the soil produces an overload of nutrients that impacts soil pH, carbon-to-nitrogen ratio, and vegetation in close proximity[10, 26-29]. A distinct CDI around the corpse is still noticeable during advanced decay. It exhibits a localized enriched pulse of soil nitrogen, carbon, and nutrient levels[10, 25]. The latter comprise potassium (K), phosphorus (P), calcium (Ca), or magnesium (Mg) and are mainly derived from cadaveric, microbial or plant material[10]. *Vass et al*. analyzed soil extracts from 3-5 cm underneath a 68 kg human corpse during active decay and detected 300 µg K/g soil, 50 µg Ca/g soil, and 10 µg Mg/g soil along with various volatile fatty acids[29]. The extent to which decomposition products diverge laterally from the cadaver was assessed in a study by *Larizza et al.*[30]. Various fatty acids (myristic, palmitic, stearic, and oleic acid) were found up to 50 cm in the lateral extent of the CDI[30]. *Barton et al.* observed a limited spread of cadaveric material in a radius of beyond 30 cm laterally from the cadaver, while an increase in moisture, electrical conductivity (EC), nitrate, ammonium, and phosphorus dominated for samples directly underneath the carcass (0 cm)[31]. The vertical migration of decomposition products within the CDI is assumed to translocate underneath a cadaver to depths of up to 15 cm[32]. Nutrient concentrations have been shown to stay elevated while a corpse proceeds through the dry stage suggesting that soil chemistry levels have not yet returned to a basal level at this point[10, 29]. *Benninger and colleagues* found concentrations of lipid-phosphorus, total nitrogen, and soil-extractable phosphorus significantly increased up to 100 days postmortem in cadaveric soils[33]. Other reports estimated the persistence of human cadaver-derived nutrients in CDI up to nearly five years[32]. Being a 'nutrient sink', the cadaver decomposition island also contributes to biodiversity by providing a beneficial habitat for microorganisms, plant growth, and the reproduction of blowflies and beetles[10]. Soil microorganisms in terrestrial ecosystems are the primary mediator for global carbon and nutrient cycling through the soil[25, 34]. However,

functional and compositional shifts in microbial communities beneath cadavers have been identified and appear to be induced by the succession of the cadaver through different stages of decomposition[35]. The work by *Cobaugh et al.* demonstrated a shift from an aerobic soil decomposer community prevalent during active decay toward anaerobic taxa at the stage of advanced decay[35]. Unfortunately, every soil environment is different, first in terms of soil texture/type and second with regard to its associated local vegetation, microorganism content, climate and geology. Factors that complicate predictions of the biochemical composition of CDI soil along with processes occurring in or around it and add to the fact that taphonomy processes are still not fully understood.

Metabolic profiling and the analysis of small molecules

'Omics' technologies implement large-scale analyses of genes (genomics), transcripts (transcriptomics), proteins (proteomics), and metabolites (metabolomics) to explore the roles, relationships, and actions of various biomolecules. Metabolomics enables a holistic view of temporal changes in metabolic profiles occurring in a biological system by measuring small, low-weight compounds of typically less than 1,000 Da[36]. Within the field of 'omics' research, multiple primary and secondary subdisciplines exist, hence, lipidomics for example, resulted as a 'daughter discipline' of metabolomics focusing on the study of the lipid metabolism[36]. With the number of distinct cellular lipids being estimated to range between 10,000 and 100,000, lipidomics has grown to a distinct field with diverse applications[37]. Current metabolomics and lipidomics disciplines are designed to either quantitively measure a predetermined small group of chemically similar compounds (targeted) or detect a broad range of metabolites in a global profiling approach (untargeted)[36, 38]. The latter is a rather exploratory approach aiming to simultaneously measure as many metabolites as possible. Given that targeted metabolomics provides a narrower scope of specific compounds, it encompasses the opportunity to also discover biomarkers. Nowadays, various analytical platforms exist to meet the demands of either one of these research approaches, yet none of the analytical techniques can measure all metabolites at once. This is why a combination of techniques

is required to increase metabolome coverage. From an analytical point of view, usually either nuclear magnetic resonance (NMR) or mass spectrometry (MS) united with a separation technique are most powerful and ideally suited to conduct metabolomics studies. NMR is non-destructive to the sample and requires minimal sample preparation but is inherently not very sensitive. Gas chromatography (GC) coupled to a quadrupole or an ion trap mass analyzer is an excellent platform for the analysis of non-polar metabolites that have a small mass-to-charge (*m/z*) range, and are easily volatilized (i.e., fatty acids). Accordingly, GC-MS tends to represent only a limited amount of information from a system as it fails to efficiently measure highly polar analytes which are better suited for liquid chromatography (LC) analysis[39]. An LC-MS approach allows for separation and detection of structurally more diverse compounds, depending on the type of the chromatography used. It also detects compounds with high polarities while removing the need for a derivatization step as necessary for GC-MS. The experimental design and research question determine optimum setup with variables including multiple LC columns, ionization techniques and types of mass analyzers to choose from. The use of high-resolution mass analyzers, usually an orbitrap or time-of-flight (TOF), is a common procedure in untargeted studies[40]. Rapidly advancing technologies in this field (for instance high-resolution mass spectrometry via a hybrid orbitrap) broaden the scope of detection by not only identifying metabolites from the current state of our (textbook) knowledge (‘known metabolites’) but by detecting thousands of unidentified spectral features (‘unknown metabolites’). These unknowns or unidentified compounds have a characteristic chromatographic and mass domain but are not included in current databases, thus exhibit an unknown structure. Although structural annotation of these unknowns is still a bottleneck of metabolomics, identification can occur in conjunction with isolation (fragmentation) and/or NMR structural analysis. Although these are promising methods, when detecting several thousand unidentified spectral features in one single run, this can be a tedious undertaking. Still, the information gained from untargeted studies provides a unique opportunity to broaden the current understanding of metabolic pathways and to expand existing libraries with novel small molecules for more comprehensive platforms with wider metabolome coverage.

Postmortem metabolomics – Its application in decomposition studies and the knowledge gap

Metabolomics can be performed *in-vivo* or *in-vitro* and is applicable to a variety of matrices ranging from solids and liquids to gases. This diversity results in its interdisciplinary application in areas of human health, biomarker discovery, toxicology, plant biology, microbiology, nutrition chemistry, and many more[40]. As biochemical changes continue to occur after death, mainly as a result of autolytic and putrefactive processes, metabolomics studies can also be used to study changes in the human body postmortem. *Akcan et al*. and *Castillo-Peinado et al.* provide an extensive overview of the potential of (metabol) omics in forensic medicine and science, and discuss how forensic specimens such as urine, blood, hair, sweat, or saliva take benefits from metabolomics[36, 41]. Despite a large amount of research, one of the most challenging forensic parameters is still the precise estimation of the time since death or the postmortem interval (PMI)[36]. Biochemical and metabolic profiles obtained from cadaveric matrices can provide in-depth information regarding the cause of death, in addition to more accurate PMI estimates when postmortem 'biochemical markers' are present in the specimen[36, 42-46]. This can help to reduce examiner bias in questions related to time since death from which traditional methods, such as those based on physical evidence from algor mortis and rigor mortis, suffer[36, 47]. Over the last decades, various metabolites have emerged as possible PMI markers. For instance, early studies in the heart and muscle tissue found lactate and pyruvate related to PMI; studies in pigs linked creatinine, succinate, and alanine with PMI; while polysaccharides, steroids, and amino acids have more recently emerged as useful for time since death estimations[48-50]. Two studies by *Donaldson and Lamont* proposed nitrogen-containing metabolites (ammonia, hypoxanthine), lactic acid, and formic acid as small biomolecular markers in postmortem blood[51, 52]. 18 amino acids, five sugars, and one carboxylic acid were among the metabolites identified by *Sato et al.* using a GC-MS/MS-based metabolomics approach in a rat model[53]. Recent literature reported taurine, niacinamide, phenylalanine, tyrosine, glycerol, xanthine, and lactate among repeatedly identified compounds at three time points postmortem in mice tissue[54]. Aside from metabolites, an increasing number of studies investigating the succession of

microbial communities during carcass decomposition have also shown promising microbial-based PMI estimates with the possibility to complement conventional entomological prediction methods[27, 47, 55-58].

The establishment of taphonomy research facilities has allowed the study of carcass decomposition in several geographical regions using various experimental designs. Studies of decomposition chemistry increased the taphonomic understanding about the degradation of decomposition products, soil chemical responses to decomposition during carcass decay, and volatile cadaver-derived compounds (VOC)[8, 10, 20, 22, 24, 29, 32, 59-61]. Yet, the primary focus of taphonomy studies when it comes to understanding the biochemistry of decomposition has been centered around soil physicochemical parameters, while global 'omics' studies have seldomly been reported. Due to its ubiquity, especially in taphonomy facilities, soil holds promising potential for such studies. Generally, soil consists of a complex mixture of minerals, decaying organic remains from microorganisms and plants, and considerable contributions from living organisms arising from root exudation, plant biomass, and bacterial production[62]. Fatty acids were reported to exist ubiquitously in soil[61]. In addition to amino acids, several carbohydrates, organic acids, and vitamins were further extracted from soils[63, 64]. To this day, *Langley et al.* performed the only postmortem lipidomics study using human cadaveric specimens (skeletal muscle)[65]. Only a tiny number of postmortem proteomics studies exist in literature investigating processes of decay in skeletal remains and if protein profiles present in such specimens permit PMI estimations[66-68]. Yet, a global metabolic profile that reflects decomposition trajectories in cadaveric specimens such as soil is currently unknown. Not a single taphonomy study using soil metabolomics in conjunction with state-of-the-art analytical instrumentation has ever been conducted. Postmortem metabolomics could help to provide a better understanding of the fundamental processes of decomposition by studying metabolic dynamics during carcass decomposition. It has potential to elucidate the influence of soil characteristics on cadaver decomposition and, conversely, the effect of the cadaver on the soil system. Assessment of metabolite degradation patterns after death could also reveal if certain groups of metabolites (including lipids) follow a time-dependent degradation pattern to potentially serve as future PMI markers. Understanding metabolic patterns of decomposition is also

important when it comes to elucidating biomolecular signatures of the cadaver decomposition island (CDI) as this could confirm the location of a decomposition site, hence provide immensely valuable insights for forensic investigations. And, last but not least, expanding current efforts in the field of taphonomy using global metabolomics complements the so far conducted biochemical groundwork to build a more comprehensive postmortem biochemical database.

CHAPTER I: POSTMORTEM METABOLIC PROFILING OF SOIL AND SKELETAL REMAINS FROM A MULTI-INDIVIDUAL GRAVE

PREFACE

This first chapter focuses on understanding metabolic dynamics occurring in the complex setting of a burial by analyzing biological samples obtained from a multi-individual grave. The use of untargeted metabolomics on grave soils and human bones allows to globally assess metabolic profiles predominating both matrices and identify potential small molecule markers by comparing results to control (soil) samples.

For this project, I was presented with the opportunity to collaborate with Dr. Amy Mundorff from the Anthropology department at the University of Tennessee, Knoxville. Her multiple peer-reviewed publications in the field of forensic anthropology make her a well-known and reputational biological anthropologist. Given this unique collaboration, I worked with Dr. Alexandra Emmons, at the time a graduate student in Dr. Mundorff's group, to elucidate metabolic and microbial signatures from biological specimens associated with buried cadavers. The combination of high-resolution mass spectrometry with a microbial sequencing approach, led to the identification of potential bacterial species and metabolites highly important in such a postmortem environment.

A version of this chapter has been submitted to mSystems and is currently under review:
Alexandra Emmons, Amy Mundorff, Katharina Hoeland, Jonathan Davoren, Sarah Keenan, David Carter, Shawn Campagna, and Jennifer DeBruyn (2021). Postmortem skeletal microbial community composition and function in buried human remains.

Contributions: The study was conceived by JD, AM, and JD. Resources were provided by JD, AM, JD, and SC. Field sampling, laboratory as well as statistical analyses were conducted by SK, AE, KH, and DC. Metabolomics laboratory and data analyses were conducted by KH. Next-generation sequencing and microbial community analysis were performed by AE. Metabolome-microbiome integration analysis was conceptualized by AE and KH. The manuscript was written by AE and KH with input from all authors.

1.1 ABSTRACT

In an anaerobic environment there is limited gas exchange coupled with reduced insect access and temperatures. Such conditions promote different decomposition dynamics than aerobic (surface) environments[11, 15, 69]. Buried remains decompose in an 'enclosed system' relative to surface carcasses ultimately resulting in longer periods before soft tissues degrade and thus prolonged decomposition rates[28]. In the past, grave soil has primarily been used to study insect and microbial community patterns[27, 47, 62, 70]. This formed the current understanding that microbial communities shift over time as decomposition progresses, which opened new directions for microbial-associated postmortem interval (PMI) estimations[28]. Grave soil biochemistry has attracted attention less frequenlty[28, 61, 71]. Especially, assessment of soil chemistry of a burial years after death solely based on metabolic signatures of decay, is a quite new endeavor. Therefore, the primary goals of our study were: (1) assess the metabolite pulse released into grave soils by buried remains at different depths of a shallow mass grave (~85 cm depth), and (2) evaluate metabolic signatures of bones from individuals within the grave.

1.2 INTRODUCTION

Decomposition progresses differently in an environment below ground compared to the soil surface. Generally, buried corpses decompose at a much slower rate than bodies above ground[11, 72]. Buried remains are situated in a unique environment, mostly protected from scavengers and other necrophagous insects. Consequently, insect-mediated degradation of soft tissue is limited, thus reducing the speed at which decay progresses[69]. Likewise, cooler ambient temperature in a burial has a similar effect. According to *Troutman et al.,* this is mainly attributed to microbial activity in soil which decelerates as soil temperature drops[69]. A temperature of 37 °C is reported as optimal for tissue degradation, while temperatures below 10 °C and over 40 °C inhibit decomposition[70]. Burial depth (shallow vs. deep burials) is an important variable that influences the degree of (a) insect access to the body and (b) temperature fluctuations[11]. In shallow burials (less than 1 meter depth), insect colonization takes place when insects lay eggs on the soil surface or reach the carcass through cracks in the soil matrix[11]. *Phoridae, Muscidae,* and *Sarcophagidae* are among the dominant fly families collected from buried carcasses, unlike *Calliphoridae* – one of the main colonizer of surface remains[11, 70]. Early studies from *Mann et al.* showed that bodies buried at a depth of one or two feet skeletonized within a few months to one year, whereas a depth of three to four feet significantly increased this period up to several years[15]. The nature of the soil also alters rates and patterns of decay. In cases where soil is especially dry, mummification can be promoted. Acidic or alkaline soils reportedly decrease microbial activity and therefore decomposition rates[11, 69, 73]. Soil environments prone to retain moisture are usually linked to the formation of adipocere leading to a retardation of decomposition porcesses[11]. Adipocere refers to a whitish residue on skeletal remains as a result of the postmortem conversion of fat tissue into a lipid mixture[61]. A gas chromatography-mass spectrometry (GC-MS) method by *Forbes et al.* provided evidence that adipocere can leach into the surrounding grave soil environment[61]. In such areas, elevated levels of dissolved organic carbon (DOC) and phosphorus have been detected[10]. Lastly, oxygen availability in a burial is greater with proximity to the soil surface; anaerobic conditions predominantly exist at the base of a grave. This controls activity and composition of

microorganisms in grave soil[69, 70]. Moreover, conditions in a mass grave also differ from those found in single burials. Mass graves have been defined as burials of two or more carcasses[69]. In mass graves where bodies are in direct contact with each other, the remains often form a contiguous and dense aggregate which may create a synergistic environment[69]. Both *Troutmann et al.* and *Mant et al*. noted differential decomposition patterns based on the corpse location in mass graves[69, 74]. A more rapid decomposition toward the top of the grave contrasted decelerated rates of decay for carcasses buried at the center or the bottom of the grave[69, 74]. Decomposition of remains buried in multi-individual graves is driven by temperature, however, *Troutman et al.* showed that oxygen deficiency prevailing at certain depths could be a major component affecting trajectories of decomposition, as well[69].

After soft tissue degradation, skeletal remains begin to slowly decompose. Diagenesis refers to the changes bones undergo after death, more specifically, the postmortem biochemical alterations as opposed to biogenesis. Mammalian bone consists of organic, inorganic components, and water. A composition that varies considerably with age and bone type[75]. The vast majority of the organic fraction is (type I) collagen – a fibrous protein. Carbonated hydroxyapatite ($Ca_5(PO_4)_3OH$) comprises the inorganic or mineral fraction[76]. Diagenesis affects the bones of the skeleton differently. Cortical (compact) bones are more densely mineralized and thus less prone to diagenesis, whereas the opposite is true for spongy (cancellous) bones which are generally more porous[77]. The composition of buried bones is a result of changes that happened pre- and post-deposition. Literature suggests that in a burial the chemical composition of bones will ultimately begin to mirror that of the surrounding soil[77]. However, the extent and speed of diagenetic processes are highly heterogeneous due to post-depositional time and the local burial environment, which includes local geology, climate, soil pH, groundwater movements, as well as soil microbial diversity[78]. Hydroxyapatite is mainly degraded or recrystallized through chemical dissolution and microbial attack[79], suggesting a correlation to phosphate solubilization[80]. Phosphate-solubilizing bacteria reportedly utilize three mechanisms of action to solubilize mineralized phosphorus from bone: the production of (1) acids, (2) chelating agents (e.g., 2-ketogluconate, citrate, oxalate, and lactate), or (3) hydrogen sulfide[81]. Collagen is mainly degraded by bacteria capable of

producing enzymes called collagenases[56]. Subsequent catabolic processes lead to the breakdown of remaining polypeptides into smaller peptides and ultimately single amino acids by hydrolytic protease activity[56].

Literature comprises several archeological studies of skeletal remains[79], yet these typically do not focus on the postmortem metabolic profiles of the depositional environment nor the buried skeleton in it. Given that subsurface decomposition is also a less commonly chosen experimental design in forensic taphonomy research, this study aimed to combine these two aspects by assessing biochemical signatures of two postmortem specimens – human bones and grave soil – to broaden our understanding of metabolic dynamics occurring in a multi-individual grave four years after burial.

1.3 EXPERIMENTAL SECTION

1.3.1 Field location and study design

For this study, three subjects obtained from the Body Donation Program at the University of Tennessee (UTK), TN, USA were buried in 2013 in a multi-individual grave at the 3-acre Anthropology Research Facility (ARF) in Knoxville, TN. A schematic representation of the burial with depth profiles is shown with the permission of Dr. Alexandra Emmons in Appendix Figure 1.9. Detailed donor demographics are listed in Appendix Table 1.1. All individuals were positioned unclothed in a stacked, crisscross fashion in the grave with individual A on the grave base and individual C placed above subject B which was located in the middle. Individuals were placed simultaneously to replicate a realistic mass grave scenario and to minimize effects related to seasonality, which is a known factor impacting decomposition rates[82]. This experimental design created inter-individual differences in decomposition states, most likely caused by different depths within the grave (see 1.4 results and discussion). In addition to this grave, a second area was excavated and backfilled with soil to serve as a control grave. No individuals were placed in the control grave. The two graves were approximately 2 m x 2 m x 0.7 m and 2 m x 4 m x 0.7 m, respectively. Donors were excavated four years after

burial in 2017. Metabolomics was performed on a subset of both soil and bone samples (see below).

1.3.2 Biological sample collection

Decomposition soil samples were collected at different depths from within the multi-individual grave: 0-5 cm, 30-35 cm, 70-75 cm, and 80-85 cm. Additionally, one sample containing adipocere and other partially decomposed organic material was sampled from within the ribcage of individual C at a depth of 40 cm. The excavations first reached human remains at a depth of 30-35 cm. The base of the grave was 70-75 cm below ground. The deepest samples were collected from a depth of 80-85 cm; around 15 cm below the base of the grave. Soil samples from different depths were collected pre-, syn-, and post-excavation. A total of n = 20 grave soil samples underwent metabolomics analyses (sample details Appendix Table 1.2). Control soils were collected from (a) the aforementioned control grave ('negative control') and (b) from an undisturbed area at a five meter distance from the multi-individual grave (depths of 0-5 cm and 30-35 cm). A 10 cm diameter auger was used to collect soils and any non-soil debris like plants or roots were manually removed. A more detailed description of the sampling procedure can be found in *Keenan et al.*[28]. In addition to metabolomics, soil samples were also subject of geochemical analyses, DNA, and nematode extractions[28].

Human skeletal remains were the second matrix. After excavation, a total of 49 bones from each of the subjects were collected and chemically treated for cleaning. After removal of the outer bone surface using a Dremel® rotary tool, bones were treated with a mixture of bleach and ethanol (10:70). A handheld drill with a 9 mm masonry bit was operated at low speed to drill holes in the bones and obtain bone powder. Bone power was used for human DNA, total DNA, and total bacterial and fungal gene abundance analyses. Metabolomics was applied to a subset of the skeletal samples (n = 41, see 1.3.3 and Appendix Table 1.2). A detailed methodology and sample description of the obtained bone/soil specimens are specified in the publications of this project[28, 82].

1.3.3 Untargeted metabolomics

Untargeted metabolomics was performed on a subset of randomly selected soil (n = 20) and bone powder samples (n = 41, A: n =14; B: n =14; C: n =13) (Appendix Table 1.2). Samples were extracted in triplicates from 70-90 mg bone powder and 70-100 mg soils using a procedure adapted from *Lu et al.*[83]. All matrices were suspended in 1.3 ml of extraction solvent (40:40:20 HPLC grade methanol, acetonitrile, water with 0.1% formic acid). Samples were vortexed and allowed to extract for 20 min at 4 ˚C while being shaken on an Orbital Platform Shaker (Bellco, Vineland, NJ). Once the extraction was complete, samples were centrifuged (5 min, 16,100 rcf, 4 °C) and the supernatant collected and transferred to new Eppendorf tubes. An additional 200 µl of extraction solvent was added to the residual specimens and re-extracted as described above. The supernatants were combined and dried to completion under a stream of nitrogen (2-3 hours). The resulting dried residue was re-suspended in 300 µl of sterile HPLC grade water and transferred to 300 µl autosampler vials for subsequent LC-MS analysis.

1.3.4 Analytical instrumentation

To perform ultra-high-performance liquid chromatography coupled to high-resolution mass spectrometry (UHPLC-HRMS) analyses, a 10 µl aliquot was injected through a Synergi 2.5 micron reverse-phase Hydro-RP 100, 100 x 2.00 mm LC column (Phenomenex, Torrance, CA), kept at 25 ˚C. The eluent was then introduced via negative electrospray ionization (ESI) into an Exactive™ Plus Orbitrap Mass Spectrometer (Thermo Scientific, Waltham, MA) through a 0.1 mm internal diameter fused silica capillary tube. The MS was run in full scan mode with a spray voltage of 3 kV. The nitrogen sheath gas was set to a flow rate of 25 psi with a capillary temperature of 300 ˚C. The acquisition gain control (AGC) target was set to $3e^6$ ions. The samples were analyzed with a resolution of 140,000. A scan window of 72 to 800 *m/z* was used from 0 to 9 minutes and of 110 to 1000 *m/z* from 9 to 25 minutes. A flow rate of 0.2 ml/min was maintained throughout the run. The length of the chromatographic analysis was 25 min. Solvent A consisted of 97:3 HPLC grade water:methanol, 10 mM tributylamine, and 15 mM acetic acid. Solvent B was HPLC grade methanol. The gradient was as follows: 0 to 5 min: 0%

B, 5 to 13 min: 20% B, 13 to 15.5 min: 55% B, 15.5 to 19 min: 95% B, 19 to 25 min: 0% B.

1.3.5 Data processing and statistical analyses

Following UHPLC-HRMS, raw files generated by Xcalibur were converted to the universal mzML format via the open-source MSConvert software as part of the ProteoWizard package[84]. Metabolomic Analysis and Visualization Engine (MAVEN) software from Princeton University was used to automatically correct the total ion chromatograms based on the retention times for each sample[85, 86]. Spectral features were manually selected based on mass accuracy (± 5 ppm mass tolerance) and retention times (≤ 2 min). Known metabolite spectra were manually selected using an in-house library with approximately 278 compounds. Normalized metabolomics data sets (normalization by mass) were uploaded to the Metaboanalyst online statistical analyzer using the following parameters: sample normalization (none), data transformation (log), and data scaling (autoscaling)[87]. The same software supplies options for uni- and multivariate statistical analyses. Partial least squares discriminant analysis (PLS-DA), which is similar to principal component analysis, was used to find differences in metabolite signatures. This analysis enables a dimension reduction along with a feature selection tool that assigns metabolites ranks based on their variable importance in projection (VIP) scores. Metabolites with a VIP score > 1.0 are generally considered significant contributors to a separation among groups. Analysis of variance (ANOVA) followed by Tukey HSD (tukey honest significant differences) was used for multiple pairwise comparisons. Differences with a p-value less than 0.05 were considered statistically significant. Normalized fold changes allowed the construction of heat maps. ANOVA plots and heat maps were generated using R software (version 1.2.5042).

The remaining spectral features from metabolomics extractions were classified as unknown or unidentified. On average multiple thousands of unidentified metabolites are detected in one run. All spectral features arising from unknown metabolites were automatically detected using XCMS (R package). Afterwards, signals from isotopes and adducts were removed with the open-source R package, CAMERA[88]. The resulting ion counts were further filtered by removing features found to be higher in blanks. To annotate

the unidentified features, Fiehn's seven golden rules algorithm can be used to assign hypothetical chemical formulae to an exact mass[89]. The hypothesized atomic H/C and O/C ratios can be used to group the unknown metabolites into major compound classes by constructing a van Krevelen diagram[90]. In such a diagram every calculated chemical formula is given a 'ratio-value' to ultimately determine a generalized compound class e.g., lipids, proteins, carbohydrates, amino-sugars, condensed hydrocarbons, or lignins.

In a collaborative effort with Dr. Alexandra Emmons, known metabolites were correlated with the microbial data obtained from 16S rRNA sequencing analyses using a sparce canonical correlation analysis (sCCA) paired with principal components analysis (PCA). R packages PMA (Penalized Multivariate Analysis, v. 1.1) and ade4 (Analysis of Ecological Data: Exploratory and Euclidean Methods in Environmental Sciences, v.) were applied. sCCA (penaltyx/penaltyz = 0.15) was used as a data reduction tool. All metabolites were log transformed (base 10) prior to analyses, and DNA degradation index, as a proxy for skeletal integrity, was added to the metabolite data set. A pseudocount of one was included to eliminate problems with zeros in log transformation.

1.4 RESULTS AND DISCUSSION

Information related to the macroscopic evaluation of the exhumed bodies described by *Emmons et al*. were important for the interpretation of our soil and bone metabolomics findings.[82] In short, the stacked fashion of the buried bodies resulted in inter-individual differences in decomposition states at excavation. In 1985, a study conducted by *Rodriguez and Bass* reported that decomposition states of buried individuals were highly dependent on burial depths and temperature[72]. Thus, in this study, skeletonization was observed for the shallowest donor (body C) with minimal residual soft tissue. Partial skeletonization and some adipocere formation with skin and soft tissues were characteristic for individual B (middle). The last donor (grave bottom, individual A) was least decomposed and nearly intact due to extensive adipocere formation which preserved underlying tissues and muscles[28]. Brain tissue residue was present in the skull and isolated decomposed muscle tissue covered in skin and adipocere was found at the

upper and lower torso including the proximal one-third of the femora and humeri[82]. Additionally, bones from each individual spanned multiple depths. Individual C was first observed at approximately 27 cm below surface and extended to a depth of 55 cm. Remains from individual B spanned depths of 34 cm and 62 cm, and those from individual A depths of 42 cm and 62 cm below ground[82].

1.4.1 Soil metabolic dynamics within a multi-individual grave

UHPLC-HRMS based untargeted metabolomics was used to profile soil metabolic changes in a grave four years after burial. A first overview of the data set was obtained by categorizing detected metabolites into seven broad compound classes according to their chemical compound attributes using KEGG (Kyoto Encyclopedia of Genes and Genomes) identifiers. By assessing all spectral features globally, 46% were linked to amino acid metabolism, 27% were identified as nucleosides, nucleotides, and analogs, and 7% as carbohydrates or carbohydrate conjugates (not shown). Lipids/lipid-like molecules and vitamins were accounted for with 5% each, while 3% of the total detected metabolome were bile acids and/or bile salts. 7% of all spectral features were grouped under the class name ‘others’ and included metabolites such as allantoin or hydroxybutyrate (data not shown). Next, the sum of relative abundances of metabolites comprising a compound class was monitored across different depths within the mass grave (Figure 1.1). We found that soils at certain depths exhibited varying metabolic profiles within the grave. In detail, compound classes dominating at 30-35 cm included bile acids, such as taurine, and nucleosides/nucleotides. Relative abundance changes of carbohydrates/carbohydrate conjugates were minor within the grave as they were detected in fairly comparable amounts at each depth. However, 27% of their overall abundance was found in soils at 70-75 cm below ground (Figure 1.1). Relative abundances of lipid-like compounds (e.g., 2-oxo-4-methylthiobutanoate, 3-methylthiopropionate), amino acids (e.g., citrulline, creatine, glutamate, glutamine, or tyrosine), vitamins such as pantothenate, as well as allantoin or hydroxybutyrate (compound class ‘others’) increased with grave depth until a depth of 40 cm. At 40 cm, abundances of these compound classes were highest but subsequently declined at 70-75 cm. Thus, subsurface soil from 40 cm seemed to exhibit a clear abundance shift – for

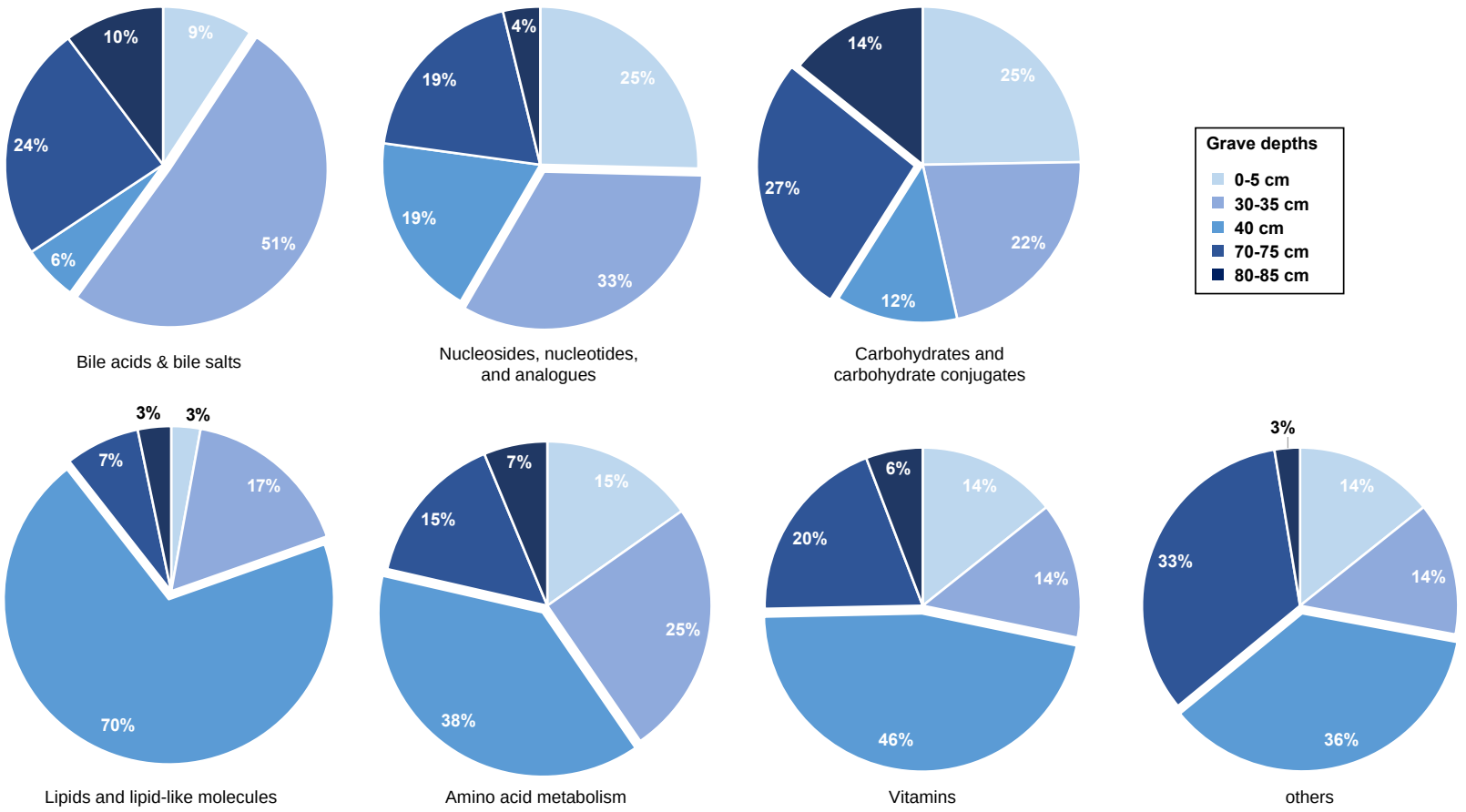

Figure 1.1 – *Overview of the distribution of compound class abundances in soils obtained from different depths within a multi-individual grave. Relative abundances of compound classes at different depths are depicted in pie charts and changes in color brightness (bright to dark blue) illustrate depths of 0-5 cm, 30-35 cm, 40 cm, 70-75 cm, and 80-85 cm, respectively.* three of the aforementioned classes abundances more than doubled compared to those detected at 30-35 cm. Interestingly, only a minor percentage of

each compound class seemed abundant at 15 cm below the base grave (80-85 cm) (Figure 1.1; abundance range across compound classes 3-14%).

Combined, abundances of compound classes at the grave surface (0-5 cm) were different when compared to those detected at different depths deeper within the burial. At a depth of 40 cm, abundances of four compound classes were highest, which reinforced and supported observations by *Kennan et al*., who showed that this soil sample also contrasted sharply from others based on nearby soil microbial ecology and biogeochemistry[28]. As the majority of metabolic changes were observed at burial depths of 30-35 cm, 40 cm, and 70-75 cm, we demonstrated differential soil chemistry responses in areas where human decomposition occurred.

To investigate the above-described global metabolic picture on a more in-depth scale, the grave metabolome was further assessed using multivariate analysis (Figure 1.2A). Consistent with Figure 1.1, PLS-DA showed diverse metabolic profiles for soils collected from within the mass grave (Figure 1.2A). A slight overlap appeared for the 0-5 cm and 30-35 cm samples, while the remaining depths formed separate clusters (Figure 1.2A). Soils collected from a depth of 40 cm grouped closely to each other. Deeper locations within the grave (70-75 cm and 80-85 cm) had more differentiation within each cluster. A driving factor for this might have been the changing diversity of microbial communities at certain excavation depths as reported by *Emmons et al.*[28, 82]. To explain some of the metabolic variation seen among all five depths, metabolites with VIP values > 1 were extracted from the PLS-DA plot and compared to results obtained from one-way ANOVA. The latter was performed to assess significance in metabolite changes among depths ($p \leq 0.05$ with Tukey's HSD correction for multiple comparisons). This analysis found significant variation in abundances for 36 metabolites, while 13 metabolites extrapolated from the PLS-DA plot had VIP scores > 1. Among those 36 and 13 compounds, eight metabolites overlapped (Figure 1.2B). These eight showed significant abundance differences at primarily either 40 cm and/or 70-75 cm below ground (Figure 1.2B). Hydroxybenzoate, homocysteine, tyrosine, and tryptophan were identified as

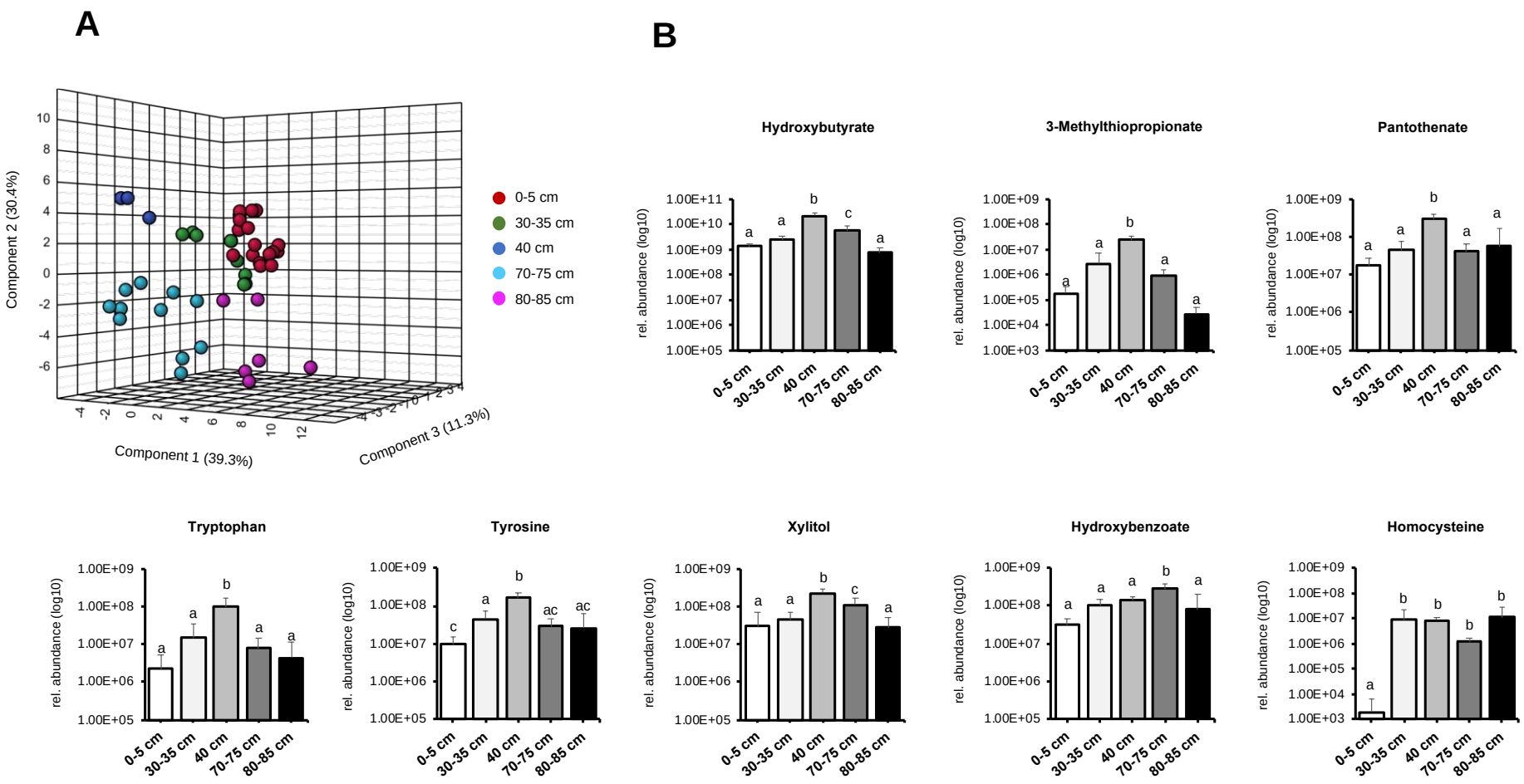

Figure 1.2 – *Intra-gave soil metabolic changes at different depths. (A) 3D PLS-DA plot of soils collected at multiple depths from the grave. (B) Most significant metabolites resulting from one-way ANOVA and VIP analysis with significant changes in relative abundances at different grave depths. Letters above bar graphs were derived via Tukey HSD post hoc tests.*

involved in the amino acid metabolism. The five-carbon sugar xylitol is commonly used in a variety of food, but is also found in smaller quantities in plants or is microbially produced from xylose[91]. Multiple origins are also known for hydroxybutyrate and the water-soluble vitamin pantothenate – both have been related to bacteria, plants, and animals[92]. The compound 3-methylthiopropionate is categorized as lipid/lipid-like molecule.

Given that all compounds were detected at 0-5 cm (grave surface), the significantly increased abundances inside the grave reinforced our hypothesis of a shift in the grave biochemistry at deeper depths. A potentially differential influx of decomposition products into the soil may have altered at these depths the intra-grave soil biochemical dynamics. A separate study of this project observed, among other parameters, high concentrations of organic sources including dissolved organic carbon (DOC) and nitrogen (DON) at 40 cm and at the grave base (70-75 cm), likely as pooled inputs from all three remains. In addition, with the base of the grave being water-saturated, oxygen availability was limited[28]. This could have driven a shift in microbial communities within the grave toward anaerobic colonizers because at around 40 cm and above, soil geochemistry parameters suggested enough oxygen for nitrification[28, 82]. *Pontiller et al.* recently described the bacterial transformation of labile DOC compounds such as amino acids, glucose, or acetate and the utilization of organic acids, oligomeric or polymeric molecules like proteins and polysaccharides[93]. Therefore, a diverse and highly variable microbiome within the grave could have impacted metabolic dynamics at specific depths.

1.4.2 Comparative analysis of grave and control soil metabolic patterns

Presently, metabolomics focused solely on decomposition-impacted soils from the multi-individual grave. Next, we compared decomposition soil samples with samples obtained from the control grave (0-5 cm and 30-35 cm). Samples from the control grave were preferred over off-grave controls, as the control grave resembles the same environmental conditions allowing direct evaluations of decomposition effects. To determine which metabolites significantly changed in abundance between the two graves (multi-individual vs. control grave), a volcano plot analysis was performed (FC threshold 1.5, p-adjusted threshold ≤ 0.05). Control grave soils from 30-35 cm were used for comparisons with decomposition soils from 30-35, 40, 70-75, and 80-85 cm, while control

soils collected at 0-5 cm were compared to those collected at 0-5 cm from the mass grave. A detailed overview of the analysis with all altered metabolites is summarized in Appendix Table 1.3. Results of the volcano plot analyses are visualized as bar graphs in Figure 1.3A. Here, the total number of metabolites with significantly altered abundances among the two grave soils is depicted by depths. For example, a depth of 0-5 cm showed 14 metabolites lowered in abundances in decomposition-impacted grave soils when compared to the control (Figure 1.3A). Yet, with increasing grave depth we noticed an increased number of compounds that were higher in relative abundance in the mass grave. Particularly, this was the case at 40 cm and to a lesser extent at 70-75 cm (Figure 1.3A, 36 metabolites and 11 metabolites, respectively). Features with higher abundance in soils from the multi-individual grave (49 features total) were further evaluated using a Venn diagram to identify common and unique metabolites among depths. As depicted in Figure 1.3B, 27 features were elevated solely at a depth of 40 cm, and two features at 70-75 cm. Seven metabolites were mutually elevated at both 40 and 70-75 cm, while two metabolites had greater abundances at all three depths when compared to control soils. Homocysteine and hydroxybenzoate comprised the latter two (Figure 1.3B). Being significantly “upregulated” in decomposition soils, a direct link to human decay processes seemed likely. Reinforcing this, a review of by *Dent et al.* links the occurrence of sulfur-containing amino acids in soils during human decay to the breakdown of proteins[16]. Homocysteine, a sulfur-containing amino acid, is formed during methionine catabolism[94]. Methionine on the other hand is one of two proteinogenic sulfur-containing amino acids. Hydroxybenzoate has not been reported in the literature as a product of human decomposition, although other benzoic acid derivatives, like methyl benzoate, were detected among compounds significant to the odor profile of human remains[95]. As subsurface decomposition processes are vulnerable to temperature, moisture and the availability of microbes[16], specific conditions in the grave could have preserved carcass-sourced metabolites in decomposition-impacted soils even four years after burial. On the contrary, adenosine, deoxycytidine, and thymidine were among the compounds with continuously higher abundances in control grave soils (Figure 1.3A, red bars and Appendix Table 1.3). All of the aforementioned compounds are nucleoside analogues or nucleosides which are structural subunits of nucleic acids. Previous studies showed the

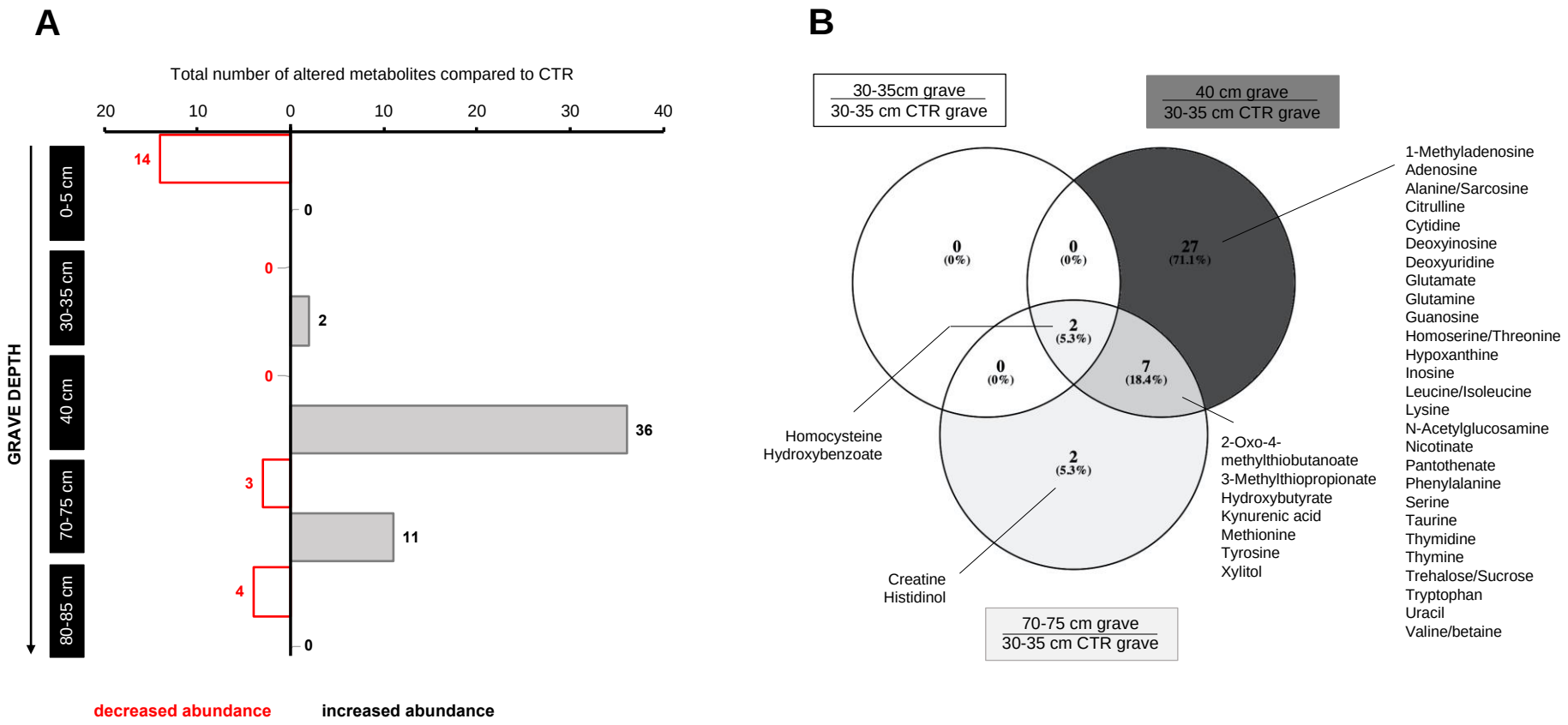

Figure 1.3 – *Postmortem metabolomics contrasting mass grave soil and control soil metabolic signatures. (A) Result of volcano plot analyses showing the total number of significantly altered metabolites at different grave soil depths when compared to soils from the control grave. Metabolites are shown as having significantly increased (grey bars) and/or decreased (red bars) abundances when compared to their abundances in controls. (B) Venn diagram using metabolites identified in (A) that had significantly increased abundances at 30-35, 40, and 70-75 cm within the mass grave in comparison to control soils. CTR = control.*

existence of nucleic acids, polynucleotides and nucleosides in soil organic matter[96, 97]. Thus, a differential microbial community composition in either one of the two soil types with microorganisms exhibiting mechanisms to release extracellular products that solubilize nucleic acids and/or other microbes equipped with necessary nucleoside transporters for facilitating uptake and incorporation of such compounds[98], seemed a plausible explanation for the detection of nucleosides in soils.

Overall, when looking at the soil metabolic responses collectively, our results revealed differential dynamics of soil metabolite abundances at different depths within the mass grave. Given that intra-grave differences in soil metabolomes between surface soils (0-5 cm) and soils of increasing depth were also significant when compared to controls, it can be assumed that soils at a depth range of 40-75 cm experienced an increased influx of human decomposition due to an additive impulse of the decay of all three bodies. Likewise, this implies that even years after a burial, soils may have the capacity to retain traces of decomposition that could aid in locating buried remains.

1.4.3 Postmortem metabolomics of buried human skeletal remains

1.4.3.1 Inter-individual comparisons

To assess metabolic signatures of bones from buried individuals, all bone samples of each individual were first analyzed comprehensively (inter-individual analysis) followed by an intra-individual analysis of several anatomical regions. For the inter-individual analysis, the PLS-DA plots showed a separation of the bone metabolomes in a multidimensional space indicating that gross bone metabolic signatures differed among all buried bodies (Figure 1.4). Bones from individual A appeared nicely clustered when compared to the entirety of samples from individual B. Similarly, bones from individual B were metabolically distinguishable from those collected from individual C (Figure 1.4). While the majority of bone samples in the PLS-DA plots did separate, a small number seemed to slightly overlap with each other – a pattern that was absent in the PLS-DA plot of individuals A and C. Here, two entirely distinct clusters were formed comprising all samples from the respective bodies (Figure 1.4). This observation was most likely caused by the study design and the way individuals were buried. With individuals A and C being located at the bottom and top of the grave, respectively, more diverse metabolic profiles

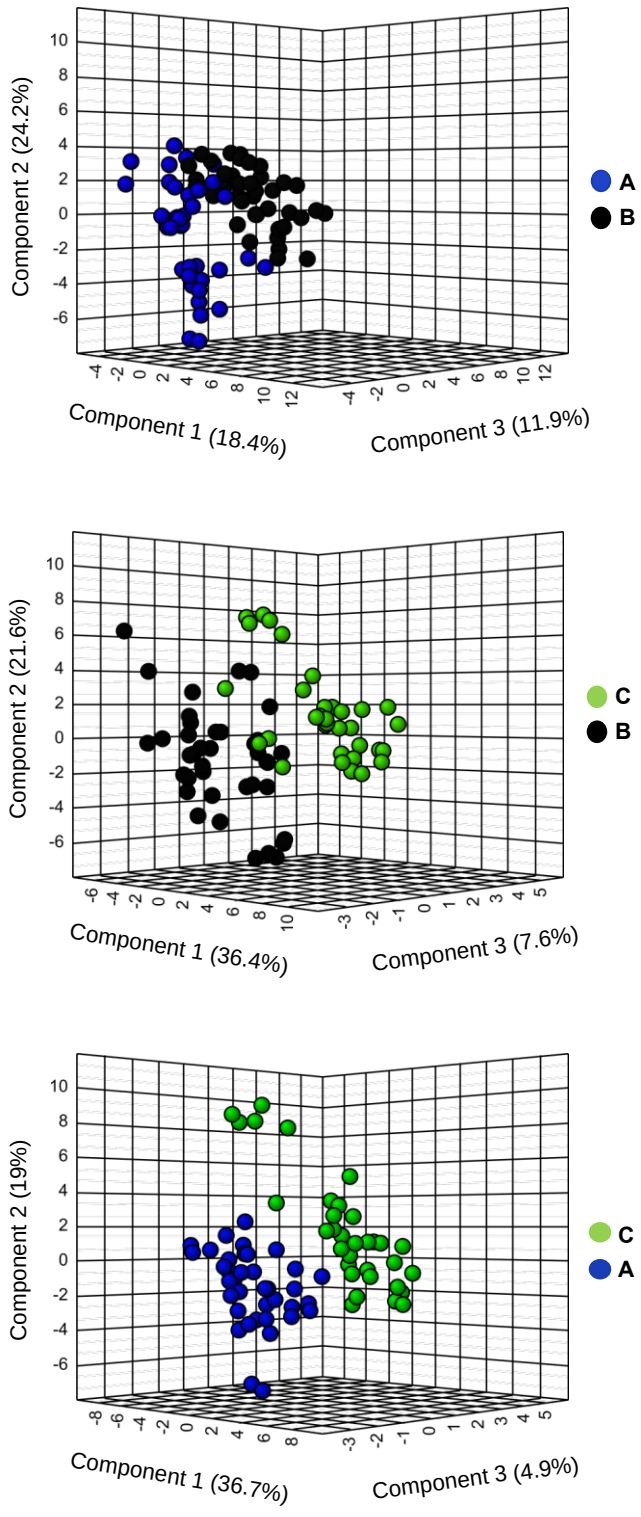

Figure 1.4 – *Inter-individual bone metabolic signatures. PLS-DA analysis of bone powder samples obtained from three donors (A, B, and C) four years after burial.*

can be expected. On the contrary, a slightly higher metabolic similarity of certain body regions for the comparisons involving donor B could have resulted from the stacked design with individual B being “sandwiched” between A and C. Bones from different individuals in close proximity or even in contact with each other could have experienced a similar decomposition environment including similar microbial communities, which ultimately led to more comparable metabolic patterns among A and B as well as B and C. The overall inter-individual variation in the bone metabolomes was impacted by a variety of factors. A few to name are general health, medication, lifestyle (tobacco, illicit drugs or alcohol abuse), or diet. All these variables form a person’s, or in this case, a cadaver’s unique (bone) metabolome. Nevertheless, it was shown that even four years after burial, bones from a multi-individual grave still contained a unique metabolic signature that could be ‘reassigned’ to an individual.

Aside from global PLS-DA analyses, we can also look at how abundances of single metabolites change across cadavers by converting a numerical value to a defined color scale (Figure 1.5). Differences in the overall patterns of metabolite abundances were particularly obvious for individual C. Lowered abundances were detected for this donor for a large variety of compounds (blue columns Figure 1.5). In contrast, A and B had overall a greater number of compounds with increased abundances (Figure 1.5 red columns). Knowing about the geochemical environments of bodies A and B compared with C, inter-individual bone metabolome differences were expected. As previously stated, decedents were stacked in the grave prior to burial, and each individual spanned multiple depths or a unique depth regime. This contributed to differential decomposition related to changes in oxygen availability, moisture, soil biogeochemistry, arthropod activity, and temperature. Additionally, cadavers A and B had greater amounts of soft tissue preservation and adipocere (body A) formation, while C was fully skeletonized. Our results coincided with observations from a previous publication of this project stating that bacterial and archaeal microbial communities from individual C deviated from A and B[82]. Donors A and B were also more likely impacted by fluctuations in groundwater. Water movement may have promoted microbial accessibility to bone surfaces and enhanced microbial intrusion by increasing bone porosity[99]. In addition, intrinsic differences in skeletal integrity may have enhanced microbial accessibility to internal bone surfaces.

Bodies A and B seemed to have greater skeletal porosity, and B had also a fused vertebral column with fused ribs 1 and 2 (publication under review).

Next, significant differential metabolite abundances based on p-values shown in Figure 1.5 were assessed with regard to VIP values obtained from the above-shown PLS-DA plots (Figure 1.4). An overview of all metabolites with VIP scores > 1 is given in Appendix Table 1.4, and selected metabolites with similar inter-individual alterations (increase or decrease) are listed in Appendix Table 1.5. Compounds with VIP scores > 1 and significant p-values (* ≤ 0.1, ** ≤ 0.05, *** ≤ 0.01) were considered most important. Among these, for instance homovanillic acid (HVA), 4-pyridoxate, and tyrosine were increased in abundance for donor A but found significantly lower in abundance in B and C (Figure 1.5, Appendix Table 1.5 p-values < 0.01). Metabolites from the energy metabolism (TCA cycle) were enriched in bones from individual B, however, lowered in the other two cadavers (e.g., aconitate, 2-oxoglutarate, citrate/isocitrate, succinate; all p-values < 0.01). Amino acid metabolism was affected most in bones of the shallowest body. While valine, N-acetylglutamate, and alanine/sarcosine were reduced relative to the other bodies, two amino acids, creatine and arginine, were found significantly higher in abundance in individual C (Figure 1.5, Appendix Table 1.5; all p-values < 0.01).

Previous work on animal and human bones revealed a great diversity of biomolecules present in the bone matrix ranging from proteins and lipids to amino acids[66, 68, 100-103]. An active exchange or substitution of chemical elements between the apatite structure of the bone and those present in the living body is important for the skeleton to store essential minerals[103]. After death, bones are still reactive and undergo constant change[77]. Most of the aforementioned factors that we suggested to be responsible for diverse inter-individual metabolic profiles also account for the here identified abundance variation of individual metabolites. Perimortem conditions, e.g. diet, underlying health conditions or mobility can affect the size, shape, and composition of the bioapatite crystals[76], thus could have also triggered different metabolic signals postmortem. Pathological conditions e.g., iron or vitamin C deficiency were reported to alter the amino acid composition of collagen[104]. Likewise, gender-induced differences might have occurred for the deepest body. Both B and C were males, while cadaver A (grave bottom)

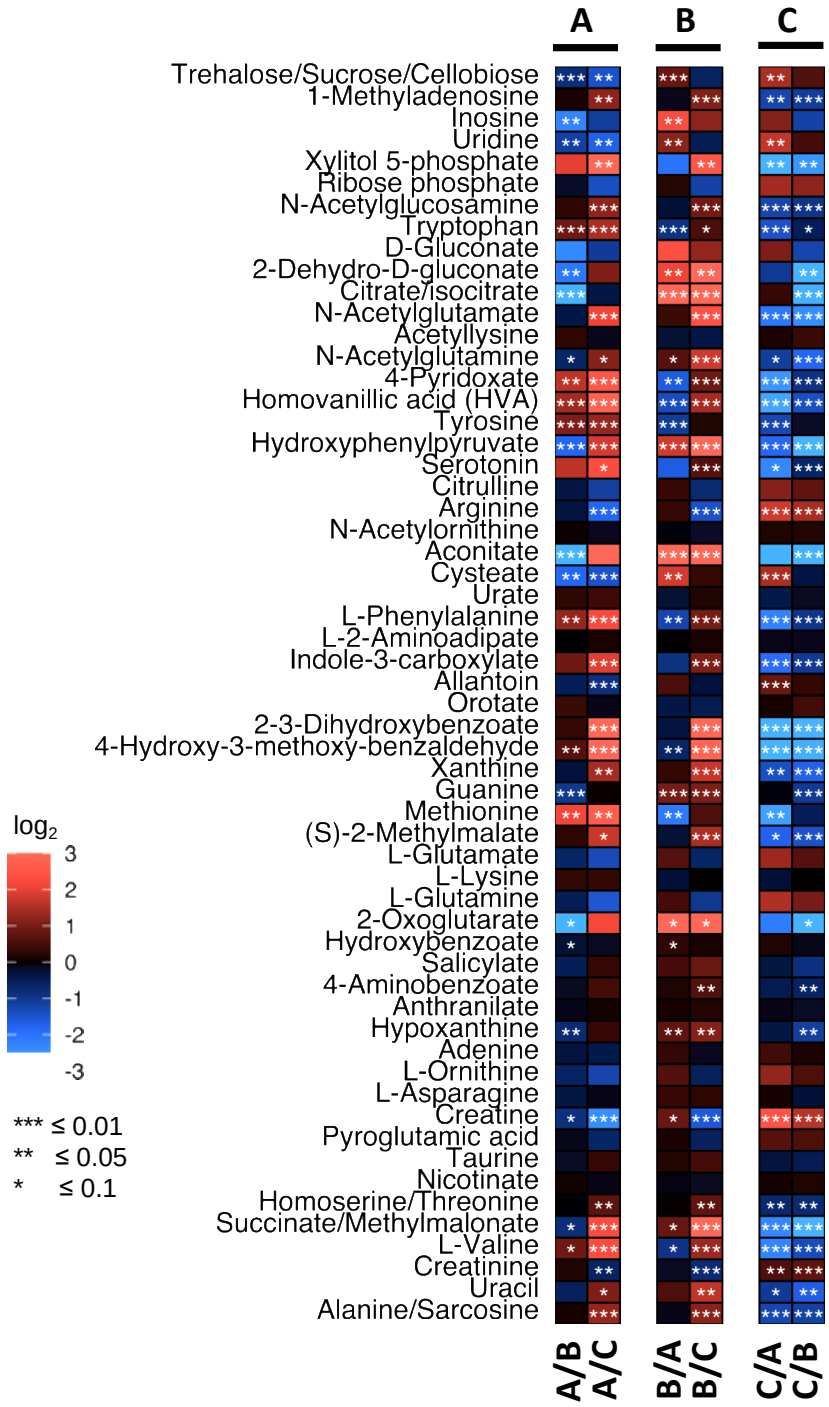

Figure 1.5 – *Heat map analysis of differential metabolites of all postmortem bone samples of individual A, B, and C. The Heat map illustrates log2 fold changes of relative metabolite abundances. Increased fold changes are indicated in red and decreases are shown in blue.*

was female. Previous studies in the living uncovered that for instance plasma HVA levels were lower in elderly men than in elderly postmenopausal women[105]. According to *Nielsen-Marsh and Hedges*, protein content in buried bone is strongly correlated with microporosity and is especially closely related to microbiological action[106]. In our study, donor C was the only fully skeletonized cadaver. Unprotected by residual soft tissue, the skeleton of C could have undergone more extensive microbial-mediated protein degradation. On the contrary, residual tissue on body B might have impacted the chemical composition of these bones to a degree where a more catabolic environment from the skeletal muscle was mirrored by bones. Catabolism of organic molecules i.e., sugars, fatty acids, and amino acids activates a metabolic main route via the TCA or citric acid cycle[107, 108], ultimately increasing the pool of TCA cycle intermediates – a hypothetical link explaining the detected compound classes of bones from individual B. Further, all decomposition processes were most likely accompanied by diverse microbial communities involved in early diagenetic processes which could become embedded within the bone matrix during cycles of demineralization and recrystallization (paper under review). During microbial catabolism, amino acids from collagen are removed for both energy and protein synthesis[56, 79].

Lastly, in a combined effort with Dr. Alexandra Emmons, a comparative analysis of metabolite-microbiome interactions modeled microbial taxa with identified metabolites using sparse canonical correlation analysis (sCCA, paper under review, data not shown). This analysis resulted in a correlation of 0.95 between the two matrices (metabolites and taxa) for individual C, with 30 features capturing most of the covariance. These features included 28 genera and 2 metabolites (acetyllysine and glutamine). For individuals A and B, which were analyzed independently from C due to significant differences in metabolite profiles, sCCA resulted in a correlation of 0.87, with 15 genera and 3 metabolites (N-acetylglutamine, N-acetylglutamate, and 2-Dehydro-D-gluconate (a.k.a., 2-ketogluconate)). These metabolites demonstrated a relationship with high human DNA degradation indices and correlated with relative abundances of *Pseudomonas* and *Lactobacillus*. An interesting result because the general mechanism through which *Pseudomonas spp*. solubilizes inorganic phosphate involves the production of gluconic acid and/or 2-ketogluconic acids via extracellular direct oxidative metabolism of

glucose[109]. The compound 2-ketogluconic acid has demonstrated efficient solubilization of inorganic phosphate from calcium phosphates including hydroxyapatite[110] (paper under review).

1.4.3.2 Intra-individual comparisons by anatomical region

To further examine the postmortem bone metabolome, an analysis focusing on six anatomical regions was conducted: skull, arm, upper torso, lower torso, leg, and foot (Appendix Table 1.6). Prior applied PLS-DA derived metabolites with VIP scores > 1 that differentiated the six body regions in each of the three donors. These metabolites (VIP > 1) were used for univariate analysis and assigned their metabolic pathways through KEGG annotation (Figure 1.6 donor A: 24 metabolites; donor B: 23 metabolites; donor C: 24 metabolites). Assessing intra-skeletal metabolic signatures, we observed that metabolite abundances differed between anatomical regions of the same body. Metabolomes from skull and foot bones of individual A were associated with a striking downregulation of metabolites from several metabolic pathways compared to other body regions. Relative increased abundances dominated for the upper and lower torso bones (Figure 1.6). Interestingly, macroscopic evaluation of the exhumed body found isolated decomposed muscle tissue covered in skin and adipocere at the upper and lower torso including the proximal one-third of the femora[82]. For the middle carcass (B) we found a less obvious overall pattern, yet the bone metabolome of the skull had decreased abundances in direct comparisons with distal bones of the body such as foot and leg bones (Figure 1.6). This trend was also consistent with results for body C. In addition, donor C showed similar to body A an altered amino acid metabolism as mostly amino acids, amino acid precursors, and derivatives revealed differential abundances. Aside from the skull and foot bones, comparisons involving arm bones yielded lowered relative metabolites abundances, as well (Figure 1.6). Compounds with higher abundances in the lower torso and leg bones belonged to the amino acid metabolism. Moreover, assessing the relationship between the in Figure 1.6 depicted relevant individual metabolites, we noticed four commonly shared compounds among all three bodies: anthranilate, creatine, N-acetylglutamine, and indole-3-carboxylate. The former three compounds are amino acids, derivatives of amino acids or are involved in the amino acid metabolism and thus

represent a source of nitrogen and carbon for microorganism and plant use[111]. The compound indole-3-carbocxylate has been detected in several microorganisms and yeasts, while in bacteria it was reported to form as degradation product of the aromatic amino acid tryptophan[112]. Likewise, anthranilic acid may also originate from the breakdown of tryptophan[112]. Differential abundances of all four metabolites between one or more body regions were also evaluated using one-way ANOVA followed by Tukey HSD post-hoc tests and results are listed in Appendix Table 1.7.

Possible explanations for the discovered intra-skeletal variation can be gathered from recent forensic literature. *Mickleburgh et al.* revealed that intra-skeletal differences in bone mineral density induced distinct differences in the variety and abundance of preserved proteins[68]. *Grupe and Turban-Just* provided an overview of amino acids extracted from matrix collagen from archaeological human bone[104]. They concluded that non-proteinogenic amino acids recovered from bones were not necessarily contaminations, but rather a marker of decomposition or microbial processes[104]. They further demonstrated a microbial invasion of bone specimens and showed that large amino acids with five or more carbon atoms were more frequently lost from collagen remnants than small amino acids to meet bioenergetic requirements of heterotrophic soil bacteria[104]. Such high carbon amino acids are more efficient in gaining energy via the citrate cycle and thus fulfill bacterial demands better[104]. Differential metabolite abundances at different anatomical regions may also be linked to the cellular skeletal composition of the analyzed regions. Different types of bone might have impacted intra-skeletal metabolic patterns. In adult mammals, cortical (compact) and cancellous (spongy) bones are the two most commonly found types of bone[76]. A higher degree of porosity is characteristic for spongy bones comprising the internal tissue of bones. Flat bones and short bones such as tarsals (foot bones), sternum, or cranial bones have typically a higher cancellous to cortical bone ratio. The external layer of bones is cortical bone, predominantly present in greater portions in the diaphysis of long bones as well as the appendicular skeleton (upper and lower extremities)[76]. A less dense bone matrix in cancellous foot bones possibly provoked leaching of soluble decomposition products into the external surrounding. Likewise, several elements from donors A and B were

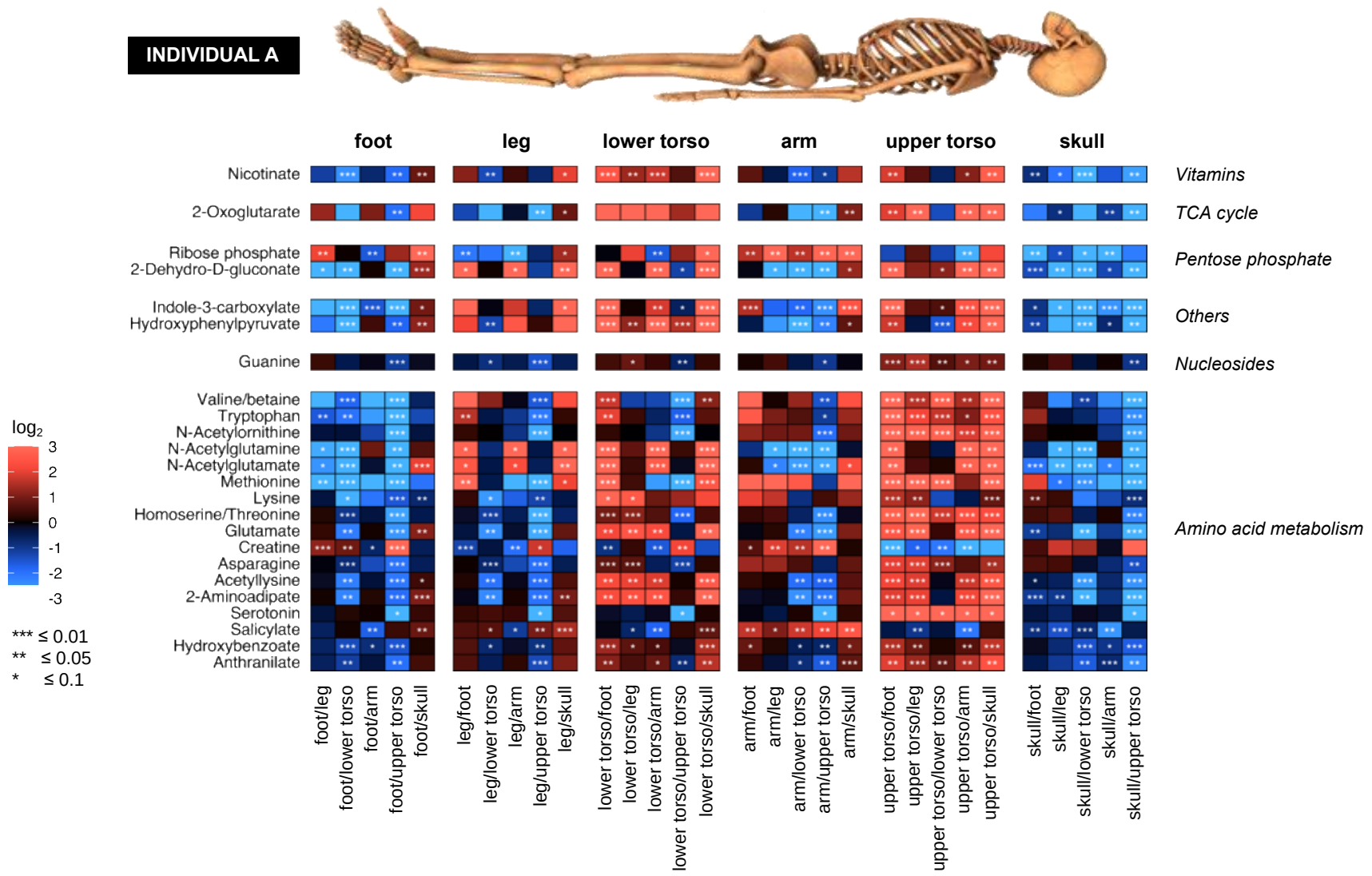

Figure 1.6 – *Intra-individual bone metabolic profiles of six anatomical regions for individuals A, B, and C. Represented metabolites were chosen based on multivariate analysis and VIP scores > 1. Metabolic pathways are listed on the right. All fold changes are log2 transformed. Increased fold changes are indicated in red and decreases are shown in blue. The skeleton on top was modified from https://www.dreamstime.com.*

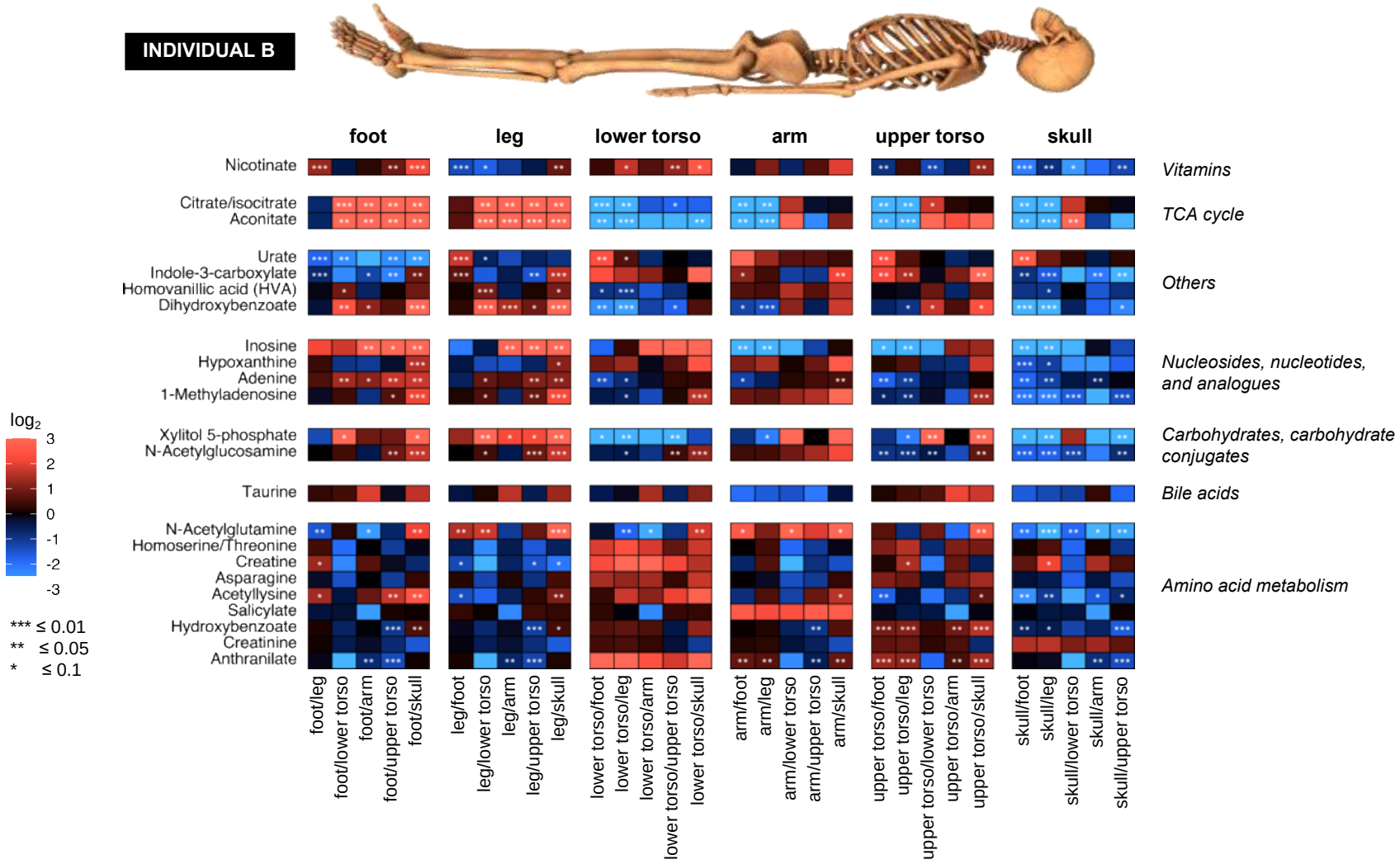

Figure 1.6 – *continued*

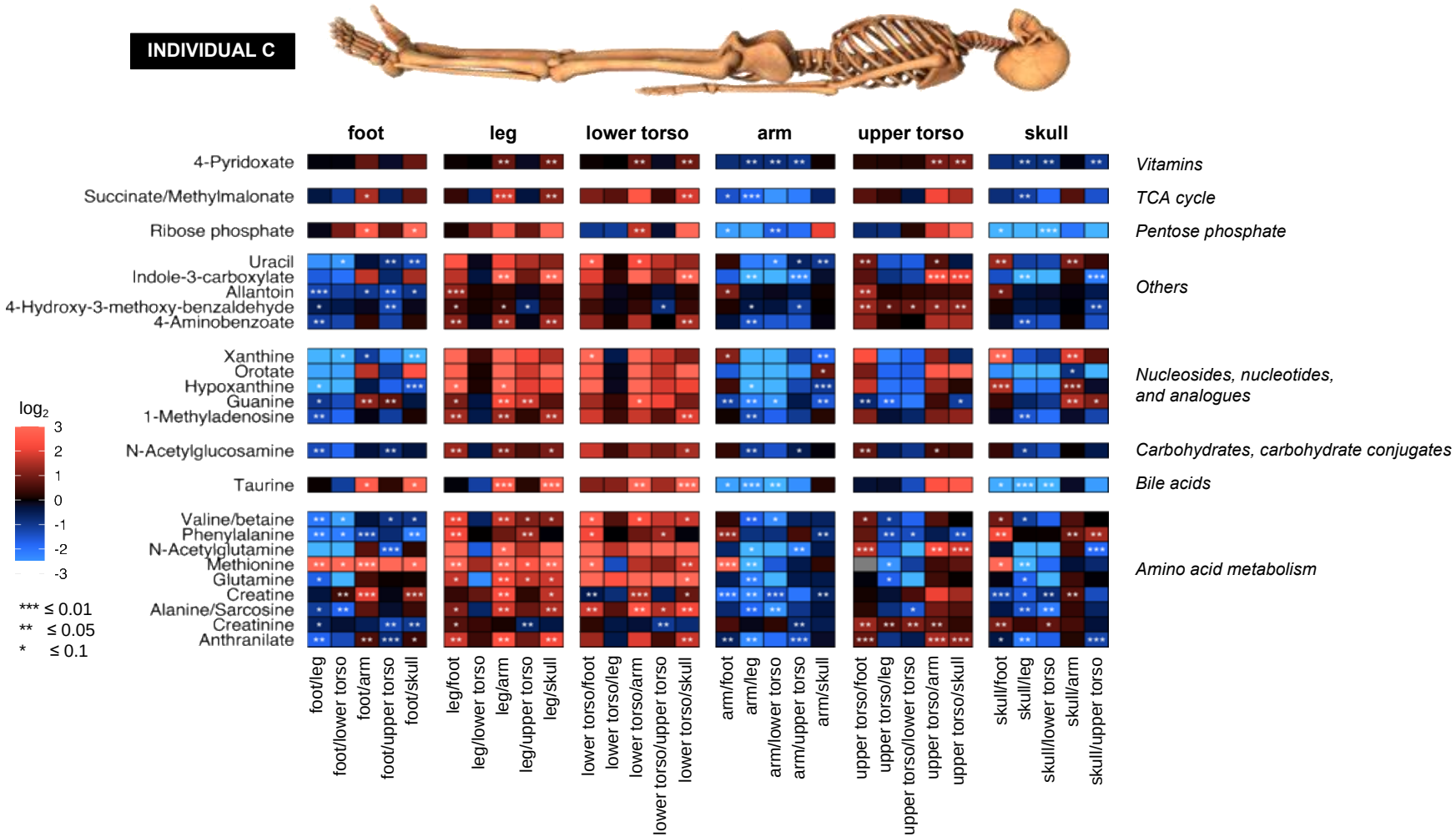

Figure 1.6 – *continued*

submerged in water at the time of disinterment due to a perched water table[82]. Such influences of site hydrology within the grave could have eased leaching of biomolecules and caused intra-skeletal variation of metabolomes[82]. Alternatively, water movement could enhance the movement of microbes and other extrinsic molecules or the intrusion of plant roots into and throughout cancellous bones[68, 79]. Hence, there could be something unique about the foot and skull microbes resulting in greater utilization of prevalent metabolites. Interestingly, according to *Child*, there is evidence for microbial inter-bone variations during decomposition[56]. During decomposition, a greater degree of putrefaction usually occurs around the intestinal region where the largest bacterial ecosystem of the human body is located. *Child* proposed that bones within the thorax and abdomen will suffer from greater effects of bacterial putrefaction and are exposed to the latter for a longer period than foot bones, long bones or the skull[56]. Potential evidence for specific microhabitats at different locations of the skeleton. Also, foot and skull bones begin the decomposition process with less soft tissue covering, and foot bones are exposed to mechanical stress during life which reduces the soft tissue mass on these bones. A reduced level of protection might have resulted in lowered metabolite abundances and/or the formation of a specific postmortem microbiome. Interestingly, complementing our results of inter-bone metabolic variety, collaborators found variable microbial diversity and richness not only among different bones but also at different sites of the same bone (e.g., midshaft vs epiphysis; paper under review).

1.4.3.3 Unidentified features of the bone metabolome

Using a high-resolution mass analyzer such as an Orbitrap enables an enormously large coverage of spectral features, containing thousands of unknown spectral *m/z* features along with known metabolites. Thus, in addition to the identified compounds that matched retention time and *m/z* of metabolites from our in-house database (knowns), 5,015 unidentified features were also detected in bone extracts. Handling the complexity of unknown spectral features is one of the current challenges in the ‘omics’ field, which is why the subsequent approach is largely exploratory. First, multivariate inter-individual analysis showed a clear separation for all performed comparisons (3D PLS-DA plots, Figure 1.7A), suggesting distinct bone metabolomes among all donors. An observation

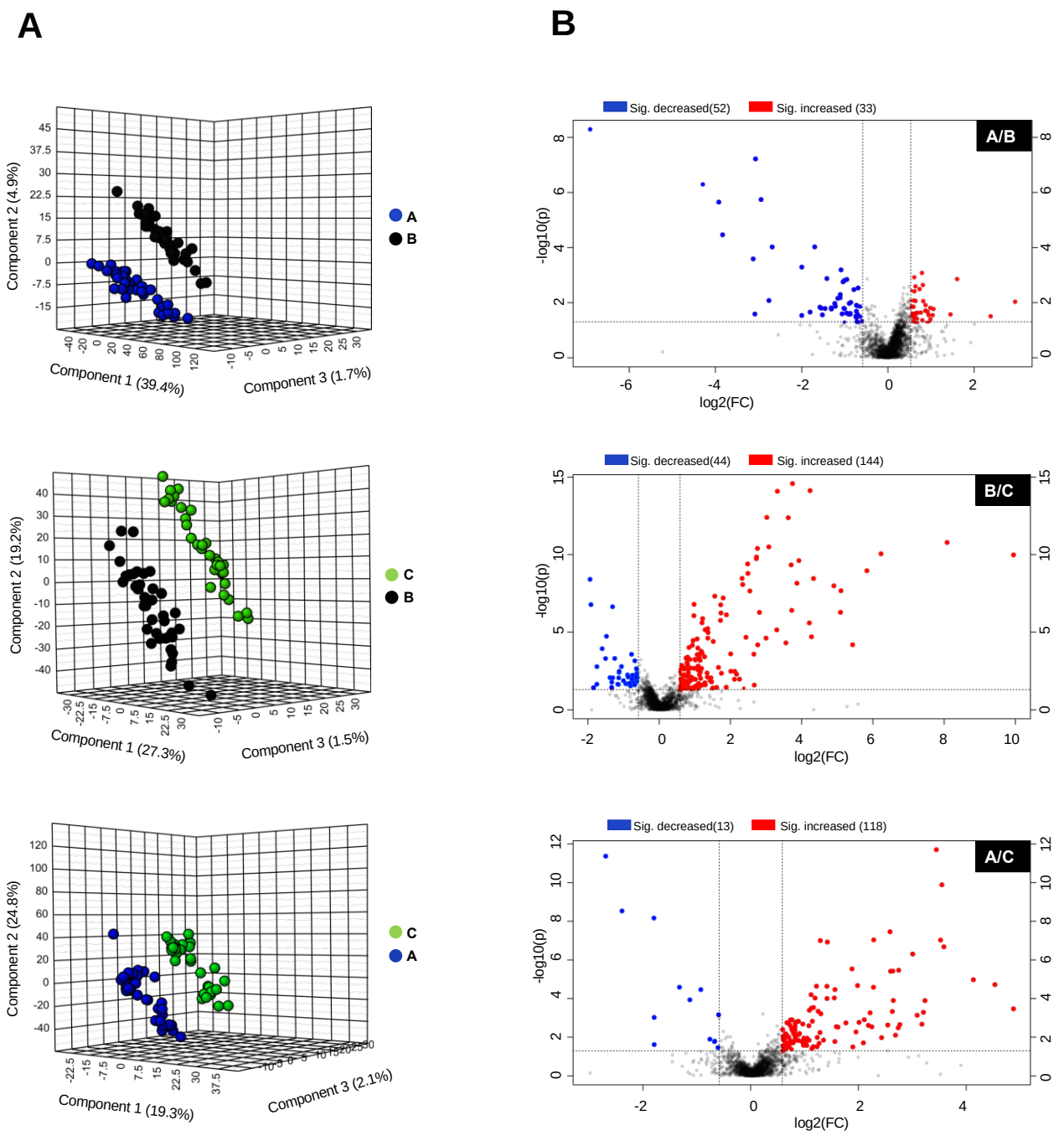

Figure 1.7 – *Unidentified features of the bone metabolome. (A) PLS-DA and (B) volcano plot analyses of bone power obtained from buried individuals (inter-individual comparisons). Volcano plots in (B) indicate the total number of unknowns significantly (= sig.) increased or decreased in abundances in a respective donor.*

already seen in Figure 1.4; however, it is noteworthy that the unknown bone metabolites revealed an even more drastic inter-individual separation in each of the PLS-DAs. A volcano plot analysis identified significantly increased or decreased unknowns based on fold change and p-value thresholds (Figure 1.7B and Appendix Table 1.8). These results also confirm previously described trends from our heat map analysis (Figure 1.5). A large number of significantly increased unknown metabolite abundances was found in bone extracts from body B (144 features) and likewise from A (118 features). Consequently, this implied drastically lowered metabolite abundances in the shallowest body C (Figure 1.7B). Similar to Figure 1.5, unknown bone metabolic profiles seemed to be relatively comparable among the deepest (A) and middle body (B) with 33 unknowns 'enriched' in A and 52 in individual B (Figure 1.7B, A vs B comparison; and Appendix Table 1.8).

Lastly, unknown features from bone extracts were assessed by anatomical region using the same approach from above. The complexity of information in the data sets was reduced by focusing on the top 25 differential unknowns with VIP values > 1 resulting from multivariate analysis (PLS-DA). These unknowns significantly discriminated the six anatomical regions in each individual. The most distal elements of the skeleton, the skull and feet, had for donor A reduced abundances as opposed to the center of the skeleton (Figure 1.8). Compounds higher in abundance were most likely available as nutrients in the grave, supporting the formation of a specific microhabitat at different locations of the body. The pattern observed for body A shifted for the middle and shallowest cadaver, as abundance profiles appeared to be less distinct. Slightly reduced abundances were still detected for the skull of individual B, yet foot and leg bones had clusters of unknowns with elevated abundances. The shallowest individual (C) had the least uniform signature. Abundance changes of unknown features were largely significant for comparisons among anatomical regions of donor A, while C had overall less significant changes (Figure 1.8). Taken together, the unknown analysis confirmed the presence of differential metabolic processes among buried individuals and at different skeletal regions postmortem – results affected by either decomposition itself or the depositional ecology. Along with Figure 1.7, diverse and variable metabolite abundances of the unknowns also reinforced our hypothesis that decomposition processes were still ongoing four years after burial.

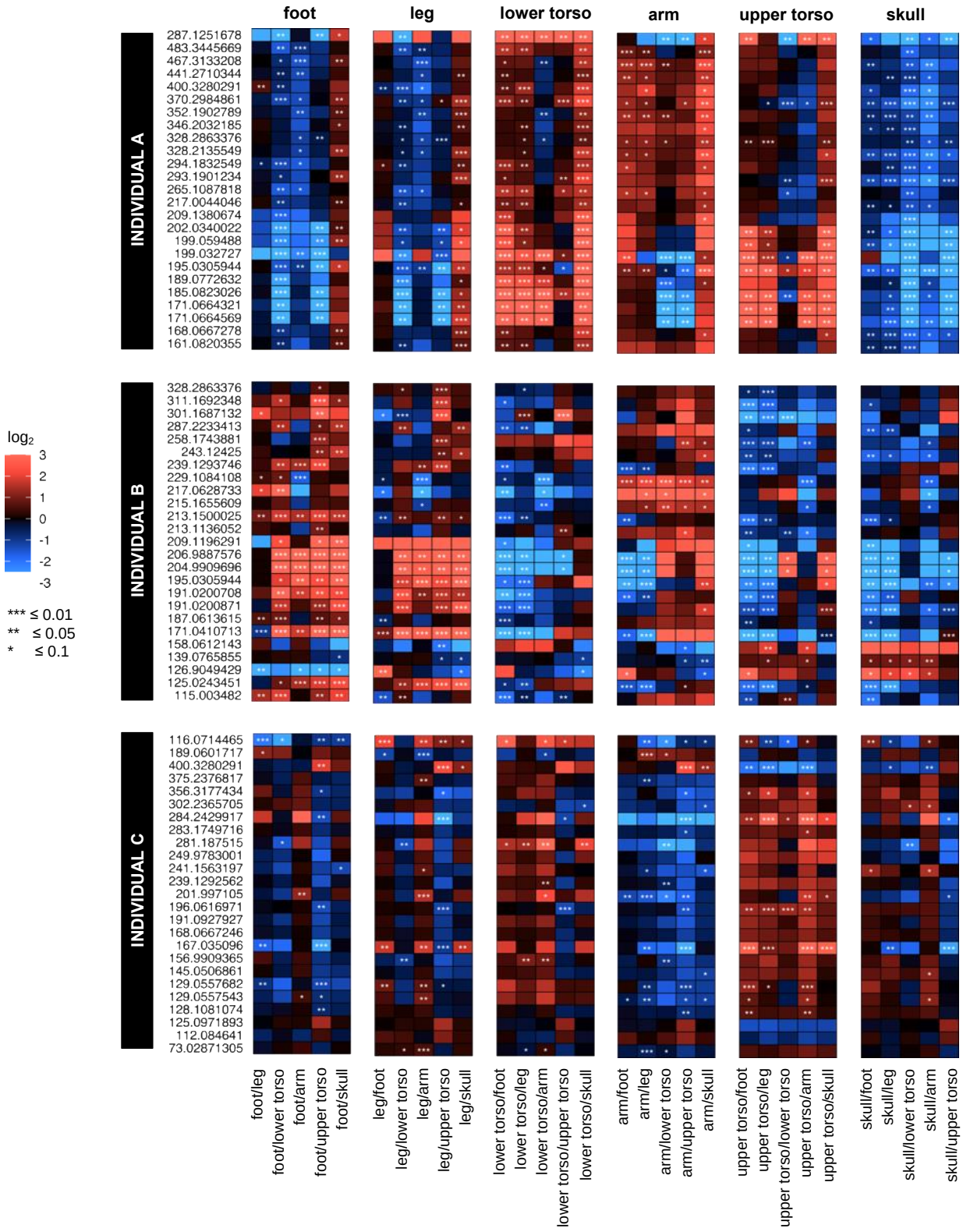

Figure 1.8 – *Masses of unidentified spectral features of the bone metabolome for each of the six anatomical regions for bodies A, B, and C. For each donor, the top 25 unknowns with VIP scores > 1 extracted from PLS-DAs are listed (intra-individual comparisons).*

Additional computational efforts were made to assign unknown compounds hypothetical chemical formulas (data not shown). In total, 11,481 empirical formulas arising from unknown *m/z* features were found. These were sorted into generalized compound classes based upon their hypothesized atomic H/C and O/C ratios in a so-called van Krevelen diagram. In such a diagram, every calculated chemical formula is given a 'ratio-value' which ultimately determines the (generalized) compound class e.g., lipids, proteins, carbohydrates, amino-sugars, condensed hydrocarbons, lignins or tannins[113]. Our clustering results suggested most of the unknown metabolites had characteristics most similar to those of lipids and condensed hydrocarbons (ratios of O/C < 0.25 and H/C 0.5-2.25). Altogether, among others, we found 1,881 unknowns similar to lipids, 1,475 seemed to fit the category of proteins, 129 amino-sugars, 135 carbohydrates, and 2,317 similar to condensed hydrocarbons, while 4,279 formulas remained with unknown designations (data not shown).

Overall, despite limitations in identifying compound classes from unidentified spectral features, the scope of our preliminary analyses showed that most of the trends observed from known biomolecules were reinforced by the unknowns. An outcome that points toward the necessity to refine and expand existing compound libraries. More comprehensive libraries could ultimately also help to solve questions of whether compounds solely arose as a result of decomposition or if they were potentially linked to plant/microbial pathways.

1.5 CONCLUSION

Subsurface decomposition is impacted by several abiotic and biotic factors differentiating decomposition trajectories from surface decay[28]. In this chapter, untargeted metabolomics was used to investigate soil and bone metabolomes present at the time of sampling in a multi-individual grave and on skeletal remains, respectively. Dissolved organic matter (DOM) in soil is a cocktail of carbohydrates, aromatic compounds, amino acids, organic acids, and fatty acids[114]. We demonstrated a diverse soil metabolic biochemistry coincided with strong spatial dynamics within the mass grave, as illustrated on shifts in metabolite abundances at different depths of the burial. Because of diverse

metabolomes *in-vivo*, we expected a considerable portion of metabolites to be likewise influenced postmortem. This was not only true for comparisons among donors but also among anatomical regions of the same skeleton. Not surprisingly, as a decomposing cadaver is a nourishing source of nitrogen and carbon, our inter- and intra-individual analyses showed amino acid profiles to be most variable. Furthermore, we displayed a trend of reoccurring lowered compound abundances dominating foot and skull bones of buried remains. An outcome suggesting specific (micro)habitats may prevailed at different locations in the grave. The unidentified spectral features of the bone metabolomes revealed similar inter- and intraindividual trends as observed for the known metabolites. Although annotation of these features is one of the bottlenecks of untargeted metabolomics, the information gained from these early untargeted studies helps to elucidate broad trends of decomposition trajectories of skeletal remains.

The interpretation of our results also demands an understanding of the limitations of this study provoked primarily by the environmental heterogeneity of the burial (biotic and abiotic). Some of the here detected metabolites sourced most likely from plant root exudates, originated from microorganisms, and/or the decay of plants and microbes. Possible artifacts in differential metabolite abundances could have further been caused due to post-excavation contamination by the application of heat during bone sampling (drilling) or storage/handling of skeletal remains at room temperature – all factors that negatively affect the stability of biomolecules. Variables related to the physical state of the bones along with individual intrinsic parameters like health conditions may have caused additional bias extremely hard to deconvolute. Yet, our work did not seek to validate any of these influences as a rather exploratory study was anticipated focused on obtaining a metabolic snapshot of soils and bones in a burial at the time of sampling. With only three individuals analyzed, a comparatively small donor size strongly motivates for more comprehensive future studies potentially considering various environmental and burial conditions, as well. This will ultimately help to complete the presented metabolic picture of subsurface decomposition trajectories.

Taken together, soils and bones retained even four years after burial diverse metabolomes formed by heterogenous influxes from human decomposition and grave ecology. Assuming decomposition was still active in the grave, we showed that grave

depth and anatomical region of skeletons revealed differential metabolic signatures postmortem. Given that buried corpses are common scenarios in forensic invetigations[47], we provided findings to contribute to the groundwork studies that might open new avenues of investigative approaches for such forensic cases.

APPENDIX

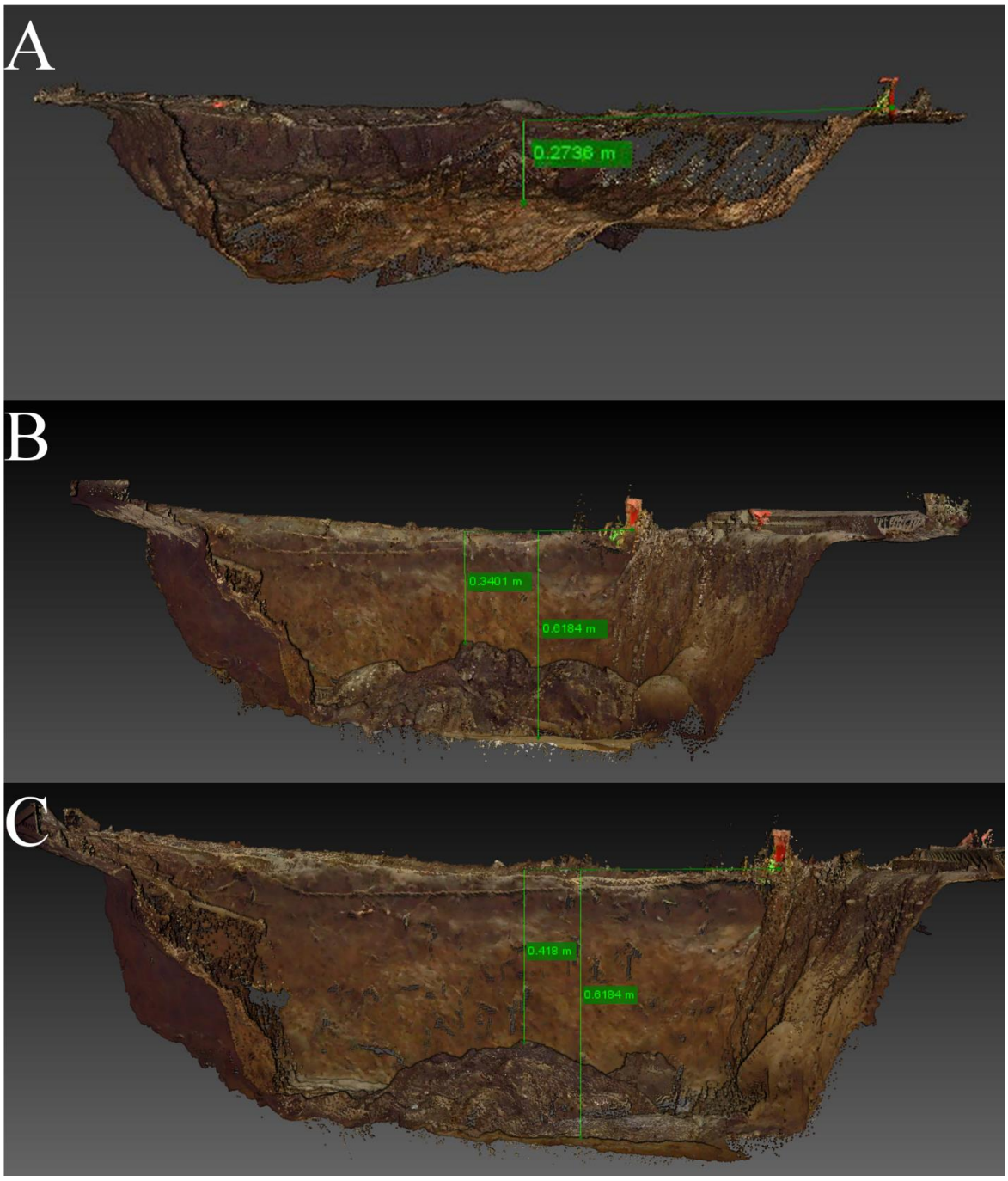

Figure 1.9 – *Depth profile of the multi-individual grave (picture permission Dr. Alexandra Emmons). (A) Top individual (donor C), (B) middle individual (donor B), and (C) bottom individual (donor A). Measurements in green indicate the span of depths in meters. Photo credit: Christina Malone.*

Table 1.1 – *Demographics of skeletonized individuals used in this study.*

Donor ID	Sample Type*	Weight (kg)	Age (yrs)	Medical History	Sex	Position in Grave	Duration of Burial
A	Soil/bone	60.3	68	Cancer	Female	Bottom	4 years
B	Soil/bone	70.8	63	COPD	Male	Middle	4 years
C	Soil/bone	51.7	63	Cancer, Coronary Artery Dx	Male	Top	4 years

* Soil obtained from a control grave served as a negative control

Table 1.2 – *Soil and skeletal samples utilized for untargeted metabolomics.*

BONE SAMPLES (n = 41)			SOIL SAMPLES (n = 20)		
Sample Code	**Individual**	**Bone**	**Sample Code**	**Sampling Location**	**Depth (cm)**
10001	A	Fibula	MGR02170001BN	Control, off-grave	0
10002	A	Sacrum	MGR02170003BN	Control, off-grave	30
10003	A	Sternum	MGR02170005BN	Control grave	0
10007	A	Femur	MGR02170007BN	Control grave	30
10009	A	Humerus	MGR02170057BN	on grave	0
10011	A	Ischium	MGR02170059BN	on grave	0
10013	A	L4	MGR03170002BN	on grave	0
10018	A	Radius	MGR03170003BN	on grave	0
10026	A	Talus	MGR03170004BN	on grave	0
10035	A	Tibia	MGR03170005BN	on grave	0
10050	A	Navicular	MGR03170006BN	on grave	30
10067	A	Temporal	MGR03170007BN	on grave	40
10031D	A	Femur	MGR03170008BN	on grave	30
10058R	A	1st Cuneiform	MGR03170009BN	on grave	30
20004	B	Sternum	MGR03170026BN	on grave	70
20008	B	L4	MGR03170027BN	on grave	85
20020	B	Talus	MGR03170028BN	on grave	70
20027	B	Navicular	MGR03170029BN	on grave	85
20048	B	Tibia	MGR03170030BN	on grave	70
20049	B	Fibula	MGR03170031BN	on grave	70
20053	B	Femur			
20066	B	Radius			
20072	B	Temporal			
20002R	B	Clavicle			
20018R	B	Calcaneus			
20022R	B	patella			
20055D	B	Femur			
20065R	B	Ulna			
30011	C	Navicular			
30036	C	Humerus			
30041	C	Radius			
30055	C	Sacrum			

Table 1.2 – *continued*

BONE SAMPLES (n = 41)			SOIL SAMPLES (n = 20)		
Sample Code	**Individual**	**Bone**	**Sample Code**	**Sampling Location**	**Depth (cm)**
30057	C	Ischium			
30061	C	Fibula			
30065	C	Femur			
30073	C	Tibia			
30079	C	Temporal			
30015D	C	1st Cuneiform			
30044R	C	ulna			
30045R	C	clavicle			
30063R	C	patella			
30063R	C	patella			

Table 1.3 – *Result of volcano plot analyses comparing relative metabolite abundances among different grave soil depths with those detected in soils in the control grave. Shown are significantly increased and decreased metabolites abundances compared to controls based on a fold change threshold of 1.5 and p-adj. threshold ≤ 0.05.*

Metabolite name	Fold change (FC)	log2(FC)	p-adjusted	-log10(p)
0-5 cm mass grave soil vs 0-5 cm control grave soil				
Inosine	0.15347	-2.7039	0.0019871	2.7018
Cytidine	0.15471	-2.6924	0.0073517	2.1336
Deoxycytidine	0.30832	-1.6975	0.010673	1.9717
Nicotinate	0.34848	-1.5209	0.010673	1.9717
Thymidine	0.38641	-1.3718	0.010673	1.9717
Glutamate	0.3198	-1.6448	0.018808	1.7256
Adenosine	0.38815	-1.3653	0.018808	1.7256
Uracil	0.29414	-1.7654	0.02282	1.6417
Leucine/Isoleucine	0.38838	-1.3645	0.029054	1.5368
Phenylalanine	0.43736	-1.1931	0.029054	1.5368
Guanosine	0.39487	-1.3405	0.031937	1.4957
Pantothenate	0.44825	-1.1576	0.041964	1.3771
Methionine	0.33675	-1.5703	0.047542	1.3229
Hypoxanthine	0.39639	-1.335	0.047542	1.3229
30-35 cm mass grave soil vs 30-35 cm control grave soil				
Hydroxybenzoate	4.8397	2.2749	0.029574	1.5291
Homocysteine	483.34	8.9169	0.045617	1.3409
40 cm mass grave soil vs 30-35 cm control grave soil				
2-Oxo-4-methylthiobutanoate	1191.7	10.219	0.00071685	3.1446
3-Methylthiopropionate	727.63	9.5071	0.00060917	3.2153
Methionine	70.948	6.1487	0.0012208	2.9134
Tryptophan	56.495	5.8201	0.0020205	2.6945
Tyrosine	37.011	5.2099	0.00048769	3.3119
Glutamate	29.442	4.8798	0.00048769	3.3119
Nicotinate	27.128	4.7617	0.00076347	3.1172
Valine/betaine	26.875	4.7482	0.00048769	3.3119
Homoserine/Threonine	26.422	4.7237	0.00048769	3.3119
Alanine/Sarcosine	23.553	4.5579	0.00048769	3.3119
Deoxyuridine	23.343	4.5449	0.00060917	3.2153
Citrulline	21.774	4.4446	0.00050679	3.2952
Leucine/Isoleucine	19.618	4.2941	0.00076347	3.1172
Glutamine	18.297	4.1936	0.00048769	3.3119
Taurine	17.125	4.098	0.0032166	2.4926
Pantothenate	16.353	4.0315	0.00060917	3.2153
Serine	15.855	3.9868	0.00071685	3.1446
hydroxybutyrate	13.745	3.7808	0.00048769	3.3119
Xylitol	9.9522	3.315	0.001597	2.7967

Table 1.3 – *continued*

Metabolite name	Fold change (FC)	log2(FC)	p-adjusted	-log10(p)
Phenylalanine	9.8269	3.2967	0.00096725	3.0145
Lysine	9.5287	3.2523	0.0033853	2.4704
Uracil	9.1846	3.1992	0.024955	1.6028
Homocysteine	7.3116	2.8702	0.00096725	3.0145
Hydroxybenzoate	6.4489	2.689	0.0015971	2.7967
Kynurenic acid	6.096	2.6079	0.00048769	3.3119
Inosine	6.0947	2.6075	0.003416	2.4665
Deoxyinosine	4.8809	2.2871	0.0027146	2.5663
Thymine	4.4736	2.1614	0.006432	2.1917
1-Methyladenosine	4.1223	2.0435	0.015258	1.8165
Guanosine	3.8163	1.9322	0.0027146	2.5663
Hypoxanthine	3.5655	1.8341	0.0021449	2.6686
Cytidine	3.0831	1.6244	0.045832	1.3388
Adenosine	2.8285	1.5	0.011098	1.9548
Thymidine	2.4776	1.3089	0.027117	1.5668
Trehalose/Sucrose	2.4675	1.303	0.011259	1.9485
N-Acetylglucosamine	2.0961	1.0677	0.033498	1.475
70-75 cm mass grave soil vs 30-35 cm control grave soil				
Hydroxybenzoate	13.103	3.7118	7.16E-06	5.145
3-Methylthiopropionate	28.118	4.8134	6.32E-05	4.1995
Homocysteine	24.224	4.5984	6.32E-05	4.1995
2-Oxo-4-methylthiobutanoate	33.786	5.0784	0.00055307	3.2572
Histidinol	33.149	5.0509	0.00055307	3.2572
Kynurenic acid	12.083	3.595	0.0013467	2.8707
Tyrosine	6.5536	2.7123	0.0071571	2.1453
Methionine	5.1955	2.3773	0.0071571	2.1453
Xylitol	4.8857	2.2886	0.0074678	2.1268
Creatine	3316.9	11.696	0.0099793	2.0009
Hydroxybutyrate	3.4864	1.8017	0.0099793	2.0009
Adenosine	0.19349	-2.3696	0.022572	1.6464
Deoxycytidine	0.13353	-2.9048	0.032913	1.4826
Thymidine	0.24504	-2.0289	0.049645	1.3041
80-85 cm mass grave soil vs 30-35 cm control grave soil				
Adenosine	0.026461	-5.24	0.0061185	2.2134
Thymidine	0.043562	-4.5208	0.0062361	2.2051
Deoxycytidine	0.03101	-5.0111	0.014847	1.8284
Deoxyinosine	0.024224	-5.3674	0.025495	1.5935

Table 1.4 – *Variable importance in projections (VIP) scores for the three inter-individual comparisons shown in Figure 1.4. Metabolites with VIP scores greater than 1 are listed. Metabolites with VIPs > 1 in 2 comparisons are bolded; those with VIPs > 1 in 3 individuals are red.*

Individuals A vs. B		Individuals A vs. C		Individuals B vs. C	
Metabolite	**VIP values**	**Metabolite**	**VIP values**	**Metabolite**	**VIP values**
Aconitate	2.1625	**4-Hydroxy-3-methoxy-benzaldehyde**	2.0745	**2-3-Dihydroxybenzoate**	1.9332
Homovanillic acid (HVA)	1.8132	**Succinate/Methylmalonate**	1.9701	**4-Hydroxy-3-methoxy-benzaldehyde**	1.7601
Citrate/isocitrate	1.7967	Homovanillic acid (HVA)	1.9638	N-Acetylglutamate	1.7483
Hydroxyphenylpyruvate	1.7084	**Creatine**	1.9565	Hydroxyphenylpyruvate	1.7252
4-Pyridoxate	1.6824	**Xanthine**	1.7634	**Succinate/Methylmalonate**	1.652
2-Dehydro-D-gluconate	1.4837	**2-3-Dihydroxybenzoate**	1.7317	Homovanillic acid (HVA)	1.6031
Guanine	1.4645	4-Pyridoxate	1.5136	**Aconitate**	1.5762
2-Oxoglutarate	1.3829	**L-Valine**	1.4796	**N-Acetylglutamine**	1.5643
D-Gluconate	1.3275	Allantoin	1.4305	**2-Dehydro-D-gluconate**	1.5133
N-Acetylglutamine	1.2898	N-Acetylglutamate	1.4053	**Xanthine**	1.4919
N-Acetylglutamate	1.282	**Indole-3-carboxylate**	1.3025	**Indole-3-carboxylate**	1.3365
Inosine	1.2541	**Arginine**	1.2517	**(S)-2-Methylmalate**	1.2981
L-Glutamate	1.227	L-Phenylalanine	1.2155	**Creatine**	1.2952
L-2-Aminoadipate	1.1995	Hydroxyphenylpyruvate	1.151	**Alanine/Sarcosine**	1.2742
Acetyllysine	1.147	**Alanine/Sarcosine**	1.1171	Hypoxanthine	1.226
(S)-2-Methylmalate	1.1467	Uracil	1.091	**L-Valine**	1.2256
Adenine	1.1454	**Trehalose/Sucrose/Cellobiose**	1.0876	1-Methyladenosine	1.1962
Cysteate	1.1401	**Xylitol 5-phosphate**	1.0532	N-Acetylglucosamine	1.1903
Tyrosine	1.1129	Tryptophan	1.0373	**2-Oxoglutarate**	1.181
Trehalose/Sucrose/Cellobiose	1.0348	Creatinine	1.0315	**Arginine**	1.1447
Uridine	1.0182	**Tyrosine**	1.0041	**Guanine**	1.1143
Serotonin	1.0141			**Citrate/isocitrate**	1.0744
				Xylitol 5-phosphate	1.0536
				4-Pyridoxate	1.0237

Table 1.5 – *VIP metabolites, fold changes, and p-values for inter-individual bone metabolomics. PLS-DA plots from Figure 1.4 were analyzed by extrapolating metabolites with VIP > 1 from all comparisons (e.g., A vs. B). Fold changes and p-values (student's t-test) resulted from pairwise univariate comparisons.*

Individual A (PLS-DAs A vs. B and A vs. C)							
	Trend of abundance change			**Fold change**		***P***	
Duplicate metabolites with VIP > 1	Individual A	Individual B	Individual C	**A/B**	**A/C**	**A/B**	**A/C**
Homovanillic acid (HVA)	increased	decreased	decreased	2.61	7.02	< 0.01	< 0.01
4-Pyridoxate	increased	decreased	decreased	3.12	5.84	< 0.01	< 0.01
Tyrosine	increased	decreased	decreased	2.13	2.45	< 0.01	< 0.01
Trehalose/Sucrose/Cellobiose	decreased	increased	increased	0.55	0.36	< 0.01	0.02

Individual B (PLS-DAs B vs. A and B vs. C)							
	Trend of abundance change			**Fold change**		***P***	
Duplicate metabolites with VIP > 1	Individual A	Individual B	Individual C	**B/A**	**B/C**	**B/A**	**B/C**
N-Acetylglutamate	decreased	increased	decreased	1.31	5.48	0.12	< 0.01
Hydroxyphenylpyruvate	decreased	increased	decreased	3.54	12.72	< 0.01	< 0.01
Aconitate	decreased	increased	decreased	33.64	277.87	< 0.01	< 0.01
N-Acetylglutamine	decreased	increased	decreased	1.60	3.48	0.09	< 0.01
2-Dehydro-D-gluconate	decreased	increased	decreased	4.23	8.90	0.04	0.02
(S)-2-Methylmalate	decreased	increased	decreased	0.83	2.78	0.99	< 0.01
2-Oxoglutarate	decreased	increased	decreased	16.23	73.10	0.09	0.09
Guanine	decreased	increased	decreased	2.01	2.06	< 0.01	< 0.01
Citrate/isocitrate	decreased	increased	decreased	9.89	7.69	< 0.01	< 0.01

Individual C (PLS-DAs C vs. A and C vs. B)							
	Trend of abundance change			**Fold change**		***P***	
Duplicate metabolites with VIP > 1	Individual A	Individual B	Individual C	**C/A**	**C/B**	**C/A**	**C/B**
4-Hydroxy-3-methoxy-benzaldehyde	increased	increased	decreased	0.08	0.13	< 0.01	< 0.01
Succinate/Methylmalonate	increased	increased	decreased	0.20	0.11	< 0.01	< 0.01
Homovanillic acid (HVA)	increased	increased	decreased	0.14	0.37	< 0.01	< 0.01
Xanthine	increased	increased	decreased	0.37	0.30	0.02	< 0.01
2-3-Dihydroxybenzoate	increased	increased	decreased	0.09	0.11	< 0.01	< 0.01
4-Pyridoxate	increased	increased	decreased	0.17	0.53	< 0.01	< 0.01
L-Valine	increased	increased	decreased	0.20	0.39	< 0.01	< 0.01
N-Acetylglutamate	increased	increased	decreased	0.24	0.18	< 0.01	< 0.01
Indole-3-carboxylate	increased	increased	decreased	0.27	0.48	< 0.01	< 0.01
Hydroxyphenylpyruvate	increased	increased	decreased	0.28	0.08	< 0.01	< 0.01
Alanine/Sarcosine	increased	increased	decreased	0.42	0.44	< 0.01	< 0.01
Xylitol 5-phosphate	increased	increased	decreased	0.04	0.17	0.05	0.01
Creatine	decreased	decreased	increased	5.50	3.02	< 0.01	< 0.01
Arginine	decreased	decreased	increased	3.49	2.75	< 0.01	< 0.01

Table 1.6 – *Overview of bone samples categorized by body regions.*

Body Region	Skeletal Element	Sample Number	Individuals
Skull	Temporal	3	A, B, C
Upper Torso	Sternum	2	A, B
	Clavicle	2	B, C
Lower Torso	Lumbar Vertebrae (L4)	2	A, B
	Sacrum	2	A, C
	Ischium	2	A, C
Leg	Femur	5	A, B, C
	Tibia	3	A, B, C
	Fibula	3	A, B, C
	Patella	2	B,C
Arm	Humerus	2	A, C
	Radius	3	A, B, C
	Ulna	2	B, C
Foot	Calcaneus	1	B
	1st Cuneiform	2	A, C
	Talus	2	A, B
	Navicular	3	A, B, C

Table 1.7 – *One-way ANOVA and Tukey post-hoc tests for creatine, anthranilate, indole-3-carboxylate, and N-acetylglutamine. Representative metabolites were selected based on previously performed PLS-DA analysis and VIP scores > 1.*

	Metabolites	ANOVA		Tukey post-hoc tests	
		F	***p***	comparisons	significance
Individual A	*creatine*	6.59	0.0003	leg/arm	p < 0.01
				leg/skull	p < 0.05
				lower torso/arm	p < 0.05
				arm/upper torso	p < 0.01
				upper torso/skull	p < 0.05
	anthranilate	3.53	0.012	foot/upper torso	p < 0.05
				upper torso/skull	p < 0.05
	N-acetylglutamine	3.68	0.0099	foot/lower torso	p < 0.05
Individual B	*creatine*	21.70	7.78e-10	foot/lower torso	p < 0.01
				leg/lower torso	p < 0.01
				lower torso/arm	p < 0.01
				lower torso/upper torso	p < 0.01
				lower torso/skull	p < 0.01
	anthranilate	43.14	5.37e-14	foot/lower torso	p < 0.01
				leg/lower torso	p < 0.01
				lower torso/arm	p < 0.01
				lower torso/upper torso	p < 0.01
				lower torso/skull	p < 0.01
	indole-3-carboxylate	11.63	1.15e-06	foot/lower torso	p < 0.01
				foot/upper torso	p < 0.01
				leg/lower torso	p < 0.01
				leg/upper torso	p < 0.01
				lower torso/arm	p < 0.05
				lower torso/skull	p < 0.01
				upper torso/skull	p < 0.01
	N-acetylglutamine	3.78	0.0079	foot/arm	p < 0.05
				lower torso/arm	p < 0.05
				arm/skull	p < 0.05
Individual C	*N-acetylglutamine*	2.80	0.0365	foot/lower torso	p < 0.05
				lower torso/arm	p < 0.05

Table 1.8 – *Summary of PLS-DA and volcano plot analysis of unknown features from human skeletal remains (inter-individual analysis). Shown is the number of differential metabolites based on VIP scores > 1 and volcano plot thresholds of fold change (FC) 1.5 as well as p-value 0.05. A total of 5,015 unknown spectral features were identified via UHPLC-HRMS analysis.*

Unidentified features of the bone metabolome (total unknowns 5,015)							
	Cutoff values	**Individual A (A/B)**		**Individual B (B/C)**		**Individual C (A/C)**	
PLS -DA	VIP > 1	849		644		596	
Volcano plot analysis	FC 1.5; p-value 0.05	85		188		131	
		Increased in A	Decreased in A	Increased in B	Decreased in B	Increased in C	Decreased in C
		33	52	144	44	13	118

CHAPTER II: SPECIES-SPECIFIC DECOMPOSITION PATTERNS – CONTRASTING HUMAN AND PIG DECOMPOSITION USING A COMPREHENSIVE 'OMICS' APPROACH

PREFACE

As opposed to the first chapter, this second chapter examines an environmental change for our postmortem metabolomics studies by contrasting species-specific surface decomposition patterns. Given that rates and patterns of decay seem to vary among species[115, 116], a comprehensive 'omics' approach was utilized to investigate the effects of human and pig decomposition on the cadaveric soil environment. This project was conducted in collaboration with Dr. Jennifer DeBruyn from the department of Biosystems Engineering and Soil Science, UTK, TN. As a microbial ecologist, Dr. DeBruyn's main research interests include decomposition and biodegradation in both agricultural and natural ecosystems. To assess species-specific decomposition profiles on a biochemical scale, human and porcine carcasses were placed simultaneously on soil surface under identical environmental conditions at an outdoor research facility and allowed to decompose naturally. Collected cadaveric soils from cadaver decomposition islands (CDI) were then evaluated for their metabolic composition. The primary conclusion resulting from this research was that human and pig decomposition differed in terms of their impacts on CDI soil biochemistry.

A version of this chapter was originally published by DeBruyn, J. M., *et al*.:

DeBruyn, J. M., Hoeland, K. M., Taylor, L. S., Stevens, J. D., Moats, M. A., Bandopadhyay, S., ... & Steadman, D. W. (2021). Comparative Decomposition of Humans and Pigs: Soil Biogeochemistry, Microbial Activity and Metabolomic Profiles. Frontiers in microbiology, 11, 3521.

Contributions: The study was conceived by JD, DS, AM, and GV. Resources were provided by JD, DS, AM, and SC. Field experiments, sampling, and laboratory analyses were conducted by JD, AD, JS, KH, MM, and SB. Metabolomics and lipidomics laboratory and data analyses were conducted by KH, MM, SD, HC, and KH. Data analysis was conducted by JD, KH, LT, JS, and AD. Manuscript writing was led by JD, KH, and LT with input from all authors.

2.1 ABSTRACT

Using pig carcasses in forensic taphonomy as human proxies is widely accepted in forensic science. Their use has been based on shared similarity with humans in parameters like skin thickness, hairiness, and patterns of insect succession. However, some field studies have demonstrated differential decomposition dynamics for non-human carcasses compared to their human analogs[24, 116-119]. After the onset of soil surface decomposition, when the active decay stage is reached, cadaveric fluids leak into the surrounding matrix and alter the soil profile around a cadaver. So far, comparative studies of soil changes among human donors and animal models have primarily been focused on assessing soil physiochemical parameters and are still fairly limited[31, 33]. Our study aimed to investigate the impact of human and pig decomposition products on the terrestrial environment beyond this point using state-of-the-art analytical 'omics' platforms. Cadaver-associated soil samples, collected from soils surrounding decomposing human and non-human (pig) carcasses placed at the Anthropology Research Facility (ARF) in Knoxville, TN, were subjected to soil physicochemical measurements performed by collaborators as well as comprehensive metabolomics and lipidomics analyses. The overall findings indicated that decomposition-impacted soils exhibited altered, species-specific molecular signatures suggesting that both mammals decompose differently on a biochemical scale.

2.2 INTRODUCTION

Carcasses are a nourishing food and nutrient source for scavengers and arthropods. Following death, bacteria and hydrolytic enzymes initiate the breakdown of cadaveric soft tissue. Proteins, carbohydrates, and lipids are among the first compounds to be further degraded into their molecular constituents. A series of subsequent postmortem changes, mainly putrefactive processes, facilitate the release of a diverse suite of decomposition products from the decaying material into the enviroment[120]. This affects plant communities, micro- as well as macrofauna in the immediate surroundings, ultimately increasing biodiversity and heterogeneity at the decomposition locality[35, 121, 122]. Literature refers to such localized and fertile areas of carcass-derived decaying organic matter as cadaver “hot spots” or cadaver decomposition islands (CDI)[35]. The interplay of the above-mentioned decomposition processes cause CDI soil to exhibit a unique, diverse physicochemical signature composed of volatile and persistent compounds[24, 35, 123].

Our current understanding of forensic taphonomy is obtained from experimental studies using human and non-human cadavers. The use of human cadavers typically faces greater restrictions, as access is limited to taphonomy facilities where donor availability and replication are problematic. Due to these challenges, animal carcasses are common alternatives in forensic studies. General similarities in anatomy and physiology favor pigs as analogs for human cadavers to study decomposition[115]. An extensive elaboration on the advantages and disadvantages accompanying the use of either of these two mammals in forensics can be found in *Matuszewski et al.*[124] However, ambivalent reports emerging from comparative studies of humans and pigs question the practicability of pigs as adequate proxies for human decomposition studies[124]. While humans and pigs appear to attract similar insect communities and succession patterns[125], there is also evidence that pigs do not capture patterns and rates of human decomposition adequately[115, 116, 126]. Furthermore, differential surface decomposition trajectories have shown to be reflected by diverse changes in soil chemistry underneath cadavers[31]. Not only the publication of this chapter, but several other studies have examined soil changes in response to human and porcine decay. Soil electrical conductivity, pH, nutrient

concentrations (C, N, P, Na, K, Ca, and Mg), and lipids (mainly fatty acids and sterols) were among common differentially affected variables[26, 31, 117, 126].

Lipids are important signaling molecules, energy storage compounds, and components of membranes. In simple terms, two broad classes of lipids exist – polar and neutral lipids. The latter typically comprise triacylglycerols and wax esters as opposed to membrane glycolipids and phospholipids, which are polar lipids[127]. Polar lipids account for approximately 90% of total lipids[59]. Phospholipids form the fundamental matrix of cellular membranes in all living cells by constituting 40% of the membrane dry matter[59, 127]. Structurally they consist of fatty acids linked by a glycerol molecule to a variable head group (Appendix Figure 2.9). A particular class of phospholipids contains numerous molecular species differing in the length of their fatty acid chains which may be fully saturated or unsaturated with double bonds[59]. Lipids comprise approximately 87% of the human fat tissue.[128] In skeletal muscle, phosphatidylcholine (PC) was reported as the most abundant phospholipid class, followed by ~30% phosphatidylethanolamine (PE) and ~7% phosphatidylinositol (PI)[129]. Likewise, evidence shows phospholipids are the major lipid component of pig muscle (38.31%)[129]. LC-MS analysis of soil organic matter listed PC (31.4%) and PE (15.6%) as the most abundant intact polar lipid classes found in soil[130]. Generally, soil receives input of lipid compounds from animals as products of exudation and decomposition in addition to contributions from plants. The galactolipid monogalactosyldiacylglycerol (MGDG) for example, is the most abundant membrane lipid in the biosphere[131]. It is the main lipid component of membranes of chloroplasts and related organelles. Accumulation of lipids in soil is largely influenced by microbes which in turn are impacted by temperature, moisture, pH, and the availability of oxygen[59]. The unique chemical properties of lipids, particularly their hydrophobic nature, increase the stability and persistence of these compounds in the postmortem environment, making them promising target compounds with versatile applications in forensic research.

Despite increasing research interest, comparative inter-species studies are still rare and thus species (dis-) similarities in decomposition trajectories inherent in cadaveric soils are not well understood. In addition, ‘omics’ studies on postmortem specimens seldomly comprise a comparative metabolomics and lipidomics approach. At this point, only one other study (*Langley et al.*) has conducted a postmortem lipidomics assay using

human skeletal muscle tissue[65]. Given these efforts, such cohort studies highlight the need for a global untargeted 'omics' approach characterizing human and pig decomposition products in CDI soils to better understand soil dynamics occurring underneath decomposing mammals.

2.3 EXPERIMENTAL SECTION

2.3.1 Study design and soil sample collection

The presented study took place during the summer of 2014 and the winter of 2014-2015. All samples were obtained from a 3-acre outdoor taphonomy facility, better known as the Anthropology Research Facility (ARF) in Knoxville, TN, USA. The enrolled human donors had no infectious diseases, were not autopsied or embalmed, and died of natural causes. The original study design included ten human donors (n = 6 females, n = 4 males) with weights ranging between 53 to 107 kg. A total of ten pig carcasses were obtained from a local farm in Knoxville and euthanized according to procedures approved in *Dautartas et al.*[116]. The weight range of the pigs was between 47 kg to 59 kg. Appendix Figure 2.2 outlines the experimental setup in the field, whereas the detailed experimental design can be found elsewhere[116, 119]. Only a subset of the cadavers originally used in a large-scale project by *Dautartas et al*. and *Steadman et al.* were utilized for our analyses. In brief, the original publication compared decomposition patterns among 45 rabbits, humans, and pigs across three seasons (winter, spring, and summer). Our follow-up study only included humans and pigs that were randomly placed on soil at a three-meter distance from each other to decompose naturally. Due to physical site constraints that limited access to soils, the summer trial included four human subjects and three pigs; the winter trial included five humans and five pigs. Tiny Tag data loggers recorded soil temperatures and internal temperatures of the cadavers. The same instruments also measured ambient temperature and humidity to calculate Accumulated Degree Days (ADD). Morphological changes on carcasses over the course of the experiment were documented using the Total Body Score (TBS) method by *Megyesi et al.*[132].

The collection procedure for soils followed a method established by *Cobaugh et al*.[35]. To ensure a coherent sampling procedure, a total of around 20 core soil samples were obtained at each sampling time point at different locations from around the carcass where the cadaver decomposition islands (CDI) caused a visible discoloration of the soils (depth ranging from 0-5 cm). Soils were subsequently homogenized in a Whirl-pack bag and stored at -20°C or -80°C until analyses in the laboratory. For each of the two trials (winter vs summer), the sampling procedure was as follows: Weekly soil sampling over a period of five weeks occurred for the summer trial which corresponded to a final ADD of 400 and a TBS of 28 for pigs and 24 for humans. For the winter trial, weekly samples were taken for the first two months, followed by a monthly soil collection for a total of 22 weeks (600 ADD and a TBS scoring of 15 for pigs and 25 for humans). Soil samples taken from approximately five meters away from the carcasses served as control soils (see Appendix Figure 2.1).

Soil physicochemical parameters were collected for winter and summer trial samples, while 'omics' experiments could only be performed on soils taken from the winter trial, as these soils had been appropriately flash-frozen in liquid nitrogen and preserved at -80°C. Improper storage of the summer trial samples made them unusable for metabolomics and lipidomics.

2.3.2 Experimental procedures

2.3.2.1 Soil physicochemistry analyses

Soils were analyzed for pH, nitrate, ammonium concentration, enzymatic activity (leucine amino peptidase activity), and soil respiration at the Department of Biosystems Engineering & Soil Science at UTK, TN, USA. Detailed information can be gained from *DeBruyn et al.*[26].

2.3.2.2 Multi-'omics' analysis: Metabolomics and lipidomics

2.3.2.2.1 Extraction methods

Metabolomics and lipidomics extractions were only performed on soil samples from the winter trial (see above). The extraction process was carried out at 4°C unless otherwise stated. Soil samples were crushed with a mortar and pestle under liquid

nitrogen and weighed into individual 2 ml Eppendorf tubes (approximately 100 mg). To each tube, 1.3 ml of extraction solvent consisting of 40:40:20 HPLC grade methanol, acetonitrile, and water supplemented with 0.1 M formic acid was added[133]. Soil particles were suspended by vortexing and incubated afterwards for 20 minutes while being shaken on an orbital platform shaker (Bellco, Vineland, NJ, USA). Following extraction, samples were centrifuged for 5 minutes at 16,100 rcf and the supernatant collected into new microcentrifuge tubes. The remaining soil was then resuspended in 200 µl extraction solvent and incubated for another 20 minutes. After centrifugation (5 min, at 16,100 rcf) the supernatant was combined with the previously collected supernatant from the first extraction step. All samples were evaporated to dryness under a stream of nitrogen gas. The resulting dried residue was resuspended in 300 µl of sterile Milli-QR grade water and transferred to autosampler vials for subsequent mass spectrometric analysis.

Lipidomics extractions followed a modified procedure described by *Bligh and Dyer*[134]. This method used two extraction solvents, 1:1 (v/v) 0.1 N hydrochloric acid:methanol (solvent 1), and 100% chloroform (solvent 2) which were added to 50-100 mg of crushed soils. 800 µl of solvent 1 and 400 µl of solvent 2 were mixed and added to the soil samples. Afterwards, samples were vortexed for 10 seconds and centrifuged (16,100 rcf for 5 min). The chloroform layer was isolated, dried under nitrogen gas, and resuspended in 9:1 (v/v) methanol:chloroform in autosampler vials prior to mass spectrometric analysis.

2.3.2.2.2 Ultra-High Performance Liquid Chromatography-High Resolution Mass Spectrometry (UHPLC-HRMS)

Mass spectrometry methods for metabolomics experiments were adapted from *Lu et al*.[83, 135]. In short, a 10 µl aliquot was injected through a Synergi 2.5 µl reverse-phase Hydro-RP 100, 100 mm x 2.00 mm liquid chromatography column (Phenomenex, Torrance, CA, United States) maintained at 25°C. The chromatographic eluent was ionized via electrospray ionization (ESI; spray voltage: 2 kV, nitrogen sheath gas: 10, capillary temperature: 320°C) and introduced to an Exactive Plus Orbitrap mass spectrometer (Thermo Fisher Scientific, Waltham, MA, United States). UHPLC-HRMS analysis was performed in negative ionization mode with a full-scan covering a range of

85 to 800 *m/z* from 0 to 9 min and 110 to 1,000 from 9 to 25 min. The resolution was set to 140,000 and the acquisition gain control (AGC) target to $3e^6$ ions. Mobile phase solvent A was composed of 97:3 water:methanol with 10 mM tributylamine and 15 mM acetic acid. Solvent B consisted of methanol. The gradient was as follows: 0 to 5 min: 0% B, 5 to 13 min: 20% B, 13 to 15.5 min: 55% B, 15.5 to 19 min: 95% B, 19 to 25 min: 0% B using a constant flow rate of 200 µl/min.

For untargeted lipidomics, 10 µl of the sample was injected onto a Kinetex hydrophilic interaction liquid chromatography (HILIC) column (150 mm x 2.1 mm, 2.6 µm; Phenomenex, Torrance, CA, USA). The mobile phases consisted of 10 mM ammonium formate in water (solvent A) and 10 mM ammonium formate in 93% acetonitrile and 7% water (solvent B). Both solvents were adjusted to a pH of 3.0. The flow rate was set to 200 µl/min and the column oven to 25°C for a run time of 35 minutes. The chromatographic gradient was as follows: t = 0 min 0% solvent A; t = 1 min 0% solvent A; t = 15 min 19% solvent A; t = 15.1 min 52% solvent A; t =25 min 52% solvent A; t = 25.1 min 0% solvent A; t = 35 min 0% solvent A. The eluent was transferred to an Exactive Plus Orbitrap mass spectrometer equipped with an electrospray ionization (ESI) source. The mass spectrometer was operated under the following settings: spray voltage: 4 kV, heated capillary 350 °C, sheath and aux gas: 25 and 10 units, respectively. Analyses were performed in both positive and negative ESI mode. Full scan and all ion fragmentation (AIF) data were gathered at a resolution of 140,000 with a mass range of 100-1,500 *m/z* and 30 eV collision energy.

2.3.2.2.3 Data processing and statistical analyses

Mass spectrometry files generated by Xcalibur were converted to mzML format using the Proteowizard package[84]. Sample retention time correction, metabolite identification, and chromatogram integration were performed using MAVEN (Metabolomic analysis and visualization engine)[85, 86]. Compounds were manually selected based on a ± 5 ppm mass and a > 2 min retention time tolerance from in-house metabolomics and lipidomics libraries (known features). Statistical analysis included uni- and multivariate approaches. Variable importance in projection (VIP) scores were calculated from partial least squares-discriminant analysis (PLS-DA) to provide a metric for determining the

influence of a metabolite on the group separation. A value > 1 indicates that the compound significantly contributes to the group differentiation. Additionally, student's t-test and volcano plot analyses were used to determine significance. The significance level was defined as $p < 0.05$ with a fold change (FC) threshold ≥ 1.5 or ≤ -1.5. Compounds meeting these thresholds in addition to a VIP cut-off > 1 were regarded as most important. Heat maps were generated in R v1.1.423 using ggplot2[136]. At the time of the study, the laboratory lipidomics analysis strategy comprised the following lipid classes: phosphatidic acids (PA), phosphatidylethanolamines (PE), phosphatidylglycerols (PG), phosphatidylinositols (PI), phosphatidylserines (PS), and monogalactosyldiacylglycerols (MGDG). XCMS, an open-source script developed to analyze chromatographic peaks generated by high-resolution mass spectrometry data, was used to annotate *m/z*-retention time (RT) pairs of unidentified (unknown) spectral features. CAMERA[137] was used to identify *m/z*-RT pairs as possible adducts and/or isotopes. These features were removed in Microsoft Excel prior to data processing to avoid potential metabolite bias. To further reduce the number of unidentified features and reduce the noise, the signal intensity had to be three times the signal intensity of the extraction and media controls. Prior to analysis, features were normalized based on mass measurements. Relative normalized intensities were then uploaded to the online statistical analyzer Metaboanalyst for multivariate analyses such as PLS-DA. The 'omics' data set is published online in the Metabolights database under study MTBLS2254.

2.4 RESULTS AND DISCUSSION

Metabolite and lipid profiles were generated for the winter trial samples, to investigate species-specific decomposition dynamics in CDI soils. As mentioned, the summer samples were not stored at -80°C and could therefore not be used for those purposes. In addition, soil physicochemistry of the winter trial soils retrospectively showed variability in the data sets according to the location of the carcass plots. Six of the plots (three humans (H1-H3) and three pigs (P1-P3), see Appendix Figure 2.10) were located on undisturbed forest soils ("lower site"), while the other four plots (two humans (H4, H5)

and two pigs (P4, P5)) were placed closer to a fence line where soils were previously disturbed by construction activities ("upper site"). As multivariate analysis of soils collected from the upper and lower sites confirmed metabolic variability among locations, the undisturbed, lower soil samples were utilized for data analyses in this chapter. An overview of the study design and the samples analyzed in this chapter are listed in Appendix Figure 2.10 and Appendix Table 2.1, respectively.

2.4.1 Contrasting biochemistry of human and pig decomposition in soil

2.4.1.1 Metabolite profiling and identification during mammalian decay

To capture the entire set of small molecular compounds in an unbiased manner, we used an untargeted UHPLC-HRMS approach to analyze extracted postmortem soil metabolomes. Overall, global metabolomics identified a total of 87 metabolites in human and porcine soils. First, to obtain a rather broad overview of the data, 11 compound classes were defined through KEGG (Kyoto Encyclopedia of Genes and Genomes) annotation and their relative abundances plotted over time (Figure 2.1). Interestingly, all compound classes in animal and human soils flowed similar general dynamics over the course of 22 weeks, yet, week-specific differences among species were noticeable. After carcass placement, relative metabolite concentrations peaked in porcine CDI soils earlier (week 3, Figure 2.1). As decay progressed, abundances rapidly declined (pigs, week 4) and fluctuated on a lowered level until a substantial increase occurred in the tenth week. Thereafter, a final rise in metabolite intensities was seen eight weeks later (pigs, week 18), before they continuously dropped to levels similar to those in week 3. Biochemical changes in human decomposition soils showed characteristically increased metabolite abundances at week 4, week 10, and week 20 (humans, Figure 2.1). Similar to pigs, relative metabolite concentrations continued to fluctuate but remained elevated past the tenth week until the 22nd week of sampling.

Broad similarities in decomposition trajectories between the two species have previously been described although differences were pointed out during their most active stages of decomposition[116]. The here observed inter-specific variability in soil biochemical responses could have been induced by differences in cadaver masses as humans were substantially larger in size (humans: 53-107 kg vs. pigs: 40-59 kg). *Spicka et al.* monitored

decomposition rates of pig carcasses of contrasting masses and reported a more rapid decay for carcasses of a mass ≤ 20 kg relative to larger cadavers[138]. Additionally, *Matuszewski et al*. summarized multiple other studies claiming that in a forensically relevant mass range (10-90 kg) small pig cadavers decompose significantly faster than larger pigs[124]. As a consequence, the rate of soil saturation with decomposition products could have been differentially impacted for lower-weight mammals in our study. Hypothesizing that smaller pig carcasses had an earlier purging of fluids from the body[139] into the surrounding soil matrix as opposed to larger humans, may explain the differential timing of the peak of compound class abundances detected in week 3 – an incline noticeable one week later in human soils (week 4 Figure 2.1). Also supported by recent work from *Barton et al.,* it seems plausible that body fat might be a factor interfering with the temporal movement of carcass fluids into the soil[31].

The flux of decomposition products in the cadaver decomposition island increased for both mammals in week 10 (Figure 2.1). Interestingly, study records showed an incline in ambient, soil, and internal carcass temperatures at day 70[26]. This might have stimulated in a positive feedback loop microorganism growth and activity increasing the flux of decomposition products into the soil up to a point of potential soil saturation with cadaveric fluids. Studies by *Bass et al.* listed ambient temperature among the most important variables influencing the rate of decay[15]. Thereafter, soil biochemistry profiles peaked for humans again in week 20, and for pigs in week 18 (Figure 2.1). Several extrinsic and/or intrinsic factors could have induced fluctuations in compound class abundances within this period. According to *Dautartas et al.,* no insect activity occurred in the initial study in the winter trial for over 100 days[116]. Thereafter, preferential insect succession and scavenging, as well as species-specific microbial activities, count among the above-indicated factors possibly relevant for differential decomposition dynamics which provoked variable soil metabolomes[116, 119].

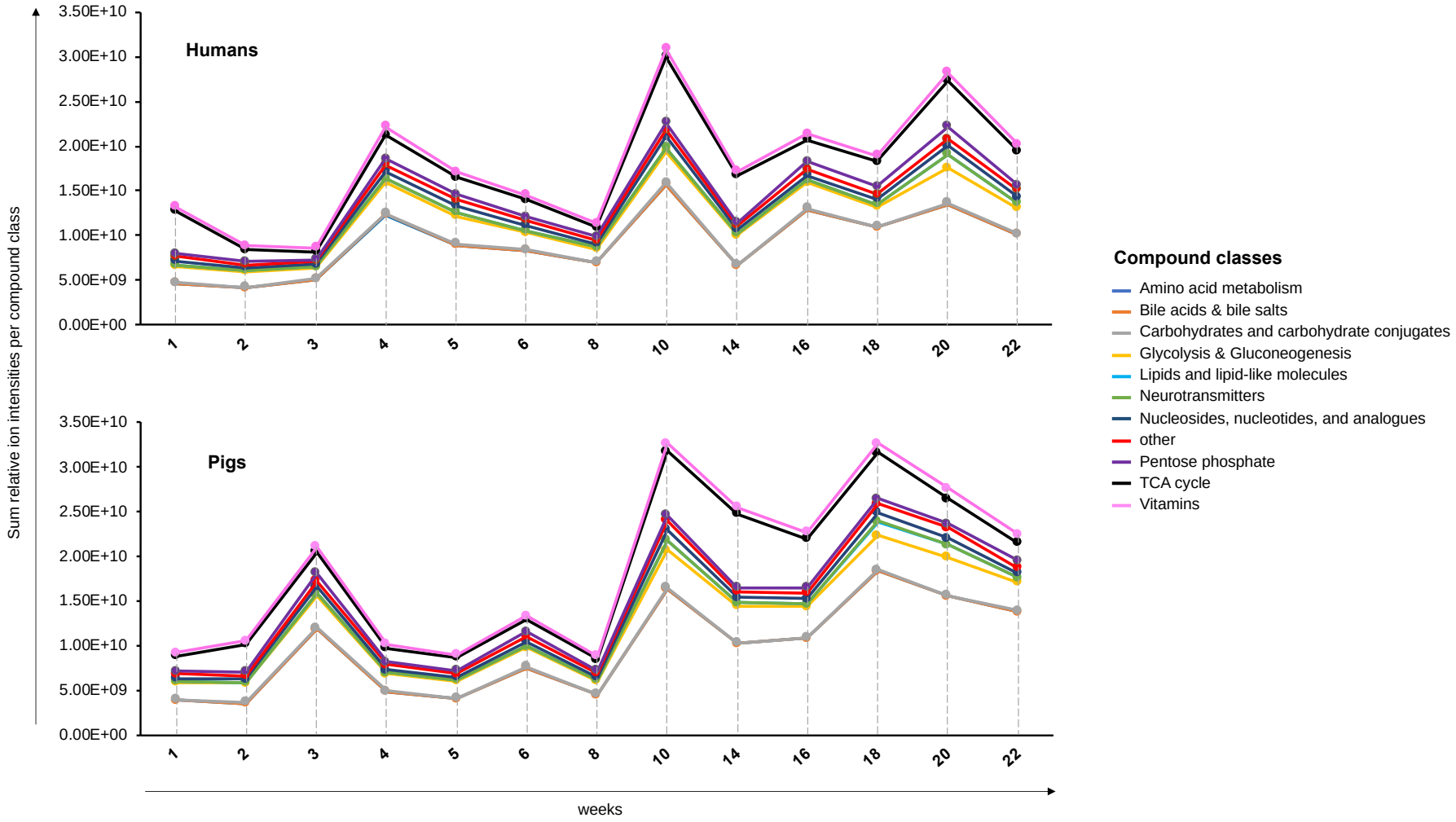

Figure 2.1 – *Line graphs showing the sum of relative ion intensities per compound class detected in CDI soils from decomposing humans (top) and pigs (bottom) over the course of 22 weeks.*

A more dynamic picture of soil metabolite changes during decomposition was obtained using heat maps (Figure 2.2). Heat maps were generated individually for human and pig soils by comparing metabolite abundances of a specific sampling week to those from the previous week to show dynamic changes throughout decomposition. Overall, metabolites linked to the amino acid metabolism depicted the most robust changes, with 37% of significant abundant changes in human and 52% in pig soils. Consistent with Figure 2.1, significant changes in metabolite abundances were concentrated for humans around weeks 4 and 10 (Figure 2.2). β-Hydroxy β-methylbutyric acid (HMB), nicotinate, and pantothenate were the only compounds with significantly increased intensities in week 4 (red column week 4/3) and week 10 (blue column week 14/10). HMB is a naturally occurring metabolite formed during the catabolism of the branched-chain amino acid leucine[140]. Nicotinate is a vitamin of the B complex reported in animal and plant tissues. It acts as precursor for the formation of coenzymes NAD and NADP[141]. Interestingly, the metabolite which exhibited the most frequent and significant abundance fluctuations throughout human decay was pantothenate, better known as vitamin B5 – a water-soluble vitamin and precursor to coenzyme A (CoA), which has an essential role in numerous biochemical processes such as the fatty acid metabolism and Krebs cycle. Vitamin B5 has also been found as nutrient in soils[64]. The 22-week pig decay showed significant metabolite changes mainly centered around weeks 3 and 10 – illustrated by an increase in abundance of 6 and 32 compounds, respectively (Figure 2.2 red columns week 3/2 and week 10/8). Of these compounds, only glutamine and glycerol-3-phosphate showed a cyclic temporal pattern and were significantly elevated at both sampling time points relative to the corresponding previous weeks. Glycerol-3-phosphate is involved in glucose, lipid, and energy metabolism, yet it also is a plant- and bacterial-derived metabolite[142]. Glutamine is the most abundant amino acid. It is also a proteinogenic amino acid, hence present in many proteins[143]. In 2002, *Vass et al.* identified a steady increase of glutamine postmortem in human liver tissue and proposed its usefulness as a postmortem interval (PMI) marker[18]. Notably, the abundance changes of the non-protein amino acid citrulline were significant in pig CDI soils for 6 out of 12 comparisons (Figure 2.2). There may be a possible link to elevated ammonium concentrations measured under decomposing pigs, which started to increase approximately around study week 5 (see

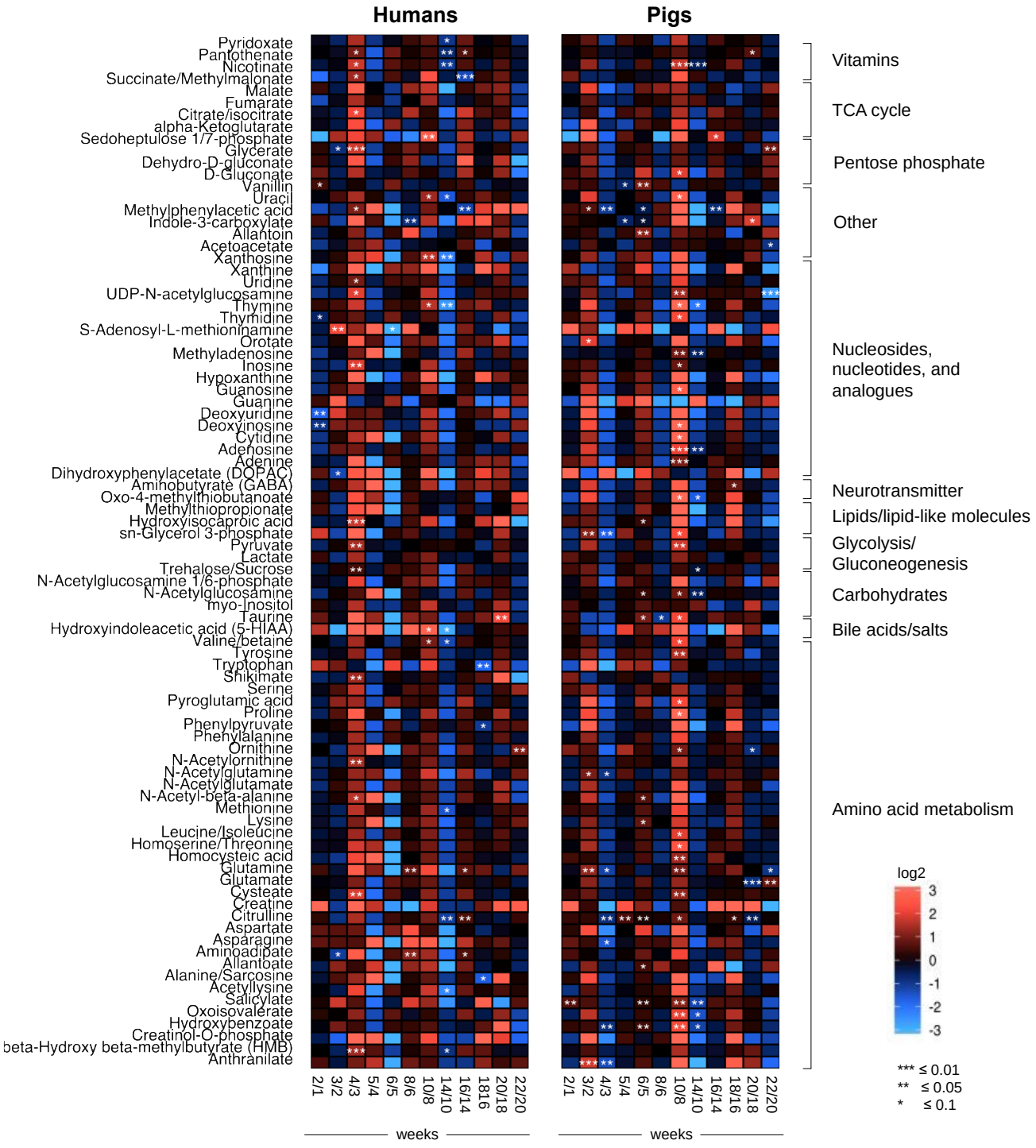

Figure 2.2 – *Changes of relative soil metabolite abundances during mammalian decomposition. Metabolites were grouped by corresponding metabolic pathways. Each plotted week was compared to the previous sampling week to show dynamic abundance changes during the decomposition period. All fold changes are log2 transformed. Increased fold changes are indicated in red and decreases are shown in blue.*

publication of this chapter)[26]. After week 5, mean ammonium concentrations in pig soils spiked as decomposition progressed in weeks 9 and 17. Ammonium ultimately contributes to the pulse of nitrogen introduced to the environment and is available to microbes and plants. As citrulline has been suggested to play a role as nitrogen modulator in higher plants, predominantly due to facilitating nitrogen assimilation, nitrogen storage, and transport[144], both variables, citrulline and ammonium, could be interconnected. This may also imply a different pool or a larger amount of (nitrifying) bacteria present in soils underneath pigs.

Next, a more in-depth weekly analysis was performed to further assess mammalian CDI soil according to its metabolic profile. Partial Least-Squares Discriminant Analysis (PLS-DA) of each week showed that soils obtained from around both decomposing mammals clustered separately for every single time point (Appendix Figure 2.11). A representative example for this finding is given in Figure 2.3A for the beginning (week 1), the middle (week 10), and the end of decomposition (week 22). Each plot illustrates a distinct separation of soil samples by species, indicating differences in the metabolic profiles of CDI soils. To examine which metabolites were responsible for the variation displayed in the PLS-DA plots, variable importance in projection (VIP) values were calculated for each week. A weekly assessment of the total number of metabolites with VIP scores > 1, found on average 35 metabolites that were important for distinguishing mammalian CDI soils each week (Figure 2.3B). The most frequent metabolites, detected in at least 7 out of 13 weeks, were further assessed by matching them to their pathways (22 metabolites, Appendix Table 2.2). Of these 22 metabolites, the majority (n = 12 compounds) were involved in amino acid metabolism and n = 5 were nucleosides, nucleotides, and analogs (Figure 2.3C). An outcome consistent with the heat map above as well as other studies which detected amino acids not only in porcine cadaveric specimens but also in soils impacted by human and other mammalian decay[18, 145]. Aside from that, soil pH was significantly different between humans, pigs, and controls. During the winter, no significant changes occurred within the first five weeks, but thereafter (starting at week 14) the lower site decomposition soils exhibited a reduced pH compared to controls (compare *DeBruyn et al.*)[26]. An increase in soil acidity (lower pH)

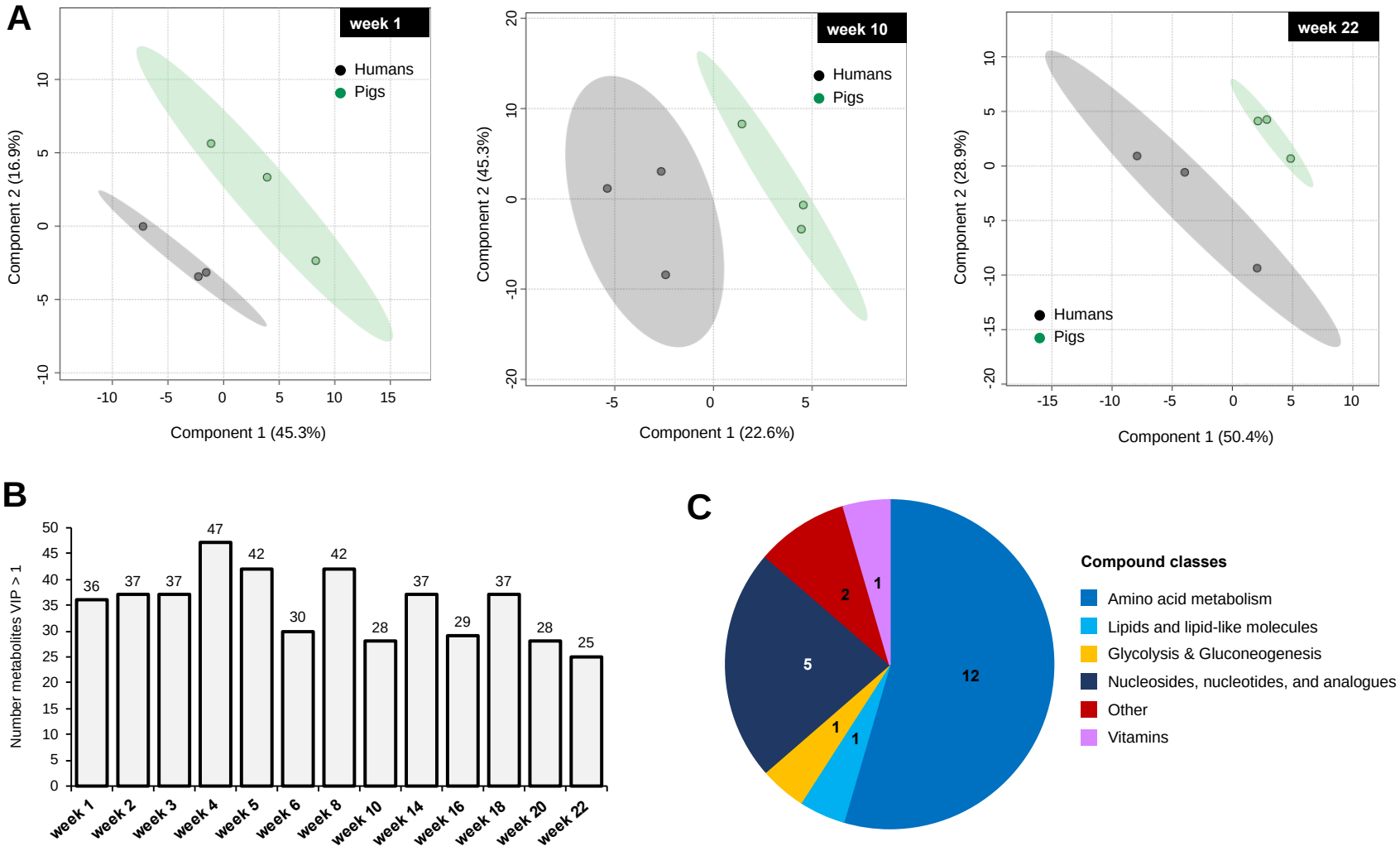

Figure 2.3 – *Postmortem metabolomics of CDI soils from human and pig carcasses. (A) 2D PLS-DA score plots of CDI soils for week 1, week 10, and week 22. Hotelling's ellipses denote 95% confidence intervals. (B) Total number of metabolites per week with VIP scores > 1 that caused a separation among soil types in PLS-DA. (C) Pathway analysis of selected VIP metabolites (n = 22, VIP > 1) detected in at least 7 out of all 13 weeks from (B).*

could have been caused by a gradual release of organic acids and amino acids into CDI soils due to general decomposition processes.

Lastly, features important in distinguishing mammalian CDI soils with VIP values > 1 were further evaluated with regard to their statistical significance. For direct pairwise comparisons, a volcano plot analysis for each time point helped to determine significant alterations in metabolite abundances. The results are illustrated in Figure 2.4. Here, the total number of metabolites with significantly different abundances in human vs pig soils is depicted over the course of decomposition (p-value and fold change thresholds < 0.05 and ≥ 1.5 or ≤ -1.5, respectively). Over the first eight weeks, several compounds were significantly higher in abundance in human soils (green bars Figure 2.4). Week 8 had with 34 metabolites the largest number of altered compounds compared to pig soils. As time progressed, this trend reversed as porcine soils showed consistently a greater number of metabolites with increased relative abundances. Consequently, these metabolites were found in decreased intensities in human soils, thus are represented in red in Figure 2.4. Overall, the analysis revealed 54 differentially abundant metabolites. However, during the decomposition period, several metabolites showed significant abundance changes for multiple of the 13 sampling weeks (compare Appendix Table 2.3). Among these, one compound, 2-oxo-4-methylthiobutanoate, was significantly altered in 5 out of 13 weeks (weeks 2, 8, 10, 18, and week 20). In three of these weeks (weeks 10, 18, 20) significant changes in metabolite abundance occurred in porcine soils. This compound is a reported methionine-derived plant secondary metabolite and is involved in humans in the methionine metabolism[146]. On the contrary, nicotinate and pyroglutamic acid had increased abundances solely in human CDI soils and showed periodic occurrence with significantly higher abundances in three sampling weeks (weeks 4, 5, and 8). The importance of nicotinate was described above. Pyroglutamic acid is fairly ubiquitously present. It can form in humans as intermediate of glutathione or protein degradation[147].

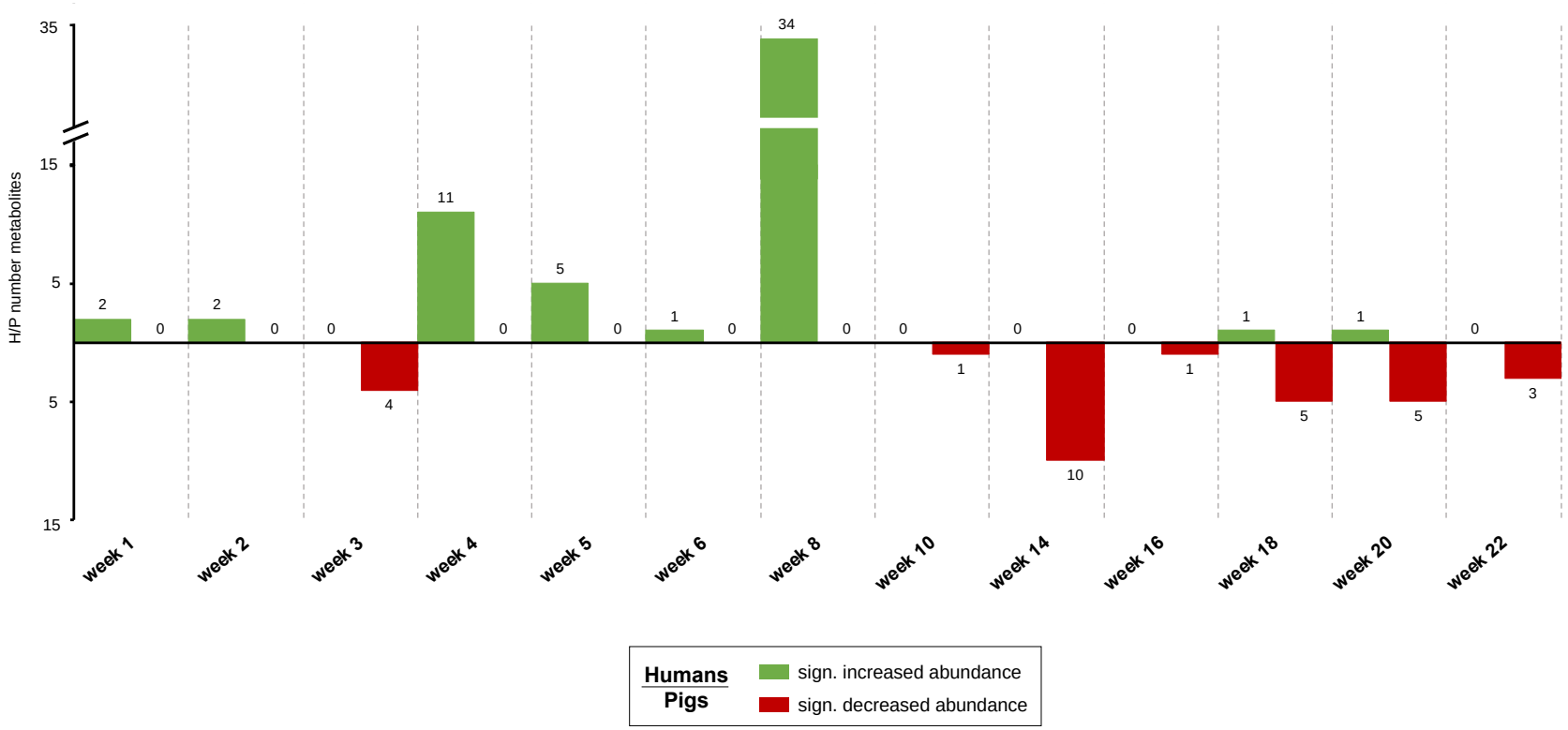

Figure 2.4 – *Total number of metabolites significantly altered in abundance in mammalian CDI soils over the course of decomposition. Shown is the total number of metabolites per week that had significantly altered intensities among both CDI soils. Increased compound abundances in human relative to pig soils are shown in green, while decreased abundances in human soils are listed in red. A summary of each individual metabolite is listed in Table 2.3. sign = significantly.*

Collectively, postmortem soil metabolomics revealed that human and pig decomposition differed with regard to metabolic patterns extracted from CDI soils. Certain compound classes dominated the pool of mammalian decomposition products, with amino acids being the major one. Differences in soil biochemistry in human- and pig-derived CDI soils implied that variable macroscopic decomposition trajectories observed by *Dautartas et al.* may induced differential metabolic patterns on a microscopic scale[116].

2.4.1.2 Inter-species lipid dynamics in mammalian CDI soils

A similar approach was taken to analyze the lipidomics data. Comprehensive lipidome profiling of human and pig soils yielded a total of 85 lipids (Appendix Table 2.4). These database-matched lipids were first classified into their lipid classes, namely phosphatidic acids (PA), phosphatidylethanolamines (PE), phosphatidylglycerols (PG), phosphatidylinositols (PI), phosphatidylserines (PS), and monogalactosyldiacylglycerols (MGDG). The most abundant lipid classes in decomposition soils were MGDG and PE with 27 and 16 detected lipids, respectively, closely followed by PS (15 lipids) and PA (12 lipids) (Figure 2.5A). PI and PG were accounted for with nine and six lipids, respectively. PE has been reported among the most abundant lipid classes in soil extracts, whereas PG, PI, PS are typically observed in lower abundances[130, 148]. The same researchers found that plant root extracts contained large amounts of MGDG[130]. This suggests that a potential contamination of soil extracts due to root/plant debris might have occurred in our samples. To assess species-specific lipid signatures, weekly PLS-DA analyses were performed. Similar to metabolic profiles, we observed differential lipid signatures during mammalian decay (Appendix Figure 2.12). Figure 2.5B exemplifies this for the beginning, middle, and end of decomposition (weeks 1, 10, and 22). Soil lipids from both mammals produced the formation of two clusters creating an inter-species divergence (Figure 2.5B). This concludes that differences in mammalian decomposition trajectories were also manifested in the soil lipidome. Following this, lipids with high importance in the group separation (VIP cut off > 1) were extracted from PLS-DA plots and further evaluated based on in how many weeks they distinguished human CDI soils from pig soils. Accordingly, lipids with VIP values > 1 that contributed in most of the 13 weeks to the formation of a distinct CDI soil lipidome are illustrated in Figure 2.5C (in seven and eight

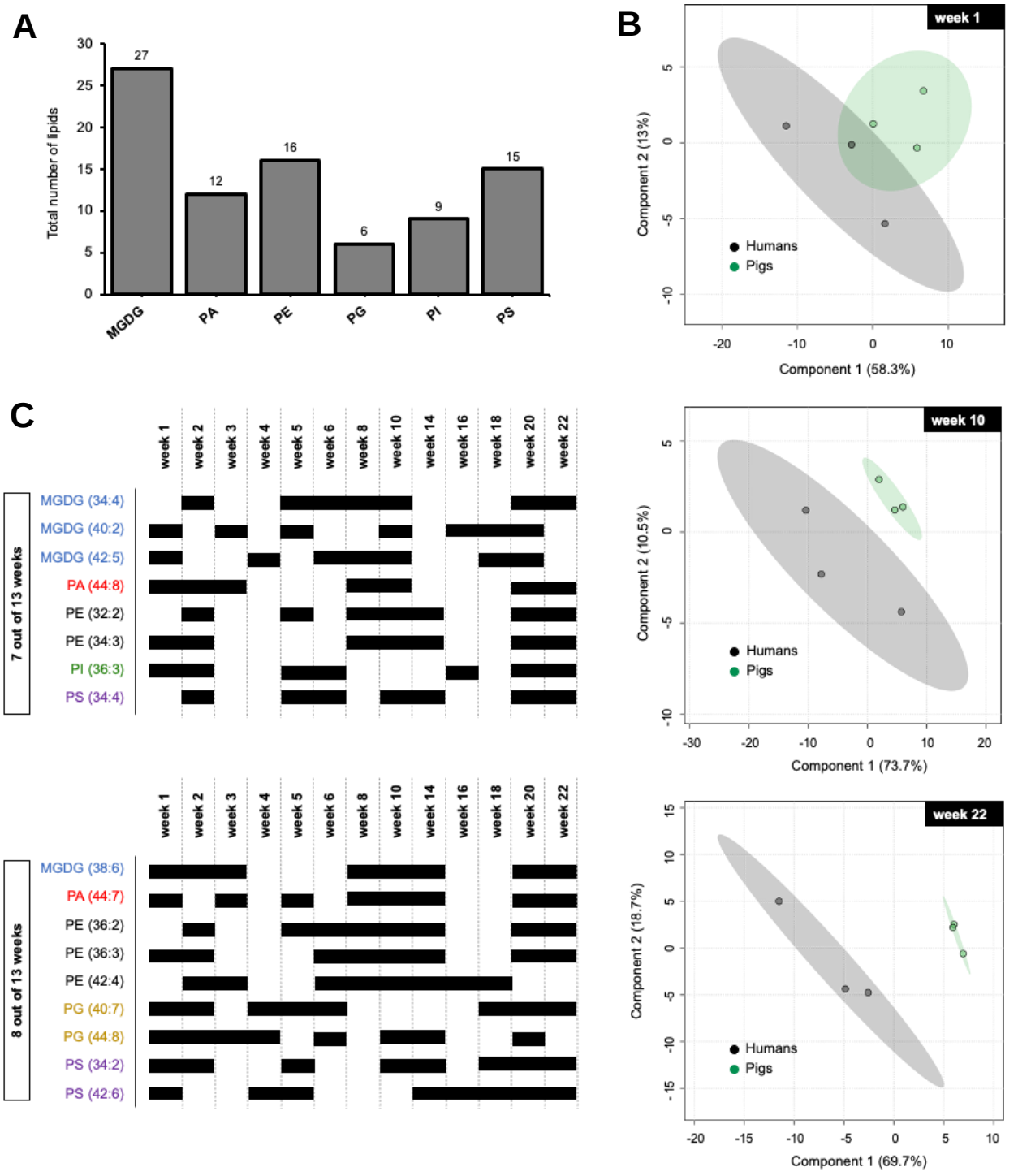

Figure 2.5 – *Postmortem lipidomics of mammalian CDI soils. (A) Cumulative number of lipids categorized by major lipid classes. (B) PLS-DA of human and pig CDI soils for week 1, week 10, and week 22. (C) Selected VIP lipids (VIP > 1) detected in 7 and 8 out of 13 weeks with high importance in differentiating pig and human CDI lipidomes. Black bars indicate in which weeks lipids were detected. PI, phosphatidylinositol; PE, phosphatidylethanolamine; PS, phosphatidylserine; PG, phosphatidylglycerol; PA, phosphatidic acid; MGDG, monogalactosyldiacylglycerol.*

weeks out of 13 weeks). The black bars in this figure indicate in which weeks certain lipids had a high importance in differentiating the two soils and they also visualize the periodic appearance of lipids during decomposition. Lipids from the class PE seemed to stand out as most important as they were repeatedly involved in separating soil lipid profiles. Also, almost every listed lipid was detected in weeks 10 and 20, and according to the metabolomics results, week 10 showed major metabolic changes, as well (see above).

To assess the significance of these results and at the same time easily visualize a large number of compounds, a heat map was generated (Figure 2.6). In total, 44 lipids showed significant differences in pig and human soils for at least one of the sampled weeks. Among them, 13 MGDG, 10 PE, 9 PS, 8 PI, 2 PG, and 2 PA were significantly altered. Over the course of 22 weeks, six lipids of the MGDG class, three of the PE class, as well as PG 40:7, PI 32:1, and PS 34:2 exhibited reoccurring significant changes in abundance among the soil types. Considering the entire decay period, three weeks had a concentration of altered lipid abundances: Week 4 (6 significantly altered lipids), week 5 (26 lipids), and week 20 (14 lipids). Generally, in weeks 4 and 5, pig soils exhibited increased lipid abundances relative to humans – this pattern reversed as decomposition progressed for week 20 (Figure 2.6, blue and red columns, respectively). The largest number of differential lipids was detected in week 5. The enrichment of lipids underneath pigs can potentially be related to the significantly reduced pH in pig decomposition soils (see publication)[26]. It can be hypothesized that greater lipid accumulation in more acidic soils might have resulted from unfavorable environmental conditions for microorganisms, which in turn may preserved lipids in pig soils from microbial degradation. A theory previously discussed in another work for other lipid classes[59]. None of the lipids that increased in abundance in pig soils in week 4 showed a significant increase in week 5, however, PE 38:6, PE 38:2, along with three MGDGs were found to be significantly elevated in animal soils during early timepoints of decay (week 5), but were reduced towards the end of active decay (week 20). Declined soil lipid concentrations in human soils in weeks 4 and 5 might represent an aftereffect from more extensive scavenging of humans compared to pigs, as reported by *Steadman et al.*[119]*.* Scavenging could have considerably reduced the overall amount of tissue left to degrade, hence retarded fluid

leakage into the surrounding soil[119]. One would assume mammals also differ in their microbiomes[31], mainly due to different dietary restrictions between the two organisms. *Parkinson* attributed the in her study observed greater diversity of soil bacterial community changes in humans compared to pigs to a more diverse human microflora[149]. Microbes are also alleged to impact the richness and diversity of released volatile organic compounds (VOC) during decay[24]. Therefore, a differential (extrinsic or intrinsic) microflora may have contributed to species- and time-specific releases of metabolites into the surrounding soil. In contrast, *Metcalf et al.* found that soil microbes did not markedly differ based on carrion type[58]. At this point, more studies focusing on the intrinsic carcass environment, rather than soil microbes, are needed to elaborate on this ambiguous state of knowledge. The overall chemical profile of adipose tissue composition also differs between humans and pigs. *Notter et al*. ascribed differences in the decay of adipose tissue to a distinct distribution of total fatty acids between species[117]. Such differences in body composition could influence decomposition patterns and soil processes underneath cadavers, and ultimately interfere with the nutrient richness available to microbes determining their growth and reproduction. Consequently, this can induce a time discrepancy regarding when liquified tissue is detectable in its molecular constituents on a biochemical scale. Another possible explanation for the postmortem inter-species metabolic fluctuation in our study.

As lipidomics is an emerging technique in the repertoire of postmortem 'omics' analyses, our results have not been reported previously. Only *Langley and colleagues* have used a lipidomics approach in a comparable outdoor setting to capture lipid profiles of the human skeletal muscle after death[65]. The authors found decreasing concentrations of PG 34:0 and PE 36:4 over the course of decay. It is important to note that CDI soil has a completely different level of biochemical complexity compared to skeletal muscle. Soil is incredibly susceptible to external influences (e.g., moisture, humidity) and experiences a microbial flux from both the internal carcass milieu as well as externally with regard to inherent soil microbes. Microbial synthesis and consumption of lipids as energy sources go along with this[130]. Although such analyses were beyond the scope of this chapter, such factors could have contributed to a more variable lipid signature in soils as opposed to a linear decline as described by *Langley et al.* On the other hand, we noticed certain

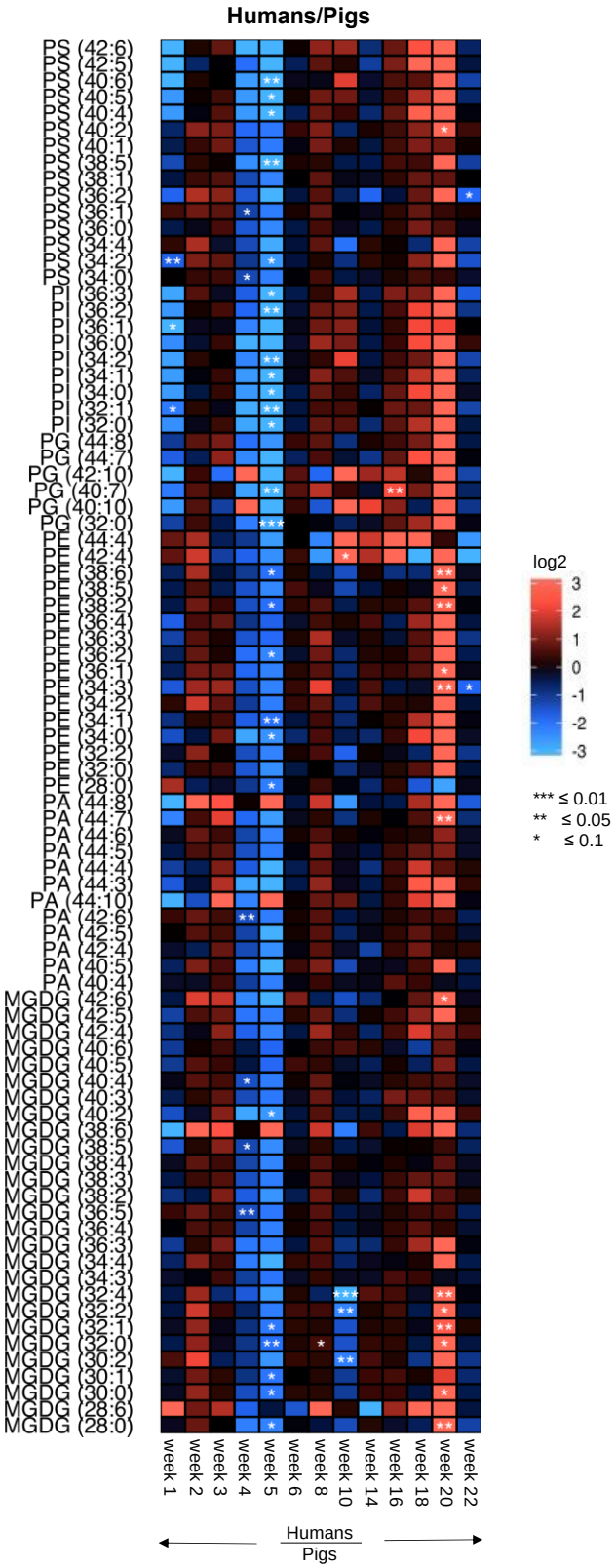

Figure 2.6 – *Changes of relative soil lipid abundances throughout mammalian decomposition. For each of the plotted weeks fold changes of metabolite abundances found in human CDI soils were compared to pig soils. Significance was calculated based on student's t-test. All fold changes are log2 transformed. Increased fold changes are indicated in red and decreases are shown in blue. For lipid class abbreviations see Figure 2.5.*

differential unsaturated phospholipids (PE 34:3, PE 38:2, PE 38:6, PG 40:7, PI 32:1, and PS 34:2) occurred periodically at multiple time points throughout decay. An interesting finding for future targeted analyses that could discover a combination of lipids as index of certain decomposition stages.

Taken together, soil lipidomics analyses exposed a pool of polar lipids in mammalian CDI soils that was largely dominated by different abundances of MGDG and PE. A reduced diversity of other phospholipid classes (PI, PG, PA, and PS) could potentially indicate the presence of certain microbial taxa that used these lipids to form membranes[150]. Different soil lipidomes underneath decomposing mammals suggested inter-species differences in decomposition patterns. Collectively – also referring to the metabolomics results – we highlighted the complexity and diversity of the postmortem biochemical soil environment; compounds in soil can have multiple mixed origins and are likewise susceptible to various extrinsic and intrinsic variables. We found that signatures of pig and human decomposition in CDI soils share many of the same compounds, however compound abundances were rarely similar at specific time points during decomposition. This supports recently published findings of volatile organic compound (VOC) analyses reporting dissimilar visual decomposition and VOC profiles for both species[126]. Overall, our work expanded the repertoire of compounds possibly important for distinguishing decomposing humans and pigs, and provided opportunities for targeted studies in the future.

2.4.1.3 Unknown features of human and pig CDI soils

One benefit of using a high-resolution mass spectrometer in full scan mode is the collection of chromatographic peaks across a large mass to charge (*m/z*) range (usually 75-1,200 *m/z*). Meaning, it is possible to identify metabolites based on their mass and retention time if those features match previously analyzed standards (known metabolites). In addition to the knowns, thousands of other spectral features did not match any compound in our in-house database. These features exhibited metabolite-like characteristics, but the exact structures were not known (unknowns or unidentified metabolites). After data reduction, signatures of 1,615 and 2,429 unidentified CDI soil

features from metabolomics and lipidomics extractions, respectively, were assessed using PLS-DA (Figure 2.7A and Figure 2.8A). PLS-DA for the unknowns demonstrated a similar distribution of the data as previously seen for the knowns (Figure 2.3A and Figure 2.5B). Unidentified compounds from lipidomics and metabolomics analyses appeared to be different among human and pig soils, illustrated by a species-specific clustering of CDI soils (Figure 2.7A and Figure 2.8A). Once again, the data suggested distinct chemical profiles for both carcasses with regard to the suite of compounds leaking into the soil. To assess which features were driving the separation in the PLS-DA plots, VIP values were extrapolated for both data sets. Using a volcano plot analysis, we calculated significant changes between both soil types for each time point (VIP > 1, FC > +/-1.5 and p-value < 0.05, Figure 2.7B and 2.8B). Unidentified features in the metabolomics data set significantly increased both in number and abundance in pig soils for weeks 3, 8, 10, and 20 (114, 119, 126, and 104 features, respectively, Figure 2.7B). In humans, the majority of unknowns higher in abundance were found in week 4 and week 8 compared to soil profiles of the same weeks from pigs (Figure 2.7B). A trend that was also reflected for the knowns when contrasting decomposition products from humans and pigs (compare Figure 2.4). Soil lipid extracts revealed major differential abundances of unidentified spectral features for weeks 5, 8, and 20 (top 3 weeks; Figure 2.8B). For the latter two weeks, a greater number of unknown lipids were significantly increased in abundance in human soils, while 423 compounds were elevated in week 5 underneath pigs (Figure 2.8B). These results confirmed the above-illustrated distribution of known lipids in decomposition soil (Figure 2.6). Here, changes in soil lipid abundances were significantly enriched in week 5 in the pig and week 20 in the human CDI soils (blue and red columns, respectively Figure 2.6).

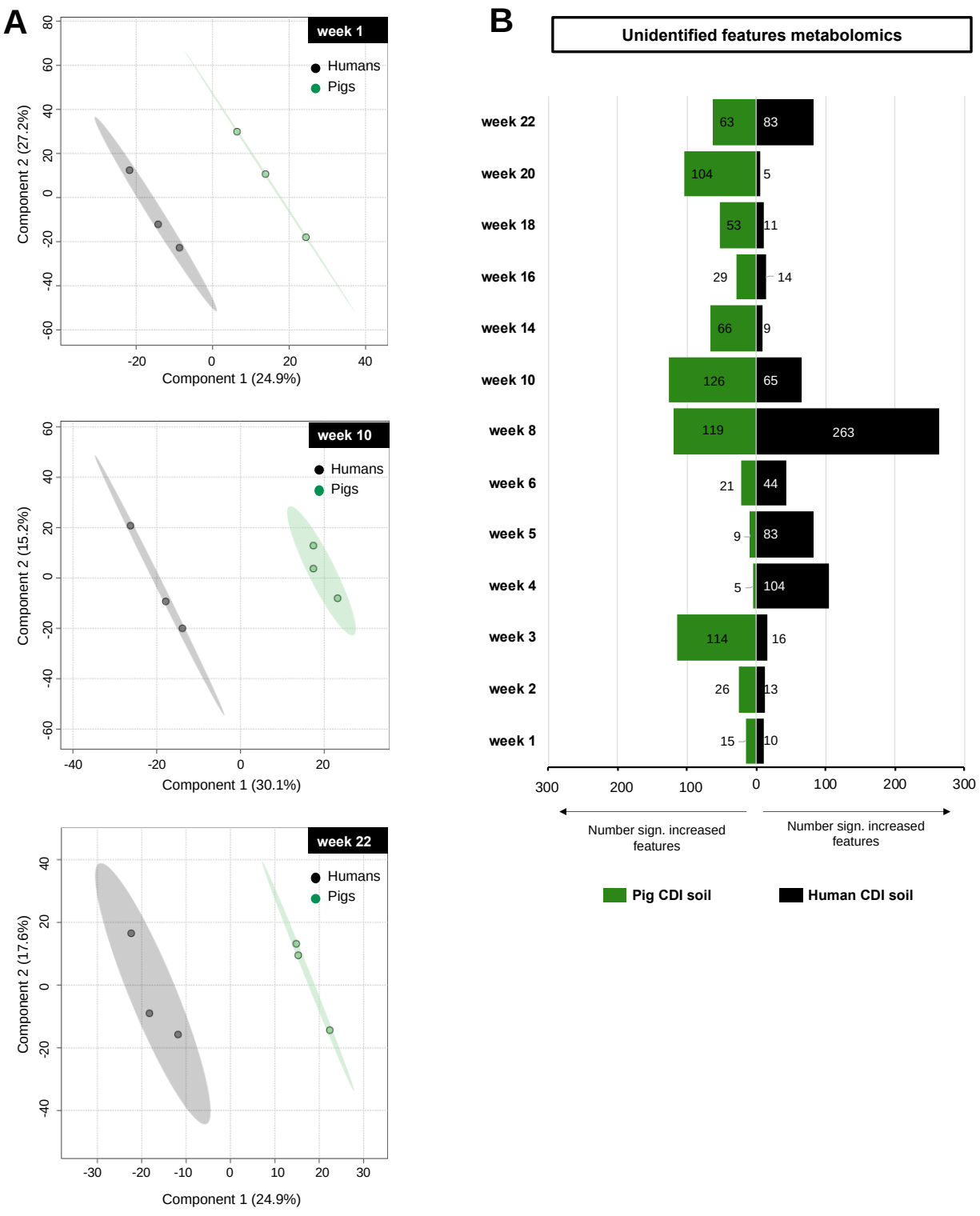

Figure 2.7 – *Unknown features of mammalian CDI soils resulting from metabolomics. (A) PLS-DA plots for weeks 1, 10, and 22. (B) Significantly increased abundances of unidentified features among pig (green) and human (black) CDI soils detected at each sampling period. Significance was based on VIP > 1, as well as a fold change cut-off +/-1.5 and p value < 0.05.*

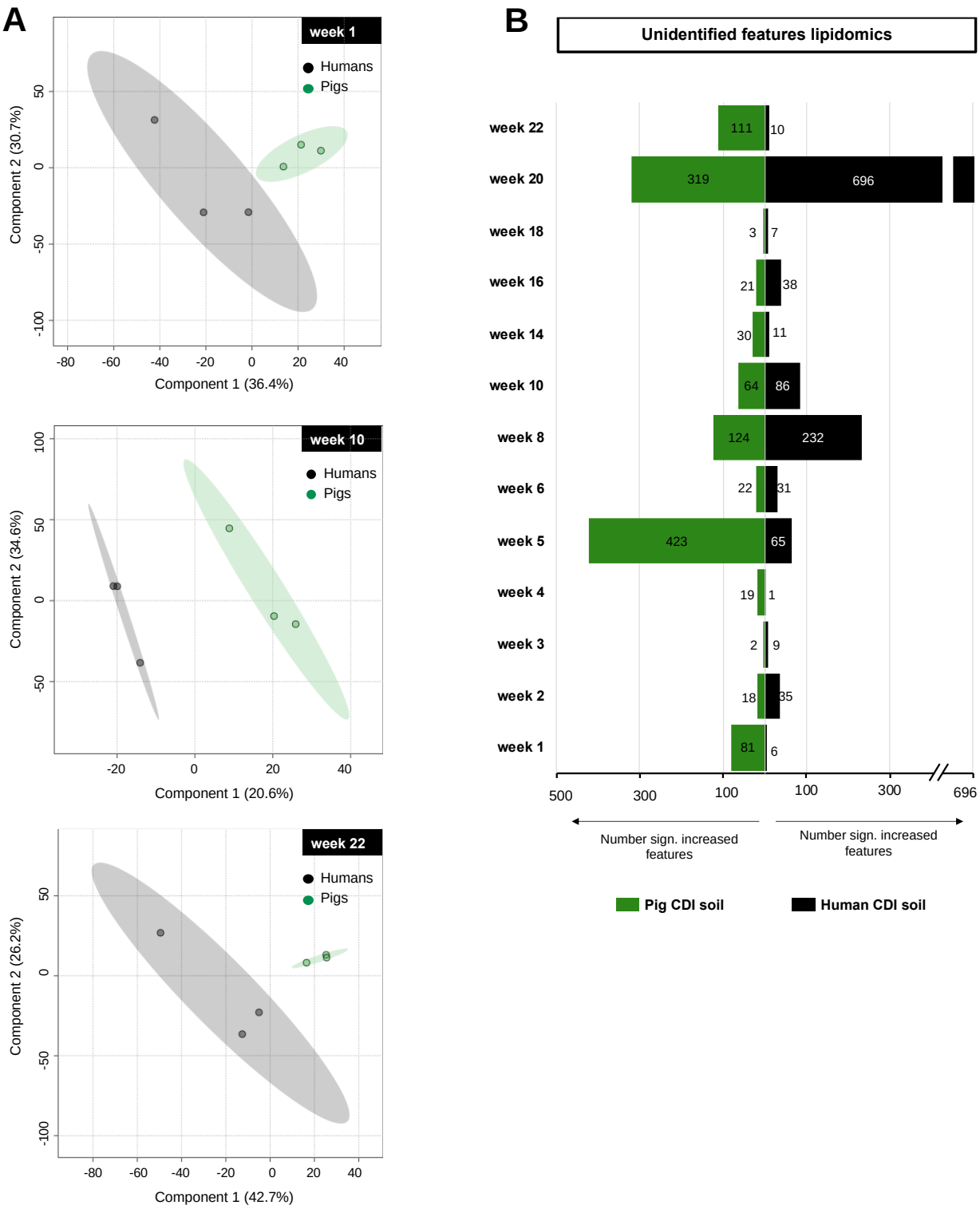

Figure 2.8 – *Unidentified lipid spectral features of mammalian CDI soils from lipidomics studies. (A) PLS-DA plots for weeks 1, 10, and 22. (B) Significantly increased abundances of unidentified features among pig (green) and human (black) CDI soils detected at each sampling week. Significance was based on VIP > 1, as well as fold change cut-off +/-1.5 and p value < 0.05.*

Collectively, these preliminary approaches to extract information from a large amount of unknown special features, revealed consistent patterns with the presented findings from the knowns in terms of species-specificity and the temporal occurrence of unknowns during mammalian decay. As the identification of unknown compounds is a major bottleneck in the 'omics' field, we still encounter various unsolved questions related to ultimate structural annotation of these spectral features. Nevertheless, we demonstrated that the unknowns hold promising potential to reflect differential biochemical signatures of mammalian decomposition trajectories in CDI soils.

2.5 CONCLUSION

Presently, this is the first study using combined untargeted metabolomics and lipidomics analytical platforms to investigate the biochemical composition of mammalian CDI soils by focusing on inter-species differences. Collectively, 'omics' analyses were congruent with the general responsiveness of the changing biochemistry of an organism after death, pointing toward the involvement of similar global metabolic pathways in decomposing humans and pigs. However, we identified a species-specific and time-dependent occurrence of compounds over the course of decay. This led to the conclusion that, from a biochemical point of view, mammalian decomposition products were distinguishable underneath cadavers in soils. Supported by weekly multivariate analyses, we noticed distinct metabolite and lipid profiles in the suite of compounds leaking from both carcasses into the soil. Citrulline for instance showed in pig CDI soils in 6 out of 12 weeks significant abundance changes, whereas pantothenate exhibited the most frequent and significant fluctuations during human decomposition. The majority of differential metabolite abundances were observed in weeks 4 and 10 for humans, and in weeks 3 and 10 for pigs. In addition, different inter-species lipid abundances were predominant for study weeks 4, 5, and 20. Overall, MGDG and PE dominated the pool of polar lipids in mammalian decomposition soil. Also, certain unsaturated phospholipids with a backbone of 32 to 40 carbon atoms (PE 34:3, PE 38:2, PE 38:6, PG 40:7, PI 32:1, and PS 34:2) showed a significant cyclic appearance throughout decay among both

species. Lastly, the analysis of unidentified spectral features revealed consistency with results obtained from the knowns. The unknown spectral features supported the fact that species-specific and temporal patterns can be extracted from the CDI of decomposing carcasses to discriminate between humans and pigs.

Explanations for the observed inter-species divergences in CDI soils were multifold. As stated above, *Dautartas et al*. and *Steadman et al.* reported that the winter trial lacked insect activity for over three months and human decomposition occurred at a much faster rate, most likely attributed to preferential scavenging[116, 119]. Body composition is another factor to consider – not only with regard to body mass and size but also differential quantity and distribution of fat[116]. Pigs also tend to have a higher moisture content, which might impact microbial activity and mobilization of decomposition products into the soil[26]. Altered inter-species lipid and metabolite abundances might have been influenced by what kind of microbial communities occurred at which time during decay as microbes are able to facilitate conversion of proteins into amino acids, metabolite production, or degradation of biomolecules[26, 130]. According to *Ding et al.,* 45-80% of soil lipids are derived from bacteria, fungi, and plants[130]. Additionally, phospholipids PE and PG are major structural components of most bacterial cell membranes[130]. Unfortunately, it was beyond the scope of this study to precisely elucidate metabolite origins. Lastly, factors involving mammalian dietary restrictions (e.g., human western diet vs. homogenous diet of farm-fed animals) together with intra-species differences such as medical history represent additional factors with the potential to impact soil responses to decomposition. Experimental limitations arise from the fact that taphonomy facilities are commonly restricted in space and donor number. Our study had a small sample size, it lacked experimental replication in all four seasons, and cadaver placement did not occur in a distance commonly used in forensic entomological research designs (at least 50 m apart)[124]. Also, with more sampling points, it would have been possible to generate a more detailed understanding of the nutrient cycling and persistence of compounds in soil postmortem, and the form in which they are retained.

Despite those limitations, our findings proposed clear species-specific biochemistry patterns of decomposition inherent in CDI soils. This does not necessarily diminish the usefulness of pig carcasses as human analogs but rather informs about

limitations and the existing margins of error of animal use in forensic taphonomy when it comes to soil chemical dynamics. Our work also strengthens the importance of ‘omics’ research as a promising forensic tool for elucidating species-specific decomposition biomarkers. Future targeted endeavors may validate the predictive accuracy of our identified compounds in terms of species uniqueness and temporal dynamics after death. Ultimately, biochemical evidence present in the fertile cadaver decomposition island can be useful in questions related to location and time of death of individuals. Regarding this, the stability of lipids seems a promising feature when it comes to answering forensically relevant questions that address long postmortem periods and/or varying environmental conditions.

APPENDIX

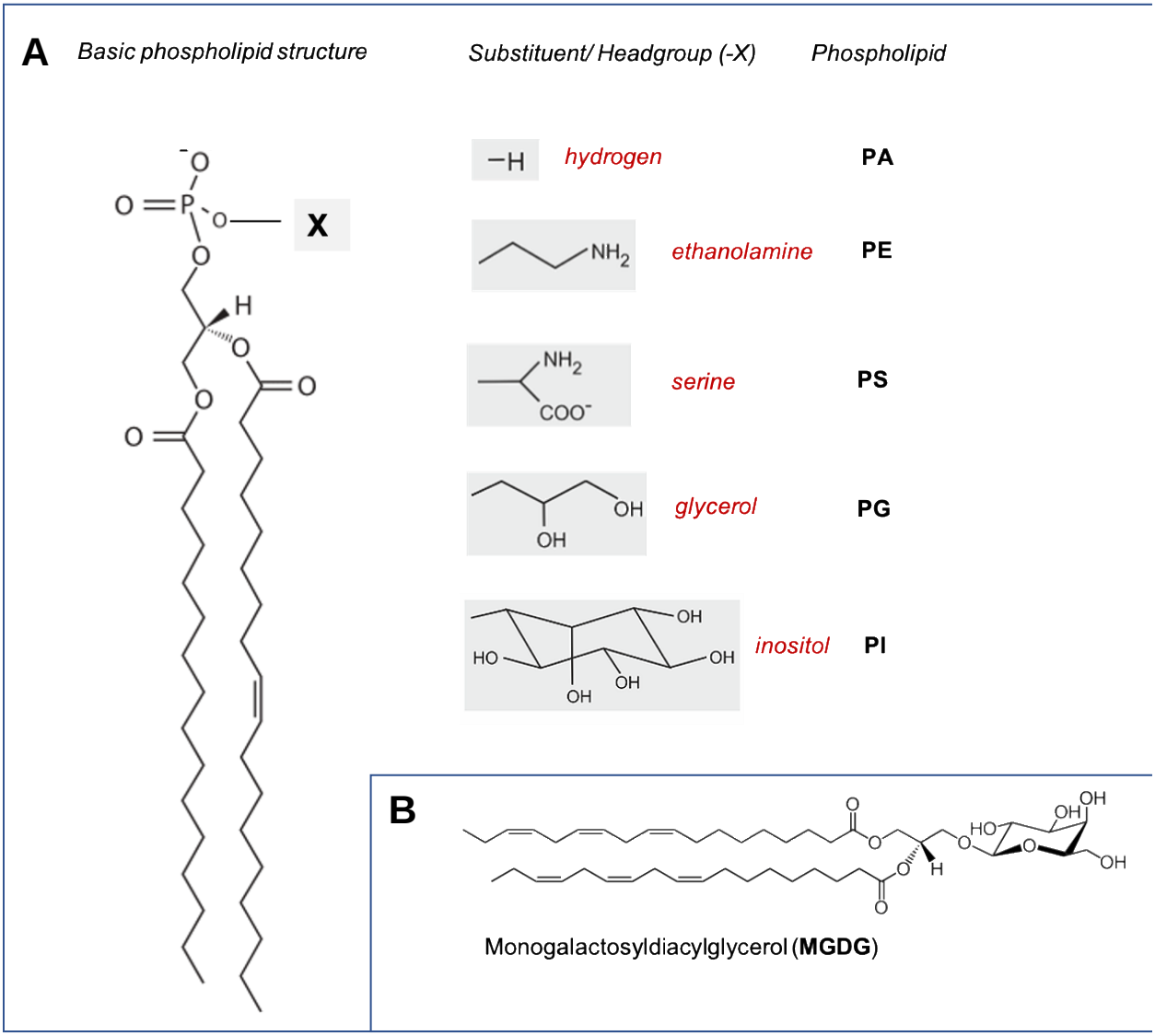

Figure 2.9 – *Overview of phospholipids in this study. (A) The structural backbone of phospholipids is a glycerol molecule linked to acyl chains via ester bonds. Headgroups are linked to glycerol via a phosphate group. A selection of possible headgroups is outlined. (B) Structure of monogalactosyldiacylglycerol (MGDG). PE phosphatidylethanolamine, PG phosphatidylglycerol, PS phosphatidylserine, PI phosphatidylinositol, PA phosphatidic acid.*

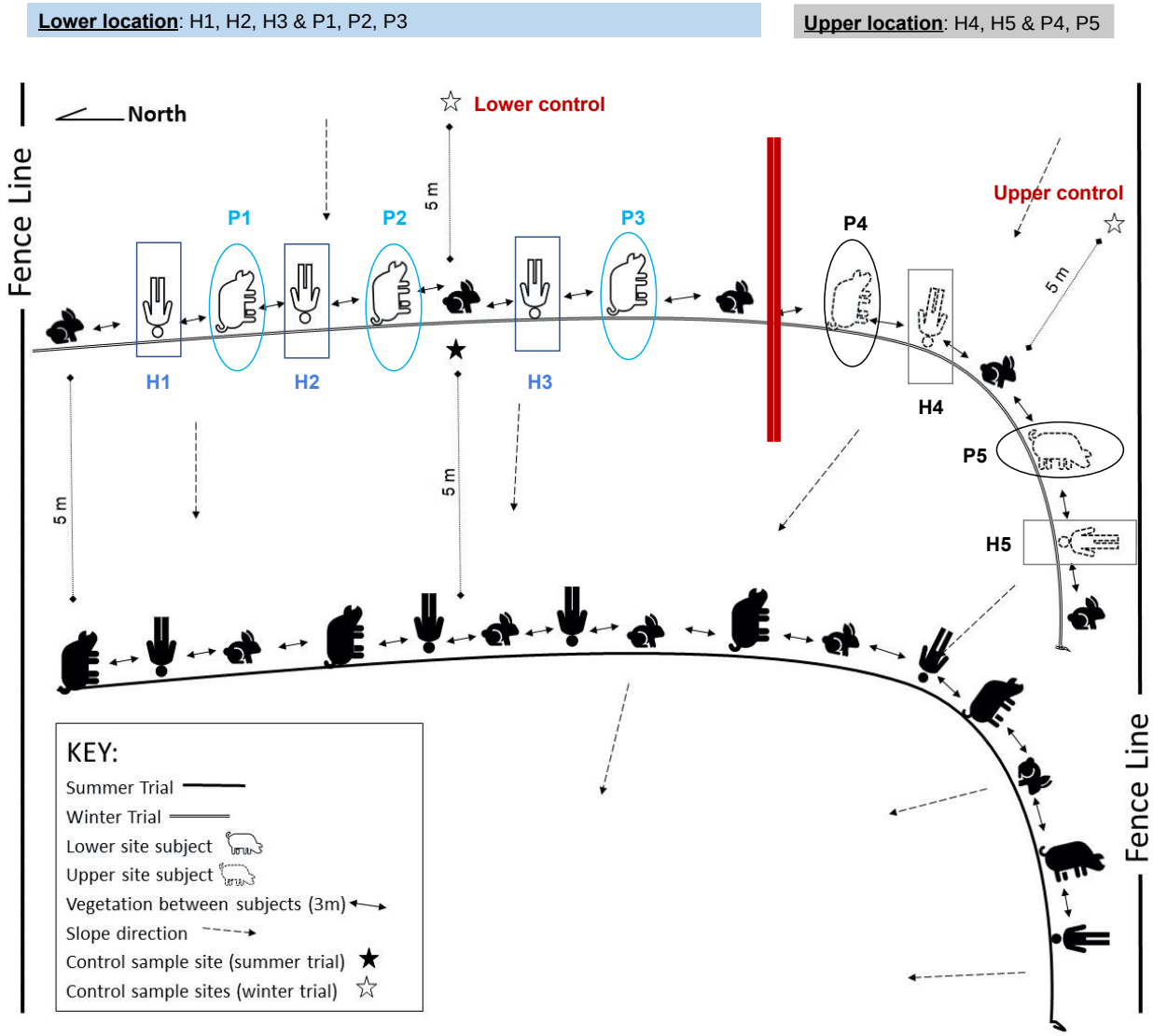

Figure 2.10 – *Study design. For the winter trial (top), five humans and five pigs were placed 3 m apart on soil surface at the Anthropology Research Facility, Knoxville, TN. Rabbit carcasses were not part of the here presented study. Soils collected from sites 5 m away from the carcasses served as controls. Four plots with two humans (H4, H5) and two pigs (P4, P5) were placed closer to a fence line ("upper site") where soils were disturbed from construction activities. Figure modified from DeBruyn et al.[26]. H = Humans, P = Pigs.*

Table 2.1 – *Overview of human and pig soil samples from all weeks and locations. Only samples from the lower location (black) were subject of metabolomics and lipidomics analyses in this chapter (Human cadavers H1, H2, H3 and Pigs P1, P2, P3).*

HUMAN SAMPLES			PIG SAMPLES			CONTROL SOIL SAMPLES		
Sample ID	**Cadaver #**	**Week**	**Sample ID**	**Cadaver #**	**Week**	**Sample ID**	**Site Location**	**Week**
HPR12140001BF	H1	Week 1	HPR12140006BF	P1	Week 1	HPR12140012BF	Lower Control	Week 1
HPR12140013BF	H1	Week 2	HPR12140018BF	P1	Week 2	HPR12140024BF	Lower Control	Week 2
HPR12140025BF	H1	Week 3	HPR12140030BF	P1	Week 3	HPR12140036BF	Lower Control	Week 3
HPR12140037BF	H1	Week 4	HPR12140042BF	P1	Week 4	HPR12140048BF	Lower Control	Week 4
HPR12140049BF	H1	Week 5	HPR12140054BF	P1	Week 5	HPR12140060BF	Lower Control	Week 5
HPR01150001BF	H1	Week 6	HPR01150006BF	P1	Week 6	HPR01150012BF	Lower Control	Week 6
HPR02150001BF	H1	Week 10	HPR01150018BF	P1	Week 8	HPR01150024BF	Lower Control	Week 8
HPR03150001BF	H1	Week 14	HPR02150006BF	P1	Week 10	HPR03150012BF	Lower Control	Week 14
HPR03150013BF	H1	Week 16	HPR03150006BF	P1	Week 14	HPR03150024BF	Lower Control	Week 16
HPR03150025BF	H1	Week 18	HPR03150018BF	P1	Week 16	HPR03150036BF	Lower Control	Week 18
HPR04150001BF	H1	Week 20	HPR03150030BF	P1	Week 18	HPR04150012BF	Lower Control	Week 20
HPR04150013BF	H1	Week 22	HPR04150006BF	P1	Week 20	HPR04150024BF	Lower Control	Week 22
HPR12140002BF	H2	Week 1	HPR04150018BF	P1	Week 22	HPR12140011BF	Upper Control	Week 1
HPR12140014BF	H2	Week 2	HPR12140007BF	P2	Week 1	HPR12140023BF	Upper Control	Week 2
HPR12140026BF	H2	Week 3	HPR12140019BF	P2	Week 2	HPR12140035BF	Upper Control	Week 3
HPR12140038BF	H2	Week 4	HPR12140031BF	P2	Week 3	HPR12140047BF	Upper Control	Week 4
HPR12140050BF	H2	Week 5	HPR12140043BF	P2	Week 4	HPR12140059BF	Upper Control	Week 5
HPR01150002BF	H2	Week 6	HPR12140055BF	P2	Week 5	HPR01150023BF	Upper Control	Week 8
HPR01150014BF	H2	Week 8	HPR01150007BF	P2	Week 6	HPR02150011BF	Upper Control	Week 10
HPR02150002BF	H2	Week 10	HPR01150019BF	P2	Week 8	HPR03150011BF	Upper Control	Week 14
HPR03150002BF	H2	Week 14	HPR02150007BF	P2	Week 10	HPR03150023BF	Upper Control	Week 16
HPR03150014BF	H2	Week 16	HPR03150007BF	P2	Week 14	HPR03150035BF	Upper Control	Week 18
HPR03150026BF	H2	Week 18	HPR03150019BF	P2	Week 16	HPR04150011BF	Upper Control	Week 20
HPR04150002BF	H2	Week 20	HPR03150031BF	P2	Week 18	HPR04150023BF	Upper Control	Week 22
HPR04150014BF	H2	Week 22	HPR04150007BF	P2	Week 20			
HPR12140003BF	H3	Week 1	HPR04150019BF	P2	Week 22			
HPR12140015BF	H3	Week 2	HPR12140008BF	P3	Week 1			
HPR12140027BF	H3	Week 3	HPR12140020BF	P3	Week 2			
HPR12140039BF	H3	Week 4	HPR12140032BF	P3	Week 3			
HPR12140051BF	H3	Week 5	HPR12140044BF	P3	Week 4			
HPR01150003BF	H3	Week 6	HPR12140056BF	P3	Week 5			
HPR01150015BF	H3	Week 8	HPR01150008BF	P3	Week 6			
HPR02150003BF	H3	Week 10	HPR01150020BF	P3	Week 8			
HPR03150003BF	H3	Week 14	HPR02150008BF	P3	Week 10			
HPR03150015BF	H3	Week 16	HPR03150008BF	P3	Week 14			

Table 2.1 – *continued*

HUMAN SAMPLES			PIG SAMPLES			CONTROL SOIL SAMPLES		
Sample ID	**Cadaver #**	**Week**	**Sample ID**	**Cadaver #**	**Week**	**Sample ID**	**Site Location**	**Week**
HPR03150027BF	H3	Week 18	HPR03150020BF	P3	Week 16			
HPR04150003BF	H3	Week 20	HPR03150032BF	P3	Week 18			
HPR04150015BF	H3	Week 22	HPR04150008BF	P3	Week 20			
HPR12140004BF	H4	Week 1	HPR04150020BF	P3	Week 22			
HPR12140016BF	H4	Week 2	HPR12140009BF	P4	Week 1			
HPR12140028BF	H4	Week 3	HPR12140021BF	P4	Week 2			
HPR12140040BF	H4	Week 4	HPR12140033BF	P4	Week 3			
HPR12140052BF	H4	Week 5	HPR12140045BF	P4	Week 4			
HPR01150004BF	H4	Week 6	HPR12140057BF	P4	Week 5			
HPR01150016BF	H4	Week 8	HPR01150009BF	P4	Week 6			
HPR02150004BF	H4	Week 10	HPR01150021BF	P4	Week 8			
HPR03150004BF	H4	Week 14	HPR02150009BF	P4	Week 10			
HPR03150016BF	H4	Week 16	HPR03150009BF	P4	Week 14			
HPR03150028BF	H4	Week 18	HPR03150021BF	P4	Week 16			
HPR04150004BF	H4	Week 20	HPR03150033BF	P4	Week 18			
HPR04150016BF	H4	Week 22	HPR04150009BF	P4	Week 20			
HPR12140005BF	H5	Week 1	HPR04150021BF	P4	Week 22			
HPR12140017BF	H5	Week 2	HPR12140010BF	P5	Week 1			
HPR12140029BF	H5	Week 3	HPR12140022BF	P5	Week 2			
HPR12140041BF	H5	Week 4	HPR12140034BF	P5	Week 3			
HPR12140053BF	H5	Week 5	HPR12140046BF	P5	Week 4			
HPR01150005BF	H5	Week 6	HPR12140058BF	P5	Week 5			
HPR01150017BF	H5	Week 8	HPR01150010BF	P5	Week 6			
HPR02150005BF	H5	Week 10	HPR01150022BF	P5	Week 8			
HPR03150005BF	H5	Week 14	HPR02150010BF	P5	Week 10			
HPR03150017BF	H5	Week 16	HPR03150010BF	P5	Week 14			
HPR03150029BF	H5	Week 18	HPR03150022BF	P5	Week 16			
HPR04150005BF	H5	Week 20	HPR03150034BF	P5	Week 18			
HPR04150017BF	H5	Week 22	HPR04150010BF	P5	Week 20			
			HPR04150022BF	P5	Week 22			

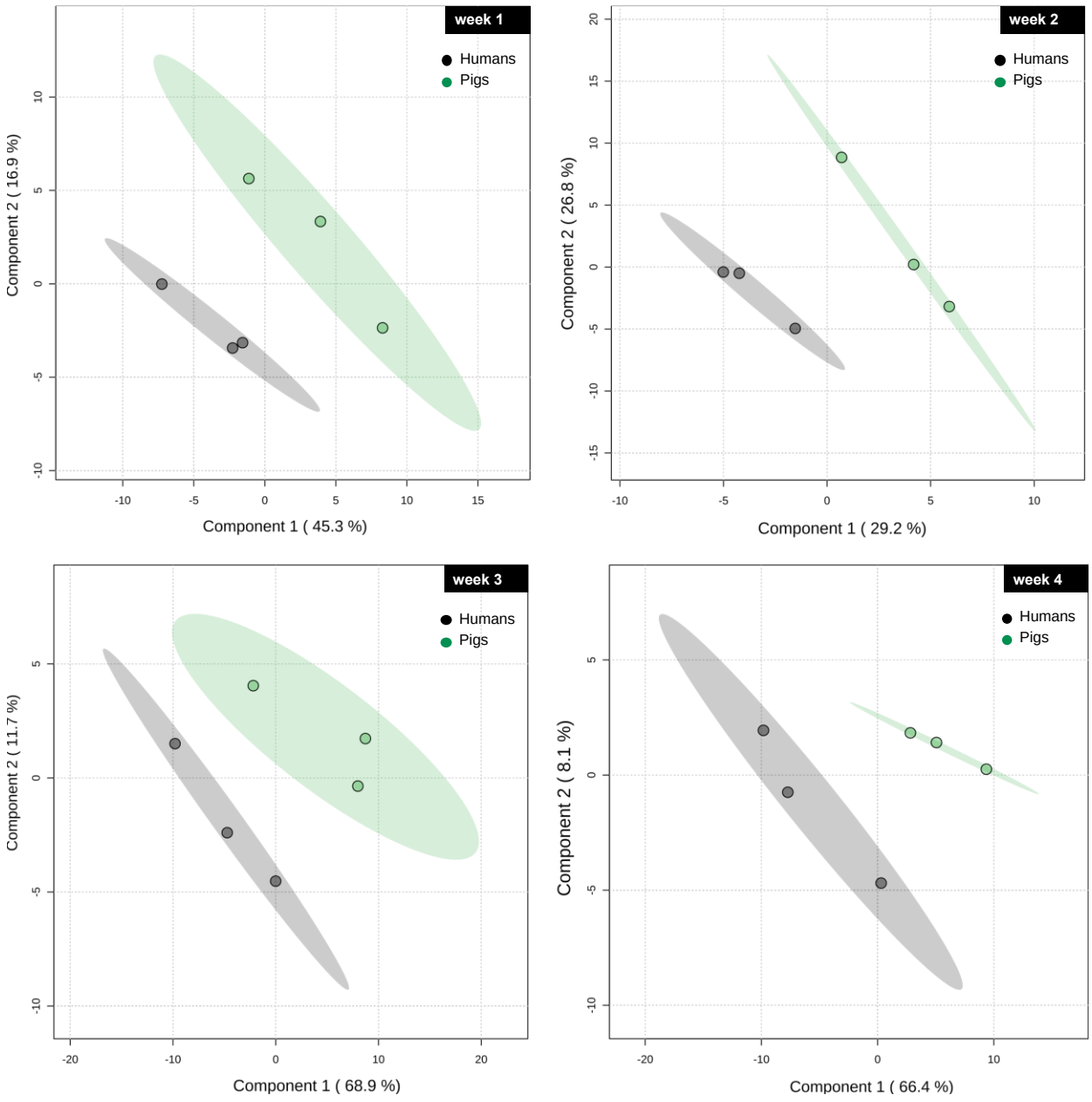

Figure 2.11 – *Postmortem metabolomics PLS-DA score plots of CDI soils from humans and pigs for all weeks.*

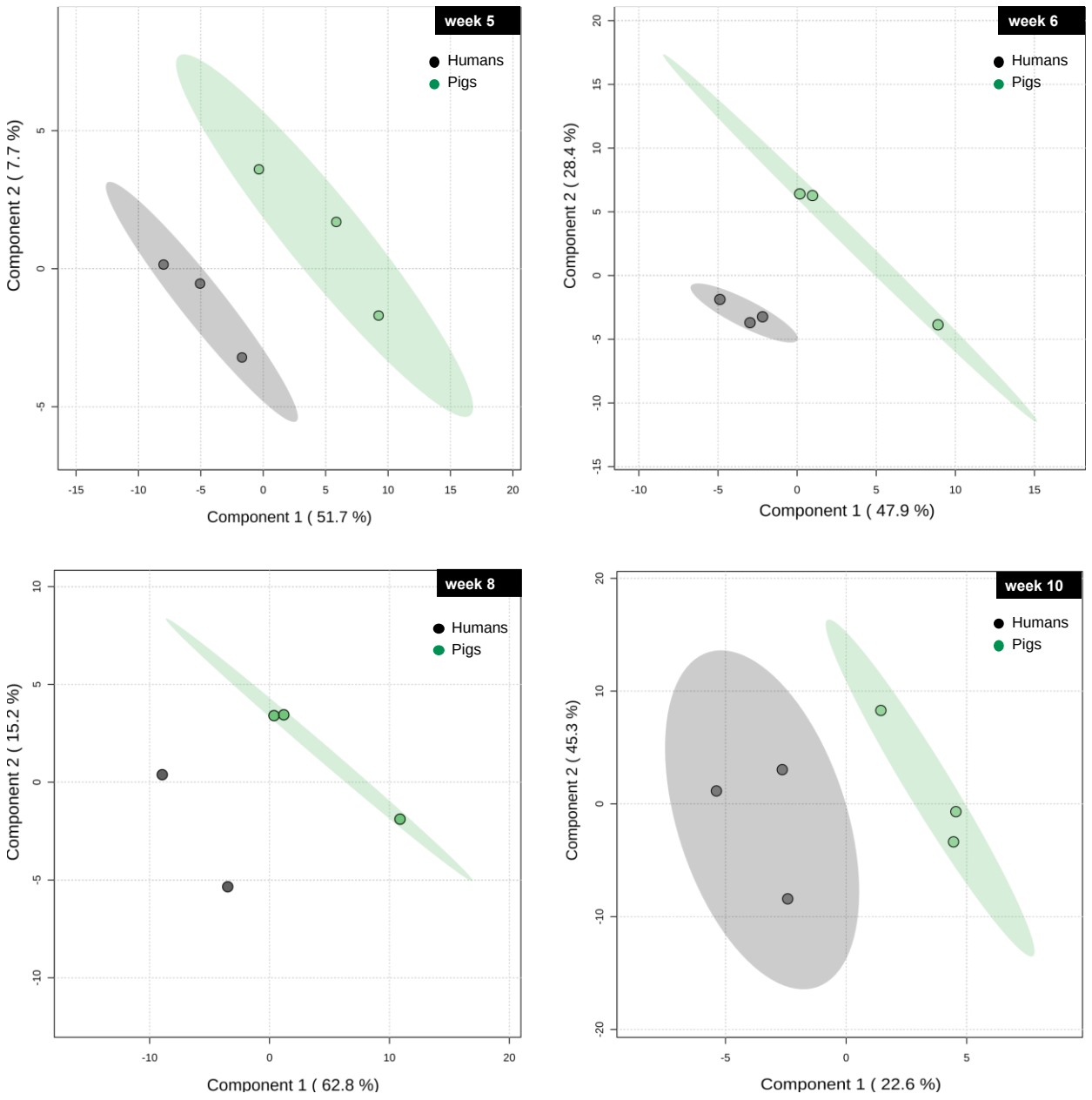

Figure 2.11 – *continued*

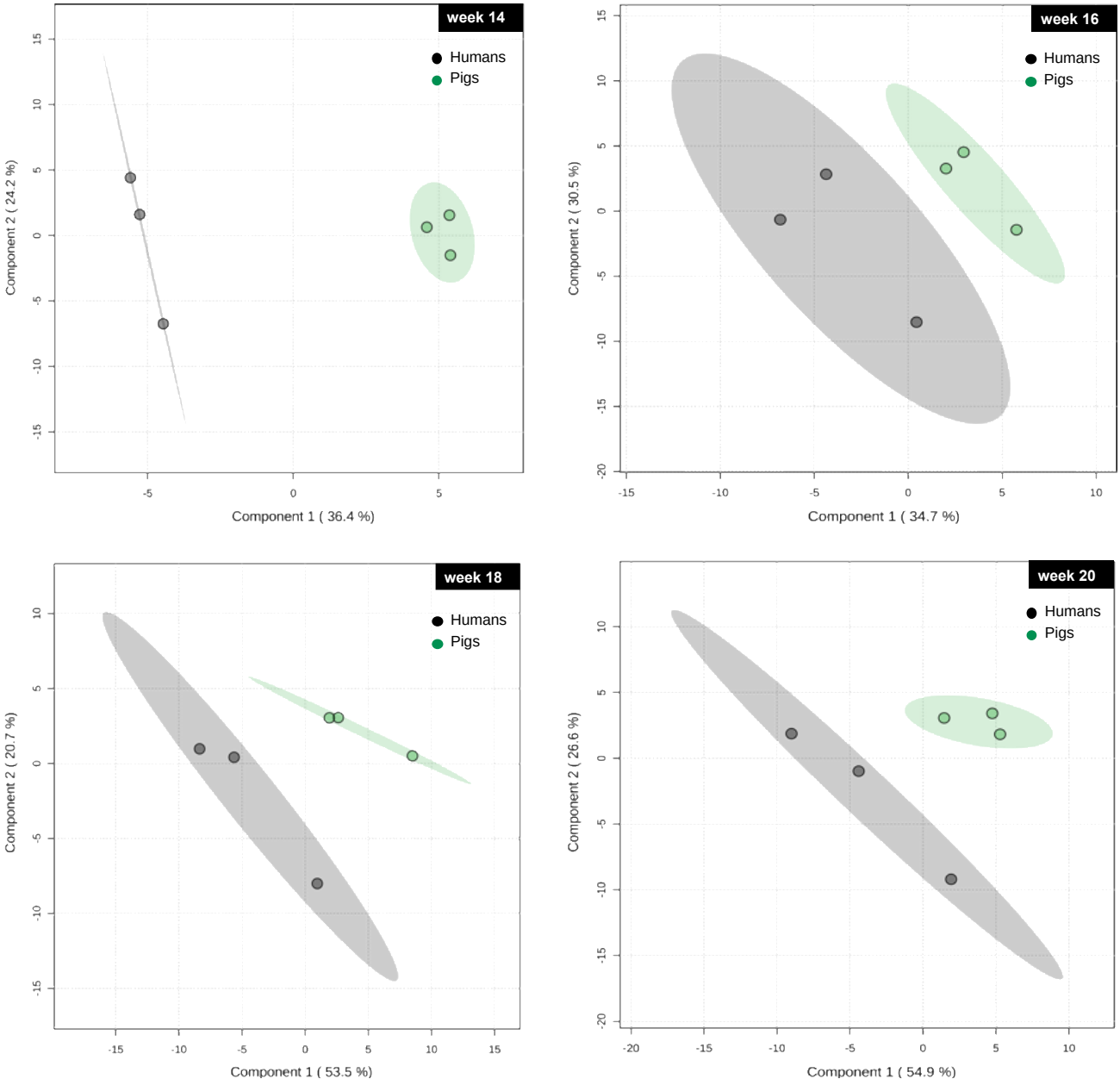

Figure 2.11 – *continued*

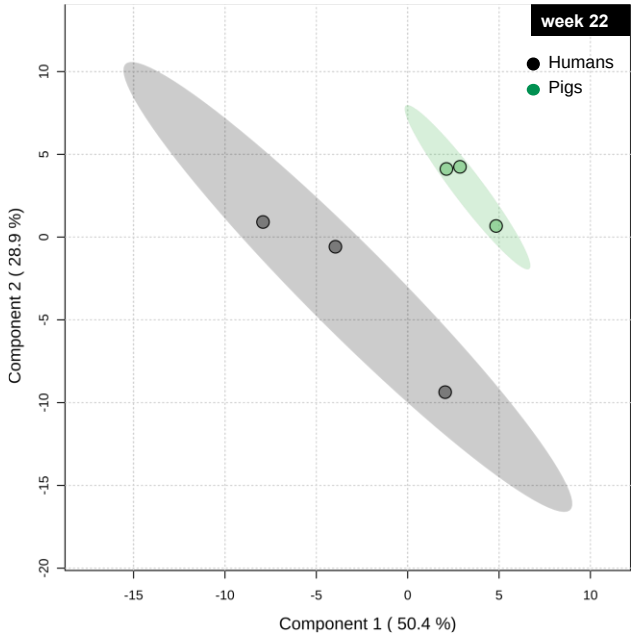

Figure 2.11 – *continued*

Table 2.2 – *VIP scores and relative abundance of metabolites in CDI soils from humans and pigs. How often each metabolite with VIP values > 1 occurred throughout the 22-week decomposition period is also listed.*

Metabolite name	Molecular weight (g/mol)	Sum relative abundance		Number of weeks VIP > 1
		Humans	*Pigs*	*Lower site*
1-Methyladenosine	281.27	2.58E+08	2.40E+08	6
2-Aminoadipate	161.16	2.02E+08	2.23E+08	5
2-Dehydro-D-gluconate	194.14	8.30E+08	3.11E+08	5
2-Oxo-4-methylthiobutanoate	148.18	2.37E+09	4.27E+09	6
2-Oxoisovalerate	116.11	7.95E+09	9.53E+09	9
3_4-Dihydroxyphenylacetate (DOPAC)	168.15	1.28E+07	5.05E+07	5
3-Methylphenylacetic acid	150.17	3.14E+08	6.07E+07	7
3-Methylthiopropionate	120.17	3.82E+07	1.14E+08	6
4-Aminobutyrate (GABA)	103.12	1.45E+08	1.03E+08	5
4-Pyridoxate	183.16	7.31E+07	7.48E+07	4
5-Hydroxyindoleacetic acid (5-HIAA)	191.18	1.39E+07	1.55E+07	3
Acetoacetate	102.09	3.66E+09	5.27E+09	6
Acetyllysine	188.22	4.12E+07	3.64E+07	4
Adenine	135.13	3.00E+08	1.76E+08	4
Adenosine	267.24	7.98E+08	8.11E+08	8
Alanine/Sarcosine	89.09	4.97E+08	5.61E+08	9
Allantoate	176.13	2.42E+07	3.11E+07	5
Allantoin	158.12	3.92E+08	2.49E+08	7
alpha-Ketoglutarate	146.10	4.10E+09	3.91E+09	4
Anthranilate	137.14	3.08E+06	9.32E+06	8
Asparagine	132.12	5.46E+06	3.40E+06	3
Aspartate	133.11	2.35E+08	3.55E+08	6
β-Hydroxy beta-methylbutyrate (HMB)	118.13	9.84E+09	9.92E+09	3
Citrate/isocitrate	192.12	1.86E+07	2.53E+07	5
Citrulline	175.19	2.81E+08	3.08E+08	7
Creatine	131.13	2.00E+06	8.04E+05	3
Creatinol-O-phosphate	197.13	1.78E+07	7.74E+06	4
Cysteate	169.16	3.33E+07	3.34E+07	6
Cytidine	243.22	4.55E+07	4.47E+07	7
D-Gluconate	196.15	1.30E+09	9.61E+08	6
Deoxyinosine	252.23	3.21E+08	3.74E+08	8
Deoxyuridine	228.20	1.57E+08	1.30E+08	6
Fumarate	116.07	1.35E+08	1.10E+08	5
Glutamate	147.13	2.26E+10	2.46E+10	5
Glutamine	146.14	2.67E+08	1.68E+08	5
Glycerate	106.08	5.46E+09	5.35E+09	5
Guanine	151.13	7.71E+06	1.13E+07	3
Guanosine	283.24	2.14E+08	2.71E+08	9
Homocysteic acid	183.18	2.86E+07	2.92E+07	2
Homoserine/Threonine	119.12	1.04E+09	1.08E+09	8
Hydroxybenzoate	152.15	7.87E+07	5.04E+07	7
Hydroxyisocaproic acid	132.16	2.41E+09	1.71E+09	8
Hypoxanthine	136.11	2.97E+08	1.62E+08	1
Indole-3-carboxylate	161.16	5.99E+07	3.20E+07	6

Table 2.2 – *continued*

Metabolite name	Molecular weight (g/mol)	Sum relative abundance		Number of weeks VIP > 1
		Humans	*Pigs*	*Lower site*
Inosine	268.23	2.35E+09	2.37E+09	5
Lactate	90.08	1.75E+10	1.94E+10	3
Leucine/Isoleucine	131.17	7.99E+09	8.56E+09	5
Lysine	146.19	5.14E+06	5.37E+06	6
Malate	134.09	7.56E+07	7.07E+07	2
Methionine	149.21	1.29E+09	1.43E+09	8
myo-Inositol	180.16	7.80E+07	9.38E+07	3
N-Acetyl-beta-alanine	131.13	7.09E+07	8.12E+07	5
N-Acetylglucosamine	221.21	1.72E+08	1.64E+08	3
N-Acetylglucosamine 1/6-phosphate	347.17	2.12E+07	2.44E+07	1
N-Acetylglutamate	189.17	6.33E+08	7.27E+08	5
N-Acetylglutamine	188.18	1.52E+07	1.63E+07	4
N-Acetylornithine	174.2	1.10E+08	1.03E+08	6
Nicotinate	123.11	3.20E+09	3.45E+09	9
Ornithine	132.16	9.93E+06	1.18E+07	7
Orotate	156.10	1.58E+08	9.73E+07	5
Pantothenate	219.23	4.98E+09	4.98E+09	5
Phenylalanine	165.19	4.22E+09	4.91E+09	7
Phenylpyruvate	164.16	3.52E+08	7.13E+08	7
Proline	115.13	4.13E+08	3.32E+08	7
Pyroglutamic acid	129.11	5.38E+10	5.37E+10	5
Pyruvate	88.06	1.59E+10	1.88E+10	7
Salicylate	138.12	1.80E+09	7.89E+08	6
Sedoheptulose 1/7-phosphate	290.16	7.28E+06	6.54E+06	4
Serine	105.09	1.36E+08	1.47E+08	6
Shikimate	174.15	2.08E+08	1.21E+08	3
sn-Glycerol 3-phosphate	172.07	8.82E+07	3.87E+07	6
Succinate/Methylmalonate	118.09	3.71E+10	3.93E+10	4
Taurine	125.15	1.58E+08	9.13E+07	5
Thymidine	242.23	6.95E+08	6.27E+08	3
Thymine	126.11	5.72E+08	5.52E+08	6
Trehalose/Sucrose	342.3	1.08E+09	1.07E+09	6
Tryptophan	204.23	1.20E+08	1.05E+08	2
Tyrosine	181.19	9.68E+08	9.71E+08	5
UDP-N-acetylglucosamine	607.35	2.67E+07	2.27E+07	9
Uracil	112.09	2.63E+09	2.69E+09	6
Uridine	244.20	8.57E+08	8.70E+08	4
Valine	117.151	4.72E+09	5.02E+09	8
Vanillin	152.15	4.24E+08	4.55E+08	1
Xanthine	152.11	8.34E+08	4.31E+08	1
Xanthosine	284.23	3.24E+07	3.01E+07	3

Table 2.3 – *Summary of all metabolites significantly altered in abundance in mammalian CDI soils. Denoted variation refers to a significant increase* (↑) *of metabolite abundances in the corresponding CDI soils (humans vs. pigs).*

	Variation	Metabolites significantly altered in relative abundance
week 1	**Humans** ↑	Alanine/Sarcosine, Deoxyinosine
	Pigs ↑	-
week 2	**Humans** ↑	2-Oxo-4-methylthiobutanoate, Phenylpyruvate
	Pigs ↑	-
week 3	**Humans** ↑	-
	Pigs ↑	3-Methylphenylacetic acid, beta-Hydroxy beta-methylbutyrate (HMB), Lactate, sn-Glycerol 3-phosphate
week 4	**Humans** ↑	Allantoin, Anthranilate, beta-Hydroxy beta-methylbutyrate (HMB), Cysteate, Deoxyuridine, Hydroxybenzoate, Hydroxyisocaproic acid, N-Acetylornithine, Nicotinate, Pyroglutamic acid, Tryptophan
	Pigs ↑	-
week 5	**Humans** ↑	Fumarate, Nicotinate, Orotate, Pyroglutamic acid, Salicylate
	Pigs ↑	-
week 6	**Humans** ↑	3-Methylphenylacetic acid
	Pigs ↑	-
week 8	**Humans** ↑	1-Methyladenosine, 2-Oxo-4-methylthiobutanoate, 2-Oxoisovalerate, 4-Aminobutyrate (GABA), 4-Pyridoxate, Acetyllysine, Alanine/Sarcosine, Anthranilate, Creatinol-O-phosphate, Cytidine, Deoxyinosine, Deoxyuridine, Glutamine, Guanosine, Homoserine/Threonine, Hydroxyisocaproic acid, Hypoxanthine, N-Acetylglucosamine, N-Acetylglutamate, N-Acetylornithine, Nicotinate, Orotate, Phenylpyruvate, Pyroglutamic acid, Salicylate, sn-Glycerol 3-phosphate, Taurine, Thymine, UDP-N-acetylglucosamine, Uracil, Uridine, Valine, Xanthine, Xanthosine
	Pigs ↑	-
week 10	**Humans** ↑	-
	Pigs ↑	2-Oxo-4-methylthiobutanoate
week 14	**Humans** ↑	-
	Pigs ↑	2-Aminoadipate, 4-Aminobutyrate (GABA), Citrulline, Cytidine, Guanosine, Hydroxyisocaproic acid, Indole-3-carboxylate, Leucine/Isoleucine, Ornithine, Phenylalanine
week 16	**Humans** ↑	-
	Pigs ↑	Fumarate
week 18	**Humans** ↑	Creatine
	Pigs ↑	2-Oxo-4-methylthiobutanoate, Alanine/Sarcosine, Aspartate, Lysine, Serine
week 20	**Humans** ↑	Taurine
	Pigs ↑	2-Oxo-4-methylthiobutanoate, Acetoacetate, Deoxyinosine, Guanosine, Ornithine
week 22	**Humans** ↑	-
	Pigs ↑	Acetoacetate, Aspartate, Glutamate

Table 2.4 *– Detected lipids and their corresponding lipid classes with relative intensities in human and pig decomposition soils. VIP scores are a result of weekly PLS-DA analyses.*

Lipid Class	Lipid	Sum rel. intensities all weeks (soils)		Lower site
		Humans (H1, H2, H3)	Pigs (P1, P2, P3)	Number of weeks VIP > 1
Monogalactosyldiacylglycerol (MGDG)	MGDG (28:0)	2.65E+06	3.53E+06	5
	MGDG (28:6)	1.64E+06	1.51E+06	4
	MGDG (30:0)	1.43E+07	1.48E+07	5
	MGDG (30:1)	3.56E+06	3.94E+06	6
	MGDG (30:2)	2.58E+06	3.00E+06	5
	MGDG (32:0)	1.29E+07	1.42E+07	6
	MGDG (32:1)	1.63E+07	1.70E+07	6
	MGDG (32:2)	6.51E+06	6.80E+06	6
	MGDG (32:4)	3.87E+06	5.51E+06	5
	MGDG (34:3)	1.06E+07	1.24E+07	5
	MGDG (34:4)	1.19E+06	1.32E+06	7
	MGDG (36:3)	2.13E+07	2.61E+07	5
	MGDG (36:4)	2.90E+07	3.09E+07	4
	MGDG (36:5)	1.17E+07	1.21E+07	5
	MGDG (38:2)	4.97E+07	5.64E+07	5
	MGDG (38:3)	6.76E+07	7.21E+07	3
	MGDG (38:4)	6.99E+07	7.21E+07	2
	MGDG (38:5)	5.89E+06	7.25E+06	6
	MGDG (38:6)	3.90E+05	3.62E+05	8
	MGDG (40:2)	2.59E+06	2.88E+06	7
	MGDG (40:3)	8.01E+06	8.77E+06	5
	MGDG (40:4)	1.73E+08	1.77E+08	3
	MGDG (40:5)	1.66E+07	1.87E+07	4
	MGDG (40:6)	2.03E+07	2.19E+07	1
	MGDG (42:4)	6.75E+07	6.69E+07	5
	MGDG (42:5)	2.66E+06	2.70E+06	7
	MGDG (42:6)	1.41E+06	1.64E+06	9
Phosphatidic acid (PA)	PA (40:4)	1.01E+07	1.17E+07	3
	PA (40:5)	1.00E+06	1.12E+06	6
	PA (42:4)	2.32E+07	2.77E+07	6
	PA (42:5)	2.80E+07	2.99E+07	6
	PA (42:6)	1.17E+07	1.21E+07	5
	PA (44:10)	1.56E+06	1.64E+06	3
	PA (44:3)	2.20E+06	2.54E+06	5
	PA (44:4)	4.68E+07	5.60E+07	5
	PA (44:5)	6.74E+07	7.07E+07	3
	PA (44:6)	6.99E+07	7.02E+07	2
	PA (44:7)	5.21E+06	5.94E+06	8
	PA (44:8)	3.52E+05	3.62E+05	7
Phosphatidylethanolamine (PE)	PE (28:0)	2.64E+06	4.27E+06	5
	PE (32:0)	1.45E+07	1.74E+07	5
	PE (32:2)	3.37E+07	4.51E+07	7
	PE (34:0)	1.01E+07	1.31E+07	3
	PE (34:1)	2.33E+07	2.61E+07	4
	PE (34:2)	7.57E+06	6.55E+06	6
	PE (34:3)	4.40E+06	4.61E+06	7
	PE (36:1)	5.36E+06	5.08E+06	6
	PE (36:2)	5.38E+07	5.92E+07	8
	PE (36:3)	8.16E+06	7.81E+06	8
	PE (36:4)	4.63E+06	4.12E+06	6
	PE (38:2)	5.61E+06	5.34E+06	6
	PE (38:5)	2.58E+06	3.36E+06	3
	PE (38:6)	2.00E+06	2.74E+06	4
	PE (42:4)	3.01E+06	4.18E+06	8

Table 2.4 – *continued*

Lipid Class	Lipid	Sum rel. intensities all weeks (soils)		Lower site
		Humans (H1, H2, H3)	Pigs (P1, P2, P3)	Number of weeks VIP > 1
	PE (44:4)	1.73E+06	2.49E+06	5
Phosphatidylglycerol (PG)	PG (32:0)	1.88E+07	2.15E+07	6
	PG (40:10)	1.95E+06	2.51E+06	3
	PG (40:7)	1.96E+06	2.04E+06	8
	PG (42:10)	1.56E+06	2.26E+06	4
	PG (44:7)	1.94E+06	2.46E+06	6
	PG (44:8)	2.60E+06	2.79E+06	8
Phosphatidylinositol (PI)	PI (32:0)	4.23E+06	4.94E+06	5
	PI (32:1)	3.30E+06	4.05E+06	5
	PI (34:0)	5.26E+06	6.22E+06	6
	PI (34:1)	9.47E+06	1.02E+07	6
	PI (34:2)	6.79E+06	6.87E+06	5
	PI (36:0)	1.81E+06	1.87E+06	4
	PI (36:1)	1.51E+06	1.62E+06	4
	PI (36:2)	3.78E+06	3.90E+06	6
	PI (36:3)	1.69E+06	1.97E+06	7
Phosphatidylserine (PS)	PS (34:0)	2.04E+07	2.28E+07	3
	PS (34:2)	4.41E+06	5.47E+06	8
	PS (34:4)	1.40E+06	1.89E+06	7
	PS (36:0)	1.49E+08	1.76E+08	5
	PS (36:1)	3.23E+07	2.99E+07	4
	PS (36:2)	2.57E+06	3.89E+06	5
	PS (38:1)	5.10E+07	5.27E+07	3
	PS (38:5)	3.01E+06	4.10E+06	5
	PS (40:1)	2.42E+08	2.41E+08	4
	PS (40:2)	7.43E+06	6.45E+06	5
	PS (40:4)	2.57E+06	2.81E+06	5
	PS (40:5)	4.55E+06	4.97E+06	5
	PS (40:6)	3.11E+06	3.37E+06	5
	PS (42:5)	6.60E+05	7.74E+05	6
	PS (42:6)	1.81E+06	1.75E+06	8

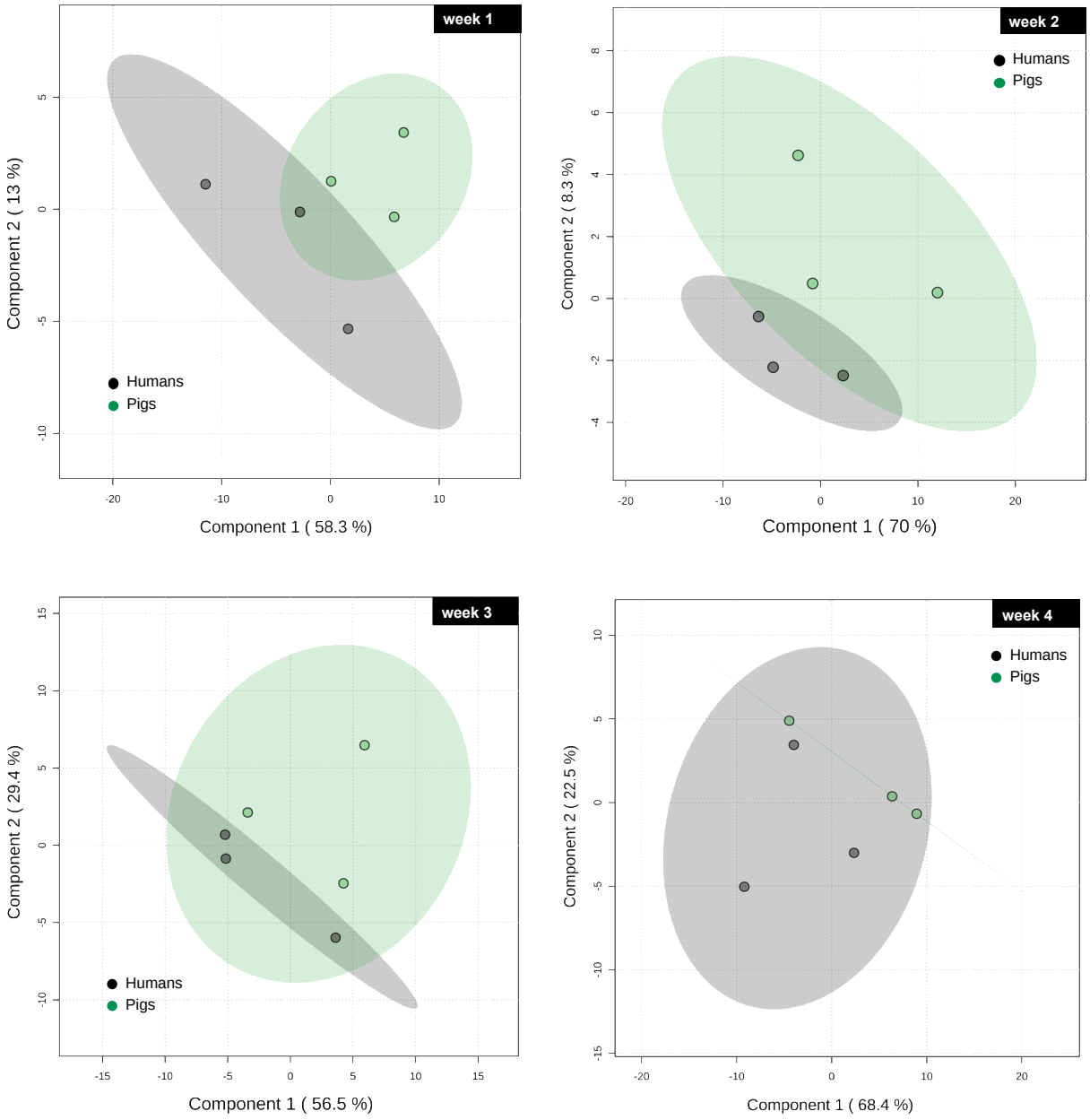

Figure 2.12 – *PLS-DA of postmortem lipidomics of CDI soils from humans and pigs for all weeks.*

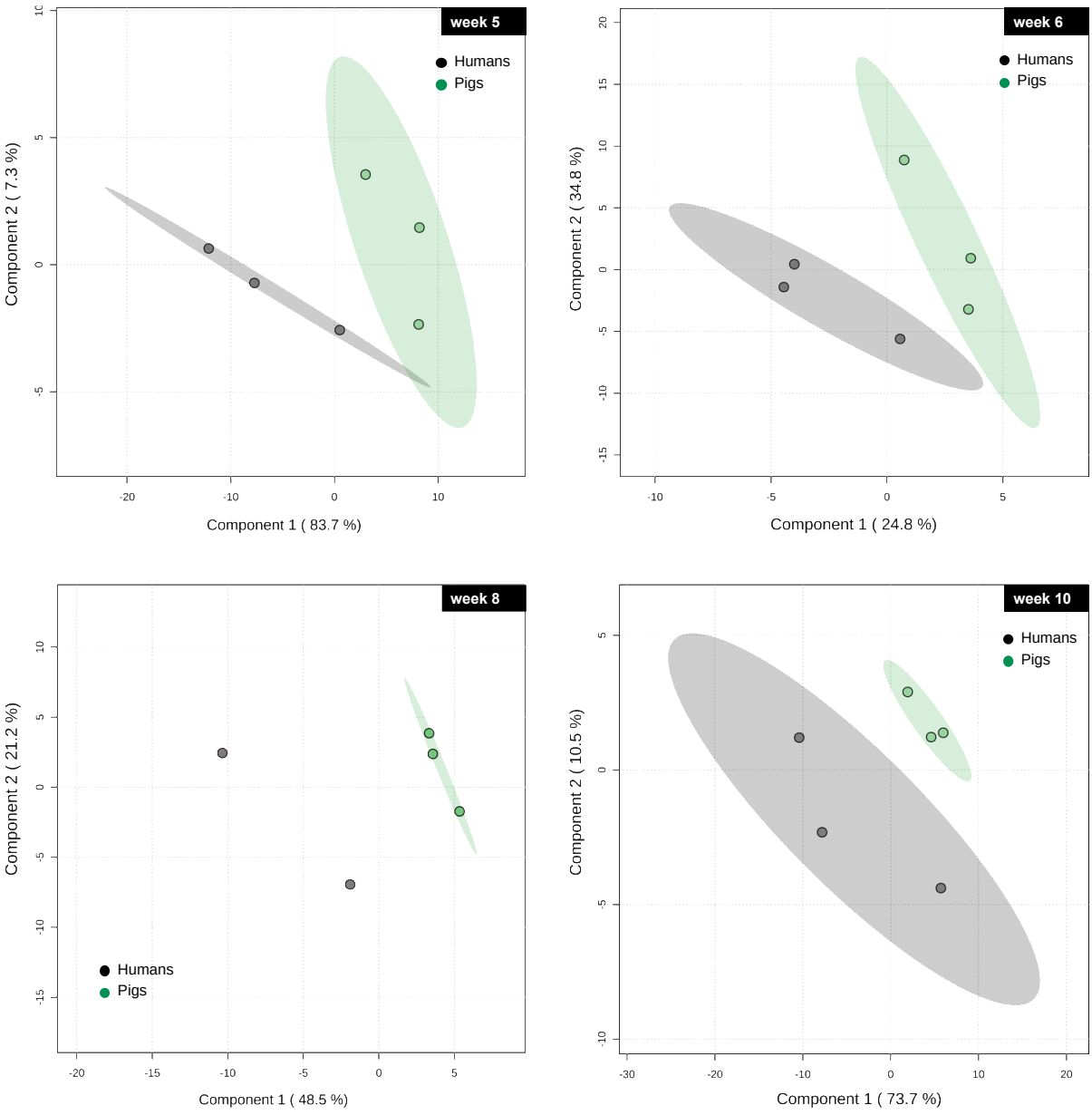

Figure 2.12 – *continued*

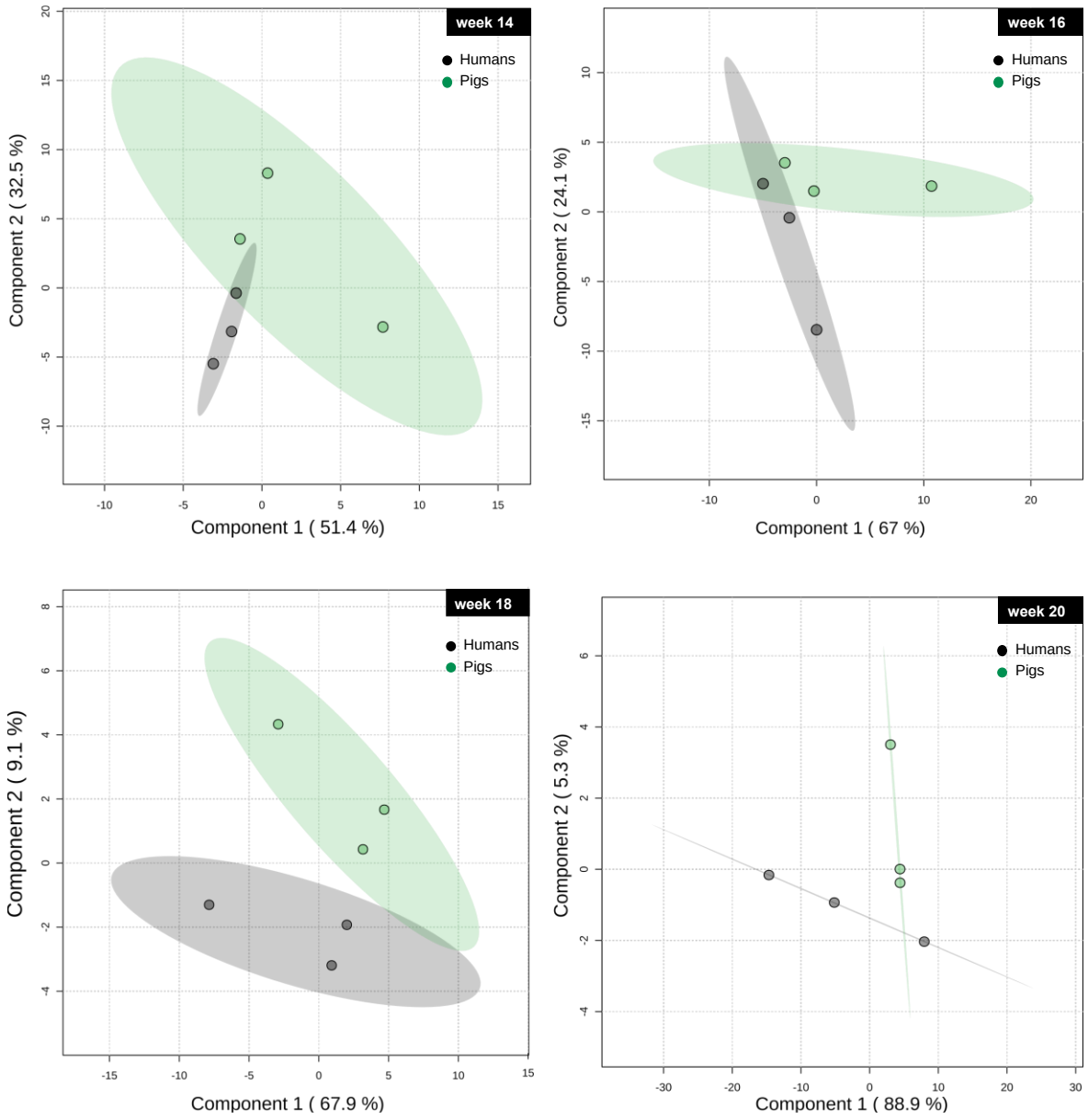

Figure 2.12 – *continued*

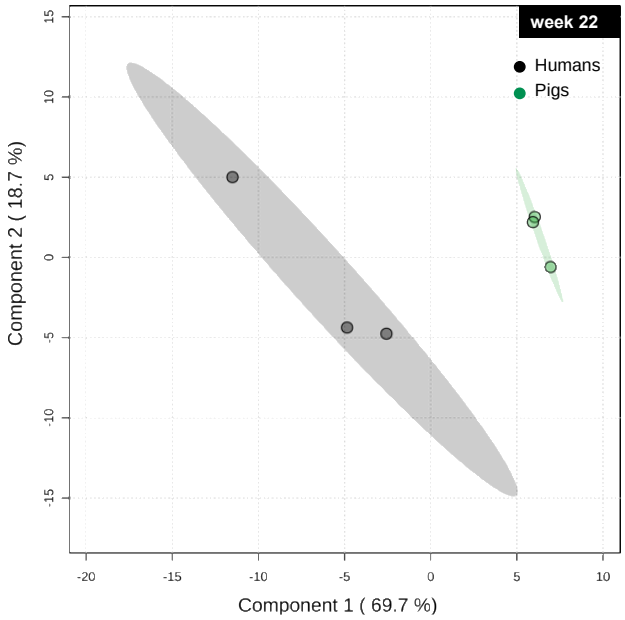

Figure 2.12 – *continued*

CHAPTER III: INTRINSIC DRIVERS OF HUMAN DECOMPOSITION – DRUG TRACING IN POSTMORTEM SPECIMENS AND DISEASE IMPACTS ON THE HUMAN POSTMORTEM METABOLOME

PREFACE

After elaborating in the previous two chapters on metabolic signatures of (a) a burial environment and (b) human and non-human surface carcass decomposition, this final chapter presents one additional variable worth investigating – intrinsic drivers of human decomposition.

Upon arrival at the University of Tennessee, Knoxville, I had the pleasure of meeting Dr. Dawnie Steadman (Department of Anthropology, UTK). She is not only the director of the Anthropology Research Facility (ARF) but moreover a highly recognized researcher in the field of forensic anthropology. In a collaborative effort between the Small Molecule Mass Spectrometry Core (BSMMSC) of UTK's chemistry department, Dr. Steadman, and Dr. DeBruyn from the Department of Biosystems Engineering & Soil Science at UTK, a project spanning almost 4.5 years was established to investigate the effects of perimortem underlying health conditions and toxicological loadings on human decomposition trajectories. As shown previously, the versatility of postmortem metabolomics to answer forensically relevant research questions both across matrices (chapter I; bone vs soil) and species (chapter II; humans vs pigs), makes it a powerful analytical platform in forensic science. Broadening the knowledge obtained from the previous chapters, this final chapter applies toxicological screening analyses and global untargeted metabolomics studies to various postmortem specimens including serum, larvae, decomposition fluid, as well as soil. With this, we aimed to not only improve our understanding of forensic taphonomy from a metabolic perspective but also provide a preliminary assessment of the impacts of perimortem health conditions (intrinsic factors) on the postmortem metabolome.

A version of this chapter is currently in preparation to be submitted to the peer-reviewed journal Forensic Science International (FSI).

3.1 ABSTRACT

Several years of research were dedicated at the 3-acre outdoor laboratory, known as the Anthropology Research Facility (ARF) in Knoxville, TN, USA, to investigate intrinsic drivers of human decomposition to ultimately draw conclusions about possible effects on time since death estimations. Our postmortem toxicological screenings illustrate how drugs and drug metabolites can be traced from a decomposing cadaver through several matrices including the surrounding soil ecosystem. In addition, comprehensive postmortem metabolomics of biological specimens provided (a) insights into the highly dynamic biochemical environment of decomposing bodies, (b) postmortem matrix-specific metabolic signatures, (c) a group of metabolites potentially useful as decomposition biomarkers in terrestrial, surface decomposition, and (d) an assessment of possible impacts of perimortem health conditions on the postmortem metabolome.

3.2 INTRODUCTION

The stages of human decomposition and the associated changes occurring in a body after death are defined elsewhere in this dissertation. Intrinsic factors are among variables that impact decomposition trajectories, yet they have rarely been subject of research. As decomposition rates of donors placed in identical environmental conditions appear to be verifiably different[119, 151], there is a need to better understand the impacts of medication on key drivers of soft tissue decomposition (insects, scavengers, and soil microbial communities). *Hayman and Oxenham* monitored two decomposing individuals with different perimortem disease history in a shed at the Forensic Research Facility of the Texas State University in San Marcos, USA. A slower rate of decomposition, no abdominal bloating, and less distinct insect activity were characteristic features for a cadaver with cancer as opposed to a donor with diabetes[151]. Underlying health conditions and/or specific perimortem medical treatments (insulin vs chemotherapy) seemed to be the most plausible cause for differential decomposition dynamics. In addition, according to *Skopyk et al.,* perimortem use of antibiotics could also impact rates of decay by altering the pre-colonization interval of insects[152]. A diminished microflora resulting from the use of such drugs could have induced a prolonged bloating stage and the lack of a phenomenon called marbling[152]. The latter was observed on two donors with a history of antibiotic treatment[152]. Evidence of differential decomposition patterns among humans has also been observed at the Anthropology Research Facility in Knoxville, TN. The above-mentioned work by *Dautartas et al.* described remarkably higher variability in decomposition patterns for simultaneously placed human donors compared to more similar rates of decomposition within the pig cohort[116]. While external conditions were identical throughout the study, the authors attributed the intra-species variation among human donors to intrinsic factors. Collectively, these studies unfold the existing knowledge gap in forensic taphonomy and the urge for human cohort studies to evaluate the impacts of intrinsic variables on decomposition in greater detail.

The metabolic fate of a drug in a living organism is generally defined by detoxification and elimination. After death, various other factors influence xenobiotic metabolism. Postmortem drug redistribution, for instance, is responsible for site- and

time-dependent concentration variations due to the passive release of drugs from drug reservoirs such as the stomach, liver, or myocardium[153]. The lack of blood circulation after death inhibits the drug transport to detoxifying organs, yet enzymes present in the blood, or those that are released by apoptotic cells, might still be able to degrade certain drugs[154]. Likewise, there is evidence of microbial-mediated alteration of drug concentrations: morphine concentrations for instance can increase postmortem due to the hydrolysis of morphine glucuronides to free morphine – a step performed by bacterial β-glucuronidases[155]. While all these factors are of great importance for forensic toxicology, the purpose of the herein presented drug screenings was directed toward a proof-of-concept study aiming to be among the first to detect drugs in multiple human cadaveric specimens (serum, decomposition fluid, soil, and larvae).

In this chapter, ultra-high-performance liquid chromatography high-resolution mass spectrometry (UHPLC-HRMS) was used to enhance the understanding of forensic taphonomy from a biochemical point of view. Postmortem metabolomics studies have emerged as a powerful tool to investigate biochemistry after death; however, they are rarely utilized on human subjects in a broad, forensically relevant framework. Previous efforts have centered around correlating specific breakdown products of macromolecules with the time since death[42, 44, 45]. For example, *Elmjsö et al.* proposed the applicability of postmortem metabolomics in death investigations when they identified pneumonia biomarkers after death that coincided with known clinically relevant antemortem compounds in patients suffering from such conditions[156]. Although the usefulness of various polysaccharides, steroids, nucleosides, and amino acids as biochemical markers for postmortem interval (PMI) estimations has sporadically been suggested by researchers[42, 44, 45], such work is still in its infancies and seldomly uses the total capability of postmortem metabolomics studies to its fullest. The novelty and uniqueness of our work lie in the complex machinery of cadaveric specimens used for both ‘omics’ and toxicological analyses, with the secondary aim of teasing apart influences of underlying medical conditions on the metabolic dynamics after death.

3.3 EXPERIMENTAL SECTION

3.3.1 Site description

This research was conducted between 2017-2021 on human donors, obtained through the University of Tennessee's Body Donation Program of the Forensic Anthropology Center (FAC), at the 3-acre woodland outdoor laboratory known as Anthropology Research Facility (ARF) in Knoxville, Tennessee, USA. Founded in 1980 by Dr. William Bass, the ARF is dedicated to the study of decomposition processes in an outdoor setting. All subjects in this study were positioned unclothed and uncaged on soil surface in randomly chosen sectors of the ARF to decompose naturally.

3.3.2 Donor collection

For this study, eligible donors had to have a perimortem medication record, no open wounds and no autopsy or embalming performed. All donors had natural causes of death. A total of n = 22 human subjects including n = 12 males and n = 10 females with an age range of 40 to 91 years were utilized. Donor characteristics such as gender, age, medical history, and prescribed drugs that were given during the last two weeks of life were recorded for each individual (Appendix Table 3.1). The medication list was available for 18 out of 22 donors. Donor Tox 014 (male, 74 years, white) was excluded from the study. He was placed on a backfilled soil site and because of this, the soil was visibly different in color and density compared to the surrounding area meaning no appropriate soil control could be obtained. A donor was unenrolled after it completed active decay as determined by the cessation of body fluids exuding from the trunk. To analyze possible disease impacts, donors were categorized based on the information listed in Appendix Table 3.1 into four major disease classes: diabetes, cancer, respiratory, and cardiovascular conditions.

3.3.3 Sample collection and sampling strategy

Samples collected for chemical analyses comprised serum, soils, larvae, and body fluids. All samples were flash-frozen in liquid nitrogen and analyzed for their toxicological and metabolic composition. Serum samples were collected at donor intake.

Approximately 4 ml central (aortic) and peripheral (femoral) blood was sampled using a veterinary spinal needle. Serum was obtained by allowing the blood to clot for 30-60 minutes at room temperature. After centrifugation (15 min at 2000 rpm), the resulting supernatant was transferred into new cryovials for storage in liquid nitrogen until toxicological analysis.

After donor placement, soil, larvae, and decomposition fluid samples were taken periodically as described below until unenrollment. Decomposition fluid and larvae sampling occurred only in case a sufficient fluid pool or larval mass was present. Both matrices were sampled from various anatomical locations around the body, immediately flash-frozen, and stored at -80 °C until analysis for metabolite and drug profiling. For fluids, a sterile 30 ml syringe was inserted into the fluid pool to collect up to 10 ml which was subsequently aliquoted into 2 ml cryovials. Insects were collected using sterile tweezers and also placed into 2 ml cryovials prior to flash-freezing. Larvae and fly samples were measured and by the entomologists Dr. Kristi Bugajski and Dr. Charity Owings.

Soil (10 g total) was obtained from within the cadaver decomposition island (CDI) using a sterile, 10 mm syringe with the top cut off. From around the cadaver, five to eight soil cores (5 cm depth) were sampled and homogenized in Whirl-pack bags. Non-soil debris such as roots or leaves of a size larger than 2 mm were manually removed using sterile tweezers prior to being flash-frozen. In addition, control soils sampled at every sampling time point from an area of approximately one meter away from each donor served as negative control.

While insect and fluid samples were sampled only when present, soil sampling time points were based on Accumulated Degree Hours (ADH) increments. ADH is a cumulative measurement of energy produced by ambient heat that drives developmental processes of insects and bacteria. At placement, small on-site data loggers placed in close proximity to donors allowed for local hourly records of temperature and relative humidity for the calculation of ADH. Decomposition and control soils were sampled upon cadaver placement (0 ADH) at 100, 250, 500, 750, 1,000, and 2,000 ADH, and thereafter at 500 ADH increments until unenrollment of the donor (no fluid excretion from the trunk). The chosen ADH increments roughly captured human decomposition independent of

season. However, some sampling time points were missed due to extreme weather, the COVID-19 pandemic, or holidays.

3.3.4 Supplement data sets – Collaborative efforts

Aside from the sample collection mentioned above, a collection of other data sets (field and laboratory data) was gathered in a collaborative effort. Field and entomological data interpretation were performed by the Department of Anthropology, UTK. Donors were observed at the ARF twice daily (mornings and afternoons) using field protocols and a Nikon D5200 digital camera to capture morphological changes with the progress of decomposition. Scavenging and insect activity was also recorded. Scavenging behavior was monitored using infrared, motion-sensing game cameras positioned near each body. In addition, the Total Body System (TBS) scoring method by *Megyesi et al.* was used to assess morphological changes throughout different regions of the decomposing body[132]. It was used to evaluate bloating, tissue discoloration, and tissue loss on the head/neck, extremities, and trunk of cadavers. The entomologists involved in the project identified the collected insects based on their developmental stage in the life cycle (1st, 2nd, 3rd instar, or migrating larvae). Microbial and soil physicochemical analyses were performed on collected fluid and soil samples in Dr. DeBruyn's laboratory at the Department of Biosystems Engineering & Soil Science, UTK. Such analyses included for instance DNA extractions (for 16S rRNA sequencing), soil moisture, pH, electrical conductivity, as well as microbial respiration measurements.

3.3.5 Experimental procedures

3.3.5.1 Untargeted postmortem metabolomics

3.3.5.1.1 Extraction method

Metabolites were extracted in triplicates from 50-70 mg soil, 30-50 mg larvae, and 50-70 mg decomposition fluid using a procedure adapted from *Lu et al.*[83]. For a detailed extraction method description, please refer to chapter I, section 1.3.3. To assure extraction and instrumental reproducibility, samples were spiked with four stable isotope-

labeled internal standards, namely orotate-15N2, vanillin-13C6, glutamate-d5, and alanine-d4 in a concentration of 100 nM.

3.3.5.1.2 Ultra-high-performance liquid chromatography-high-resolution mass spectrometry (UHPLC-HRMS)

For UHPLC-HRMS analyses a Synergi 2.5 micron reverse-phase Hydro-RP 100, 100 x 2.00 mm LC column (Phenomenex, Torrance, CA) was used. The Exactive™ Plus Orbitrap Mass Spectrometer (Thermo Scientific, Waltham, MA) was operated in negative electrospray ionization (ESI) mode with parameters listed in chapter I, section 1.3.4. Solvent A consisted of 97:3 HPLC grade water:methanol, 10 mM tributylamine, and 15 mM acetic acid. Solvent B was HPLC-grade methanol. The gradient was set as follows: 0 to 5 min: 0% B, 5 to 13 min: 20% B, 13 to 15.5 min: 55% B, 15.5 to 19 min: 95% B, 19 to 25 min: 0% B. All other parameters are identical to those listed in chapter I.

3.3.5.2 Postmortem toxicology

Commercially available toxicology standard stocks (diluted in methanol, >99% purity) were purchased from Restek, Bellefonte, PA. Nicotine, morphine, lorazepam, oxycodone, and fentanyl were purchased individually. Two pharmaceutical drug mixtures containing (a) acetaminophen, caffeine, carbamazepine, ciprofloxacin HCL, erythromycin, fluoxetine HCl, sulfamethoxazole, trimethoprim, and (b) gemfibrozil, ibuprofen, naproxen, triclosan were also purchased. Standards were used for method validation purposes, to ensure extraction and instrumental reproducibility, as well as for quantitation. Prior to extractions, standard solutions were diluted to working stocks. Quantitative analysis was performed using external calibration curves. In brief, each methanol-based standard mixture was diluted with methanol to a concentration of 65 ng/ml. Following, serial dilutions were prepared to a minimum of 1 pg/ml. Extractions were carried out using 100 µl serum. All other matrices were extracted as described in section 3.3.5.1.1 and used thereafter for toxicological screens. Next, 5 µl of the samples were injected onto a Raptor Biphenyl column (100mm × 2.1 mm ID) with 2.7-µm particle size in combination with a guard column (Raptor Biphenyl EXP guard column cartridge 5mm, 2.1mm ID, 2.7-µm). Separation was performed using the following mobile phases and

gradient: (A) water + 0.1% formic acid + 2 mM ammonium formate, (B) methanol + 0.1% formic acid + 2 mM ammonium formate; t = 0 min, 5% B; t = 9 min, 100% B, t = 10 min, 100% B; t = 10.1 min, 5% B; t = 12 min, 5% B. A consistent flow rate was maintained at 0.6 ml/ min. The eluent was introduced into a Q Exactive™ Plus Hybrid Quadrupole-Orbitrap via positive electrospray ionization (heated ESI) using the parameters: sheath gas flow = 25 psi, auxiliary gas unit flow = 10, spray voltage = 3.0 kV. The capillary heater temperature was set to 300 °C. A full scan MS analysis (*m/z* 70-1,050) was performed, while samples were analyzed for a total duration of 12 minutes with a resolution of 140,000. The AGC (acquisition gain control) target was set to $3e^6$ ions.

3.3.5.3 Data processing and statistical analyses

LC-MS raw files generated by Xcalibur were converted and processed in MAVEN (Metabolomic analysis and visualization engine)[85, 86] in the same manner as mentioned above (chapter II, section 2.3.2.2.3). Known metabolite spectra from postmortem metabolomics experiments were manually selected using an in-house metabolite database with 278 metabolites, whereas toxicological screens were analyzed using an adapted drug database from Restek[157]. After normalization, metabolomics data were uploaded to Metaboanalyst for uni- and multivariate statistical analyses[87]. Before statistical analysis data were auto-scaled and log-transformed to minimize discrepancy and obtain a Gaussian distribution. Partial least squares-discriminant analysis (PLS-DA) was utilized to find differences in metabolic profiles. Being a supervised multivariate analysis, PLS-DA can be prone to overestimation of the model. Thus, cross-validation testing using Metaboanalyst was performed to evaluate the used models. Metabolites with variable importance in projection (VIP) scores > 1.0 were considered significant contributors to a separation among groups. One-way analysis of variance (ANOVA) followed by Tukey HSD (honestly significant difference) was used for multiple pairwise comparisons. Differences with a p-value less than 0.05 were considered statistically significant. Normalized fold changes allowed for the calculation of p-values for the construction of heat maps. Both ANOVA plots and heat maps were generated in R, version 1.2.5042[158]. Using Spearman correlation analyses, we assessed associations among metabolites and time (ADH). Pathway analyses were performed using KEGG

(Kyoto Encyclopedia of Genes and Genomes) and/or Metaboanalyst[159]. As sampling time points were highly variable among donors, percent ADH (% ADH) categories were used as a more uniform and comprehensive comparison strategy. Percent ADH was calculated by dividing the sample ADH by the total ADH. The total ADH is the amount of time required by each subject to complete active decomposition. Lastly, in collaborative work with Dr. Russell Zaretzki from the Business Analytics & Statistics department at UTK, we developed a Random Forest machine-learning algorithm to address classification and regression questions using the soil metabolomics data set. A Random Forest algorithm builds a large number of trees using subsets of features from the original data set and makes predictions based on a subset of features that are best capable of classifying the samples into manually chosen categories. For all predictions, R's Random Forest algorithm was used. To gain an understanding of the importance of the predictions, R's VIP package was applied along with the importance function from the random forest package which computes an importance score using an average decrease in node purity as measured by the Gini index. The Gini index measures node purity as the sum of the squared proportions of each class in the node. The more a feature contributes to creating splits with pure nodes the greater its importance[160]. Currently, ongoing data analyses for this project involve lipidomics studies on larvae, fluid, and soil samples as well as data evaluation of the unknown spectral features from both metabolomics and lipidomics runs.

3.4 RESULTS AND DISCUSSION

3.4.1 General decomposition characteristics

Table 3.1 in this chapter's appendix lists donor demographics, prescribed drugs, medical conditions, and causes of death. Most donors reported the use of numerous medications based on a variety of underlying illnesses which highlights a key limitation with regard to data processing. A total of 187 drugs were reported among which lorazepam, morphine, ondansetron, and levothyroxine were most frequently prescribed. N = 30 drugs were analgesics, followed by antihypertensives and anxiolytics comprising n = 26 and n = 18 drugs, respectively. Over 55% of donors were known smokers and

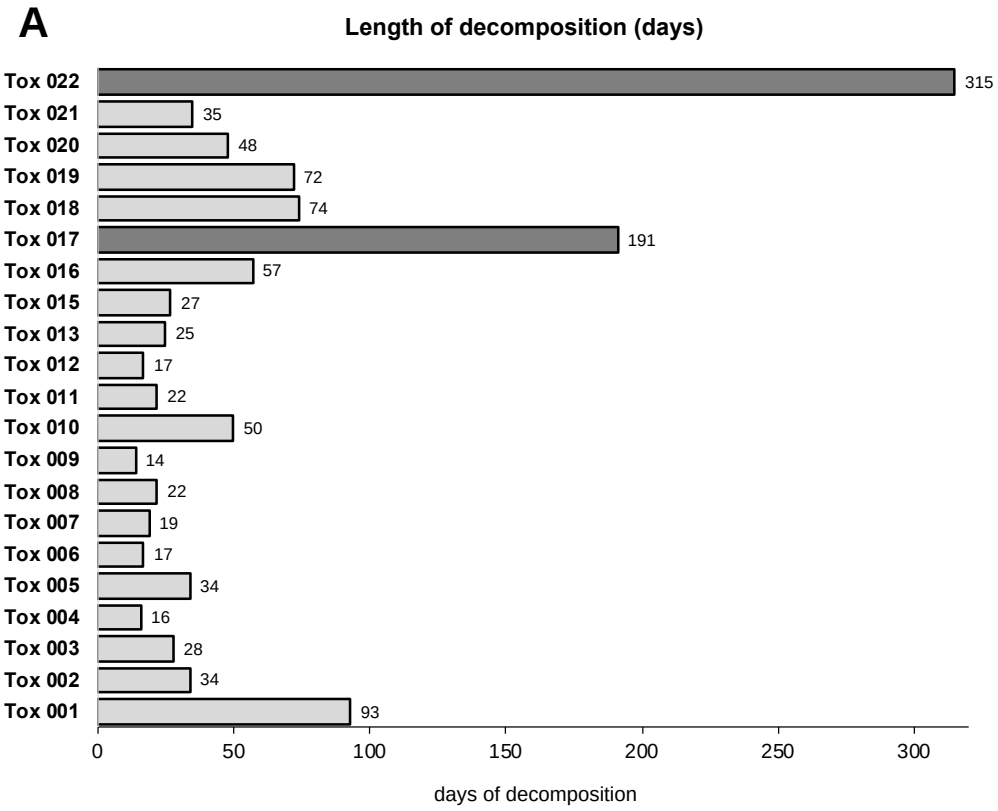

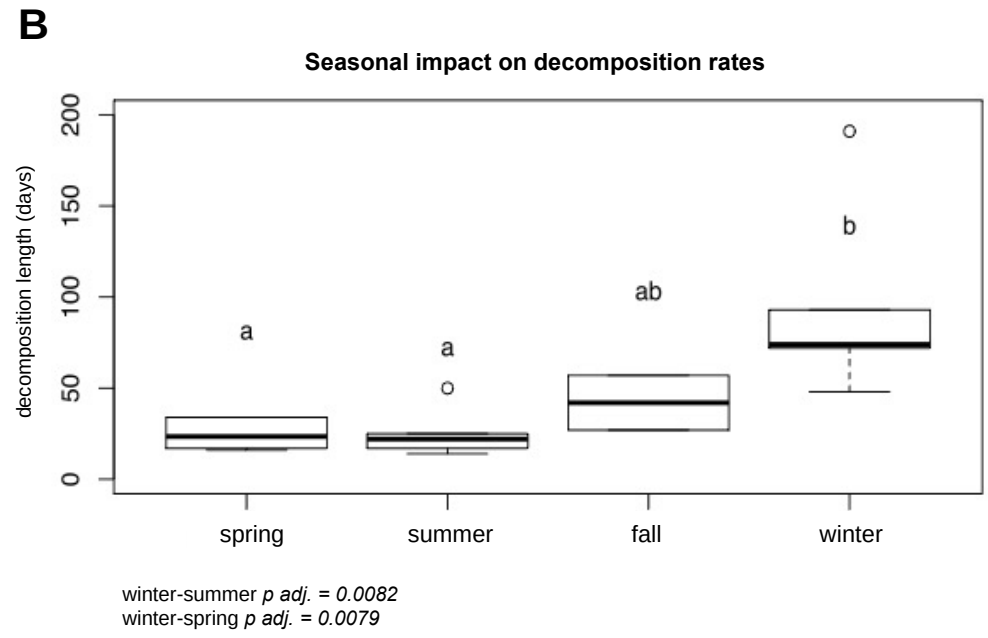

Figure 3.1 – *Length of decomposition. (A) Bar graph comparing the total days required to complete active decay between donors. Slowest decomposition rates are highlighted in dark grey (n = 191 and n = 315 days). (B) One-way ANOVA showing seasonal impacts on the length of decay. P-values were derived via Tukey HSD.*

more than one-third had high blood pressure. Strokes, pulmonary or metabolic disorders comprised 30% of other commonly reported health conditions.

Over the course of this study, it took on average approximately 58 days (57.62 days) in the given environmental setting to complete active decay (Appendix Table 3.2). Aside from Tox 017 and Tox 022, the decomposition periods of all donors ranged from 14 to 93 days (Figure 3.1A). It took 191 and 315 days for Tox 017 and Tox 022, respectively to decompose – the longest decomposition periods observed in this study. The season of placement (spring, summer, fall, or winter) seemed to impact rates of decomposition as donors placed in the winter decomposed slower compared to those placed in the spring (ANOVA, $p = 0.0079$) and summer (ANOVA, $p = 0.0082$) (Figure 3.1B). Environmental factors such as climate, season, and humidity have been reported among the major disturbance factors affecting decomposition trajectories, mainly because they influence a cascade of subsequent factors including, but not limited to, insect succession patterns, scavenging, or microorganism diversity[161-163].

3.4.2 Postmortem toxicology

3.4.2.1 Method validation

All toxicological screenings were performed based on an established and published analytical method from Restek with the same intended use for which it was originally validated[164]. The above-listed reference solutions were used for method validation. Reference standards and method validation parameters are provided in Appendix Figure 3.14. In short, all standards with a concentration of 1 mg/ml were mixed with methanol to obtain working standard solutions with a concentration of 65 ng/ml for each standard. The working solution was serially diluted with methanol. Standards detected along the 12-minute analysis are listed with their spectral features in Appendix Figure 3.14A. The linear range, R^2, limits of detection (LOD), and limits of quantitation (LOQ) were also determined (Appendix Figure 3.14B). Prior to using project samples, test serum collected from a donor not enrolled in this study was successfully used to test the extraction and instrumental method. The serum samples were analyzed for their drug composition against the Raptor drug database containing 231 drugs in total. Minimal retention time shifts seen between this database and the obtained standards ran in-house

allowed for confident identification of 10 drugs from this donor (Appendix Figure 3.14C). Acetaminophen, morphine, fentanyl, and lorazepam were matched directly to standards, while the other six drugs were identified based on monoisotopic mass and retention time (Appendix Figure 3.14C). Following these results, the extraction and screening method was utilized on matrices from enrolled study donors.

3.4.2.2 Drug screens of different cadaveric specimens

The original research strategy comprised a presence/absence drug screen of serum. Over the course of this project, this was expanded toward a more comprehensive analysis including all other postmortem matrices. Relative and absolute abundances of drugs detected in each of the matrices are summarized in Appendix Tables 3.3 and 3.4, respectively. The toxicological screenings performed on all donors led to the overall conclusion that not only parent drugs but also certain drug metabolites were detectable and traceable in different specimens after death (Appendix Table 3.3). Overall, n = 61 drugs were detected among 22 donors. Drug and drug metabolites shown in green in Appendix Table 3.3 were listed on the donor's medical list and confirmed by analytical analysis. Drugs in yellow were detected but not prescribed, and compounds in blue refer to individuals with no medical history. The density of the color indicates relative drug concentration. Highest concentrations were either detected in decomposition fluid (47%) or serum (29%), although detectable amounts were found in larvae and CDI soils, as well.

Postmortem toxicology of Tox 019 exemplifies this trend of trackability for the analgesic morphine by demonstrating a defined route of the drug from the cadaver into the environment (Figure 3.2A). Not only was morphine present in the serum but in larvae that were feeding on the cadaver, as well as in different fluid pools on the body. It was eventually found in the soil around the carcass. Specifically, central serum obtained from the aorta (4327.46 ng/ml) yielded a significantly higher morphine concentration than serum obtained from the femoral artery (peripheral serum; 170.07 ng/ml) (Figure 3.2A, Appendix Table 3.4). A difference most likely caused by postmortem redistribution (PMR). It is assumed that PMR occurs both in central and peripheral blood, yet blood from the aorta might be more prone to PMR due to drug diffusion from major organs resulting from

a decline in pH postmortem (pH 7.4 to pH 5.4) which increases the permeability of tissue cell membranes[165].

Furthermore, the developmental stage of decomposers seemed to influence drug detectability. An instar is a developmental stage of the larval form of the insect. Briefly, insects that enter the larval life cycle undergo three instars (1st, 2nd, and 3rd) before they migrate away from the food source to pupate. Lower intensities of morphine in insects from donor Tox 019 seemed to correlate with an advanced developmental stage. Initially, higher drug concentrations were detected in a sample mixture of 1st and 2nd instar larvae and then decreased in 3rd instar samples from 57% to 37%, respectively (Figure 3.2A, $p = 0.01$). A mixture of 2nd and 3rd instar larvae showed with 6% the lowest amount of morphine ingested by the insects. Dependent on certain stages of the life cycle, an insect's ability or disability to metabolize the drug might explain differential drug concentrations. During the first stages of development, larvae continuously consume tissue from the cadaver leading to a potential build-up of drugs within the body. Once larvae reach a certain developmental stage, feeding might be a secondary purpose given that metabolic changes direct the development toward the adult stage[166]. Unfortunately, limited entomological identification of each decomposer complicates testing this hypothesis for multiple donors. Drugs such as methadone, codeine, antibiotics, zolpidem, or heroin have reportedly been used in entomological studies to investigate growth and development impairments in forensically relevant species (mostly *Calliphoridae*)[167-175]. As opposed to our field study, such studies were typically performed under controlled experimental conditions by exposing flies to a food source spiked with drugs. The theory that consumed drugs might have induced physiological and developmental alterations in the adult insect is currently under investigation by collaborators.

The analysis of drug concentrations from fluid showed inconclusive results. Overall, we noticed concentration fluctuations for different ADH and body locations, yet no common trend was found among donors. Decomposition-impacted soils on the other hand revealed a cross-donor trend. Morphine-containing body fluid that leaked into the soil around Tox 019, accumulated over time, and reached maximum concentrations at 3,000 and 5,500 ADH (Figure 3.2A). A more detailed soil toxicological analysis using fold change comparisons of relative drug abundances found in cadaveric and control soils

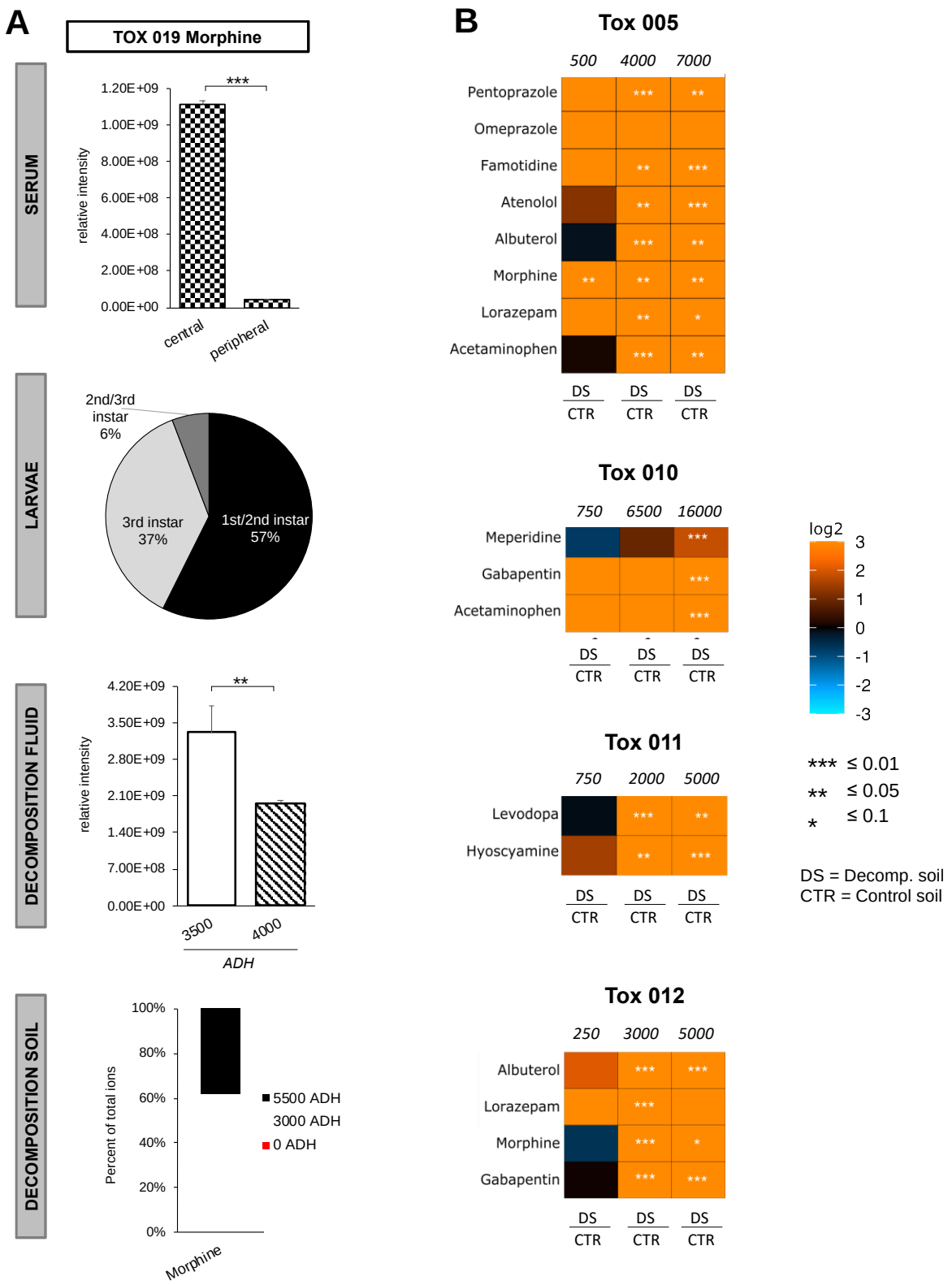

Figure 3.2 – *Toxicological analyses of different human postmortem matrices. (A) Detection of morphine in serum, larvae, fluid, and soil collected from donor Tox 019. (B) Comparison of normalized fold changes calculated for decomposition (DS) and control (CTR) soils for three time points (ADH) during decay. Significant changes in drug abundances are indicated as asterisks.*

confirmed this observation (Figure 3.2B). Increased drug concentrations in decomposition soils became statistically significant for time points near the beginning and end of active decay. Generally, human decomposition can be classified into five broad stages – fresh, bloating, active, advanced, and dry. At the end of the bloating stage with the onset of active decay, the abdominal cavity eases the internal pressure created by putrefactive processes and ultimately leaks cadaveric fluids into the surrounding soil. This explains why decomposition-impacted soils possessed elevated drug concentrations as decay progressed (Figure 3.2B). As of today, no other approach has been made to use either decomposition fluid or soil from decomposing humans for large-scale drug detection purposes.

Taken together, this is the first field study of its kind using a postmortem toxicological approach to comprehensively demonstrate, first the presence of drugs after death in various cadaveric matrices, and secondly their continuous path through the latter with eventual accumulation in a completely new ecosystem.

3.4.3 Postmortem metabolomics

3.4.3.1 Investigating the human postmortem metabolome

Throughout this project, more than 8,000 samples were handled, thousands of metabolites detected, and multiple terabytes of data generated which provided a massive data set for hypothesis testing. On average, untargeted data evaluation revealed over 100 known spectral features per donor for every analyzed matrix.

3.4.3.1.1 Metabolic signatures of decomposers, decomposition fluid, and CDI soil

Decomposition fluid, soil, and larvae from 22 donors were extracted to analyze their metabolomes. To gain a better understanding of metabolite affiliations, compounds were categorized into 11 broad compound classes using KEGG (Kyoto Encyclopedia of Genes and Genomes) identifiers (Appendix Figure 3.15). Pathway analysis found minor inter-matrix differences with on average 40% of metabolites linked to the amino acid metabolism, 19% were identified as nucleosides, nucleotides, and analogs, and 8% classified as lipids or lipid-like molecules. Krebs cycle, glycolysis, and gluconeogenesis were accounted for with 4% each. After death, cessation of protein synthesis steadily

increases the pool of amino acids in cellular compartments. The breakdown of tissues and cells releases not only different amino acids but permits proteases unhindered access to proteins, ultimately resulting in proteolysis – the breakdown of proteins into polypeptides and amino acids. Additionally, proteinogenic amino acids have been reported to steadily increase following death which makes them potential targets for PMI biomarkers[18, 43, 51]. Furthermore, microorganisms utilize amino acids to synthetize proteins to ensure reproduction and growth[176]. Multiple researchers found a decline in soil pH underneath decomposing humans with the progress of decay[26, 31]. Likewise, collaborators noticed a decrease in soil pH for n = 16 out of 22 donors. Such an increase in acidity (lower pH) could be linked to a gradual release of organic acids, e.g., fatty or amino acids into the soil (unpublished data).

Next, we conducted partial least squares discriminant analyses (PLS-DA) using all known metabolites detected in our samples. The metabolite profiles from the three matrix groups (decomposition fluid, soil, larvae) were sufficient to obtain a distinct clustering of these specimens using the first two principal components with 40.9% and 8.4% of explained variance (Figure 3.3A). Component 1 demonstrated separation of the larvae and decomposition soil (CDI) samples, and the second component was necessary for a distinct clustering of the fluid samples. We further identified the compounds that drove the separation among matrices by assigning a variable importance of projection score (VIP) to each metabolite. The top 30 discriminating metabolites with the highest VIP values and thus greatest contribution to matrix separations are presented in a VIP score plot in Figure 3.3B. Interestingly, relative metabolite concentrations of the VIP metabolites had a fairly consistent pattern across matrices – highest abundances were characteristic for larvae compared to fluid and soil (lowest) (Figure 3.3B, heat scale). In total, for all three matrices, 73 metabolites had VIP scores > 1 (Appendix Table 3.5). Among these key metabolites, pathway analysis categorized 47.9% as amino acids, amino acid precursors and/or derivatives; 18% of all VIP metabolites were nucleosides, nucleotides, and analogs (Figure 3.3C). According to Metaboanalysts' pathway enrichment analysis, the two most significantly over-represented pathways were (a) purine metabolism ($p < 0.001$) with 11 VIP metabolites (glutamine, GDP, dGMP, GMP, ATP, ADP, AMP, adenosine, IMP, hypoxanthine, and urate), and (b) arginine metabolism/urea cycle ($p < 0.001$) with 8

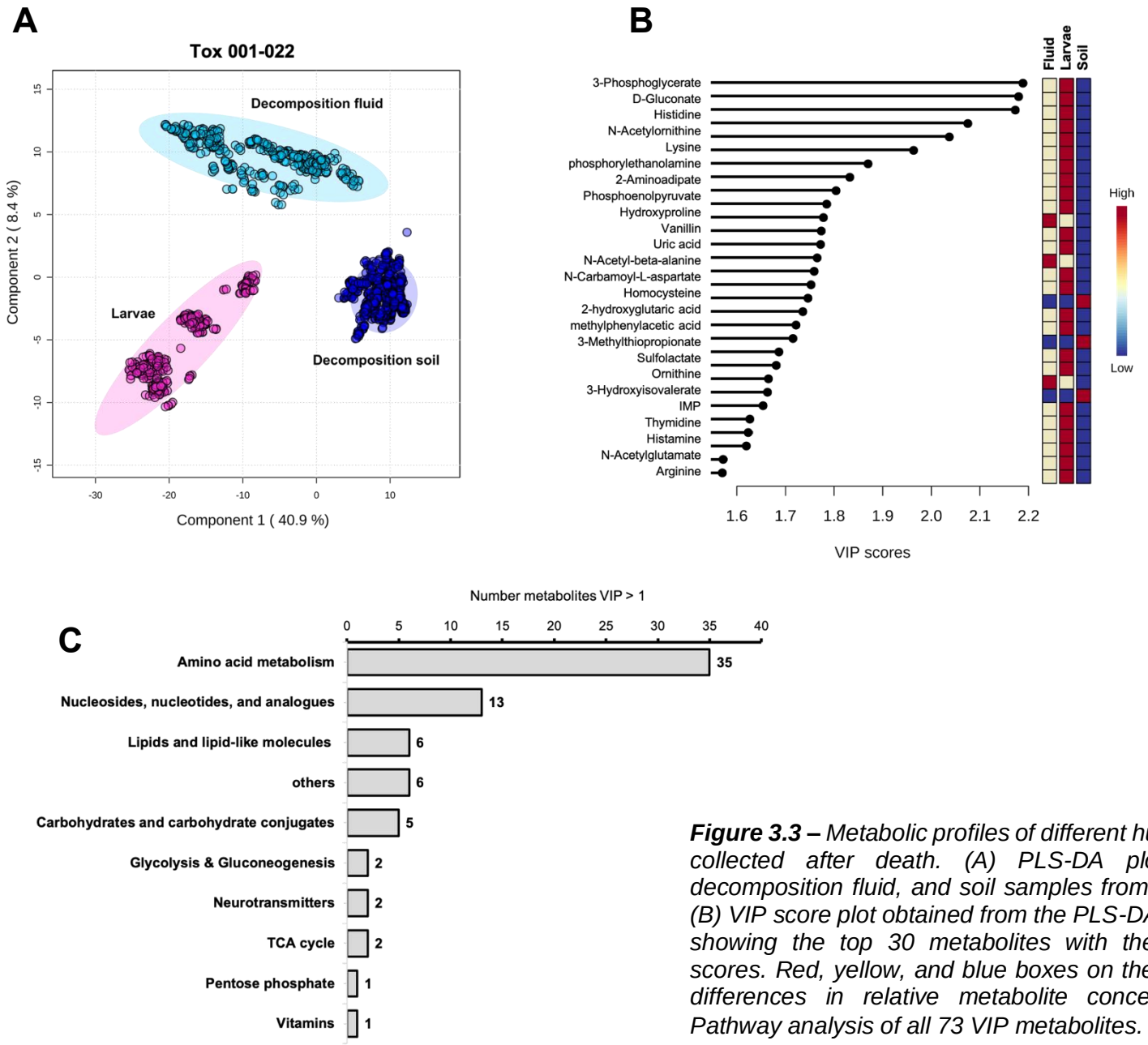

Figure 3.3 – *Metabolic profiles of different human matrices collected after death. (A) PLS-DA plot of larvae, decomposition fluid, and soil samples from Tox 001-022. (B) VIP score plot obtained from the PLS-DA model in (A), showing the top 30 metabolites with the highest VIP scores. Red, yellow, and blue boxes on the right indicate differences in relative metabolite concentrations. (C) Pathway analysis of all 73 VIP metabolites.*

metabolites (aspartate, arginine, citrulline, N-acetylornithine, ornithine, glutamine, 2-oxoglutarate, N-acetyl-L-glutamate). Amino acid catabolism after death results in waste ammonia which enters the urea cycle. Intermediates of the purine degradation pathway identified in our study have been detected in other postmortem metabolic studies and possibly resulted from the breakdown of nucleic acids [54].

Following this inter-matrix comparison, we were also interested in investigating metabolic profiles of each matrix individually (intra-matrix approach). Hence, PLS-DA plots were generated for each matrix for all 22 donors (Appendix Figure 3.16). Overall, we noticed that the entirety of larvae, fluid, and soil samples collected from each donor had a unique donor-specific metabolic signature that was either fairly similar among certain cadavers (closely grouped clusters) or distinct (separated clusters). Underlying reasons for intra-matrix differences were multifold. No two live individuals have an identical metabolism which is why we expected the postmortem metabolome to behave similarly and exhibit inter-individual variability. Different microbial communities, insect physiology, diverse insect species, or seasonal impacts are other plausible factors inducing possible variability of donor metabolomes. Consequently, this led to an intra-donor analysis. For fluids collected on Tox 005, we noticed a fairly large separation of these samples in the intra-matrix PLS-DA (Figure 3.4A). Subsequent intra-donor analysis (Figure 3.4B) revealed a potential impact of sampling time point (ADH) and location on metabolic diversity. For instance, fluid from the groin and leg each formed overlapping groupings with similar sampling times of 2,000-2,500 ADH and 3,500-4,084 ADH, respectively (Figure 3.4B). Although sampled at comparable times, 3,000 ADH (leg) and 3,500 ADH (abdomen), these fluid samples appeared to be metabolically distinguishable as they clustered far apart. This could have reflected different microhabitats prevailing at fairly distant anatomical regions of the cadaver. The observation that the suite of metabolites seemingly differed dependent on the anatomical region and decomposition time, meaning ADH, continued for the remaining two matrices. Metabolomes of larvae feeding on Tox 003 revealed three distinct groupings of 1,000, 3,500, and 4,500 ADH (Figure 3.5B). In two of the clusters, samples were obtained from the mouth and eyes, which separated along the first component from insects that were migrating away from

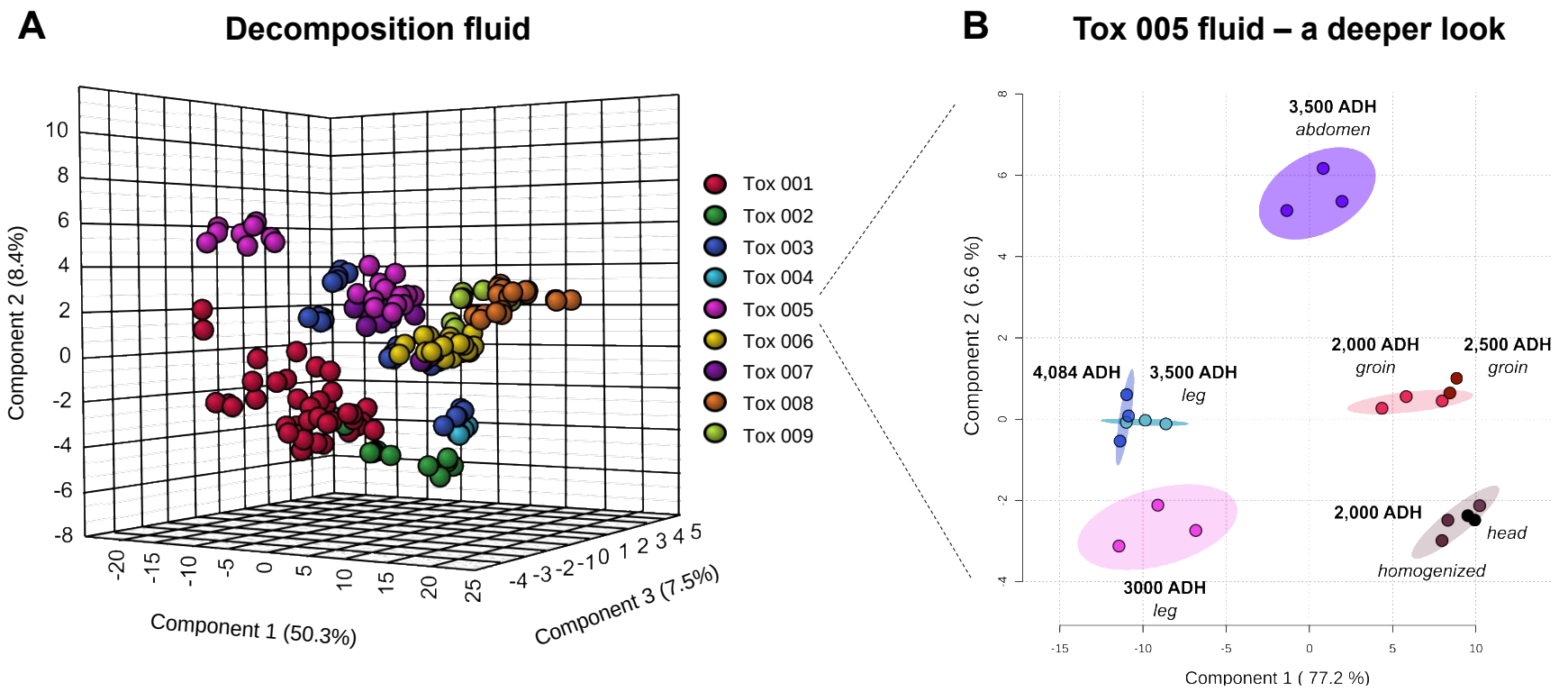

Figure 3.4 – *Postmortem metabolomics of decomposition fluid. (A) Intra-matrix analysis using PLS-DA for decomposition fluid samples from Tox 001-009. (B) Intra-donor analysis exemplified on fluid samples from Tox 005. The PLS-DA score plot shows distinguishable metabolic signatures based on sampling time point (ADH) and anatomical location.*

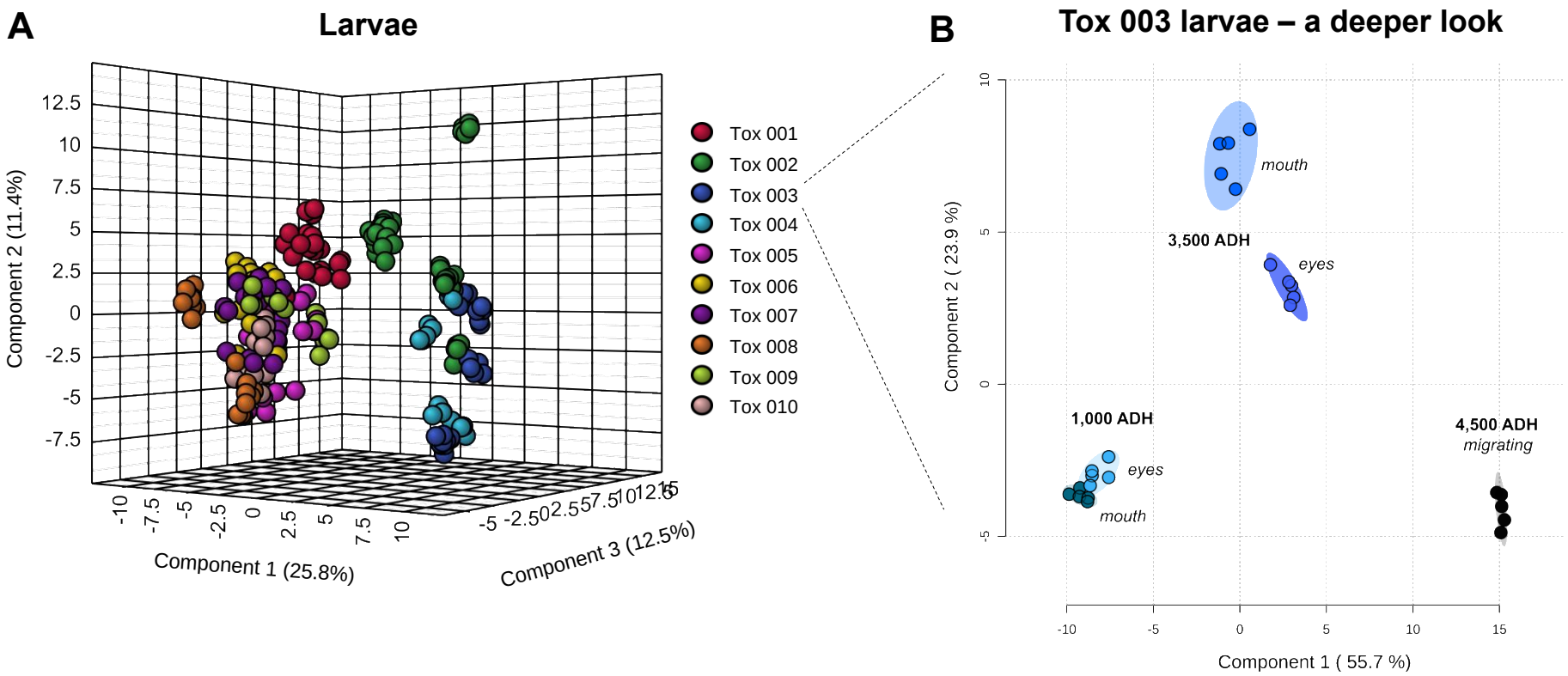

Figure 3.5 – *Postmortem metabolomics of larvae. (A) Intra-matrix analysis using PLS-DA for larvae samples collected from Tox 001-010. (B) Intra-donor analysis exemplified on larvae obtained from Tox 003. The PLS-DA score plot shows distinguishable metabolic signatures based on sampling time point (ADH) and anatomical location.*

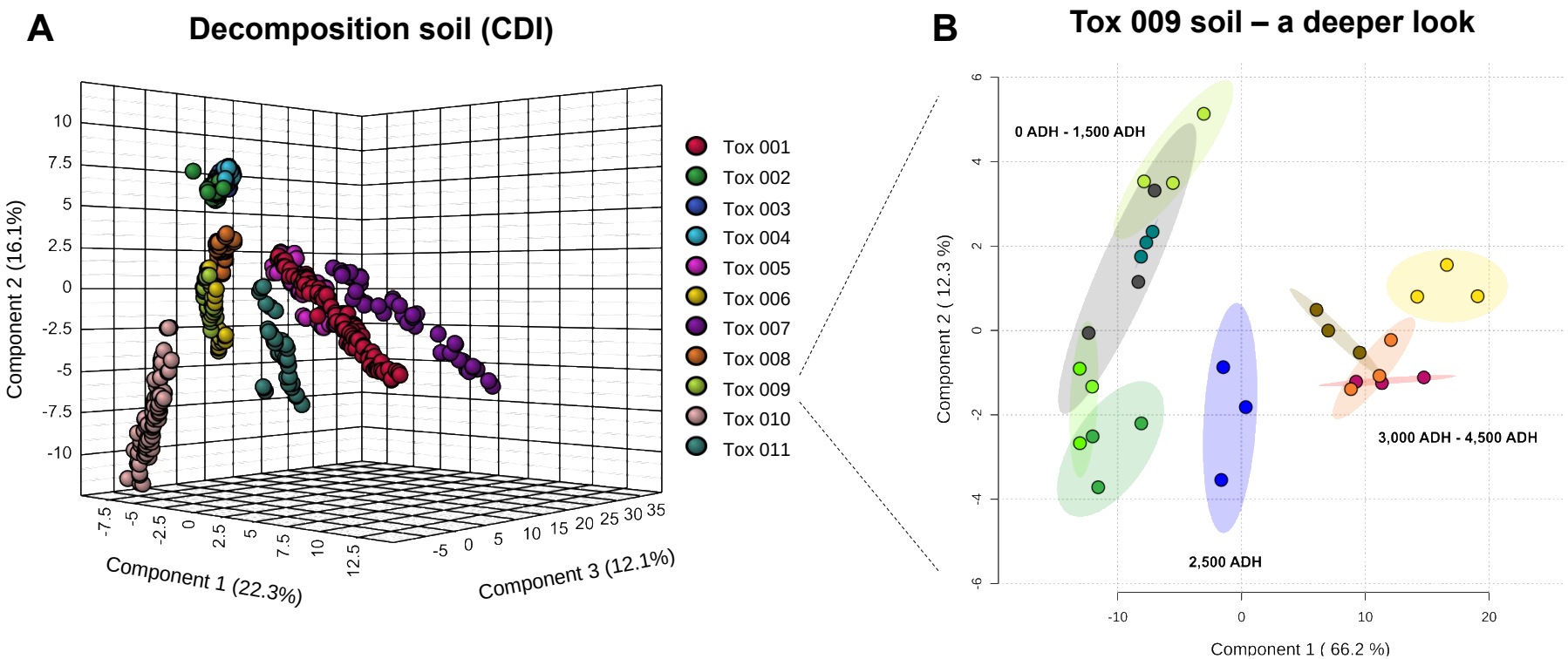

Figure 3.6 – *Postmortem metabolomics of decomposition soil (CDI). (A) Intra-matrix analysis using PLS-DA for soil samples from Tox 001-011. (B) Intra-donor analysis exemplified on soils obtained from the CDI of Tox 009. The PLS-DA score plot shows distinguishable metabolic signatures based on when sampling occurred during decomposition.*

the body. A more detailed analysis of soils collected from the CDI of Tox 009 reaffirmed possible time-depended influences (Figure 3.6B). Of the three broad clusters in this plot, multiple overlapping groups spanning a period of 0-1,500 ADH, as well as 3,000-4,500 ADH appeared to be more similar in their metabolomes compared to samples obtained at 2,500 ADH during decomposition. These samples remained separate and did not contribute to the overlapping clusters generated by all other soil samples.

Due to the nature of the experimental design, soil samples had a higher consistency in terms of when sampling occurred because specific ADH increments determined sampling time points throughout the entire decomposition period. Also, soil was the only matrix for which controls were available. This led to a final comparative analysis among decomposition and control soils for the soil matrix. First, we demonstrated for each donor distinguishable metabolomes inherent in both soil types (Appendix Figure 3.17). Subsequent heat map analyses revealed significantly increased metabolite abundances in cadaveric soils compared to controls prevalent for later decomposition periods. Figure 3.7 exemplifies this for Tox 009. The soil metabolome beneath this donor seemingly changed past the 2,500 ADH marker. As cadaveric fluid purges from the body during active decay, it creates a cadaver decomposition island around the carcass. During this time of decay, an accumulative influx of a diverse suite of metabolites can be expected. *Dekeirsschieter et al.* confirmed this theory by isolating the highest number of volatile carcass-derived compounds during stages of active and early advanced decay[22]. Contrasting this, early ADH time points showed inconsistent changes in metabolite abundances (Figure 3.7) – potentially a result of a differential community pool of microorganisms in the CDI during early decomposition events[35]. Likewise, variation in microbial activity due to fluctuations in temperature or moisture could have contributed to this. Moreover, metabolites are also a microbial food source for growth and survival, which could have diminished the detection of certain compounds in soils up to a point before the onset of active decay, where subsequent purging of fluids induced greater soil saturation with biomolecules. It is noteworthy that this global pattern described for Tox 009 was noted, to a greater or lesser extent, for all 22 donors. A cross-donor evaluation found that the number of significantly increased metabolites in cadaveric soils (fold

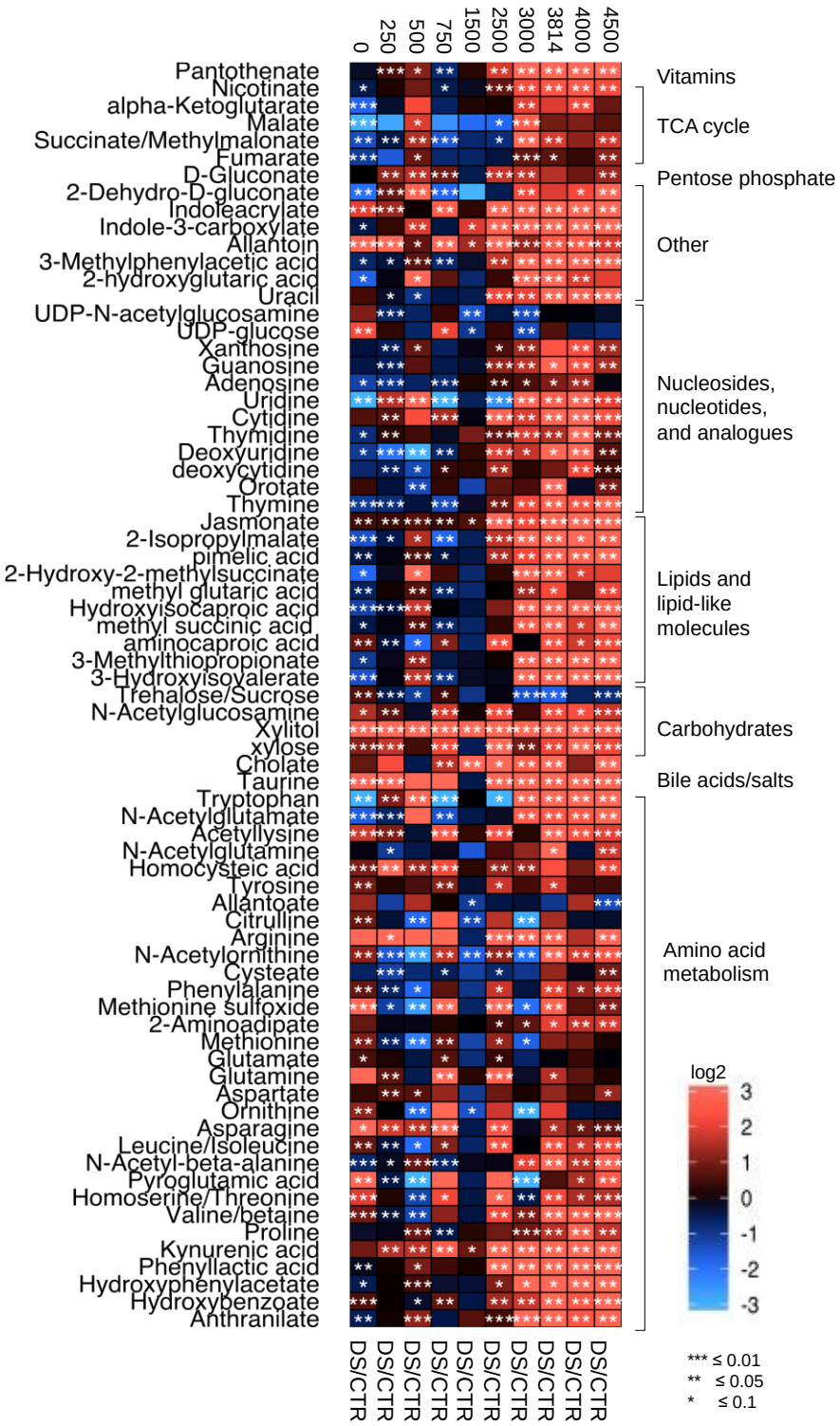

Figure 3.7 – *Heat map of relative metabolite abundances in decomposition (DS) and control (CTR) soils detected for Tox 009. Data are plotted as log_2-transformed fold changes with an increase in metabolite abundance in red and a decrease shown in blue. P-values are the result of student's t-tests. ADH is listed above and metabolic pathways are shown on the right.*

change ≥ 1.5, p-value ≤ 0.05) increased from on average 27 at placement (0% ADH) to 41 metabolites by the time cadavers were halfway decomposed (25-50% ADH), up to 49 and 52 metabolites at 75% and 100% ADH, respectively (Appendix Figure 3.18). Lastly, we assigned soil biomolecules their metabolic pathways using the KEGG database (Figure 3.7). The biochemical soil environment during decay reflected a sequential breakdown of macromolecules (nucleic acids, proteins, carbohydrates, lipids) into their corresponding monomers. An outcome supported by analyses from collaborators showing an increase in soil electrical conductivity and β-glucosidase (an enzyme involved in the breakdown of sugars) as decomposition progressed (unpublished data).

3.4.3.1.2 Metabolome alterations over the course of decomposition

The above section implied that biochemical signatures in CDI soils were highly variable over time postmortem. Thus, further efforts were made to deconvolute this time-dependent profile using the soil metabolomics data. This data set was the only one with sampling time points spanning the complete decomposition period, yet irregular ADH increments existed across donors. To compensate for this, data were split by percent ADH (0%, 25%, 50%, 75%, and 100% ADH) to allow for inter-donor comparisons and analyzed using supervised, multivariate models (Figure 3.8A). Consistent with the findings above, multiple donors (exemplified on Tox 001, 012, and 021) demonstrated differential metabolic dynamics as decomposition progressed (Figure 3.8A). Given the distinguishable cluster formation at each postmortem interval spanning 0% to 100% ADH, the metabolic composition of CDI soils appeared to shift over time. Samples of the 0% and 25% ADH clusters created for Tox 001 and 012 a more distinct group away from the remaining three ADH classes with samples taken at 50% ADH remaining separate (Figure 3.8A). A pattern that roughly reflected early (0%-25% ADH), middle (50% ADH), and later timepoints of decomposition (75%-100% ADH). The 50% ADH sample for Tox 021 appeared metabolically more similar to samples from 75%-100% ADH. They formed a close grouping in the PLS-DA plot with distinct signatures compared to the beginning of decomposition (0%-25% ADH) (Figure 3.8A). We further tested whether these observed changes had a robust predictive value when considering all donors. In a donor-comprehensive analysis (PLS-DA performed individually for all 22 donors), compounds

driving a time-dependent shift in the soil metabolomes were identified based on their VIP scores. Figure 3.8B lists metabolites with VIP scores > 1 extracted from more than half of the 22 PLS-DA plots and shows how often they contributed to significant changes in the soil metabolome upon the onset of decay. For instance, pantothenate was found to have VIP scores greater than 1 in 17 out of 22 donors, thus suggesting it significantly contributed to differential clustering of the five ADH classes in the PLS-DA plot of these donors. Taurine and indole-3-carboxylate were found in CDI soils from 14 donors among metabolites with VIP > 1. Collectively, the compounds in Figure 3.8B emerged as driving factors for the vast majority of donors causing soil metabolic profiles to vary during decomposition. Generally, decaying cadavers are a concentrated nutrient source that stimulates the biogeochemical cycling of energy and nutrients within the natural ecosystem – they affect nitrogen, phosphorus, and carbon pools in the soil by providing a significant source of proteins and amino acids[177]. Similar to our results, a temporal occurrence of biomolecules across the early, intermediate, and late postmortem interval (PMI) was reported by *Locci and colleagues*[42].

Subsequent Spearman rank correlation analyses assessed the linearity of pantothenate, taurine, and indole-3-carboxylate abundances (top three compounds from Figure 3.8B) throughout decomposition (Figure 3.8C). A p-value < 0.05 determined significant correlations (Appendix Table 3.6). N = 16 donors had a significant positive correlation when extrapolating pantothenate concentrations over the investigated ADH range. Abundances of taurine in CDI soils revealed for 11 donors a continuous increase over time; while indole-3-carboxylate had for 12 subjects positive metabolite-ADH associations. This demonstrated that we were not only able to identify which variables contributed most to dynamic decomposition patterns in soils but also visualize their cyclic, linear nature after death. Even though this correlation analysis focused on only three metabolites, it can be considered a preliminary proof-of-concept study for future metabolite-based PMI prediction models. According to literature, several volatile organic compounds (VOC), amino or fatty acids have been reported among promising candidates for PMI estimations[18, 24, 29, 145, 178]. Taurine, a major constituent of bile, was found to positively correlate with late PMI samples from ovine aqueous humor (PMI > 1,000 min)[42]. For the same metabolite, *Zelentsova et al.* demonstrated its slow and regular postmortem

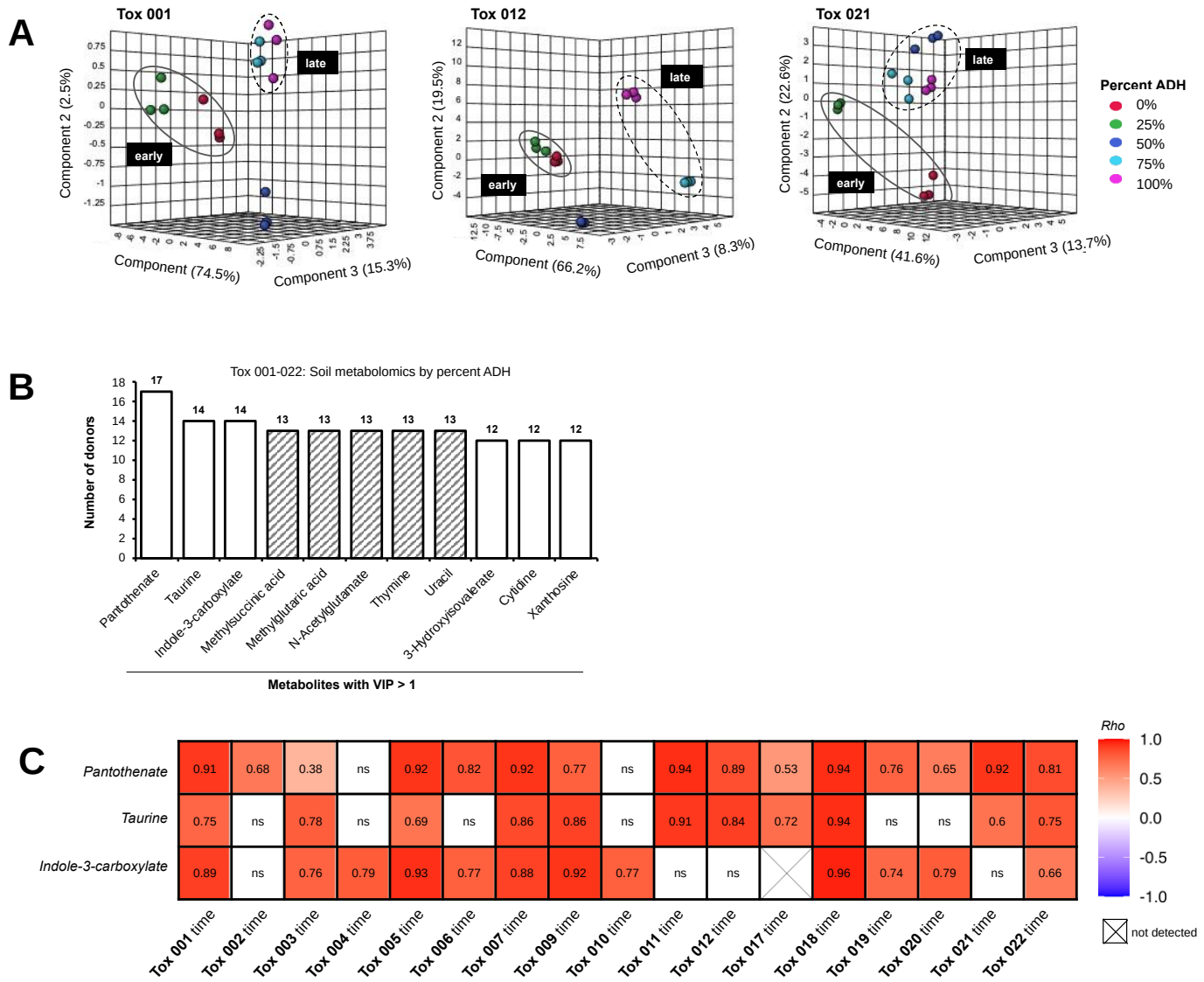

Figure 3.8 – *Dynamics of the soil metabolome during human decomposition. (A) PLS-DA of soil metabolomics analyzed by percent ADH. 'Early' and 'late' refers to soil samples taken at the beginning and end of decomposition, respectively. (B) Metabolites with VIP > 1 from PLS-DA analyses from all 22 donors. (C) Spearman correlation analysis of metabolite-time correlations for the top 3 metabolites from (B). Only significant metabolite-ADH correlations based on Spearman's Rho and p < 0.05 are listed. Tox 008, 013, 015, and 016 had no significant correlation for all three metabolites. Ns = not significant.*

increase over time in a rabbit model[46]. Proteolytic processes after death produce gases, sulfur compounds, and phenolic molecules including indoles[16]. Specifically, the decomposition product indole is formed from the breakdown of the aromatic amino acid tryptophan and counts to the well-known bacterial-produced products of decay[43]. Various researchers have listed indole among frequently occurring compounds postmortem[22, 43, 176, 179]. Zhou et al. postulated that indole and its derivatives may attract necrophagous flies and are quorum-sensing molecules affecting biofilm formation in bacteria which can impact colonization, growth, and metabolism of other microbes involved in carcass decomposition[176]. Pantothenate has only been mentioned by Kaszynski et al. [180]. It was found among the top compounds with a significant Pearson coefficient correlating with the time elapsed after death in a prediction model in mice serum (R^2: 0.9369; p-value: 0.0001) [180]. However, the authors lacked further evaluation of this result. Pantothenate is better known as vitamin B5 – a water-soluble vitamin and precursor to coenzyme A (CoA). The latter is essential for numerous biochemical processes such as the fatty acid metabolism and Krebs cycle. Vitamin B5 has also been reported among the nutrients prevailing in soils[64].

3.4.3.1.3 Potential soil metabolic biomarkers of decomposition

A unique metabolic composition and time-dependent changes in the biochemical profiles over the course of decay were two promising features of cadaveric soils initiating further biomarker discovery analyses. As sampling increments for larvae and decomposition fluid varied strongly based on when the specimens were present on donors, both data sets did not align with the chosen ADH classes (0%-100% ADH) and were therefore not a major focus of the subsequent approach.

Assuming that the molecules leaking from a decomposing body into the surrounding soil were sufficient to differentiate among decomposition and control soils (Appendix Figure 3.17), a Random Forest classification model was developed. Random Forest algorithms typically handle unbalanced and massive data sets produced by high-throughput analyses fairly well and are robust to data overfitting. First, it was intended to identify groups of metabolites that could help to accurately classify a soil sample as decomposition or control soil. Our preliminary machine learning approaches identified

several metabolites as highly correlated with decomposition soils (Figure 3.9A). Performance evaluation of the model showed that it correctly classified in the test data set 889 out of 960 samples as decomposition samples, yielding a class error of 0.0732. For the controls, 944 out of 968 samples were classified correctly, giving a 0.0248 class error (Figure 3.9A). Overall, the Random Forest algorithm predicted control and decomposition samples with a 96% accuracy. The out-of-bag (OOB) estimate of error rate for the test data set was 4.9%. The 30 top-ranked metabolites based on their importance for the identification of the two soil types included among others the previously identified metabolites taurine, pantothenate, and indole-3-carboxylate (Figure 3.9A).

To evaluate the strength of metabolites in predicting a time point during decomposition, a prediction model was built using only the decomposition soil metabolomics data. Predictions from this model were plotted against actual outcomes and a simple linear regression model was fit to illustrate the strength of the linear relationships between predicted and actual ADH. The response modeled was percent ADH (current ADH/maximum ADH for the donor). Thus, a Random Forest regression model was used to create a predictive model for percent ADH based on relative soil metabolite concentrations. The model indicated that it was possible to estimate how long a body has been decaying relative to the maximum ADH solely based on soil metabolic profiles. The differences between the actual and predicted ADH are illustrated in the regression plot in Figure 3.9B. An R^2-value of 0.87 and a p-value < 2.2e-16 implied great linearity and overall performance of the model. According to the model, the metabolic features with the highest predictive importance to correctly predict percent ADH intervals were for instance pantothenate, taurine, kynurenic acid, indole-3-carboxylate, and others (Figure 3.9B). The reoccurrence of pantothenate, taurine, and indole-3-carboxylate was noteworthy and confirmed our results from the previous section. This strong association between the predictive model and the actual outcomes suggested that metabolic signatures found in cadaveric soils could be characteristic of decomposition periods measured as percent ADH. We acknowledge the fact that this result not necessarily indicated time in the traditional PMI sense. Our results refer to our maximum ADH, meaning final timepoints of decomposition as determined based on the end of active

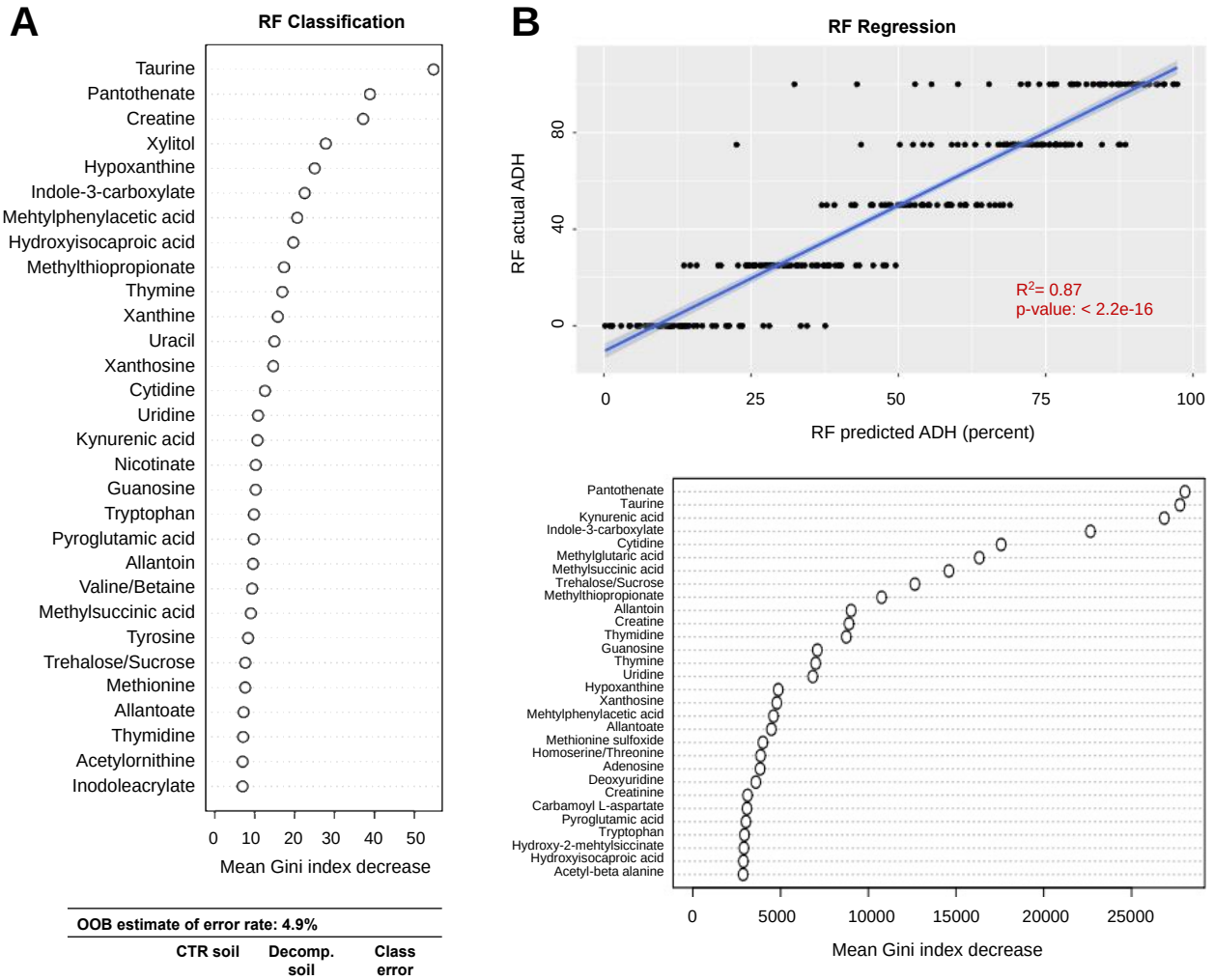

OOB estimate of error rate: 4.9%

	CTR soil	Decomp. soil	Class error
CTR soil	944	24	0.0248
Decomp. soil	71	899	0.0732

Figure 3.9 – *Random Forest (RF) models trained on the soil metabolomics data. (A) Random forest classification model to distinguish between decomposition and control soils. Illustrated are the 30 top-ranked metabolites based on their importance for the identification of the two soil types. The model accuracy is depicted below. OOB = out-of-bag. (B) Random Forest regression model using metabolite abundances found in decomposition soil to predict percent ADH (0%, 25%, 50%, 75%, 100% ADH). Each black dot represents a soil sample. A list of features with high predictive power to correctly predict a certain time point after death is shown on the bottom. RF = Random Forest.*

decay. Thus, they may be considered as morphological descriptor with loose correlation to time.

Taken together, these preliminary results encourage future research on certain groups of metabolites to evaluate their benefit as a complementary forensic tool to existing PMI estimation methods to reduce the error in time since death predictions. Literature sporadically shows application of machine learning methods to generate microbial-based PMI prediction models utilizing 16S rRNA gene markers from grave soil or carcass skin as candidates for highly accurate predictions[57]. Recently, *Zhang et al.* reported predictions of the postmortem interval within 1.82 ± 0.33 days by using a model built on grave soil and microbial communities[47]. Overall, this postmortem metabolomics section demonstrated that, from a metabolic perspective, human decomposition was not consistent among donors. Individual-, matrix-, and time-specific metabolic trends were extracted from analyzed cadaveric specimens showing great susceptibility of postmortem metabolomes to various extrinsic and intrinsic factors.

3.4.3.2 Impact of medical conditions on the postmortem metabolome

We elaborated in section 3.4.2.2 on how drugs took a defined path through cadaveric specimens to enter the ecosystem surrounding a decomposing body. As subsequent postmortem metabolomics analyses revealed a highly diverse metabolic make-up of those specimens, we further investigated the impact of intrinsic factors on the postmortem metabolome. Four broad disease classes were defined according to literature and common age-related medical conditions (cancer, diabetes, cardiovascular, and respiratory conditions)[151]. Categorization of donors in these classes was based on medical information listed in Appendix Table 3.1. None of the tested medical conditions seemed to significantly influence the rate of decomposition (Figure 3.10, diabetes $p = 0.13$; cancer $p = 0.70$; cardiovascular and respiratory conditions $p = 0.22$ and $p = 0.38$, respectively). These findings diverge from studies by *Hayman and Oxenham* as well as *Skopyk et al.,* in which macroscopic changes during decomposition were hypothesized to result from perimortem medication use[151, 152]. However, our donor size was limited to only $n = 22$ individuals which ultimately might have impacted statistical significance.

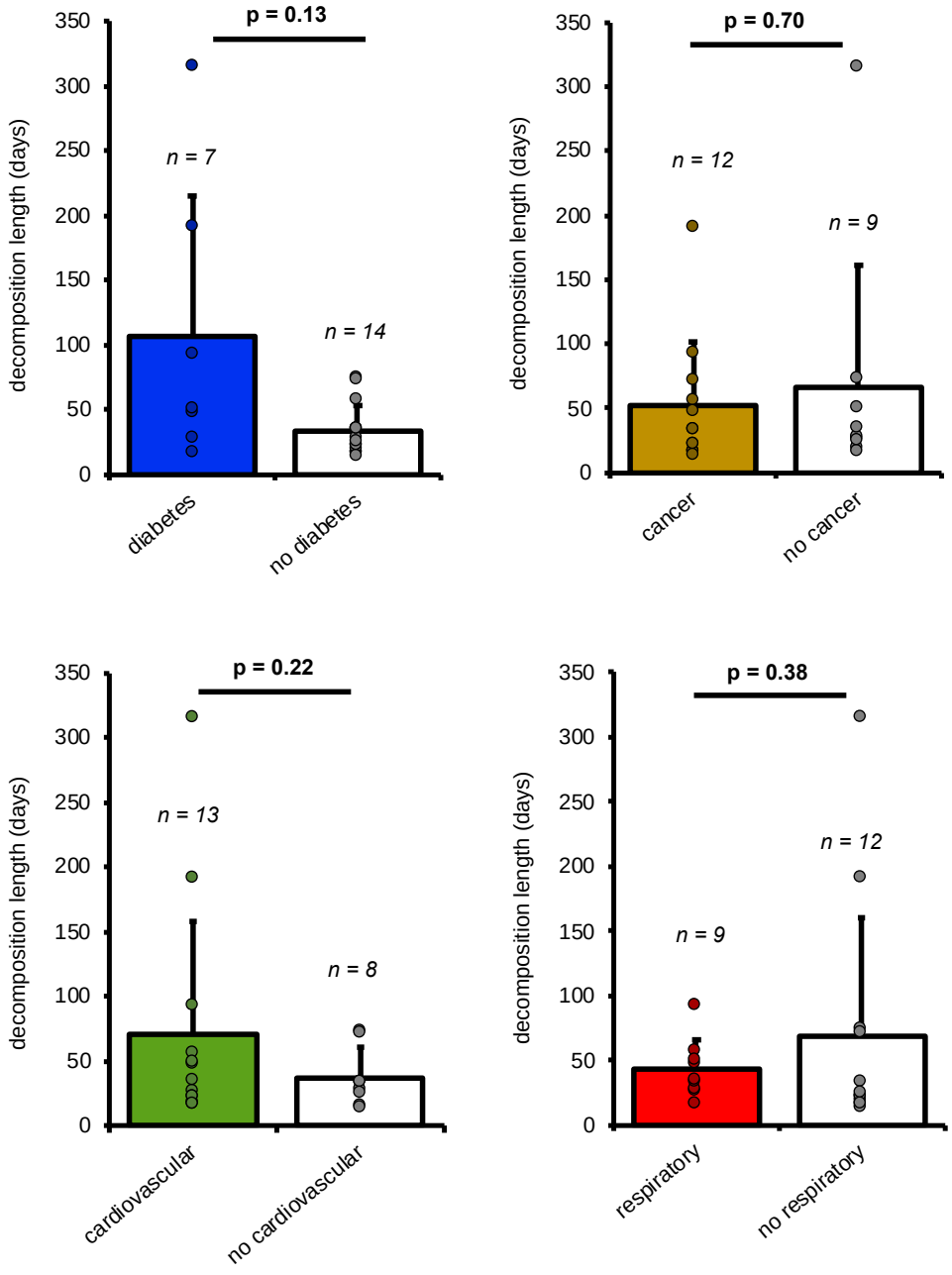

Figure 3.10 – *Disease impacts on decomposition length. The total days required to complete active decomposition were compared between donors with (color) and without (grey) certain medical conditions. All 22 subjects were categorized into four major disease classes. All p-values resulted from student's t-tests. Cancer donors: Tox 001, 002, 004, 005, 006, 008, 009, 011, 016, 017, 019, 020. Diabetes class: Tox 001, 010, 012, 015, 017, 020, 022. Respiratory: Tox 001, 003, 005, 006, 010, 015, 016, 020, 021 and cardiovascular: Tox 001, 006, 007, 008, 010, 011, 012, 015, 016, 017, 020, 021, 022.*

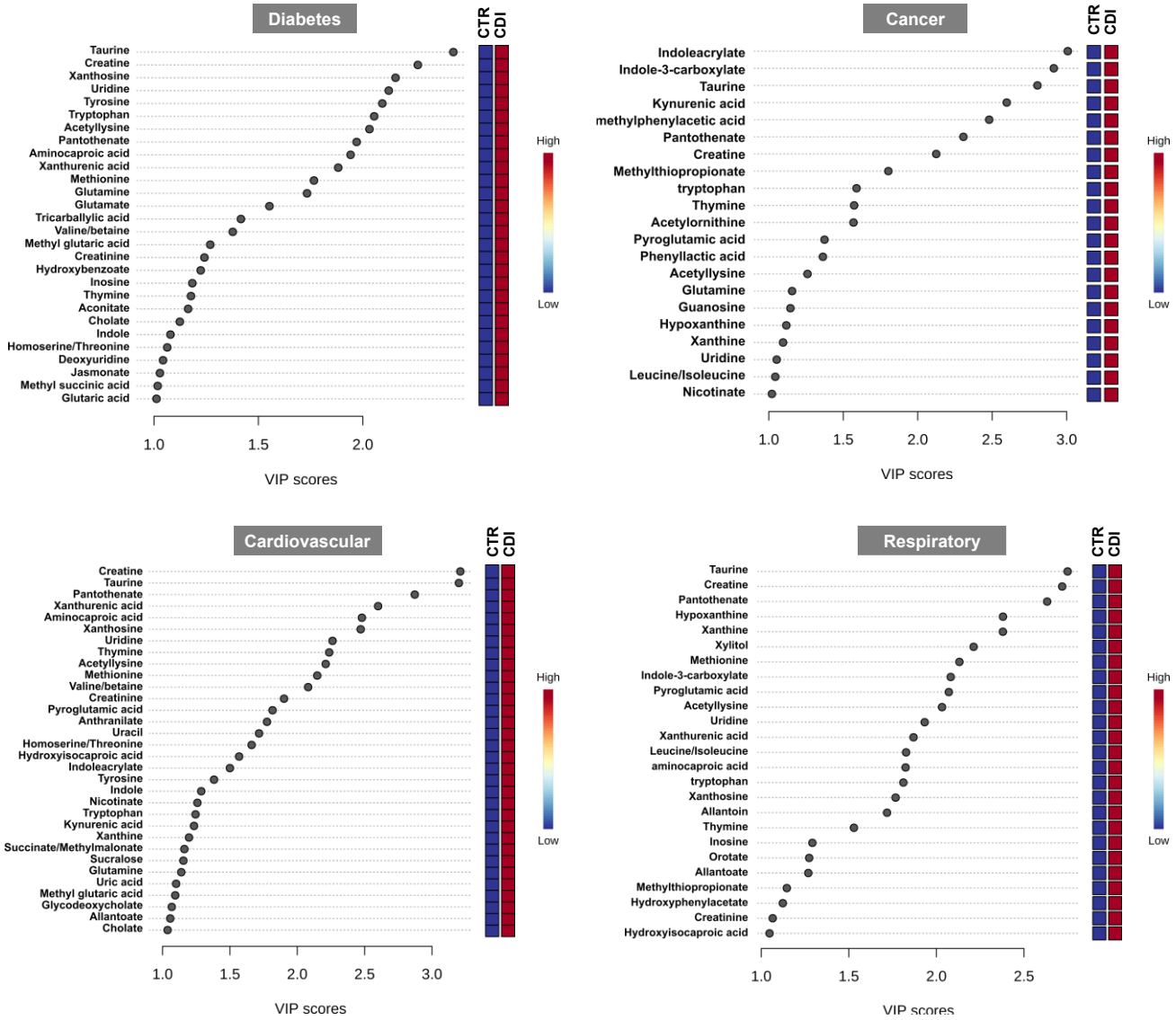

Figure 3.11 – *Disease impacts on the postmortem metabolome considering CDI (= disease) and control soils. All 22 donors were categorized into four major disease classes (Appendix Table 3.7). Shown are VIP score plots with metabolites identified by PLS-DA (VIP > 1). Colored boxes indicate relative concentrations of the corresponding metabolites in each soil group (red, increased relative abundance; blue, decreased relative abundance).*

To investigate possible disease impacts on the metabolome after death, subsequent metabolomics analysis contrasted soils collected from donors with certain diseases with control soils. We used the above-mentioned four major disease classes, however, considered for each class only donors whose medication and disease history was least complex but most applicable for one class (Appendix Table 3.7). For instance, only Tox 002, 004, 009, and 019 suffered solely from cancer (colon cancer: Tox 002; lung cancer: Tox 004, 009, 019), thus these subjects comprised the cancer disease class. Soils from the CDI from all donors comprising one class were collectively compared to control soils from the same individuals using PLS-DA. Cluster formation in PLS-DA plots was assessed using corresponding VIP score plots to identify metabolites significant in distinguishing disease soils from controls (VIP cut-off > 1, Figure 3.11). Throughout all disease classes, higher relative abundances of differential metabolites were exclusively detected in disease (CDI) soils – not a single metabolite was found with lower intensities in this soil type (Figure 3.11). Tissue breakdown and accumulation of body fluids which ultimately leak into the soil beneath a carcass assumingly increased the biochemical heterogeneity in disease soils compared to those from an area with no carcass (controls).

The in Figure 3.11 listed metabolites with VIP scores greater than 1 that emerged for each disease class as differentially abundant among the two soil types were next visualized in a Venn diagram (Figure 3.12). This helped to discriminate metabolites common to or distinct for the four diseases. Seven metabolites (center of Venn diagram) were commonly shared among all classes, which means they provoked for each disease class distinct soil metabolomes between control and CDI soils. Interestingly, of these metabolites, six were previously identified by our Random Forest classification model as highly predictive to classify decomposition soil (taurine, creatine, uridine, tryptophan, pantothenate, thymine) (Figure 3.12 table). This again highlighted their potential in being considered ‘decomposition biomarkers’. For disease-specific metabolites – diabetes (8), cancer (4), cardiovascular (6), and respiratory condition (4) – we further investigated their importance by performing inter-disease comparisons across multiple postmortem specimens. Figure 3.13 illustrates relative metabolite abundances in soil, fluid, and larvae samples from for instance decaying cancer donors and contrasts these metabolic profiles

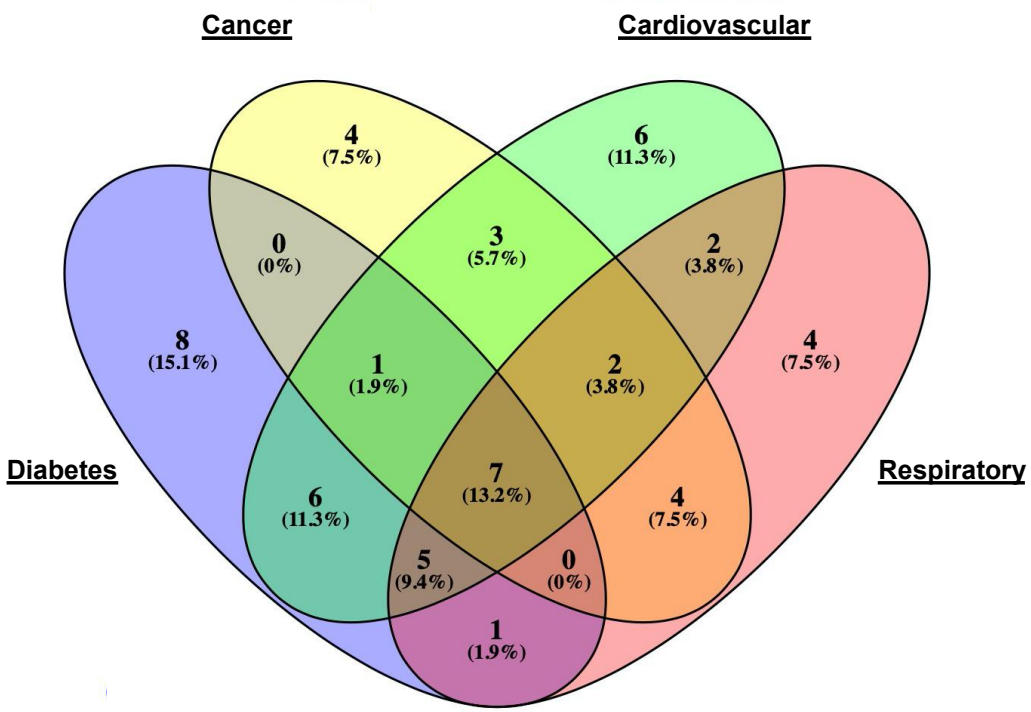

Exclusive metabolites for each disease class			
Diabetes (8)	***Cancer (4)***	***Cardiovascular (6)***	***Respiratory (4)***
Glutamate	Methylphenylacetic acid	Anthranilate	Xylitol
Tricarballylic acid	Acetylornithine	Uracil	Allantoin
Hydroxybenzoate	Phenyllactic acid	Succinate/Methylmalonate	Orotate
Aconitate	Guanosine	Sucralose	Hydroxyphenylacetate
Deoxyuridine		Uric acid	
Jasmonate		Glycodeoxycholate	
Methyl succinic acid			
Glutaric acid			

Commonly shared metabolites
Taurine
Creatine
Uridine
Tryptophan
Acetyllysine
Pantothenate
Thymine

Figure 3.12 – *Venn diagram of common and unique features in disease-impacted soils. For each disease class only metabolites with VIP > 1, as shown in the score plots in Figure 3.11, were considered. Seven soil metabolites were commonly shared among all diseases and are listed in pink in the table below the Venn diagram.*

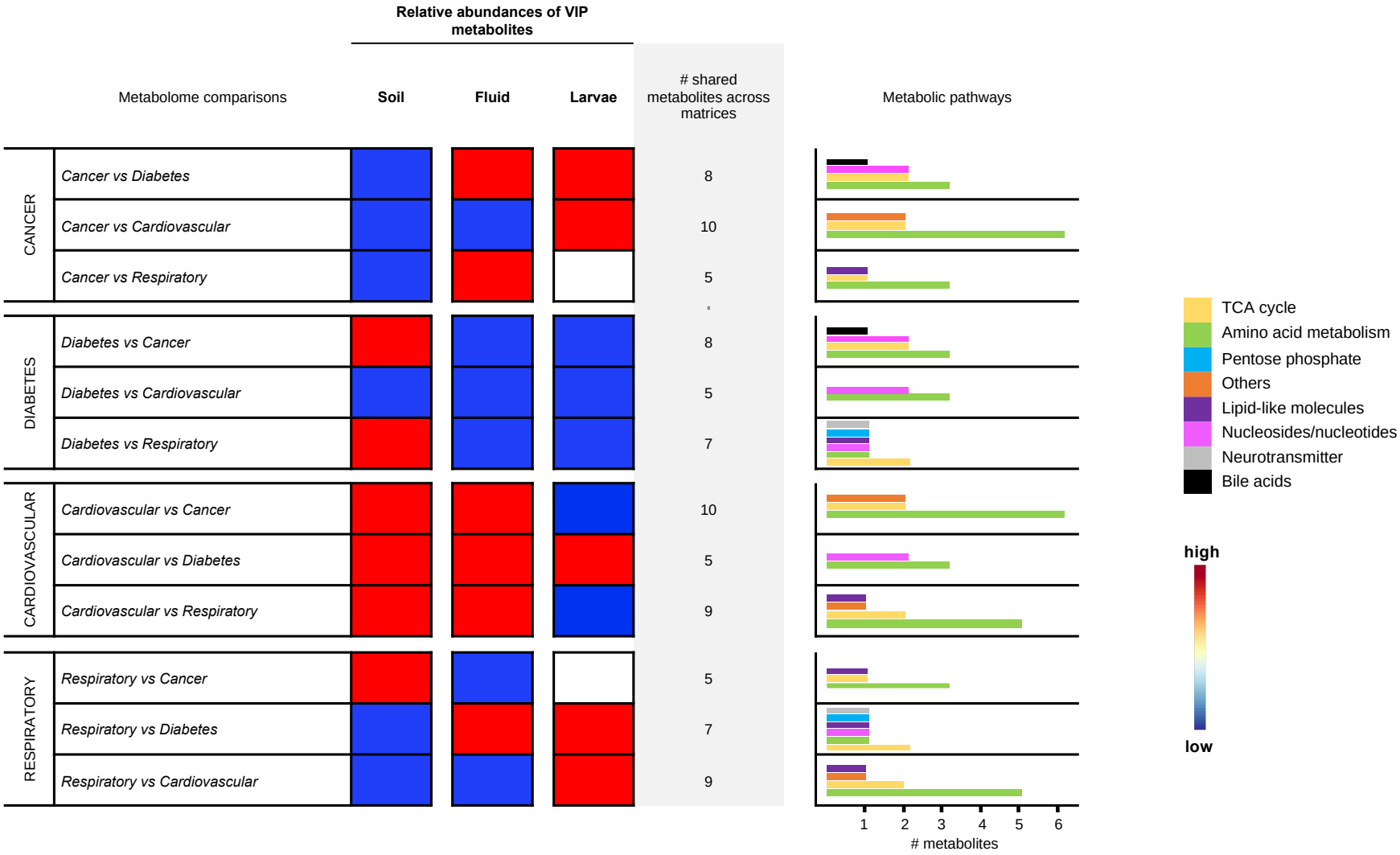

Figure 3.13 – *Impact of medical conditions on the postmortem metabolome considering all postmortem specimens (soil, fluid, larvae). Only metabolites that significantly (VIP > 1) contributed to diverse postmortem metabolomes between disease classes were considered. Colors in the table indicate increased (red) or decreased (blue) relative metabolite abundances of > 60% metabolites in soil, fluid, or larvae. The total number of identical VIP metabolites that was found throughout all matrices is greyed out. For these compounds metabolic pathways were assigned.*

with those from the remaining three disease classes. To visualize general metabolic trends, metabolites that significantly (VIP >1) contributed to diverse postmortem metabolomes in e.g., cancer versus diabetic donors, were assigned a color. This color scale reads as follows: According to the total number of significantly distinct metabolites from VIP and volcano plot analyses, a red color indicates that more than 60% of metabolites had increased abundances in the respective disease. The opposite is true for blue. Blue refers to decreased abundances of > 60% of the total differential metabolites. First, when comparing trends within one matrix but across disease classes (e.g., cancer vs diabetes, cancer vs cardiovascular, cancer vs respiratory), we noticed that cancer CDI soils tended to have decreased metabolite abundances. Fluid collected from diabetic donors yielded consistently decreased metabolite intensities when compared to cancer, respiratory, and cardiovascular classes. Interestingly, this pattern continued to exist in larvae samples. Both soil and fluid samples from cardiovascular donors revealed increased metabolic activity.

Next, when comparing metabolic signatures across matrices (Figure 3.13), we found that only comparisons between donors with diabetes and cardiovascular illnesses had consistent patterns throughout matrices. Overall, 50% of the inter-matrix comparisons showed that the metabolic signature inherent in CDI soils was identical to the one found in the fluid. Likewise, for fluid and larvae samples 50% of the disease comparisons returned identical signatures. Only 16.7% of comparisons had an identical metabolic pattern for soil and larvae samples. For these inter-matrix comparisons, we also calculated how often the same metabolite was detected in each of the three matrices. The total number of identical VIP metabolites that occurred consistently throughout all matrices is greyed out in Figure 3.13. Lastly, these compounds were evaluated by assigning them metabolic pathways. Pathways for each individual metabolite are listed in Appendix Table 3.8. Of note, while amino acid metabolism appeared relevant for all four diseases, the highest number of ‘metabolite-pathway matches’ was found for subjects with a cardiovascular impairment. Cardiovascular diseases are the leading cause of death worldwide[181]. Altered plasma levels of branched-chain amino acids (BCAA; leucine, isoleucine, valine) have been associated with a high cardiometabolic risk[181-183]. Recent research suggests a direct relationship between BCAA and the pathogenesis of coronary

artery disease/artherosclerosis[181, 182]. Similarly, an integrated transcriptomics-metabolomics approach by *Sun et al.* related a suppressed BCAA catabolic gene expression to the accumulation of branched-chain α-keto acids, which was identified as significant in promoting heart failure in mice[183]. Interestingly, our results revealed valine among significantly different amino acids in all three matrices when comparing metabolic profiles of decomposing donors with circulatory conditions to those who had cancer and to those with respiratory issues (valine p-values < 0.01 for all matrices). Diabetes exhibited seemingly the greatest postmortem metabolic variety. The most diverse selection of pathways was detected for this class with overall most metabolites identified as nucleotides/nucleosides or analogs thereof. Knowledge about the role of purine and/or pyrimidine metabolism in diabetes is still incomplete. However, evidence for an accelerated nucleotide synthesis in diabetic erythrocytes exists – an acceleration that may also stimulate nucleotide breakdown which was shown by *Dudzinska* due to increased concentrations of nucleotide degradation products[184]. Among the significantly altered inter-matrix metabolites related to donors with respiratory illnesses, five compounds were intermediates of the tricarboxylic acid (TCA) cycle. A review by *Zhao et al.* elaborated on the metabolic reprogramming in the pathogenesis of chronic lung diseases including bronchopulmonary dysplasia (BPD), chronic obstructive pulmonary disease (COPD), and lung fibrosis[185]. Possible links between the TCA cycle and these disorders manifest in a reduced rate of mitochondrial respiration (BPD and lung fibrosis) or a disrupted lipid metabolism (COPD)[185]. We discovered four TCA cycle intermediates (alpha-ketoglutarate, $p < 0.01$; succinate, $p < 0.01$; fumarate, $p < 0.01$; and malate, $p < 0.01$) from comparisons among the classes respiratory vs cancer, respiratory vs diabetes, and respiratory vs cardiovascular (compare Appendix Table 3.8). Lastly, pathway analysis for the cancer class yielded a high number of compounds related to energy and amino acid metabolism. *Lieu et al.* outlined the importance of amino acids in the cancer metabolism and their interplay with the TCA cycle promoting ontogenetic activity. The latter is facilitated by the incorporation of e.g., glutamate, BCAAs, and threonine into TCA cycle intermediates which produce ATP and thus energy for cell growth. Amino acids also serve as nitrogen or carbon donors for nucleosides which in turn are crucial for cancer cell growth or contribute to regulate lipid biosynthesis[186].

Collectively, our pilot data analysis strategy to determine metabolic disturbances associated with the decomposition of donors having cancer, diabetes, or cardiovascular and respiratory perimortem disease profiles, identified certain metabolic trends that distinguished between the four disease classes. Our results identified various postmortem disease 'phenotypes' that had distinct metabolic trends associated with each one. We do acknowledge the fact that each of the illnesses translate to an incredibly heterogeneous and complex metabolic picture in the living organism, which is why currently ongoing data analyses aim to further deconvolute this picture and correlate known metabolic disease signatures with our postmortem metabolomics results. An undertaking that will most certainly also profit from the performed lipidomics analyses (data analysis ongoing). Additionally, unknown spectral features from all donors are currently under evaluation, as well. In the meantime, researchers may choose to select from our presented results pathways of their interest to perform follow-up experiments using targeted studies.

3.5 CONCLUSION

Using global metabolomics, it was shown that we can not only assign a decomposing body a particular metabolic signature but also specify the latter on an even smaller matrix-specific level with the potential to uncover intrinsic influences. The established time-dependent metabolic sequences of such changes may ultimately provide chemical biomarkers for a more precise classification of decomposition stages. Given the accuracy of our Random Forest models, this work provided groups of metabolites as potentially useful for this undertaking. In addition, it was shown that drugs in a decomposing body cycled through different cadaveric specimens. On their route into the surrounding ecosystem, it is assumed that drugs impact both insect physiology and resident soil microbes – aspects that will be evaluated in future collaborative efforts. Being the first global postmortem metabolomics field study of its kind, our metabolomics approach using cadaver-derived matrices (fluid, soil, larvae) reported metabolic changes consistent with global molecular mechanisms after death to compensate for hypoxia (see

dissertation introduction). We identified numerous metabolites important in the postmortem environment, of which future studies will have to determine their potential as biomarkers. Furthermore, this was the first human postmortem field study focused on elucidating a disease-specific metabolic signatures of decaying bodies. Above-discussed preliminary results are currently under investigation in our lab and will be compiled with outcomes from collaborators.

There are a few noteworthy limitations to this study that should be kept in mind for data interpretation. Firstly, inconsistent sampling increments (ADH), not only among donors but also for different matrices, complicated data alignment. Along with this, the lack of a healthy control donor and the fact that no two donors assigned to a disease class had identical medical profiles, created an additional lack of transparency. Secondly, all humans enrolled in this study varied considerably in their body mass (range 34-170 kg). Total body mass including body fat composition could interfere with tissue liquefaction and subsequent movement of fluids into the soil. Lastly, heterogeneity in the data may also be attributed to perimortem lifestyle, genetic background and, most importantly, external conditions such as weather during sampling. When performing metabolomics studies, a sample size that allows for statistically robust results is crucial. It remains to be seen if a larger donor size will confirm our findings. Studies in a controlled laboratory environment using mice are planned complementary experiments. Mice can be controlled for diet, body weight, and population. Injecting them with selected drugs will help to assess drug effects on microbes, insects, and the postmortem metabolome more ‘directly’ and evaluate the relevance of our trends observed in the field.

APPENDIX

Table 3.1 – *Donor demography and medical information.*

Donor ID	Sex	Age	Stature (cm)	Weight (lb)	Cause of Death	Medical Conditions	Medications
Tox 001	F	63	170.5	214	Coronary Artery Disease, Diabetes, Hypertension	Asthma, COPD, Diabetes, Hypothyroidism, Multiple Sclerosis, GERD, IBS, Chronic Kidney Disease, Ovarian Cancer, ASCVD, Coronary Artery Disease, Hypertension, Hypercalcemia, Vitamin D Deficiency, Depression, Tobacco Use	Albuterol, Amlodipine, Atorvastatin, Carvedilol, Clopidogrel, Cymbalta, Gabapentin, Lantus, Levothyroxine, Lisinopril, Nitroglycerin, Novolog, Oxybutynin, Pantoprazole, Trelegy
Tox 002	F	78	162	117	Colon Cancer	Hypothyroidism, Colon Cancer, Depression, Tobacco Use, Alcohol Abuse	Aspirin, Atorvastatin, Digoxin, Levothyroxine, Losartan, Paroxetine, Tizanidine, Valium, Xanax
Tox 003	M	71	170	127	COPD	COPD, Pancreatitis, Tobacco Use, Alcohol Abuse	Med List Not Obtained
Tox 004	F	84	147	92	Lung Cancer	Lung Cancer, Tobacco Use	Haldol, Lidocaine, Lorazepam, Morphine
Tox 005	F	71	157	126	Pneumonia, Adult Respiratory Distress Syndrome	Pneumonia, Adult Respiratory Distress Syndrome, Breast Cancer	Acetaminophen, Albuterol, Amlodipine, Atenolol, Calcium-Vitamin D, Enoxaparin, Famotidine, Furosemide, Ibuprofen, Iron, Letrozole, Levothyroxine, Lorazepam, Morphine, Omeprazole, Ondansetron, Oxycodone, Palbociclib, Pantoprazole, Sodium Chloride
Tox 006	M	64	162	144	Lymphoma, Renal Failure, Stroke, Heart Disease	COPD, Chronic Renal Failure, Lymphoma, Peripheral Artery Disease, Stroke, Tobacco Use	Allopurinol, Atorvastatin, Buspirone, Citalopram, Eliquis, Furosemide, Hydrocodone-Acetaminophen, Klor-Con, Lorazepam, Metoprolol
Tox 007	M	89	179	185	Congestive Heart Failure	CHF, Stroke, Tobacco Use	Aspirin, Furosemide, Lisinopril, Metoprolol, Warfarin
Tox 008	M	40	160	137	Leukemia	Ulcers, Leukemia, Stroke	Gabapentin, Ondansetron, Oxycodone, Ponatinib, Ranitidine, Warfarin
Tox 009	F	72	158	131	Lung Cancer	Lung Cancer, Tobacco Use	Albuterol, Atropine, Hyoscyamine, Lorazepam, Metoprolol, Morphine, Ondansetron, Scopolamine, Sodium Chloride
Tox 010	M	65	177	374	COPD, Hypertension, Pneumonia	COPD, Pneumonia, Diabetes, Hypertension	Med List Not Obtained

Table 3.1 – *continued*

Donor ID	Sex	Age	Stature (cm)	Weight (lb)	Cause of Death	Medical Conditions	Medications
Tox 011	M	81	170	140	Parkinson's Disease	Kidney Cancer, Stroke, Parkinson's Disease	Acetaminophen, Bisacodyl, Hyoscyamine, Lorazepam, Morphine, Prochlorperazine
Tox 012	F	77	154	154	Renal Disease, Seizures, TIA, Diabetes, Cerebral Hemorrhage	Diabetes, Hyperparathyroidism, Chronic Kidney Disease, Stroke, Dementia, Seizures	Albuterol, Aspirin, Buspirone, Cymbalta, Gabapentin, Geodon, Haldol, Ibuprofen, Lantus, Lisinopril, Lorazepam, Morphine, Voltaren
Tox 013	M	54	174	278	Asphyxia via Ligature Hanging	Migraines, Depression, Sleep Apnea, Erectile Dysfunction	Ambien, Imitrex, Sildenafil
Tox 015	M	78	164	84	Pulmonary Fibrosis	Diabetes, Hypertension, Pulmonary Fibrosis	Acetaminophen, Colace, Fentanyl, Glimepiride, Guaifenesin, Hydrocodone-Acetaminophen, Levothyroxine, Lorazepam, MiraLax, Morphine, Ondansetron
Tox 016	M	62	184	280	Chronic Hypoxic and Hypercapnic Respiratory Failure, Advanced COPD, Obstructive Sleep Apnea	COPD, Seasonal Allergies, GERD, Skin Cancer, Congestive Heart Failure, Peripheral Artery Disease, Stroke, Hypertension, Hyperlipidemia, Depression, Tobacco Use, Alcohol Abuse	Albuterol, Clonidine, Clopidogrel, Hydrochlorothiazide, Lisinopril, Meloxicam, Metoprolol, Omeprazole, Pantoprazole, Spironolactone
Tox 017	F	62	160	311	Congestive Heart Failure	Diabetes, Hypothyroidism, GERD, Constipation, Uterine Cancer, Congestive Heart Failure, Ventricular Hypertrophy, TIA, DVT, Hypertension, Hyperlipidemia, Vitamin B12 Deficiency, Hypomagnesemia, Anemia, Bipolar Disorder, Insomnia, Paroxysmal Nocturnal Dyspnea, Benzodiazepine Dependence, Opiate Dependence, Restless Leg Syndrome, Rosacea	Albuterol, Amlodipine, Aspirin, Belsomra, Bevespi Aerosphere, Clonazepam, Colace, Eliquis, Ezetimibe, Furosemide, Hydrocodone-Acetaminophen, Iron, Januvia, Levothyroxine, Lidocaine, Magnesium, Mirapex, Montelukast, Myrbetriq, Omeprazole, Promethazine, Sodium Chloride, Trulicity, Xanax
Tox 018	F	85	146	75	Parkinson's Disease	Parkinson's Disease	Acetaminophen, Atropine, Bactroban, Biofreeze Roll-On, Carbidopa-Levodopa, Escitalopram, Guaifenesin, Hydrocodone-Acetaminophen, Hyoscyamine, Milk of Magnesia, Senna

Table 3.1 – *continued*

Donor ID	Sex	Age	Stature (cm)	Weight (lb)	Cause of Death	Medical Conditions	Medications
Tox 019	F	67	152	100	Lung Cancer	Hypothyroidism, Breast Cancer, Lung Cancer, Tobacco Use	Atorvastatin, Cyclobenzaprine, Dexamethasone, Haldol, Hydrocodone-Acetaminophen, Ibuprofen, Lamotrigine, Levothyroxine, Lorazepam, Morphine, Omeprazole, Ondansetron, Promethazine, Ropinirole
Tox 020	M	91	164	185	Respiratory Failure, Emphysema	COPD, Emphysema, Seasonal Allergies, Diabetes, GERD, Chronic Kidney Disease, Prostate Cancer, Coronary Artery Disease, Hypertension, Hyperlipidemia, Insomnia, Tobacco Use, Alcohol Abuse	Acetaminophen, Albuterol, Bisacodyl, Famotidine, Flutamide, Furosemide, Haldol, Hydralazine, Hydromorphone, Hyoscyamine, Isosorbide Mononitrate, Lorazepam, Metoprolol, Ondansetron, Senna, Tramadol, Xanax
Tox 021	M	71	162.5	211	Acute Respiratory Failure	Acute Kidney Injury, Alcohol Abuse, Ascites, ASCVD, Congestive Heart Failure, COPD, Gout, Stroke, Tobacco Abuse	Med list not obtained
Tox 022	F	60	155	199	Blunt force trauma	Bipolar, Diabetes, Hypertension, Schizophrenia	Med list not obtained

Table 3.2 – *Additional donor information.*

Donor ID	Date of Death	Date of Placement	Date Removed	Days Observed	Season of Placement	Last ADH Recorded
Tox 001	2/19/19	2/25/19	29 May 19	93	Winter	16,225
Tox 002	3/9/19	3/13/19	15 Apr 19	34	Spring	3,997
Tox 003	3/30/19	4/2/19	29 Apr 19	28	Spring	4,569
Tox 004	4/21/19	4/23/19	8 May 19	16	Spring	3,520
Tox 005	4/21/19	4/26/19	29 May 19	34	Spring	8,652
Tox 006	5/8/19	5/13/19	29 May 19	17	Spring	4,399
Tox 007	5/13/19	5/16/19	3 June 19	19	Spring	6,099
Tox 008	6/4/19	6/10/19	2 July 19	22	Summer	6,813
Tox 009	6/20/19	6/24/19	8 July 19	14	Summer	4,934
Tox 010	7/5/19	7/9/19	28 Aug 19	50	Summer	17,476
Tox 011	7/30/19	7/31/19	20 Aug 19	22	Summer	7,238
Tox 012	9/19/19	9/20/19	7 Oct 19	17	Summer	6,037
Tox 013	9/17/19	9/20/19	15 Oct 19	25	Summer	7,479
Tox 015	10/20/19	10/22/19	18 Nov 19	27	Fall	1,425
Tox 016	10/29/19	11/4/19	30 Dec 19	57	Fall	1,532
Tox 017	11/29/19	12/4/19	12 Jun 20	191	Winter	18,460
Tox 018	1/7/20	1/10/20	24 Mar 20	74	Winter	4,028
Tox 019	1/22/20	1/28/20	9 Apr 20	72	Winter	5,607
Tox 020	3/8/20	3/11/20	28 Apr 20	48	Winter	6,006
Tox 021	9/3/20	9/8/20	13 Oct 20	35	Summer	7,526
Tox 022	9/25/20	10/2/20	13 Aug 21	315	Fall	46,500

A

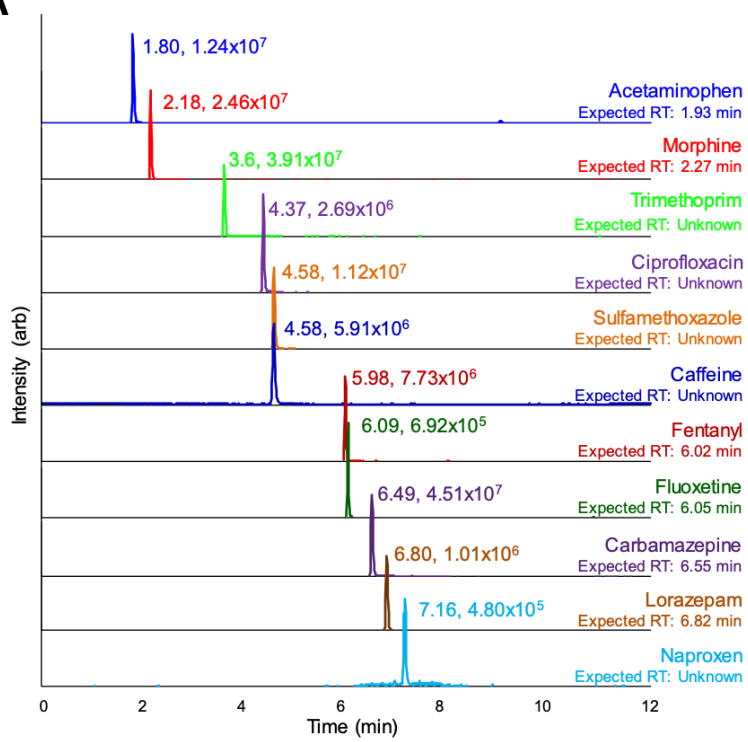

B

Validation parameters for each drug standard

Reference standard	*Linear range (ng/ml)*	*Linearity (R^2)*	*Limit of detection (ng/ml, LOD)*	*Limit of quantitation (ng/ml, LOQ)*
Acetaminophen	1 – 65	>0.99	2.51	7.62
Trimethoprim	5 – 65	0.98	13.68	41.45
Ciprofloxacin	35 – 65	0.94	17.01	51.55
Caffeine	1 – 65	>0.99	2.83	8.58
Sulfamethoxazole	1 – 65	>0.99	4.10	12.42
Fluoxetine	35 – 65	0.94	27.13	82.22
Naproxen	1 – 65	0.99	4.58	13.88
Lorazepam	5 – 65	0.99	10.30	31.21
Morphine	1 – 65	0.99	7.02	21.28
Fentanyl	35 – 65	0.87	21.64	65.57
Oxycodone	5 – 65	0.99	10.88	32.97
Nicotine	5 – 65	0.99	10.59	32.09

Figure 3.14 – *Extracted ion chromatograms (EICs) and method validation parameters. (A) EICs of standards as well as expected and actual retention times and intensities for each drug. (B) Linearity parameters, LOD, and LOQ of detected drug standards. (C) Method validation on a test donor with donor EICs shown in black and standard EICs shown in color (left) together with EICs of the other six drugs detected from the donor (right). The expected retention time is shown below the name and the actual retention time of each drug is listed above spectral features. Times shown in black are the most likely match to the drug.*

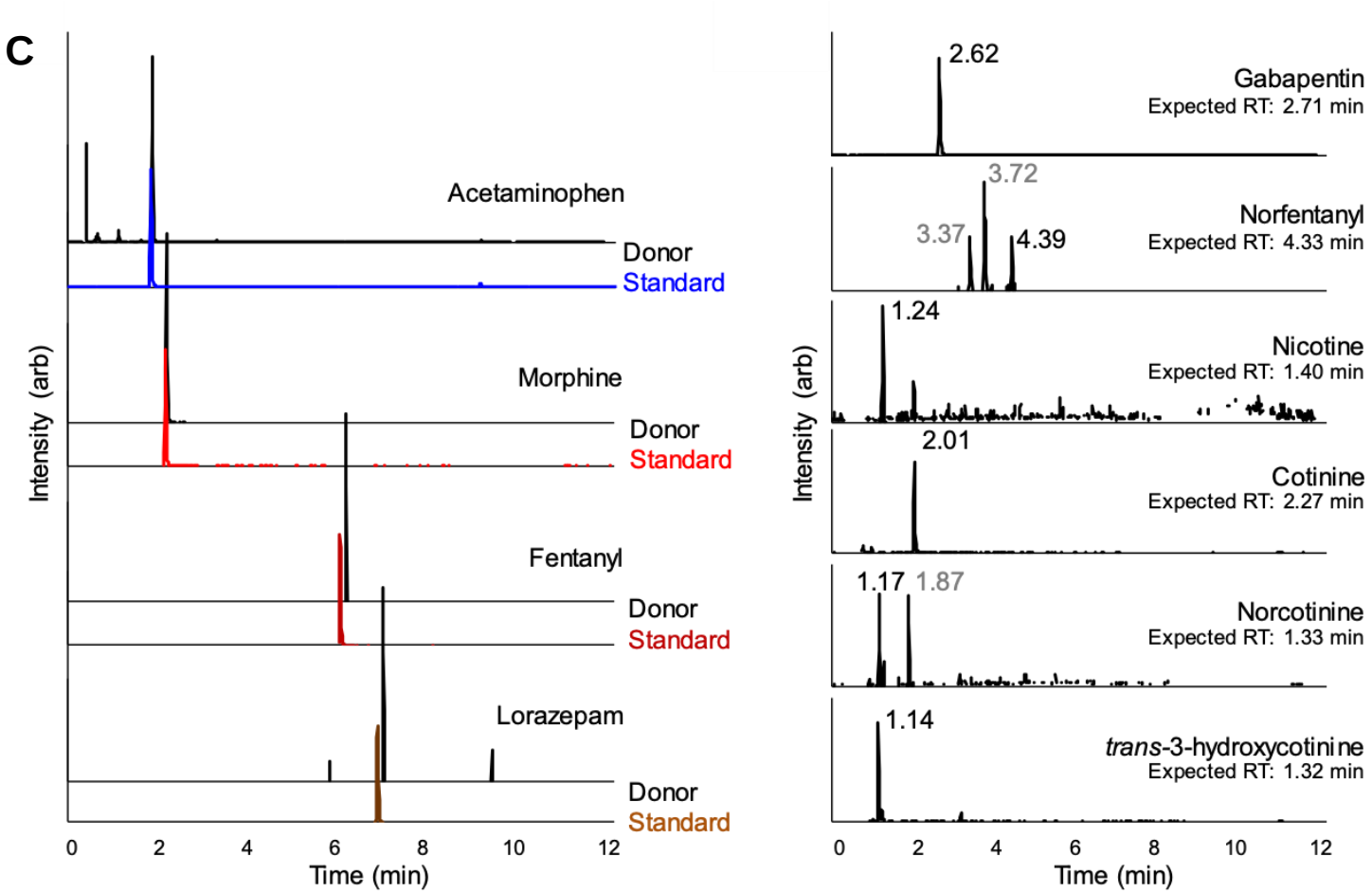

Figure 3.14 – *continued*

Table 3.3 – *Postmortem toxicology of different human specimens using UHPLC-HRMS.*

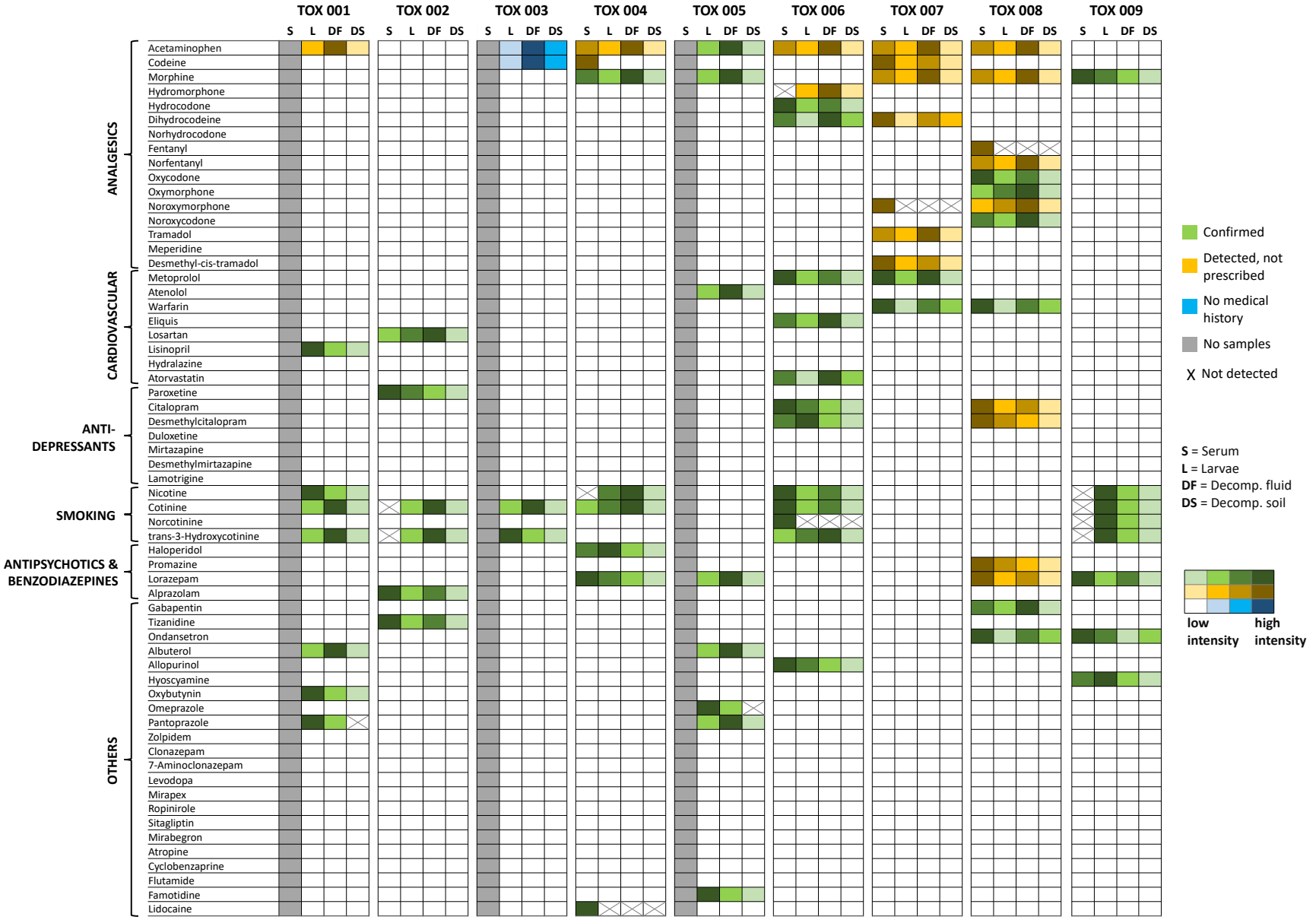

Table 3.3 – *continued*

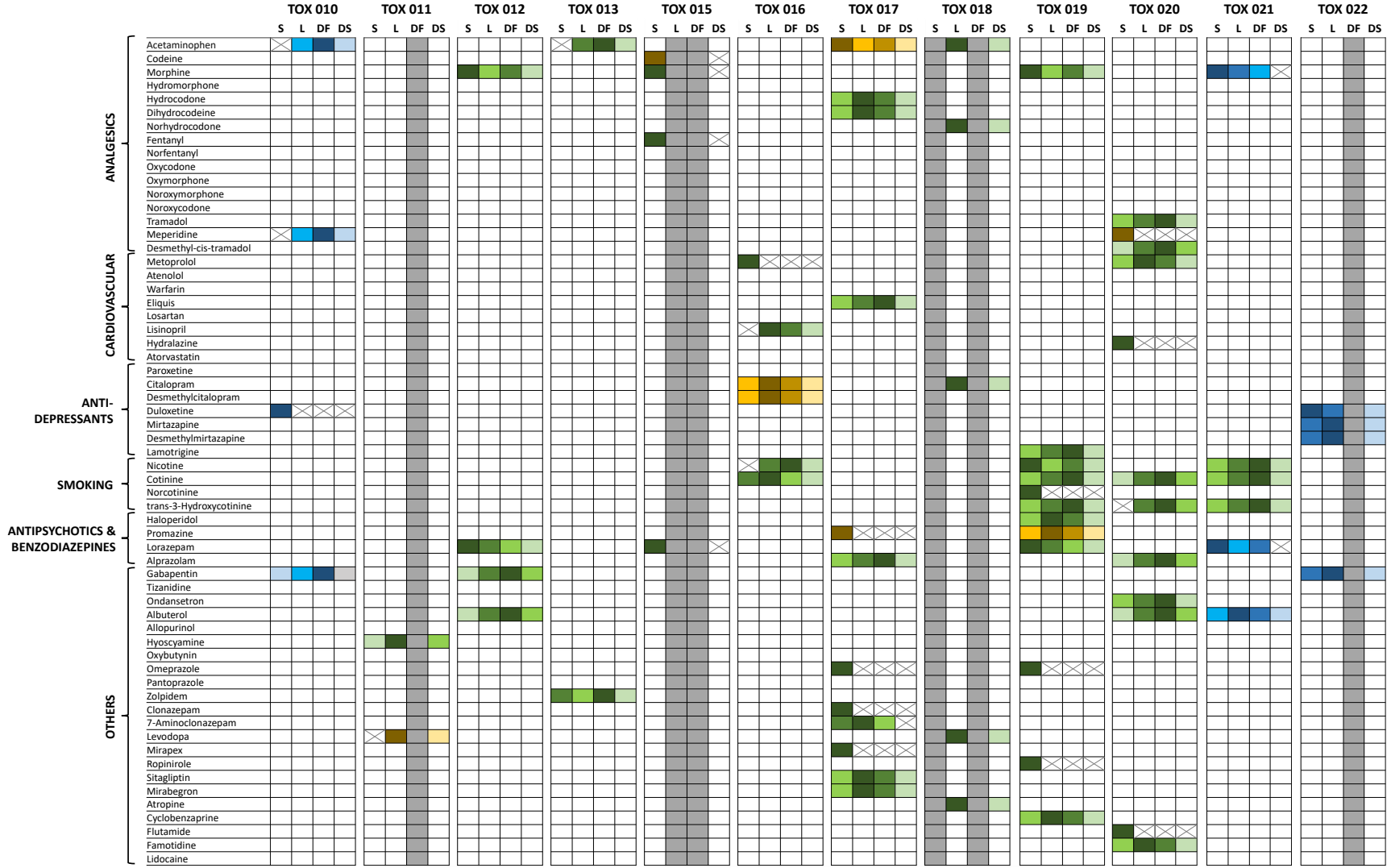

Table 3.4 – *Absolute postmortem drug concentrations in different human matrices (in ng/ml). Commercially available drug standards included acetaminophen (A), fentanyl (F), lorazepam (L), morphine (M), nicotine (N), and oxycodone (O). No serum could be obtained from donor Tox 001, 003, 005, and 018. No larvae and fluid samples were collected for Tox 015. Tox 014 was excluded from the study. C = central serum (aorta), P = peripheral serum (femoral vein).*

	SERUM						LARVAE					
	Concentration drug standards (in ng/ml)						Concentration drug standards (in ng/ml)					
Donor ID	**A***	**F**	**L**	**M**	**O**	**N**	**A**	**F**	**L**	**M**	**O**	**N**
Tox 001							8.71-1912.78					15.36-111.52
Tox 002												
Tox 003							4.70-47.86					
Tox 004	C: 262.92 P: 226.80		C: 69.66 P: 59.02	C: 543.21 P: 93.12			0.71-18.86		1.04-53.71	10.42-193.77		2.13-13.30
Tox 005							4.00-96.80		3.90-15.55	2.89-31.15		
Tox 006	C: 9616.33 P: 3705.44					C: 321.21 P: 150.62	186.33-1448.68					9.06-52.27
Tox 007	C: 6451.37 P: 4956.87			C: 189.39 P: 97.53			14.48-1522.26			29.84-271.73		
Tox 008	C: 1109.2 P: 679.75	C: 630.70 P: 351.66	C: 95.50 P: 34.97	C: 34.00 P: 17.23	C: 1033.29 P: 371.63		5.67-167.05		1.88-8.60	4.30-28.77	36.73-88.71	
Tox 009			C: 134.31 P: 102.96	C: 245.21 P: 244.55					1.39-57.71	7.33-133.53		8.22-13.10
Tox 010							19.49-75.70					
Tox 011												
Tox 012			C: 397.52 P: 37.71	C: 30071.04 P: 304.31					2.37-54.11	57.40-291.12		
Tox 013							76.31-173.28					
Tox 015		C: 43.03 P: 44.13	C: 13.10 P: 19.77	C: 186.57 P: 138.99								

Table 3.4 – *continued*

	SERUM						LARVAE					
	Concentration drug standards (in ng/ml)						Concentration drug standards (in ng/ml)					
Donor ID	**A***	**F**	**L**	**M**	**O**	**N**	**A**	**F**	**L**	**M**	**O**	**N**
Tox 016												2.48-5.66
Tox 017	C: 7774.00 P: 5904.16						26.80-291.08					
Tox 018							10.72					
Tox 019			C: 108.46 P: 61.63	C: 4327.46 P: 170.07		C: 97.18l P: 44.76				58.64-645.53	7.01-76.38	1.10-2.00
Tox 020												
Tox 021			C: 383.10 P: 257.51	C: 39.11 P: 37.23		C: 70.14 P: 46.12			24.38-179.31	4.79-65.18		7.02-73.60
Tox 022												

	DECOMPOSITION FLUID						DECOMPOSITION SOIL					
	Concentration drug standards (in ng/ml)						Concentration drug standards (in ng/ml)					
Donor ID	**A***	**F**	**L**	**M**	**O**	**N**	**A**	**F**	**L**	**M**	**O**	**N**
Tox 001	454.48-6516.36					25.72-108.06	0.63-2.94					2.38-3.56
Tox 002												
Tox 003	157.60-1483.72						1.11-164.68					
Tox 004	253.76		18.02	477.31		26.56	1.22-6.76		0.94-5.85	0.20-6.83		2.35-3.24
Tox 005	20.93-2358.64		3.74-56.15	1.93-243.55			1.48-40.06		1.22-4.40	0.08-20.40		
Tox 006	7324.05-12938.32					53.30-214.09	7.24-284.48					2.97-9.44
Tox 007	8302.81-10738.76			514.42-884.39			8.83-476.52			0.10-125.48		
Tox 008	1699.50-3308.79		3.79-50.43	59.93-357.14	68.82-245.98		4.01-6.47		1.04	0.11-4.69	0.71-8.01	
Tox 009			19.97-29.04	0.84-21.96		6.35-12.03			1.63-6.57	0.14-17.55		2.99-3.51

Table 3.4 – *continued*

	DECOMPOSITION FLUID						DECOMPOSITION SOIL					
	Concentration drug standards (in ng/ml)						Concentration drug standards (in ng/ml)					
Donor ID	**A***	**F**	**L**	**M**	**O**	**N**	**A**	**F**	**L**	**M**	**O**	**N**
Tox 010	0.20-2096.55						0.12-46.85					
Tox 011												
Tox 012			17.51-24.41	20.74-758.61					2.34-17.27	11.63-13.14		
Tox 013	64.37-396.50						9.41-339.24					
Tox 015												
Tox 016						4.48-5.23						0.17-0.23
Tox 017	7.23-2332.75						0.12-3.89					
Tox 018							0.25-0.48					
Tox 019			13.07-56.84	488.02-827.48		2.28-3.12			1.36-2.54	5.45-8.77		0.02-0.13
Tox 020												
Tox 021			109.45	4.79		42.69						
Tox 022												

** A=Acetaminophen, F= Fentanyl, L= Lorazepam, M= Morphine, O= Oxycodone, N= Nicotine*
C= Central, P= Peripheral

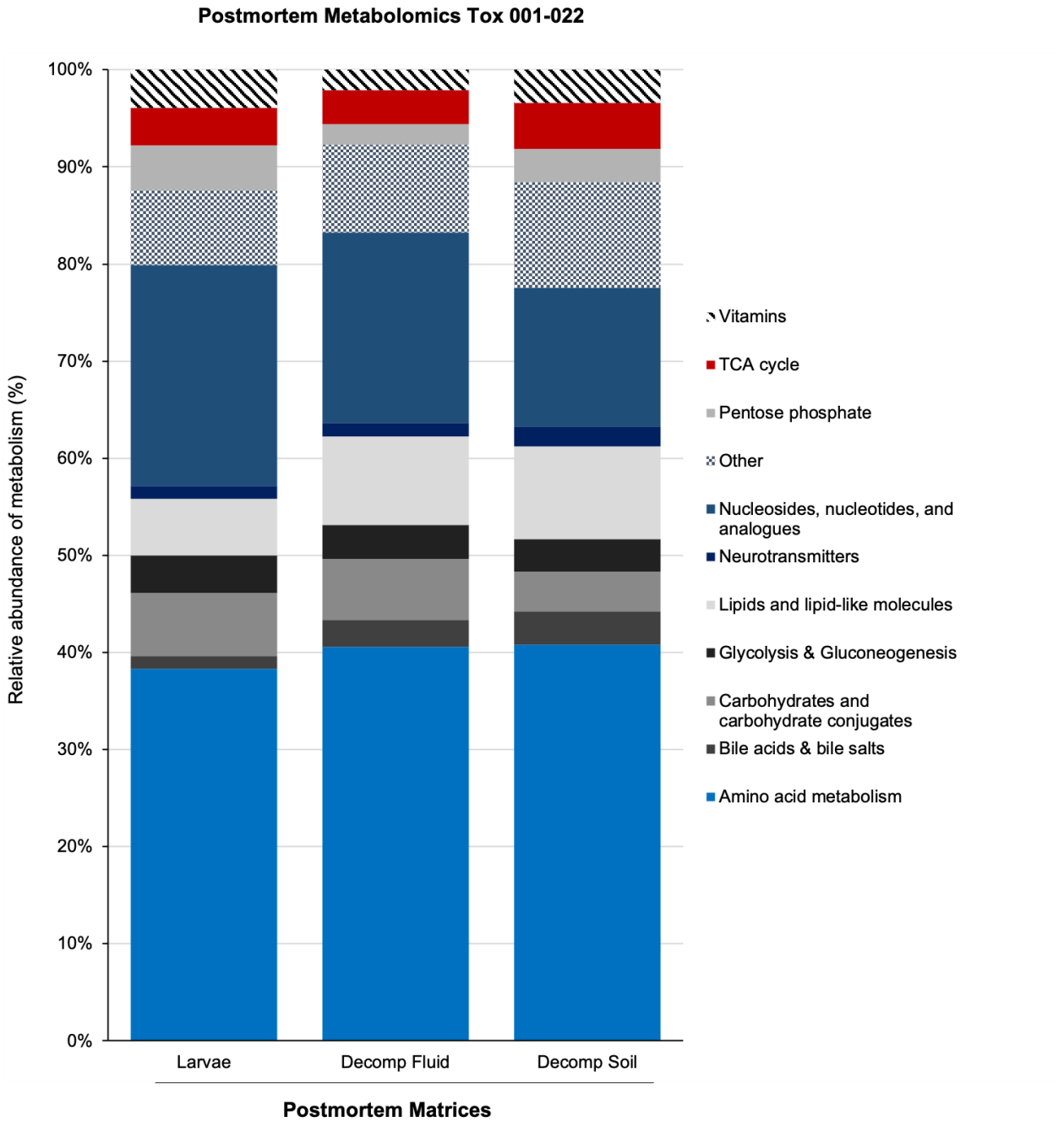

Figure 3.15 – *Relative abundance of metabolites in three postmortem matrices collected over the course of decomposition until the end of active decay. Compound classes are shown on the right. In each of the matrices, most of the detected metabolites (around 40%) were linked to the amino acid metabolism.*

Table 3.5 – *VIP scores for metabolites driving separations between decomposition fluid, soil, and larvae samples from all 22 donors.*

Metabolite name	VIP scores
3-Phosphoglycerate	2.6463
D-Gluconate	2.5789
Histidine	2.5544
N-Acetylornithine	2.3479
Lysine	2.3105
phosphorylethanolamine	2.2375
2-Aminoadipate	1.9459
Phosphoenolpyruvate	1.9381
Hydroxyproline	1.9378
Vanillin	1.9352
Uric acid	1.9005
N-Acetyl-beta-alanine	1.8917
N-Carbamoyl-L-aspartate	1.8855
Homocysteine	1.8818
2-hydroxyglutaric acid	1.8412
methylphenylacetic acid	1.815
3-Methylthiopropionate	1.8053
Sulfolactate	1.8018
Ornithine	1.7967
3-Hydroxyisovalerate	1.7848
IMP	1.764
Thymidine	1.7549
Histamine	1.7333
N-Acetylglutamate	1.7202
Arginine	1.7172
Acetylornithine	1.7085
ADP	1.6648
GMP	1.6582
4-Pyridoxate	1.6449
Asparagine	1.5738
Proline	1.5507
Fructose 1_6-bisphosphate	1.5297
homocitrulline	1.5275
4-Aminobutyrate (GABA)	1.4876
2-Isopropylmalate	1.4837
Glutathione	1.4707
Adenosine	1.4306
Hydroxylysine	1.4251
Cystathionine	1.4119

Metabolite names	VIP scores
N-Acetylglucosamine	1.4047
2-Oxo-4-methylthiobutanoate	1.4003
Xanthurenic acid	1.3945
Kynurenic acid	1.3881
GDP	1.3831
2-Oxoisovalerate	1.3688
Methyladenosine	1.3648
Phenylpyruvate	1.347
Tyrosine	1.3294
Malate	1.3009
2-Hydroxy-2-methylsuccinate	1.2857
Glutamine	1.2813
Sedoheptoluse bisphosphate	1.2797
Phenylalanine	1.276
D-Glucarate	1.2496
Aspartate	1.2314
3-Methylphenylacetic acid	1.2277
Xylose	1.214
Hydroxyisovalerate	1.2108
Citraconate	1.2096
Methionine sulfoxide	1.1977
Cystine	1.1717
Acetylglucosamine	1.1571
N-Acetylglutamine	1.1501
Dihydroorotate	1.1468
Acetyl-beta-alanine	1.1365
ATP	1.1295
Methylthiopropionate	1.1233
alpha-Ketoglutarate	1.1132
Creatinine	1.1079
Hypoxanthine	1.102
Dopamine	1.066
1-Methyladenosine	1.0526
Serine	1.0496
UDP-glucuronate	1.0473
Phenyllactic acid	1.0387
Anthranilate	1.0384
AMP/dGMP	1.036
NADP+	1.0185
Citrulline	1.0052

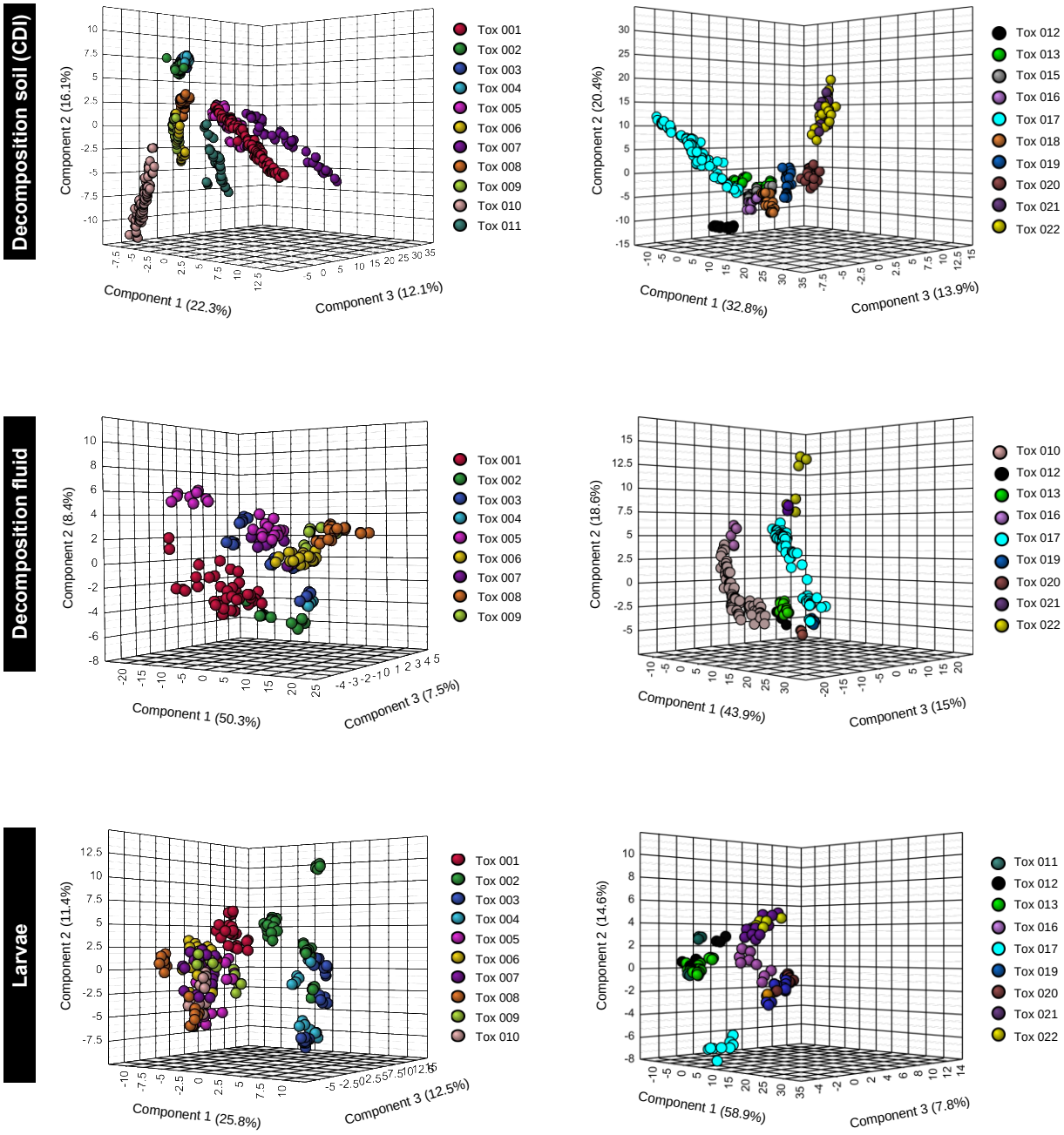

Figure 3.16 – *Intra-matrix multivariate analyses (PLS-DA) of larvae, decomposition fluid, and CDI soils for Tox 001-Tox 022.*

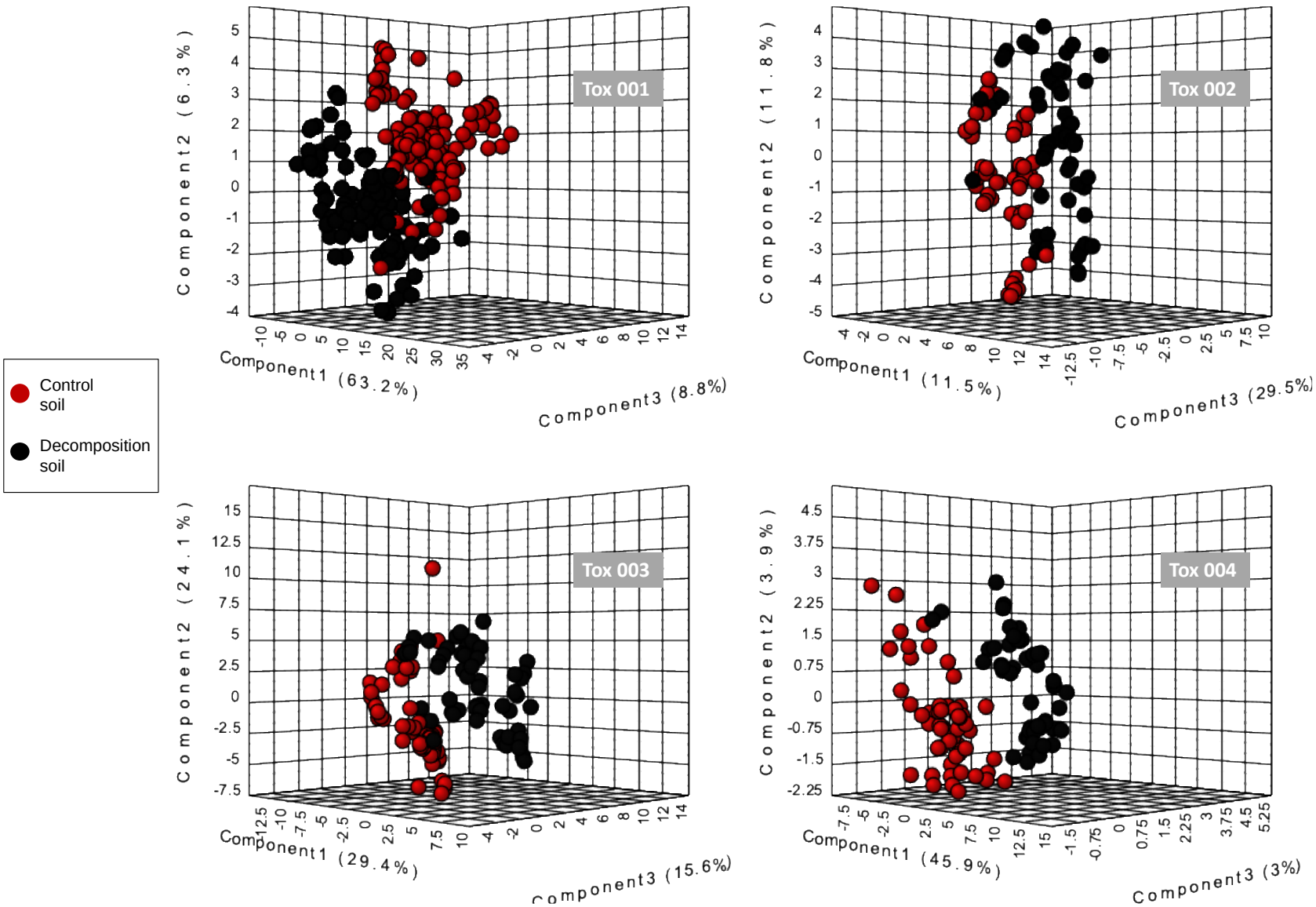

Figure 3.17 – *PLS-DA of metabolomics of control and decomposition soils for all 22 donors.*

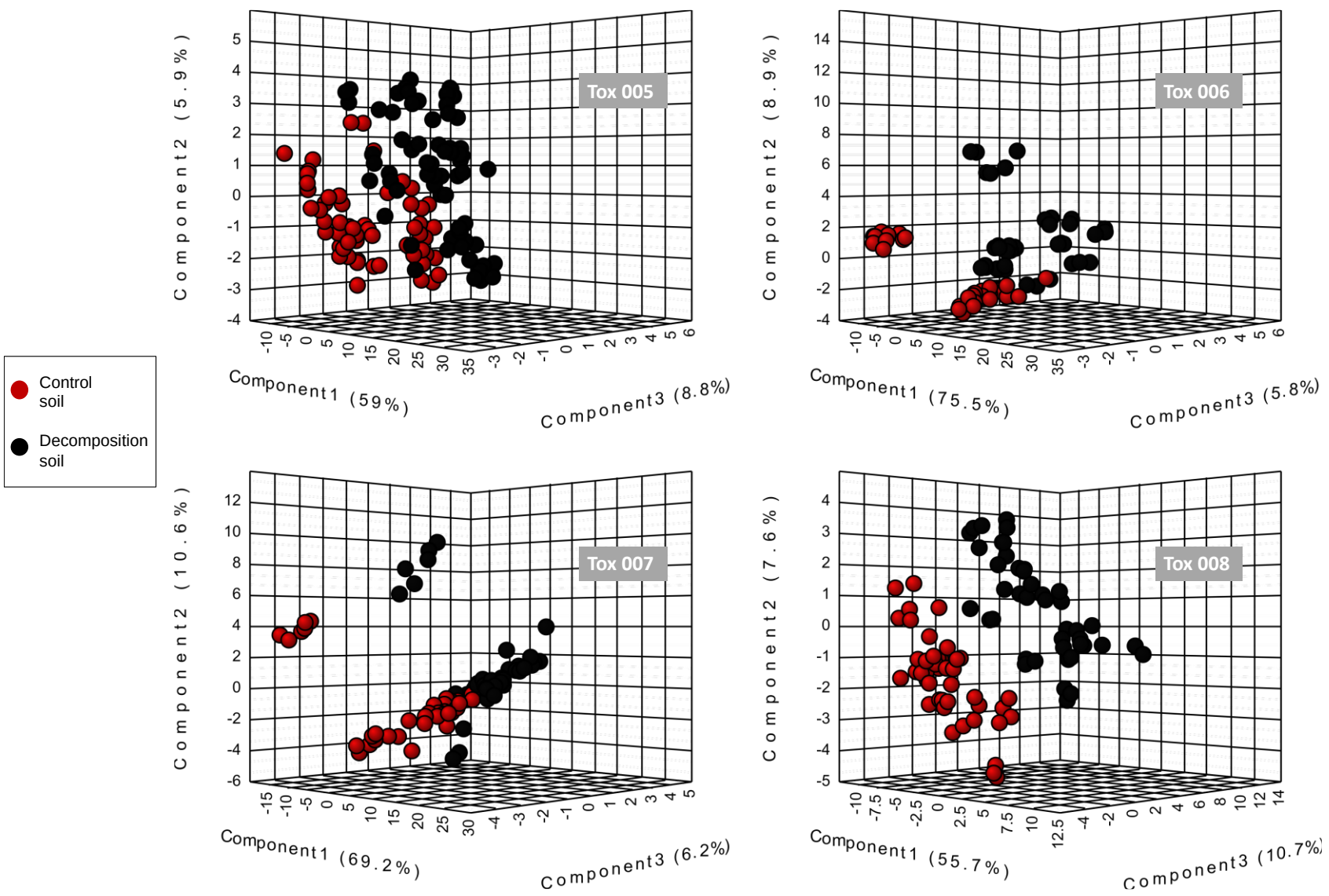

Figure 3.17 – *continued*

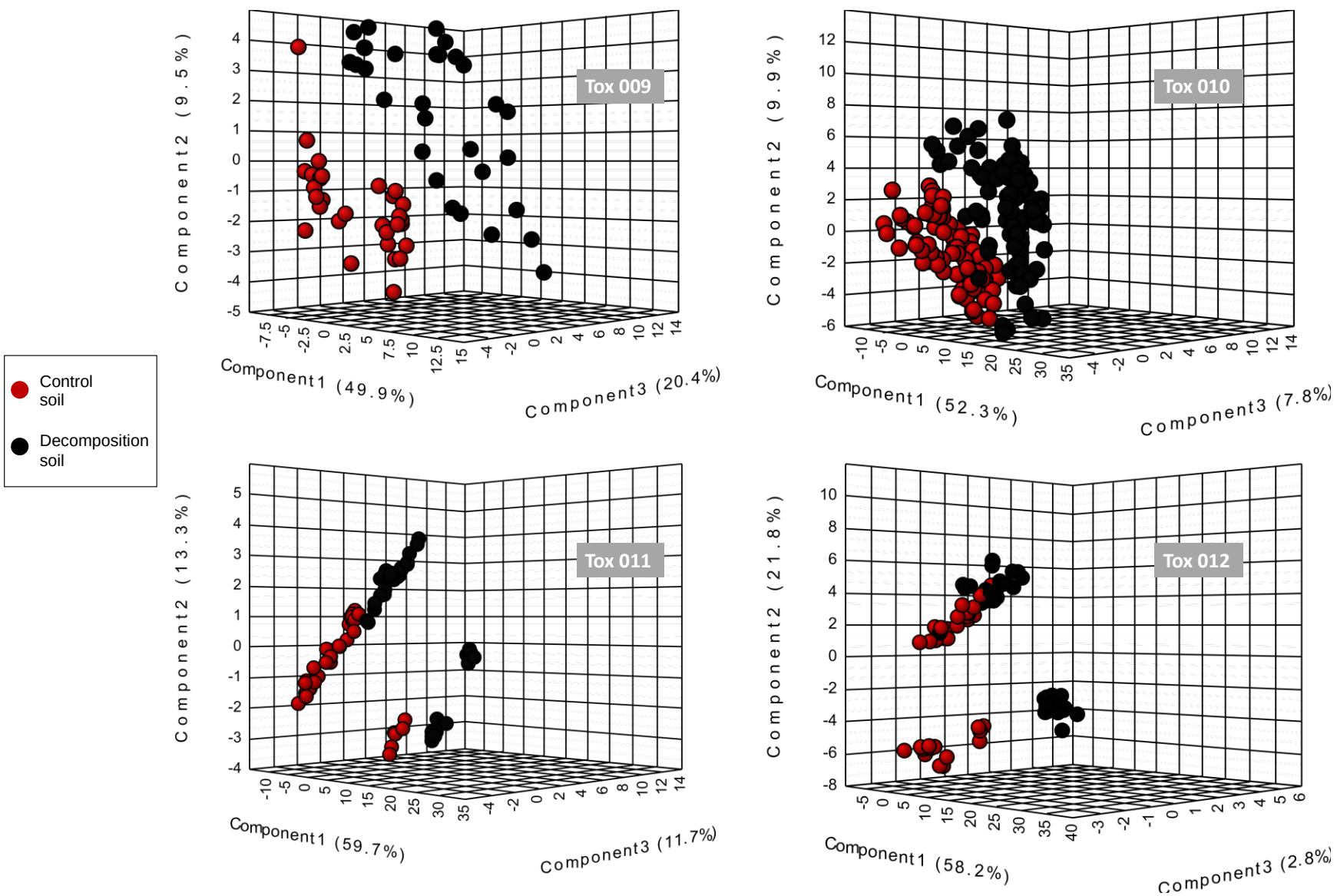

Figure 3.17 – *continued*

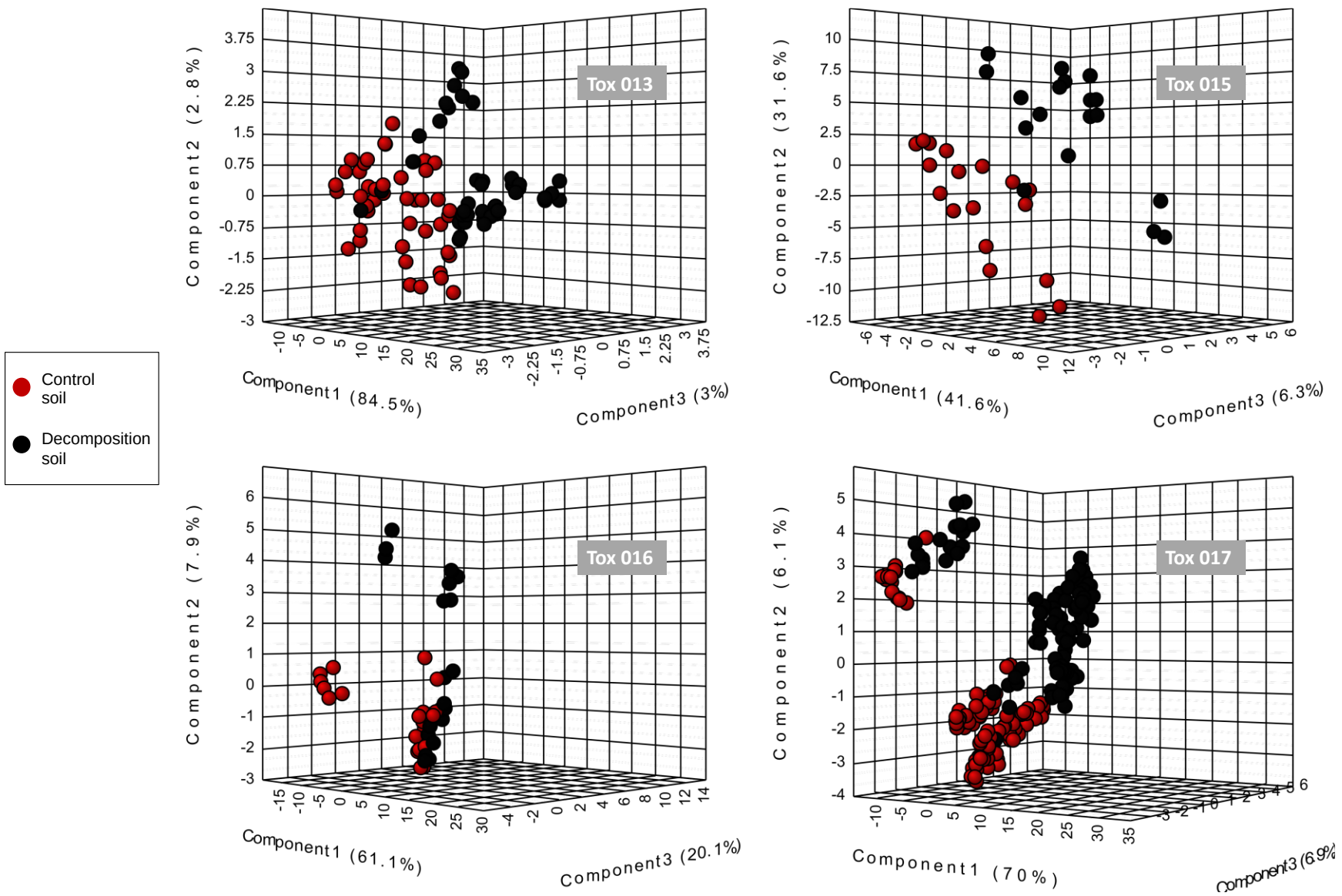

Figure 3.17 – *continued*

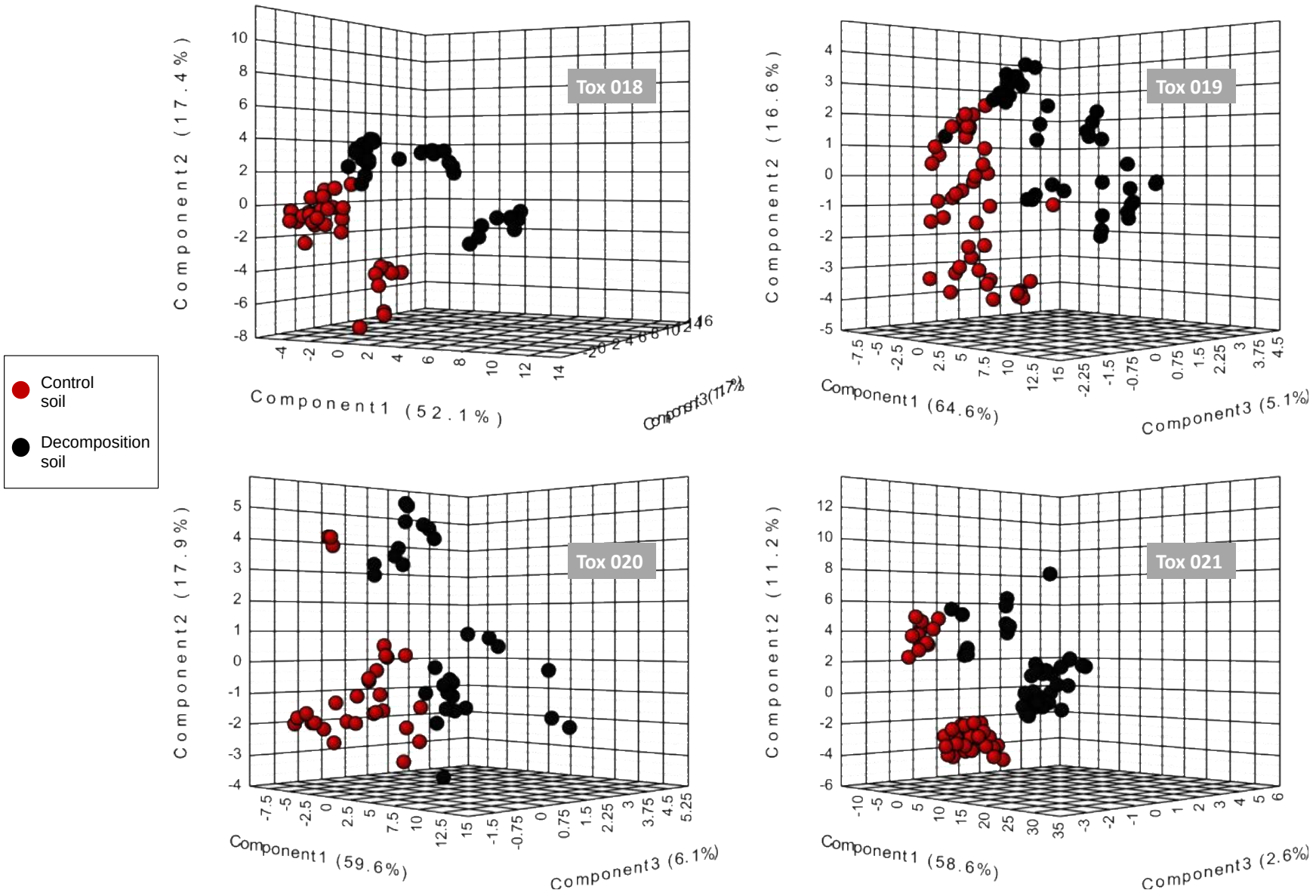

Figure 3.17 – *continued*

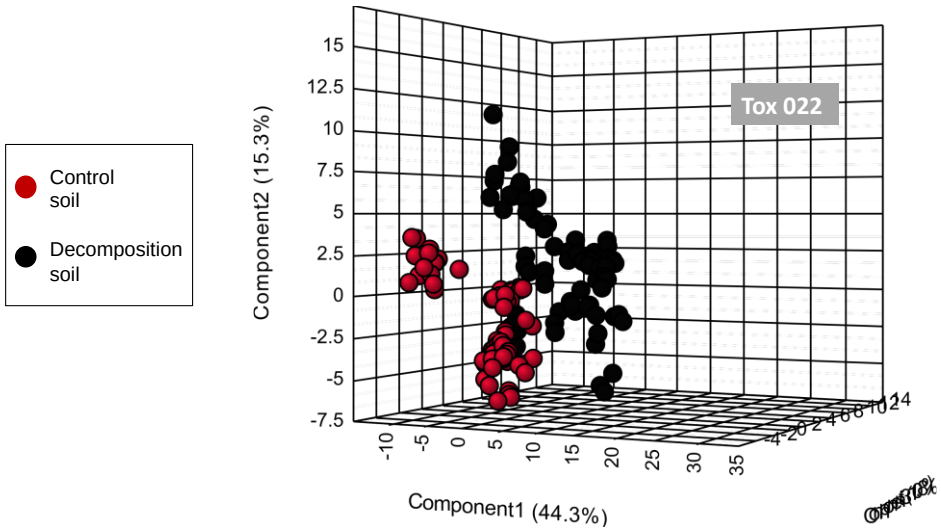

Figure 3.17 – *continued*

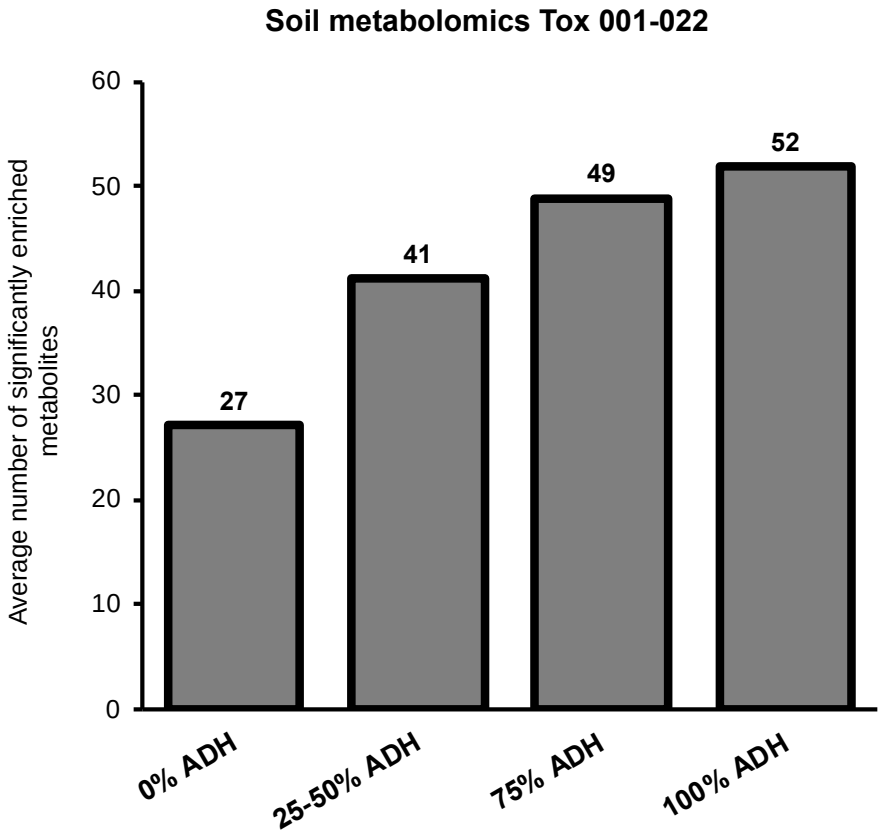

Figure 3.18 – *Number of significantly increased metabolites in decomposition compared to control soils across the entire decomposition period for all 22 donors. All donor samples were grouped by percent ADH. A 25-50% ADH class was necessary as certain donors did not have a specific ADH sample that classified for both 25% and 50% ADH. A significant increase was determined using cut-offs for fold change (decomposition soil/control soil) ≥ 1.5 and p-value ≤ 0.05.*

Table 3.6 – *Spearman rank correlation analysis. P-values for indole-3-carboxylate, taurine, and pantothenate. A p-value of < 0.05 determined significance.*

	Spearman p-values		
Tox ID	**indole-3-carboxylate**	**taurine**	**pantothenate**
Tox 001	< 0.001	< 0.001	<0.001
Tox 002	0.089	0.650	0.018
Tox 003	0.008	0.023	0.043
Tox 004	0.008	0.836	0.782
Tox 005	< 0.001	0.003	< 0.001
Tox 006	< 0.001	0.302	< 0.001
Tox 007	< 0.001	< 0.001	0.003
Tox 008	0.845	0.630	0.973
Tox 009	< 0.001	0.003	0.002
Tox 010	< 0.001	0.081	0.375
Tox 011	0.299	< 0.001	< 0.001
Tox 012	0.489	0.008	0.002
Tox 013	0.297	0.126	0.098
Tox 015	0.945	0.289	0.852
Tox 016	*Not detected*	0.878	0.404
Tox 017	*Not detected*	0.001	0.001
Tox 018	< 0.001	0.002	< 0.001
Tox 019	0.024	0.210	0.021
Tox 020	< 0.001	0.629	0.040
Tox 021	0.094	0.020	< 0.001
Tox 022	< 0.001	< 0.001	< 0.001

Table 3.7 – *Study donors grouped based on their medical profiles into four broad disease classes (diabetes, cancer, cardiovascular, and respiratory conditions). In the table on the bottom, donors with minor co-morbidities (listed in parentheses) were selected as the 'best' fit for each of the four classes and used for investigating disease impacts on the postmortem metabolome.*

Donors categorized by disease classes			
Diabetes	**Cancer**	**Cardiovascular condition**	**Respiratory condition**
Tox 001	Tox 001	Tox 001	Tox 001
Tox 010	Tox 002	Tox 006	Tox 003
Tox 012	Tox 004	Tox 007	Tox 005
Tox 015	Tox 005	Tox 008	Tox 006
Tox 017	Tox 006	Tox 010	Tox 010
Tox 020	Tox 008	Tox 011	Tox 015
Tox 022	Tox 009	Tox 012	Tox 016
	Tox 011	Tox 015	Tox 020
	Tox 016	Tox 016	Tox 021
	Tox 017	Tox 017	
	Tox 019	Tox 020	
	Tox 020	Tox 021	
		Tox 022	

Donors per diseases class with minor co-morbidities			
Diabetes	**Cancer**	**Cardiovascular condition**	**Respiratory condition**
Tox 012 (also circulatory)	Tox 002	Tox 007	Tox 003
Tox 022 (also circulatory)	Tox 004	Tox 008 (also cancer)	Tox 005 (also cancer)
	Tox 009	Tox 011 (also cancer)	Tox 021 (also circulatory)
	Tox 019	Tox 012 (also diabetes)	
		Tox 021 (also respiratory)	
		Tox 022 (also diabetes)	

Table 3.8 – *Inter-matrix comparisons for each of the four disease classes. Shown is the total number of identical VIP metabolites (blue) that occurred consistently in soil, fluid, and larvae. These metabolites contributed to a distinguishable postmortem metabolome for each of the disease comparisons. Metabolites were also assigned their metabolic pathways.*

	Disease class comparisons	Total number of identical VIP metabolites in soil, fluid, and larvae	Metabolic pathways
CANCER	Cancer vs Diabetes	**Alpha-ketoglutarate**	*TCA cycle*
		Tyrosine	*Amino acid metabolism*
		Glutamate	*Amino acid metabolism*
		Malate	*TCA cycle*
		Hydroxybenzoate	*Amino acid metabolism*
		Guanosine	*Nucleosides, nucleotides, and analogues*
		Deoxycytidine	*Nucleosides, nucleotides, and analogues*
		Glycine	*Bile acids & bile salts*
	Cancer vs Cardiovascular	**Succinate/Methylmalonate**	*TCA cycle*
		Proline	*Amino acid metabolism*
		Valine/betaine	*Amino acid metabolism*
		Uracil	*other*
		Homoserine/Threonine	*Amino acid metabolism*
		Serine	*Amino acid metabolism*
		Dimethylglycine	*Amino acid metabolism*
		Tricarballylic acid	*Other*
		Alpha-ketoglutarate	*TCA cycle*
		Creatinine	*Amino acid metabolism*
	Cancer vs Respiratory	**Creatine**	*Amino acid metabolism*
		Tyrosine	*Amino acid metabolism*
		Aminocaproic acid	*Lipids and lipid-like molecules*
		Citrulline	*Amino acid metabolism*
		Fumarate	*TCA cycle*
DIABETES	Diabetes vs Cancer	**Alpha-ketoglutarate**	*TCA cycle*
		Tyrosine	*Amino acid metabolism*
		Glutamate	*Amino acid metabolism*
		Malate	*TCA cycle*
		Hydroxybenzoate	*Amino acid metabolism*
		Guanosine	*Nucleosides, nucleotides, and analogues*
		Deoxycytidine	*Nucleosides, nucleotides, and analogues*
		Glycine	*Bile acids & bile salts*
	Diabetes vs Cardiovascular	**Xanthosine**	*Nucleosides, nucleotides, and analogues*
		Glutamate	*Amino acid metabolism*
		Guanosine	*Nucleosides, nucleotides, and analogues*
		Deoxycytidine	*Nucleosides, nucleotides, and analogues*
		Ornithine	*Amino acid metabolism*
	Diabetes vs Respiratory	**Malate**	*TCA cycle*
		Alpha-ketoglutarate	*TCA cycle*
		Dopamine	*Neurotransmitter*
		Citraconate	*Lipids and lipid-like molecules*
		Deoxycytidine	*Nucleosides, nucleotides, and analogues*
		Gluconolactone	*Pentose phosphate*
		Allantoate	*Amino acid metabolism*

Table 3.8 – *continued*

	Disease class comparisons	Total number of identical VIP metabolites in soil, fluid, and larvae	Metabolic pathways
CARDIOVASCULAR	Cardiovascular vs Cancer	**Succinate/Methylmalonate**	*TCA cycle*
		Proline	*Amino acid metabolism*
		Valine/Betaine	*Amino acid metabolism*
		Uracil	*other*
		Homoserine/Threonine	*Amino acid metabolism*
		Serine	*Amino acid metabolism*
		Dimethylglycine	*Amino acid metabolism*
		Tricarballylic acid	*Other*
		Alpha-ketoglutarate	*TCA cycle*
		Creatinine	*Amino acid metabolism*
	Cardiovascular vs Diabetes	**Xanthosine**	*Nucleosides, nucleotides, and analogues*
		Glutamate	*Amino acid metabolism*
		Guanosine	*Nucleosides, nucleotides, and analogues*
		Deoxycytidine	*Nucleosides, nucleotides, and analogues*
		Ornithine	*Amino acid metabolism*
	Cardiovascular vs Respiratory	***Dimethylglycine***	*Amino acid metabolism*
		Valine/Betaine	*Amino acid metabolism*
		Homoserine/Threonine	*Amino acid metabolism*
		Uracil	*Other*
		Proline	*Amino acid metabolism*
		Serine	*Amino acid metabolism*
		Succinate/Methylmalonate	*TCA cycle*
		Alpha-ketoglutarate	*TCA cycle*
		Citraconate	*Lipids and lipid-like molecules*
RESPIRATORY	Respiratory vs Cancer	**Creatine**	*Amino acid metabolism*
		Tyrosine	*Amino acid metabolism*
		Aminocaproic acid	*Lipids and lipid-like molecules*
		Citrulline	*Amino acid metabolism*
		Fumarate	*TCA cycle*
	Respiratory vs Diabetes	**Malate**	*TCA cycle*
		Alpha-ketoglutarate	*TCA cycle*
		Dopamine	*Neurotransmitter*
		Citraconate	*Lipids and lipid-like molecules*
		Deoxycytidine	*Nucleosides, nucleotides, and analogues*
		Gluconolactone	*Pentose phosphate*
		Allantoate	*Amino acid metabolism*
	Respiratory vs Cardiovascular	***Dimethylglycine***	*Amino acid metabolism*
		Valine/Betaine	*Amino acid metabolism*
		Homoserine/Threonine	*Amino acid metabolism*
		Uracil	*Other*
		Proline	*Amino acid metabolism*
		Serine	*Amino acid metabolism*
		Succinate/Methylmalonate	*TCA cycle*
		Alpha-ketoglutarate	*TCA cycle*
		Citraconate	*Lipids and lipid-like molecules*

CONCLUSION

Advances in analytical chemistry have enabled the design of high-resolution mass spectrometry platforms which were used in the presented studies to investigate metabolic signatures of mammalian decomposition at an outdoor taphonomy facility in Knoxville, Tennessee, USA. Our work exemplifies the exploratory nature of several chemometric strategies that opened new avenues for future forensic taphonomy studies. 'Omics' platforms yield a great knowledge gain when it comes to understanding overall decomposition trajectories. The above chapters demonstrated how versatile, complex, and dynamic the postmortem metabolome is, yet, at the same time susceptible to a likewise complex amount of intrinsic and extrinsic factors. Knowing this, it requires a similarly diverse approach to capture these dynamics. Rapidly developing state-of-the-art analytical platforms will meet these needs even better in the near future and therefore allow a more superior understanding of taphonomy on a metabolic level. This is promising particularly when it comes to the estimation of the time since death. Using a group of metabolites as decomposition biomarkers may augment current techniques to increase the precision and accuracy of such estimates.

Conversely, all of the studies in this dissertation have also revealed clear limitations. Generally, it should be noted that our outcomes refer solely to the local environment and soil type prevailing at the Anthropology Research Facility (ARF) in Knoxville, Tennessee. Accordingly, the varying experimental outdoor designs found across literature challenged the interpretation of our results. How and to which extent the postmortem metabolomes from decomposing remains differ for scenarios at other taphonomy facilities such as the one in Sydney (AFTER, Australian Facility for Taphonomic Experimental Research) remains to be determined. Certainly, one of the most intense criticisms that taphonomy facilities face are related to the contamination or saturation of soil with decomposition-derived products that makes it incredibly challenging to obtain a feasible molecular baseline from within these facilities[124, 187]. Studies by *Damann et al.* revealed a high similarity of soils obtained within the ARF in Knoxville when compared to samples taken from approximately 1 km away in a similar forest biome[187]. Characteristic ARF soil features comprised elevated pH, total nitrogen, water, and lipid

phosphorus in areas of high decomposition[187]. The proposed homogenization of ARF soils was speculated to result from a continuous decomposition input spanning over 40 years of research. The same researchers suggested that soil chemistry at ARF has most likely not yet returned to a baseline level and soil microbial communities could have adapted to the prevalent soil composition. Furthermore, with our metabolic snapshot it is fairly difficult to provide definite conclusions about if changes in metabolite abundances were of catabolic or anabolic nature, nor if compounds were of plant, human, or microbial origin. A topic that will remain to be elucidated in future work.

Nevertheless, the performed untargeted studies considerably contributed to the taphonomy groundwork broadening the understanding of fundamental processes of decomposition and the cycling of decomposition products from carcasses into the surrounding ecosystem. This dissertation demonstrated the potential of postmortem metabolomics throughout several different research designs, matrices, as well as species. Through comprehensive literature research, we have tentatively interpreted the observed findings with the hope to attract enough scientific curiosity for future research to obtain a more holistic view of the metabolic signature of decomposition. To our knowledge, only a few other studies have investigated the postmortem biochemical environment on such a detailed molecular scale with superior analytical instrumentation. We demonstrated that postmortem samples taken from a burial were susceptible to the heterogenous microhabitat prevailing at different burial depths and likewise on several skeletal remains. Additionally, we identified differential metabolite signatures in the cadaver decomposition island (CDI) from decomposing humans and pigs. From a biochemical perspective, decay progressed on a different scale among both mammals. When it comes to deconvoluting intrinsic drivers of human decomposition, we showed the urge for more interdisciplinary research to verify our exploratory findings and definitively pinpoint impacts of diseases on decomposition. Given this, our work was most certainly the first that ‘reassigned’ a unique toxicological profile to a decomposing cadaver along with the novelty of detecting drugs in various cadaveric specimens (serum, larvae, decomposition fluid, and soil). The proposed use of certain groups of metabolites (especially pantothenate and taurine) as biomarkers in PMI estimations may help to reduce examiner bias and increase approximation reliability by narrowing down the time

frame of when death occurred. We hope that implications of future studies will provide supportive information for forensic toxicologists, medical examiners, and law enforcement agencies with regard to estimating the time since death.

Lastly, the attentive reader might have recognized that soil organic matter was the only constant matrix throughout all three chapters. Not only decomposition but also control soils were obtained for all projects, which is why a currently ongoing comparative inter-study analysis aims to determine if there is a coinciding metabolic signature of decomposition soil (data not shown). During the early stages of data consolidation, multivariate analysis has drawn attention to a selected number of metabolites enriched in decomposition-impacted soils. Specifically, creatine, methionine, and taurine were the only amino acids consistently and significantly increased in abundance in cadaveric soils from (a) a burial (chapter I), (b) pig and human cadavers (chapter II), and (c) solely human cadavers (chapter III) (inter-study p-value range for creatine, methionine, taurine $p = 0.04 – 4.89E\text{-}115$). An exciting result considering the fact that both taurine and methionine are sulfur-containing amino acids. Microbial decomposition of free sulfur-containing amino acids can produce volatile sulfur compounds which were previously detected in decomposition studies by *Dekeirsschieter et al.* and *Statheropoulos et al.*[22, 188]. Creatine is a non-proteinogenic amino acid. 95% of creatine can be found in the skeletal muscle[189]. It is also a metabolite of arginine, glycine and methionine[189]. Studies with rats and mice have shown marked increases in creatine in blood and tissues over the early postmortem interval (24-72 h)[54, 190].

REFERENCES

1. Nolan, A.-N. Investigating the peptide profile of decomposition fluid by liquid chromatography mass spectrometry to assist in the determination of the post-mortem interval (PMI). Murdoch University, 2020.
2. Goff, M. L., Early post-mortem changes and stages of decomposition in exposed cadavers. *Experimental and applied acarology* **2009,** *49* (1), 21-36.
3. Damann, F. E., Human Decomposition Ecology at the University of Tennessee Anthropology Research Facility. **2010**.
4. Stadler, S. Analysis of the volatile organic compounds produced by the decomposition of pig carcasses and human remains. 2013.
5. Comstock, J. L.; Desaulniers, J.-P.; LeBlanc, H. N.; Forbes, S. L., New decomposition stages to describe scenarios involving the partial and complete exclusion of insects. *Canadian Society of Forensic Science Journal* **2015,** *48* (1), 1-19.
6. Clark, M. A.; Worrell, M. B.; Pless, J. E., Postmortem changes in soft tissues. *Forensic taphonomy: the postmortem fate of human remains* **1997**, 151-164.
7. Buis, R. C. The validation of human decomposition fluid as a cadaver-detection dog training aid. 2016.
8. Nolan, A.-N. D.; Mead, R. J.; Maker, G.; Speers, S. J., A review of the biochemical products produced during mammalian decomposition with the purpose of determining the post-mortem interval. *Australian Journal of Forensic Sciences* **2020,** *52* (4), 477-488.
9. Hau, T. C.; Hamzah, N. H.; Lian, H. H.; Hamzah, S., Decomposition process and post mortem changes. *Sains Malaysiana* **2014,** *43* (12), 1873-1882.
10. Carter, D. O.; Yellowlees, D.; Tibbett, M., Cadaver decomposition in terrestrial ecosystems. *Naturwissenschaften* **2007,** *94* (1), 12-24.
11. Forbes, S. L., Decomposition chemistry in a burial environment. In *Soil analysis in forensic taphonomy*, CRC Press: 2008; pp 215-236.
12. Pinheiro, J.; 00E3o, Decay process of a cadaver. *Forensic anthropology and medicine: complementary sciences from recovery to cause of death* **2006**, 85-116.

13. Dautartas, A. M., The effect of various coverings on the rate of human decomposition. *Masters Theses* **2009**, 69.
14. Wescott, D. J., Recent advances in forensic anthropology: decomposition research. *Forensic sciences research* **2018,** *3* (4), 278-293.
15. Mann, R. W.; Bass, W. M.; Meadows, L., Time since death and decomposition of the human body: variables and observations in case and experimental field studies. *Journal of Forensic Science* **1990,** *35* (1), 103-111.
16. Dent, B. B.; Forbes, S. L.; Stuart, B. H., Review of human decomposition processes in soil. *Environmental geology* **2004,** *45* (4), 576-585.
17. Janaway, R. C.; Percival, S. L.; Wilson, A. S., Decomposition of human remains. In *Microbiology and aging*, Springer: 2009; pp 313-334.
18. Vass, A. A.; Barshick, S.-A.; Sega, G.; Caton, J.; Skeen, J. T.; Love, J. C.; Synstelien, J. A., Decomposition chemistry of human remains: a new methodology for determining the postmortem interval. *Journal of Forensic Science* **2002,** *47* (3), 542-553.
19. Vass, A. A., Odor mortis. *Forensic Science International* **2012,** *222* (1-3), 234-241.
20. Cablk, M. E.; Szelagowski, E. E.; Sagebiel, J. C., Characterization of the volatile organic compounds present in the headspace of decomposing animal remains, and compared with human remains. *Forensic science international* **2012,** *220* (1-3), 118-125.
21. Statheropoulos, M.; Spiliopoulou, C.; Agapiou, A., A study of volatile organic compounds evolved from the decaying human body. *Forensic science international* **2005,** *153* (2-3), 147-155.
22. Dekeirsschieter, J.; Stefanuto, P.-H.; Brasseur, C.; Haubruge, E.; Focant, J.-F., Enhanced characterization of the smell of death by comprehensive two-dimensional gas chromatography-time-of-flight mass spectrometry (GCxGC-TOFMS). *PLoS One* **2012,** *7* (6), e39005.
23. Brasseur, C.; Dekeirsschieter, J.; Schotsmans, E. M.; de Koning, S.; Wilson, A. S.; Haubruge, E.; Focant, J.-F., Comprehensive two-dimensional gas chromatography–time-of-flight mass spectrometry for the forensic study of cadaveric

volatile organic compounds released in soil by buried decaying pig carcasses. *Journal of chromatography A* **2012,** *1255*, 163-170.

24. Vass, A. A.; Smith, R. R.; Thompson, C. V.; Burnett, M. N.; Dulgerian, N.; Eckenrode, B. A., Odor analysis of decomposing buried human remains. *Journal of Forensic Sciences* **2008,** *53* (2), 384-391.

25. Aitkenhead-Peterson, J. A.; Alexander, M. B.; Bytheway, J. A.; Carter, D. O.; Wescott, D. J., Applications of soil chemistry in forensic entomology. *Forensic entomology: International dimensions and frontiers* **2015,** *283*.

26. DeBruyn, J. M.; Hoeland, K. M.; Taylor, L. S.; Stevens, J. D.; Moats, M. A.; Bandopadhyay, S.; Dearth, S. P.; Castro, H. F.; Hewitt, K. K.; Campagna, S. R., Comparative Decomposition of Humans and Pigs: Soil Biogeochemistry, Microbial Activity and Metabolomic Profiles. *Frontiers in microbiology* **2021,** *11*, 3521.

27. Hopkins, D.; Wiltshire, P.; Turner, B., Microbial characteristics of soils from graves: an investigation at the interface of soil microbiology and forensic science. *Applied Soil Ecology* **2000,** *14* (3), 283-288.

28. Keenan, S. W.; Emmons, A. L.; Taylor, L. S.; Phillips, G.; Mason, A. R.; Mundorff, A. Z.; Bernard, E. C.; Davoren, J.; DeBruyn, J. M., Spatial impacts of a multi-individual grave on microbial and microfaunal communities and soil biogeochemistry. *PloS one* **2018,** *13* (12), e0208845.

29. Vass, A. A.; Bass, W. M.; Wolt, J. D.; Foss, J. E.; Ammons, J. T., Time since death determinations of human cadavers using soil solution. *Journal of Forensic Science* **1992,** *37* (5), 1236-1253.

30. Larizza, M.; Forbes, S. L., Detection of fatty acids in the lateral extent of the cadaver decomposition island. *Geological Society, London, Special Publications* **2013,** *384* (1), 209-219.

31. Barton, P. S.; Reboldi, A.; Dawson, B. M.; Ueland, M.; Strong, C.; Wallman, J. F., Soil chemical markers distinguishing human and pig decomposition islands: a preliminary study. *Forensic Science, Medicine and Pathology* **2020,** *16* (4), 605-612.

32. Fancher, J.; Aitkenhead-Peterson, J.; Farris, T.; Mix, K.; Schwab, A.; Wescott, D.; Hamilton, M., An evaluation of soil chemistry in human cadaver decomposition

islands: Potential for estimating postmortem interval (PMI). *Forensic science international* **2017,** *279*, 130-139.

33. Benninger, L. A.; Carter, D. O.; Forbes, S. L., The biochemical alteration of soil beneath a decomposing carcass. *Forensic science international* **2008,** *180* (2-3), 70-75.

34. Anderson, B.; Meyer, J.; Carter, D. O., Dynamics of ninhydrin-reactive nitrogen and pH in gravesoil during the extended postmortem interval. *Journal of Forensic Sciences* **2013,** *58* (5), 1348-1352.

35. Cobaugh, K. L.; Schaeffer, S. M.; DeBruyn, J. M., Functional and structural succession of soil microbial communities below decomposing human cadavers. *PloS one* **2015,** *10* (6), e0130201.

36. Castillo-Peinado, L.; de Castro, M. L., Present and foreseeable future of metabolomics in forensic analysis. *Analytica chimica acta* **2016,** *925*, 1-15.

37. Marchand, J.; Guitton, Y.; Martineau, E.; Royer, A.-L.; Balgoma, D.; Le Bizec, B.; Giraudeau, P.; Dervilly, G., Combining mass spectrometric platforms for lipidome investigation-Application to the characterisation of disruptions in the lipid profile of pig serum upon β-agonist treatment. *bioRxiv* **2020**.

38. Fiehn, O.; Weckwerth, W., Deciphering metabolic networks. *European Journal of Biochemistry* **2003,** *270* (4), 579-588.

39. Fiehn, O., Metabolomics—the link between genotypes and phenotypes. *Functional genomics* **2002**, 155-171.

40. Szeremeta, M.; Pietrowska, K.; Niemcunowicz-Janica, A.; Kretowski, A.; Ciborowski, M., Applications of Metabolomics in Forensic Toxicology and Forensic Medicine. *International Journal of Molecular Sciences* **2021,** *22* (6), 3010.

41. Akcan, R.; Taştekin, B.; Yildirim, M. Ş.; Aydogan, H. C.; Sağlam, N., Omics era in forensic medicine: Towards a new age. *Turkish journal of medical sciences* **2020,** *50* (5), 1480-1490.

42. Locci, E.; Stocchero, M.; Noto, A.; Chighine, A.; Natali, L.; Napoli, P. E.; Caria, R.; De-Giorgio, F.; Nioi, M.; d'Aloja, E., A 1 H NMR metabolomic approach for the estimation of the time since death using aqueous humour: an animal model. *Metabolomics* **2019,** *15* (5), 76.

43. Pesko, B. K.; Weidt, S.; McLaughlin, M.; Wescott, D. J.; Torrance, H.; Burgess, K.; Burchmore, R., Postmortomics: The potential of untargeted metabolomics to highlight markers for time since death. *OMICS: A Journal of Integrative Biology* **2020,** *24* (11), 649-659.
44. Rousseau, G.; Chao de la Barca, J. M.; Rougé-Maillart, C.; Teresiński, G.; Chabrun, F.; Dieu, X.; Drevin, G.; Mirebeau-Prunier, D.; Simard, G.; Reynier, P., Preliminary Metabolomic Profiling of the Vitreous Humor from Hypothermia Fatalities. *Journal of Proteome Research* **2021,** *20* (5), 2390-2396.
45. Zelentsova, E. A.; Yanshole, L. V.; Melnikov, A. D.; Kudryavtsev, I. S.; Novoselov, V. P.; Tsentalovich, Y. P., Post-mortem changes in metabolomic profiles of human serum, aqueous humor and vitreous humor. *Metabolomics* **2020,** *16* (7), 1-10.
46. Zelentsova, E. A.; Yanshole, L. V.; Snytnikova, O. A.; Yanshole, V. V.; Tsentalovich, Y. P.; Sagdeev, R. Z., Post-mortem changes in the metabolomic compositions of rabbit blood, aqueous and vitreous humors. *Metabolomics* **2016,** *12* (11), 1-11.
47. Zhang, J.; Wang, M.; Qi, X.; Shi, L.; Zhang, J.; Zhang, X.; Yang, T.; Ren, J.; Liu, F.; Zhang, G., Predicting the postmortem interval of burial cadavers based on microbial community succession. *Forensic Science International: Genetics* **2021,** *52*, 102488.
48. Banaschak, S.; Rzanny, R.; Reichenbach, J.; Kaiser, W.; Klein, A., Estimation of postmortem metabolic changes in porcine brain tissue using 1 H-MR spectroscopy—preliminary results. *International journal of legal medicine* **2005,** *119* (2), 77-79.
49. Harada, H.; Maeiwa, M.; Yoshikawa, K.; Ohsaka, A., Identification and quantitation by 1H-NMR of metabolites in animal organs and tissues. An application of NMR spectroscopy in forensic science. *Forensic science international* **1984,** *24* (1), 1-7.
50. Kang, Y.-R.; Park, Y. S.; Park, Y. C.; Yoon, S. M.; JongAhn, H.; Kim, G.; Kwon, S. W., UPLC/Q-TOF MS based metabolomics approach to post-mortem-interval discrimination: mass spectrometry based metabolomics approach. *Journal of Pharmaceutical Investigation* **2012,** *42* (1), 41-46.
51. Donaldson, A.; Lamont, I., Metabolomics of post-mortem blood: identifying potential markers of post-mortem interval. *Metabolomics* **2015,** *11* (1), 237-245.

52. Donaldson, A. E.; Lamont, I. L., Biochemistry changes that occur after death: potential markers for determining post-mortem interval. *PloS one* **2013,** *8* (11), e82011.
53. Sato, T.; Zaitsu, K.; Tsuboi, K.; Nomura, M.; Kusano, M.; Shima, N.; Abe, S.; Ishii, A.; Tsuchihashi, H.; Suzuki, K., A preliminary study on postmortem interval estimation of suffocated rats by GC-MS/MS-based plasma metabolic profiling. *Analytical and bioanalytical chemistry* **2015,** *407* (13), 3659-3665.
54. Mora-Ortiz, M.; Trichard, M.; Oregioni, A.; Claus, S. P., Thanatometabolomics: introducing NMR-based metabolomics to identify metabolic biomarkers of the time of death. *Metabolomics* **2019,** *15* (3), 1-11.
55. Carter, D. O.; Yellowlees, D.; Tibbett, M., Temperature affects microbial decomposition of cadavers (Rattus rattus) in contrasting soils. *Applied Soil Ecology* **2008,** *40* (1), 129-137.
56. Child, A. M., Microbial taphonomy of archaeological bone. *Studies in conservation* **1995,** *40* (1), 19-30.
57. Metcalf, J. L.; Parfrey, L. W.; Gonzalez, A.; Lauber, C. L.; Knights, D.; Ackermann, G.; Humphrey, G. C.; Gebert, M. J.; Van Treuren, W.; Berg-Lyons, D., A microbial clock provides an accurate estimate of the postmortem interval in a mouse model system. *elife* **2013,** *2*, e01104.
58. Metcalf, J. L.; Xu, Z. Z.; Weiss, S.; Lax, S.; Van Treuren, W.; Hyde, E. R.; Song, S. J.; Amir, A.; Larsen, P.; Sangwan, N., Microbial community assembly and metabolic function during mammalian corpse decomposition. *Science* **2016,** *351* (6269), 158-162.
59. binti Johari, I. S., Lipidomic characterisation and profiling of soil for forensic investigations. **2018**.
60. Carter, D. O.; Filippi, J.; Higley, L. G.; Huntington, T. E.; Okoye, M. I.; Scriven, M.; Bliemeister, J., Using ninhydrin to reconstruct a disturbed outdoor death scene. *Journal of Forensic Identification* **2009,** *59* (2), 190-195.
61. Forbes, S. L.; Keegan, J.; Stuart, B. H.; Dent, B. B., A gas chromatography-mass spectrometry method for the detection of adipocere in grave soils. *European Journal of Lipid Science and Technology* **2003,** *105* (12), 761-768.

62. Procopio, N.; Ghignone, S.; Williams, A.; Chamberlain, A.; Mello, A.; Buckley, M., Metabarcoding to investigate changes in soil microbial communities within forensic burial contexts. *Forensic Science International: Genetics* **2019,** *39*, 73-85.
63. Swenson, T. L.; Jenkins, S.; Bowen, B. P.; Northen, T. R., Untargeted soil metabolomics methods for analysis of extractable organic matter. *Soil Biology and Biochemistry* **2015,** *80*, 189-198.
64. Vranova, V.; Rejsek, K.; Formanek, P., Aliphatic, cyclic, and aromatic organic acids, vitamins, and carbohydrates in soil: a review. *The Scientific World Journal* **2013,** *2013*.
65. Langley, N. R.; Wood, P.; Herling, P.; Steadman, D. W., Forensic Postmortem Interval Estimation from Skeletal Muscle Tissue: A Lipidomics Approach. *Forensic Anthropology* **2019,** *2* (3), 152-157.
66. Procopio, N.; Chamberlain, A. T.; Buckley, M., Intra-and Interskeletal proteome variations in fresh and buried bones. *Journal of proteome research* **2017,** *16* (5), 2016-2029.
67. Prieto-Bonete, G.; Pérez-Cárceles, M. D.; Maurandi-López, A.; Pérez-Martínez, C.; Luna, A., Association between protein profile and postmortem interval in human bone remains. *Journal of proteomics* **2019,** *192*, 54-63.
68. Mickleburgh, H. L.; Schwalbe, E. C.; Bonicelli, A.; Mizukami, H.; Sellitto, F.; Starace, S.; Wescott, D. J.; Carter, D. O.; Procopio, N., Human Bone Proteomes before and after Decomposition: Investigating the Effects of Biological Variation and Taphonomic Alteration on Bone Protein Profiles and the Implications for Forensic Proteomics. *Journal of proteome research* **2021,** *20* (5), 2533-2546.
69. Troutman, L.; Moffatt, C.; Simmons, T., A preliminary examination of differential decomposition patterns in mass graves. *Journal of forensic sciences* **2014,** *59* (3), 621-626.
70. Iancu, L.; Junkins, E. N.; Necula-Petrareanu, G.; Purcarea, C., Characterizing forensically important insect and microbial community colonization patterns in buried remains. *Scientific reports* **2018,** *8* (1), 1-16.

71. von der Lühe, B.; Prost, K.; Birk, J. J.; Fiedler, S., Steroids aid in human decomposition fluid identification in soils of temporary mass graves from World War II. *Journal of Archaeological Science: Reports* **2020,** *32*, 102431.
72. Rodriguez, W. C.; Bass, W. M., Decomposition of buried bodies and methods that may aid in their location. *Journal of Forensic Science* **1985,** *30* (3), 836-852.
73. Turner, B.; Wiltshire, P., Experimental validation of forensic evidence: a study of the decomposition of buried pigs in a heavy clay soil. *Forensic Science International* **1999,** *101* (2), 113-122.
74. Mant, A. K. A study in exhumation data. University of London, 1950.
75. Pate, F. D.; Hutton, J. T., The use of soil chemistry data to address post-mortem diagenesis in bone mineral. *Journal of Archaeological Science* **1988,** *15* (6), 729-739.
76. Kendall, C.; Eriksen, A. M. H.; Kontopoulos, I.; Collins, M. J.; Turner-Walker, G., Diagenesis of archaeological bone and tooth. *Palaeogeography, Palaeoclimatology, Palaeoecology* **2018,** *491*, 21-37.
77. Department, D. U. F. A. a. A. Bone Diagenesis (decay). https://www.futurelearn.com/info/courses/forensic-archaeology-and-anthropology/0/steps/67871 (accessed Aug 26, 2021).
78. López-Costas, O.; Lantes-Suárez, Ó.; Cortizas, A. M., Chemical compositional changes in archaeological human bones due to diagenesis: Type of bone vs soil environment. *Journal of Archaeological Science* **2016,** *67*, 43-51.
79. Matthiesen, H.; Eriksen, A. M. H.; Hollesen, J.; Collins, M., Bone degradation at five Arctic archaeological sites: Quantifying the importance of burial environment and bone characteristics. *Journal of Archaeological Science* **2021,** *125*, 105296.
80. Marchiafava, V.; Bonucci, E.; Ascenzi, A., Fungal osteoclasia: a model of dead bone resorption. *Calcified tissue research* **1974,** *14* (1), 195-210.
81. Föllmi, K., The phosphorus cycle, phosphogenesis and marine phosphate-rich deposits. *Earth-Science Reviews* **1996,** *40* (1-2), 55-124.
82. Emmons, A. L.; Davoren, J.; DeBruyn, J. M.; Mundorff, A. Z., Inter and intra-individual variation in skeletal DNA preservation in buried remains. *Forensic Science International: Genetics* **2020,** *44*, 102193.

83. Lu, W.; Clasquin, M. F.; Melamud, E.; Amador-Noguez, D.; Caudy, A. A.; Rabinowitz, J. D., Metabolomic analysis via reversed-phase ion-pairing liquid chromatography coupled to a stand alone orbitrap mass spectrometer. *Analytical chemistry* **2010,** *82* (8), 3212-3221.
84. Martens, L.; Chambers, M.; Sturm, M.; Kessner, D.; Levander, F.; Shofstahl, J.; Tang, W. H.; Römpp, A.; Neumann, S.; Pizarro, A. D., mzML—a community standard for mass spectrometry data. *Molecular & Cellular Proteomics* **2011,** *10* (1), R110. 000133.
85. Clasquin, M. F.; Melamud, E.; Rabinowitz, J. D., LC-MS data processing with MAVEN: a metabolomic analysis and visualization engine. *Current protocols in bioinformatics* **2012,** *37* (1), 14.11. 1-14.11. 23.
86. Melamud, E.; Vastag, L.; Rabinowitz, J. D., Metabolomic analysis and visualization engine for LC− MS data. *Analytical chemistry* **2010,** *82* (23), 9818-9826.
87. Chong, J.; Wishart, D. S.; Xia, J., Using MetaboAnalyst 4.0 for comprehensive and integrative metabolomics data analysis. *Current protocols in bioinformatics* **2019,** *68* (1), e86.
88. Treutler, H.; Neumann, S., Prediction, detection, and validation of isotope clusters in mass spectrometry data. *Metabolites* **2016,** *6* (4), 37.
89. Kind, T.; Fiehn, O., Seven Golden Rules for heuristic filtering of molecular formulas obtained by accurate mass spectrometry. *BMC bioinformatics* **2007,** *8* (1), 1-20.
90. Rivas-Ubach, A.; Liu, Y.; Bianchi, T. S.; Tolic, N.; Jansson, C.; Pasa-Tolic, L., Moving beyond the van Krevelen diagram: A new stoichiometric approach for compound classification in organisms. *Analytical chemistry* **2018,** *90* (10), 6152-6160.
91. Zhao, Z.; Xian, M.; Liu, M.; Zhao, G., Biochemical routes for uptake and conversion of xylose by microorganisms. *Biotechnology for biofuels* **2020,** *13* (1), 1-12.
92. Mierziak, J.; Burgberger, M.; Wojtasik, W., 3-Hydroxybutyrate as a Metabolite and a Signal Molecule Regulating Processes of Living Organisms. *Biomolecules* **2021,** *11* (3), 402.

93. Pontiller, B.; Martínez-García, S.; Lundin, D.; Pinhassi, J., Labile dissolved organic matter compound characteristics select for divergence in marine bacterial activity and transcription. *Frontiers in microbiology* **2020,** *11*, 2365.
94. Miller, A. L., The methionine-homocysteine cycle and its effects on cognitive diseases.(Homocysteine & Cognitive). *Alternative medicine review* **2003,** *8* (1), 7-20.
95. DeGreeff, L. E.; Furton, K. G., Collection and identification of human remains volatiles by non-contact, dynamic airflow sampling and SPME-GC/MS using various sorbent materials. *Analytical and bioanalytical chemistry* **2011,** *401* (4), 1295-1307.
96. Senesi, N.; Loffredo, E., The chemistry of soil organic matter. In *Soil physical chemistry*, CRC press: 2018; pp 239-370.
97. Phillips, D. A.; Joseph, C. M.; Hirsch, P. R., Occurrence of flavonoids and nucleosides in agricultural soils. *Applied and environmental microbiology* **1997,** *63* (11), 4573-4577.
98. Tsuchiya, K.; Sano, T.; Tomioka, N.; Kohzu, A.; Komatsu, K.; Shinohara, R.; Shimode, S.; Toda, T.; Imai, A., Incorporation characteristics of exogenous 15N-labeled thymidine, deoxyadenosine, deoxyguanosine and deoxycytidine into bacterial DNA. *PloS one* **2020,** *15* (2), e0229740.
99. Hedges, R. E.; Millard, A. R., Bones and groundwater: towards the modelling of diagenetic processes. *Journal of Archaeological Science* **1995,** *22* (2), 155-164.
100. Toppe, J.; Albrektsen, S.; Hope, B.; Aksnes, A., Chemical composition, mineral content and amino acid and lipid profiles in bones from various fish species. *Comparative Biochemistry and Physiology Part B: Biochemistry and Molecular Biology* **2007,** *146* (3), 395-401.
101. Narayanan, A.; Khanchandani, P.; Borkar, R. M.; Ambati, C. R.; Roy, A.; Han, X.; Bhoskar, R. N.; Ragampeta, S.; Gannon, F.; Mysorekar, V., Avascular necrosis of femoral head: a metabolomic, biophysical, biochemical, electron microscopic and histopathological characterization. *Scientific reports* **2017,** *7* (1), 1-16.
102. Evershed, R. P.; Turner-Walker, G.; Hedges, R. E.; Tuross, N.; Leyden, A., Preliminary results for the analysis of lipids in ancient bone. *Journal of Archaeological Science* **1995,** *22* (2), 277-290.

103. Alldritt, I.; Whitham-Agut, B.; Sipin, M.; Studholme, J.; Trentacoste, A.; Tripp, J. A.; Cappai, M. G.; Ditchfield, P.; Devièse, T.; Hedges, R. E., Metabolomics reveals diet-derived plant polyphenols accumulate in physiological bone. *Scientific reports* **2019,** *9* (1), 1-12.
104. Grupe, G.; Turban-Just, S., Amino acid composition of degraded matrix collagen from archaeological human bone. *Anthropologischer Anzeiger* **1998**, 213-226.
105. Giltay, E. J.; Kho, K. H.; Blansjaar, B. A.; Verbeek, M. M.; Geurtz, P. B. H.; Geleijnse, J. M.; Gooren, L. J., The sex difference of plasma homovanillic acid is unaffected by cross-sex hormone administration in transsexual subjects. *Journal of endocrinology* **2005,** *187* (1), 109-116.
106. Nielsen-Marsh, C. M.; Hedges, R. E., Patterns of diagenesis in bone I: the effects of site environments. *Journal of Archaeological Science* **2000,** *27* (12), 1139-1150.
107. Martínez-Reyes, I.; Chandel, N. S., Mitochondrial TCA cycle metabolites control physiology and disease. *Nature communications* **2020,** *11* (1), 1-11.
108. Breusch, F., Citric acid cycle; sugar and fat breakdown in tissue metabolism. *Science (Washington)* **1943,** *97*, 490-492.
109. Miller, S. H.; Browne, P.; Prigent-Combaret, C.; Combes-Meynet, E.; Morrissey, J. P.; O'Gara, F., Biochemical and genomic comparison of inorganic phosphate solubilization in Pseudomonas species. *Environmental microbiology reports* **2010,** *2* (3), 403-411.
110. Moghimi, A.; Tate, M., Does 2-ketogluconate chelate calcium in the pH range 2.4 to 6.4? *Soil Biology and Biochemistry* **1978,** *10* (4), 289-292.
111. Vinolas, L.; Healey, J.; Jones, D., Kinetics of soil microbial uptake of free amino acids. *Biology and fertility of soils* **2001,** *33* (1), 67-74.
112. Davis, P. J.; Gustafson, M. E.; Rosazza, J. P., Formation of indole-3-carboxylic acid by Chromobacterium violaceum. *Journal of bacteriology* **1976,** *126* (1), 544-546.
113. Van Krevelen, D., Graphical-statistical method for the study of structure and reaction processes of coal. *Fuel* **1950,** *29*, 269-284.
114. NandaKafle, G.; Christie, A. A.; Vilain, S.; Brözel, V. S., Growth and extended survival of Escherichia coli O157: H7 in soil organic matter. *Frontiers in microbiology* **2018,** *9*, 762.

115. Connor, M.; Baigent, C.; Hansen, E. S., Testing the use of pigs as human proxies in decomposition studies. *Journal of forensic sciences* **2018,** *63* (5), 1350-1355.
116. Dautartas, A.; Kenyhercz, M. W.; Vidoli, G. M.; Meadows Jantz, L.; Mundorff, A.; Steadman, D. W., Differential decomposition among pig, rabbit, and human remains. *Journal of forensic sciences* **2018,** *63* (6), 1673-1683.
117. Notter, S. J.; Stuart, B. H.; Rowe, R.; Langlois, N., The initial changes of fat deposits during the decomposition of human and pig remains. *Journal of Forensic Sciences* **2009,** *54* (1), 195-201.
118. Schoenly, K. G.; Haskell, N. H.; Hall, R. D.; Gbur, J. R., Comparative performance and complementarity of four sampling methods and arthropod preference tests from human and porcine remains at the Forensic Anthropology Center in Knoxville, Tennessee. *Journal of Medical Entomology* **2007,** *44* (5), 881-894.
119. Steadman, D. W.; Dautartas, A.; Kenyhercz, M. W.; Jantz, L. M.; Mundorff, A.; Vidoli, G. M., Differential scavenging among pig, rabbit, and human subjects. *Journal of forensic sciences* **2018,** *63* (6), 1684-1691.
120. Luong, S.; Forbes, S. L.; Wallman, J. F.; Roberts, R. G., Monitoring the extent of vertical and lateral movement of human decomposition products through sediment using cholesterol as a biomarker. *Forensic science international* **2018,** *285*, 93-104.
121. Swift, M. J.; Heal, O. W.; Anderson, J. M.; Anderson, J., Decomposition in terrestrial ecosystems. **1979**.
122. van Klink, R.; van Laar-Wiersma, J.; Vorst, O.; Smit, C., Rewilding with large herbivores: Positive direct and delayed effects of carrion on plant and arthropod communities. *PloS one* **2020,** *15* (1), e0226946.
123. Keenan, S. W.; Schaeffer, S. M.; Jin, V. L.; DeBruyn, J. M., Mortality hotspots: nitrogen cycling in forest soils during vertebrate decomposition. *Soil Biology and Biochemistry* **2018,** *121*, 165-176.
124. Matuszewski, S.; Hall, M. J.; Moreau, G.; Schoenly, K. G.; Tarone, A. M.; Villet, M. H., Pigs vs people: the use of pigs as analogues for humans in forensic entomology and taphonomy research. *International journal of legal medicine* **2020,** *134* (2), 793-810.

125. Wang, Y.; Ma, M.-y.; Jiang, X.-y.; Wang, J.-f.; Li, L.-l.; Yin, X.-j.; Wang, M.; Lai, Y.; Tao, L.-y., Insect succession on remains of human and animals in Shenzhen, China. *Forensic science international* **2017,** *271*, 75-86.
126. Knobel, Z.; Ueland, M.; Nizio, K. D.; Patel, D.; Forbes, S. L., A comparison of human and pig decomposition rates and odour profiles in an Australian environment. *Australian Journal of Forensic Sciences* **2019,** *51* (5), 557-572.
127. Şen Özdemir, N.; Parrish, C. C.; Parzanini, C.; Mercier, A., Neutral and polar lipid fatty acids in five families of demersal and pelagic fish from the deep Northwest Atlantic. *ICES Journal of Marine Science* **2019,** *76* (6), 1807-1815.
128. Thomas, L. W., The chemical composition of adipose tissue of man and mice. *Quarterly Journal of Experimental Physiology and Cognate Medical Sciences: Translation and Integration* **1962,** *47* (2), 179-188.
129. Heden, T. D.; Neufer, P. D.; Funai, K., Looking beyond structure: membrane phospholipids of skeletal muscle mitochondria. *Trends in Endocrinology & Metabolism* **2016,** *27* (8), 553-562.
130. Ding, S.; Lange, M.; Lipp, J.; Schwab, V. F.; Chowdhury, S.; Pollierer, M. M.; Krause, K.; Li, D.; Kothe, E.; Scheu, S., Characteristics and origin of intact polar lipids in soil organic matter. *Soil Biology and Biochemistry* **2020,** *151*, 108045.
131. Riekhof, W. R.; Benning, C., Glycerolipid biosynthesis. In *The Chlamydomonas sourcebook*, Elsevier: 2009; pp 41-68.
132. Megyesi, M. S.; Nawrocki, S. P.; Haskell, N. H., Using accumulated degree-days to estimate the postmortem interval from decomposed human remains. *Journal of Forensic Science* **2005,** *50* (3), 1-9.
133. Rabinowitz, J. D.; Kimball, E., Acidic acetonitrile for cellular metabolome extraction from Escherichia coli. *Analytical Chemistry* **2007,** *79* (16), 6167-6173.
134. Bligh, E. G.; Dyer, W. J., A rapid method of total lipid extraction and purification. *Canadian journal of biochemistry and physiology* **1959,** *37* (8), 911-917.
135. Mueller, L. O.; Borstein, S. R.; Tague, E. D.; Dearth, S. P.; Castro, H. F.; Campagna, S. R.; Bailey, J. K.; Schweitzer, J. A., Populations of Populus angustifolia have evolved distinct metabolic profiles that influence their surrounding soil. *Plant and Soil* **2020**, 1-13.

136. Wickham, H., ggplot2: elegant graphics for data analysis Springer; New York; 2009. *URL http://had. co. nz/ggplot2/book.[Google Scholar]*.
137. Kuhl, C.; Tautenhahn, R.; Bottcher, C.; Larson, T. R.; Neumann, S., CAMERA: an integrated strategy for compound spectra extraction and annotation of liquid chromatography/mass spectrometry data sets. *Analytical chemistry* **2012,** *84* (1), 283-289.
138. Spicka, A.; Johnson, R.; Bushing, J.; Higley, L. G.; Carter, D. O., Carcass mass can influence rate of decomposition and release of ninhydrin-reactive nitrogen into gravesoil. *Forensic science international* **2011,** *209* (1-3), 80-85.
139. Komar, D.; Beattie, O., Effects of carcass size on decay rates of shade and sun exposed carrion. *Canadian Society of forensic science journal* **1998,** *31* (1), 35-43.
140. Kovarik, M.; Muthny, T.; Sispera, L.; Holecek, M., Effects of β-hydroxy-β-methylbutyrate treatment in different types of skeletal muscle of intact and septic rats. *Journal of physiology and biochemistry* **2010,** *66* (4), 311-319.
141. National Center for Biotechnology Information (2021). PubChem Compound Summary for CID 937, N. R. S., 2021 from https://pubchem.ncbi.nlm.nih.gov/compound/Nicotinate., National Center for Biotechnology Information (2021). PubChem Compound Summary for CID 937, Nicotinate. Retrieved September 15, 2021 from https://pubchem.ncbi.nlm.nih.gov/compound/Nicotinate.
142. Information, N. C. f. B., National Center for Biotechnology Information (2021). PubChem Compound Summary for CID 439162, Sn-Glycerol 3-phosphate. . **2021,** (Retrieved July 24, 2021).
143. Cruzat, V.; Macedo Rogero, M.; Noel Keane, K.; Curi, R.; Newsholme, P., Glutamine: metabolism and immune function, supplementation and clinical translation. *Nutrients* **2018,** *10* (11), 1564.
144. Song, Q.; Joshi, M.; DiPiazza, J.; Joshi, V., Functional relevance of citrulline in the vegetative tissues of watermelon during abiotic stresses. *Frontiers in Plant Science* **2020,** *11*, 512.
145. Swann, L. M.; Busetti, F.; Lewis, S. W., Determination of amino acids and amines in mammalian decomposition fluid by direct injection liquid chromatography-

electrospray ionisation-tandem mass spectrometry. *Analytical Methods* **2012,** *4* (2), 363-370.

146. Kroymann, J.; Textor, S.; Tokuhisa, J. G.; Falk, K. L.; Bartram, S.; Gershenzon, J.; Mitchell-Olds, T., A gene controlling variation in Arabidopsis glucosinolate composition is part of the methionine chain elongation pathway. *Plant Physiology* **2001,** *127* (3), 1077-1088.

147. Kumar, A.; Bachhawat, A. K., Pyroglutamic acid: throwing light on a lightly studied metabolite. *Current Science* **2012**, 288-297.

148. Warren, C., A liquid chromatography–mass spectrometry method for analysis of intact fatty-acid-based lipids extracted from soil. *European Journal of Soil Science* **2018,** *69* (5), 791-803.

149. Parkinson, R., Bacterial communities associated with human decomposition. **2009**.

150. Warren, C. R., Soil microbial populations substitute phospholipids with betaine lipids in response to low P availability. *Soil Biology and Biochemistry* **2020,** *140*, 107655.

151. Hayman, J.; Oxenham, M., Peri-mortem disease treatment: a little known cause of error in the estimation of the time since death in decomposing human remains. *Australian Journal of Forensic Sciences* **2016,** *48* (2), 171-185.

152. Skopyk, A. D.; Forbes, S. L.; LeBlanc, H. N., Recognizing the Inherent Variability in Dipteran Colonization and Decomposition Rates of Human Donors in Sydney, Australia. *Journal of Clinical and Health Sciences* **2021,** *6* (1 (Special), 102-119.

153. Pélissier-Alicot, A.-L.; Gaulier, J.-M.; Champsaur, P.; Marquet, P., Mechanisms underlying postmortem redistribution of drugs: a review. *Journal of analytical toxicology* **2003,** *27* (8), 533-544.

154. Butzbach, D. M., The influence of putrefaction and sample storage on post-mortem toxicology results. *Forensic science, medicine, and pathology* **2010,** *6* (1), 35-45.

155. Peters, F. T.; Steuer, A. E., Antemortem and postmortem influences on drug concentrations and metabolite patterns in postmortem specimens. *Wiley Interdisciplinary Reviews: Forensic Science* **2019,** *1* (1), e1297.

156. Elmsjö, A.; Vikingsson, S.; Söderberg, C.; Kugelberg, F. C.; Green, H., Post-Mortem Metabolomics: A Novel Approach in Clinical Biomarker Discovery and a Potential Tool in Death Investigations. *Chemical Research in Toxicology* **2021**.
157. Chormatography, R. P., Big Pain Assays Aren't a Big Pain with the Raptor Biphenyl
LC Column.
158. Team, R. C., R: A language and environment for statistical computing. **2013**.
159. Kanehisa, M., Toward understanding the origin and evolution of cellular organisms. *Protein Science* **2019,** *28* (11), 1947-1951.
160. Hastie, T.; Tibshirani, R.; Friedman, J., *The elements of statistical learning: data mining, inference, and prediction*. Springer Science & Business Media: 2009.
161. Giles, S. B.; Harrison, K.; Errickson, D.; Márquez-Grant, N., The effect of seasonality on the application of accumulated degree-days to estimate the early post-mortem interval. *Forensic Science International* **2020,** *315*, 110419.
162. Griffiths, K.; Krosch, M. N.; Wright, K., Variation in decomposition stages and carrion insect succession in a dry tropical climate and its effect on estimating postmortem interval. *Forensic Sciences Research* **2020,** *5* (4), 327-335.
163. Smith, J. K., Raccoon Scavenging and the Taphonomic Effects on Early Human Decomposition and PMI Estimation. **2015**.
164. Lupo, S., "The Big Pain": Development of Pain-Free Methods for Analyzing 231 Multiclass Drugs and Metabolites by LC-MS/MS. *MS. Lit. Cat.# CFAR2309-UNV* **2016**.
165. Apple, F. S., A better understanding of the interpretation of postmortem blood drug concentrations. *Journal of analytical toxicology* **2011,** *35* (6), 381-383.
166. Bhat, M. A.; Shrivastav, A. B.; Qureshi, S. R.; Quadri, S. A., Forensic exploitation of veterinary entomology. *Int J Agro Vet Med Sci* **2011,** *5* (4), 429-437.
167. Kshvary, D.; Rassi, Y.; OSHAGHI, M. A.; RAFIZADEH, S.; ALIMOHAMMADI, A. M.; NAMADI, M. S.; PARKHIDEH, S. Z., Analysis of the effect of methadone and temperature on the development rate of Calliphora vicina (Diptera: Calliphoridae): A forensically important fly. *Nusantara Bioscience* **2020,** *12* (2).
168. Ishak, N.; Ahmad, A. H.; Nor, S. A. M.; Ahmad, A., Developmental cycle and growth of lucilia cuprina (diptera: Calliphoridae) fed on heroin: Implications for post-

mortem interval (pmi) estimation in forensic investigations. *ESTEEM Acad. J* **2018,** *14*, 63-71.
169. Wang, S.; Zhang, C.; Chen, W.; Ren, L.; Ling, J.; Shang, Y.; Guo, Y., Effects of methamphetamine on the development and its determination in Aldrichina grahami (Diptera: Calliphoridae). *Journal of medical entomology* **2020,** *57* (3), 691-696.
170. Oliveira, H. G.; Gomes, G.; Morlin Jr, J. J.; Von Zuben, C. J.; Linhares, A. X., The effect of Buscopan® on the development of the blow fly Chrysomya megacephala (F.)(Diptera: Calliphoridae). *Journal of forensic sciences* **2009,** *54* (1), 202-206.
171. Al-Shuraym, L. A.; Al-Mekhlafi, F. A.; Abd Al Galil, F. M.; Alhag, S. K.; Al-Keridis, L. A.; Ali El Hadi Mohamed, R.; Wadaan, M. A.; Al-Khalifa, M. S., Effect of Zolpidem Tartrate on the Developmental Rate of Forensically Important Flies Chrysomya megacephala (Diptera: Calliphoridae) and Chrysomya saffranea. *Journal of Medical Entomology* **2021**.
172. Gosselin, M.; Di Fazio, V.; Wille, S. M.; Fernandez, M. d. M. R.; Samyn, N.; Bourel, B.; Rasmont, P., Methadone determination in puparia and its effect on the development of Lucilia sericata (Diptera, Calliphoridae). *Forensic science international* **2011,** *209* (1-3), 154-159.
173. El-Samad, L. M.; Tantawi, T. I.; El-Ghaffar, H. A.; Beltagy, B. I.; El-Abd, E., The effect of morphine on the development rate of flies (Diptera: Calliphoridae, Sarcophagidae) reared on rabbit carcasses containing this drug and its implications to postmortem interval estimates. *Swed J BioSci Res* **2020,** *1* (1), 28-38.
174. Kharbouche, H.; Augsburger, M.; Cherix, D.; Sporkert, F.; Giroud, C.; Wyss, C.; Champod, C.; Mangin, P., Codeine accumulation and elimination in larvae, pupae, and imago of the blowfly Lucilia sericata and effects on its development. *International journal of legal medicine* **2008,** *122* (3), 205-211.
175. Preußer, D.; Bröring, U.; Fischer, T.; Juretzek, T., Effects of antibiotics ceftriaxone and levofloxacin on the growth of Calliphora vomitoria L.(Diptera: Calliphoridae) and effects on the determination of the post mortem-interval. *Journal of Forensic and Legal Medicine* **2021**, 102207.
176. Zhou, R.; Yu, Q.; Li, T.; Long, M.; Wang, Y.; Feng, T.; Su, W.; Yang, J.; Li, H., Carcass decomposition influences the metabolic profiles and enriches noxious

metabolites in different water types by widely targeted metabolomics. *Chemosphere* **2021,** *269*, 129400.
177. Macdonald, B. C.; Farrell, M.; Tuomi, S.; Barton, P. S.; Cunningham, S. A.; Manning, A., Carrion decomposition causes large and lasting effects on soil amino acid and peptide flux. *Soil Biology and Biochemistry* **2014,** *69*, 132-140.
178. Statheropoulos, M.; Agapiou, A.; Spiliopoulou, C.; Pallis, G. C.; Sianos, E., Environmental aspects of VOCs evolved in the early stages of human decomposition. *Science of the Total Environment* **2007,** *385* (1-3), 221-227.
179. Vass, A. A., Beyond the grave-understanding human decomposition. *Microbiology today* **2001,** *28*, 190-193.
180. Kaszynski, R. H.; Nishiumi, S.; Azuma, T.; Yoshida, M.; Kondo, T.; Takahashi, M.; Asano, M.; Ueno, Y., Postmortem interval estimation: a novel approach utilizing gas chromatography/mass spectrometry-based biochemical profiling. *Analytical and bioanalytical chemistry* **2016,** *408* (12), 3103-3112.
181. Grajeda-Iglesias, C.; Aviram, M., Specific amino acids affect cardiovascular diseases and atherogenesis via protection against macrophage foam cell formation. *Rambam Maimonides medical journal* **2018,** *9* (3).
182. Zaric, B. L.; Radovanovic, J. N.; Gluvic, Z.; Stewart, A. J.; Essack, M.; Motwalli, O.; Gojobori, T.; Isenovic, E. R., Atherosclerosis Linked to Aberrant Amino Acid Metabolism and Immunosuppressive Amino Acid Catabolizing Enzymes. *Frontiers in Immunology* **2020**, 2341.
183. Sun, H.; Olson, K. C.; Gao, C.; Prosdocimo, D. A.; Zhou, M.; Wang, Z.; Jeyaraj, D.; Youn, J.-Y.; Ren, S.; Liu, Y., Catabolic defect of branched-chain amino acids promotes heart failure. *Circulation* **2016,** *133* (21), 2038-2049.
184. Dudzinska, W., Purine nucleotides and their metabolites in patients with type 1 and 2 diabetes mellitus. *Journal of biomedical science and engineering* **2014,** *2014*.
185. Zhao, H.; Dennery, P. A.; Yao, H., Metabolic reprogramming in the pathogenesis of chronic lung diseases, including BPD, COPD, and pulmonary fibrosis. *American Journal of Physiology-Lung Cellular and Molecular Physiology* **2018,** *314* (4), L544-L554.

186. Lieu, E. L.; Nguyen, T.; Rhyne, S.; Kim, J., Amino acids in cancer. *Experimental & molecular medicine* **2020,** *52* (1), 15-30.
187. Damann, F. E.; Tanittaisong, A.; Carter, D. O., Potential carcass enrichment of the University of Tennessee Anthropology Research Facility: a baseline survey of edaphic features. *Forensic Science International* **2012,** *222* (1-3), 4-10.
188. Statheropoulos, M.; Agapiou, A.; Zorba, E.; Mikedi, K.; Karma, S.; Pallis, G. C.; Eliopoulos, C.; Spiliopoulou, C., Combined chemical and optical methods for monitoring the early decay stages of surrogate human models. *Forensic Science International* **2011,** *210* (1-3), 154-163.
189. Wu, G., *Amino acids: biochemistry and nutrition*. CRC Press: 2013.
190. Dai, X.; Fan, F.; Ye, Y.; Lu, X.; Chen, F.; Wu, Z.; Liao, L., An experimental study on investigating the postmortem interval in dichlorvos poisoned rats by GC/MS-based metabolomics. *Legal Medicine* **2019,** *36*, 28-36.

VITA

Originally from Germany, Katharina Höland grew up in Grossrinderfeld, Baden-Württemberg. After high school, she attended the Julius-Maximilians-University of Würzburg (JMU), Germany and received a Bachelor and Master of Science in biomedicine. During her time at JMU, she explored her passion for forensics by acquiring an internship as a medicolegal death investigator at the Institute of Legal Medicine in Würzburg, Germany. From this experience came the desire to pursue a career in forensic science. For her graduate studies she chose the University of Tennessee, Knoxville with the reputational Forensic Anthropology Center (FAC) which enabled to combine her future endeavors with state-of-the-art analytical chemistry. This is why she continued her educational path by pursuing a Doctor of Philosophy degree in chemistry with a concentration in analytical chemistry and a focus in forensics. Her research interests are centered around studying the mechanisms of human decomposition by assessing metabolic changes occurring postmortem.